Studies on Photocatalytic Conversion of CO_2 in Water over Layered Double Hydroxides

SHOJI IGUCHI

2016

Preface

On December 12, 2015, 186 countries concluded a new international agreement on reduction of climate change at *the 2015 United Nations Climate Change Conference* (COP 21) held in Paris. This agreement asked all countries to make an action plan which intends to keep the rise in the global average temperature below 2 degree Celsius compared to pre-industrial levels by diminution of the greenhouse gas emission. It is known that the concentration of atmospheric CO_2, which is one of the most serious causes of global climate changes, increases year by year because energy consumption derived from fossil fuels has been steadily increased. The total energy consumption in whole world was approximately 15 tera-watt in 2010, and more than 80% of it was generated from fossil fuels such as coal, oil, and natural gas. It is obvious that the suppression of energy consumption should be urgent issue for us. For developing countries, however, reduction in the use of fossil fuels directly prevent them from the economic growth because there are many merits for them in utilizing fossil fuels, such as easy handling, high calorific value, low cost, easy transportation, and easy set up to use. Hence, the developed countries including Japan should drive attempts to convert the energy source from fossil fuels to renewable energy, such as wind, solar, biomass, etc. In that sense, the use of solar light as the energy source is an attractive theme for many researchers because total energy demand in whole world can be provided by 0.03% of sunlight falling onto the land area of world. The photocatalytic conversion of CO_2 into useful chemicals, which transform the light energy into the chemical energy, is promising process to create an artificial carbon cycling system driven by the renewable energy source from the point of view of two issues; the reduction of atmospheric CO_2 concentration and the utilizing the solar energy. Lately, kinds of Japanese corporations such as Toyota Central R&D Labs., Inc. (Toyota Motor Group), Panasonic Corporation, and Toshiba Corporation respectively address developments of the artificial photosynthesis using photoelectrochemical devices, indicating that the momentum for researching on the solar-light driven artificial photosynthesis heightens. The studies on heterogeneous photocatalysis such as developments of new photocatalysts, mechanistic studies, elucidation in the roles of cocatalyst, and investigation on the surface properties of photocatalyst which influence the activities, should give the remarkable and conspicuous achievements to such an utilitarian systems. Based on

this consideration, the author carried out the researches focused on the development in the photocatalysis of new materials; layered double hydroxides.

In the present thesis, the author found that the photocatalytic activities of Ni^{2+}-based layered double hydroxides (LDHs) for the conversion of CO_2 in an aqueous media under UV light irradiation. As compared to the cases of typical semiconductor photocatalysts, the selectivity toward CO formation among the reduction products was sufficiently high because the reduction of proton (H^+) into H_2 was obviously suppressed. The improvements in activity for the conversion of CO_2 were achieved by the addition of chloride ion (Cl^-) into the reaction solution, the coordination of LDH properties via substituting metal components and fluorination. Moreover, LDH-based composite photocatalyst (LDH-Ga_2O_3) exhibited elegant performance for the photocatalytic conversion of CO_2 into CO.

The studies presented in this thesis were carried out at Department of Molecular Engineering, Graduate School of Engineering, Kyoto University from 2013 through 2016 under the supervision of Professor Tsunehiro Tanaka. The author wishes to express his sincere gratitude to Professor Tsunehiro Tanaka for his guidance, philosophical suggestions, and continual encouragement throughout this work. In addition, the author should make special acknowledgements to Associate Professor Kentaro Teramura for his grateful guidance, valuable suggestions, fruitful discussions, strict but heartwarming advices, and careful reviewing of the manuscripts. Grateful thanks should be made to Associate Professor Saburo Hosokawa for his helpful advices and pointed suggestions. Special thanks should also be made to Professor Tetsuya Shishido at Tokyo Metropolitan University for his grateful advices, helpful suggestions, and tenderhearted encouragement. Cordial thanks are given to Professor Hisao Yoshida at Kyoto University, Professor Tomoko Yoshida at Osaka City University, Professor Ryu Abe at Kyoto University, and Dr. Masanobu Higashi at Kyoto University for their encouragements and valuable discussions at the conference. The author is deeply grateful to seniors of his laboratory, Dr. Shinya Furukawa, Dr. Tomoyuki Kitano, Dr. Lidan Deng, Dr. Hiroyuki Asakura, Dr. Zheng Wang, and Dr. Akira Yamamoto for their useful advices to experiments, instructive suggestions, and exact discussions concerned to this study, in addition to continual encouragements throughout this work. The author wishes to express his sincere gratitude to Professor Salvatore Coluccia and Professor Gianmario Martra for

their heartwarming hospitality and valuable discussion when I stayed in Turin, Italy to measure *in-situ* FT-IR spectra although FT-IR studies on LDHs are not presented in this thesis. The author shows gratitude to the staffs of SPring-8 at JASRI in Hyogo prefecture for measurements of XAFS. The author should make thanks to Dr. Takeshi Morikawa at Toyota Central R&D Labs., Inc. for offering samples in the collaborative XAFS experiments. Associate Professor Hitoshi Ishida at Kitasato University and Associate Professor Yasuaki Tokudome at Osaka Prefecture University are acknowledged for their kind offer of ruthenium complexes and high surface area Ni−Al LDHs, respectively. In addition, the author is deeply grateful to Associate Professor Yusuke Yoshinaga at Tokyo Gakugei University and Dr. Kaori Omata at NIT Suzuka College for their continual encouragements throughout this work.

The author is also indebted to Mr. Yuto Mizuno who have cooperated the photocatalytic conversion of CO_2 using various LDHs (Chapter 1), Mr. Hirotaka Ishii who have cooperated the investigation on the effect of chloride ion (Chapter 2), Mr. Soichi Kikkawa who have cooperated the photoelectrochemical and electrochemical measurements (Chapter 5), and Mr. Yudai Hasegawa who have cooperated the investigation on both the incorporation of transition metals into LDH structure (Chapter 4) and the photocatalytic conversion of CO_2 using LDH-Ga_2O_3 composite photocatalyst (Chapter 6) for their collaborations, diligent working, and instructive discussion about this work. Thanks should be made to Secretary Ms. Ayako Tanaka and Ms. Mami Nishio for their kind aids in official affairs. The author is also grateful to all the members of the laboratory led by Professor Tsunehiro Tanaka.

Finally, the author sincerely thanks his parents Yukinobu and Kaori Iguchi, brother Yoshito Iguchi, and grandparents Akuri Iguchi, Takashi and Masa Ito for their understanding and encouragement.

Shoji Iguchi

Kyoto

December 2015

CONTENTS

Preface

General Introduction …….. 001

Chapter 1 Photocatalytic Conversion of CO_2 in an Aqueous Solution Using Various Kinds of Layered Double Hydroxides……..... 019

Chapter 2 Effect of the Chloride Ion as a Hole Scavenger on the Photocatalytic Conversion of CO_2 in an Aqueous Solution over Ni−Al Layered Double Hydroxides……. 035

Chapter 3 Photocatalytic Conversion of CO_2 in Water Using Fluorinated Layered Double Hydroxides as Photocatalysts..……. 055

Chapter 4 Preparation of Transition Metal-containing Layered Double Hydroxides and Application to the Photocatalytic Conversion of CO_2 in Water..... 075

Chapter 5 Investigation on Electrochemical and Photoelectrochemical Properties of Ni−Al LDH Photocatalyst…….. 097

Chapter 6 Improvement in the Photocatalytic Activity for the Conversion of CO_2 in Water by Modification of Ga_2O_3 with Mg−Al Layered Double Hydroxide……. 117

Summary …….. 135

Appendix $ZnTa_2O_6$ Photocatalyst Synthesized via Solid State Reaction for Conversion of CO_2 into CO in Water……..…….. 139

List of Publications …….. 159

General Introduction

Catalytic Reduction of CO_2

Development in the chemical fixation of CO_2 which imitates the photosynthesis system of green plants in nature has been one of the biggest issues for scientists [1]. It is known that CO_2 molecule, which consists of two C = O double bonds to form a linear shape, is the most oxidized form of carbon, and then stable and inert compound in the chemical reactions, indicating that energy injection for the activation of CO_2 molecule is required to achieve the chemical fixation of CO_2. The standard reduction potentials of CO_2 are given in Table 1 in volts relative to the normal hydrogen electrode (pH = 7) [2, 3].

Table 1 Standard potentials of redox reactions related to CO_2 [2, 3]

Reaction										E^o / V vs. NHE
CO_2			+	e^-	$\longrightarrow$	$CO_2^{\bullet-}$				−1.90
CO_2	+	$2H^+$	+	$2e^-$	$\longrightarrow$	HCOOH	+	H_2O		−0.61
CO_2	+	$2H^+$	+	$2e^-$	$\longrightarrow$	CO	+	H_2O		−0.52
CO_2	+	$4H^+$	+	$4e^-$	$\longrightarrow$	HCHO	+	H_2O		−0.48
CO_2	+	$6H^+$	+	$6e^-$	$\longrightarrow$	CH_3OH	+	H_2O		−0.38
CO_2	+	$8H^+$	+	$8e^-$	$\longrightarrow$	CH_4	+	$2H_2O$		−0.24

Catalytic Hydrogenation of CO_2: Hydrogenation of CO_2 into CO, CH_3OH, and CH_4 using both homogeneous and heterogeneous catalysts have been investigated for several decades to produce an artificial fuel originated from abundant atmospheric CO_2. As reviewed by Gong et al. [4], homogeneous catalysts exhibit sufficient activity and selectivity, but the reuse and regeneration are doubtful. That review also says, on the other hand, heterogeneous catalysts are favorable in the points of stability, separation, handling, and reuse, as well as reactor design, which reflects in lower costs for large-scale productions [4]. It is generally known that kinds of supported cupper catalysts are active for the hydrogenation of CO_2. Actually, pilot-scale plants for methanol production from H_2 and CO_2 using efficient heterogeneous catalysts have been demonstrated [5]. Moreover, the recent advance in the H_2 production process using natural energy sources, which might cause the falling in

price of H_2 and the enhancement in supply stability, will improve the fuel production process based on the hydrogenation of CO_2 over heterogeneous catalysts.

Electrochemical Reduction of CO_2: Electrochemical reduction of CO_2 in an aqueous media has been also widely demonstrated, and remarkable results and consideration were reported in 1980s and 1990s by Hori et al [6]. Metal electrodes are divided into four groups in the cathodic reduction of CO_2 in aqueous inorganic salt solution [6]; for CO formation metals (Au, Ag, Zn, Pd, and Ga), for $HCOO^-$ formation metals (Pb, Hg, In, Sn, Cd, and TI), for hydrocarbon formation metal (Cu), and for H_2 formation metals (Ni, Fe, Pt, and Ti). It is generally considered that metal cathode electrodes which permit $CO_2^{\bullet-}$ (carbon dioxide anion radical) adsorbed on yield CO as a reduction product, while $HCOO^-$ was mainly produced at those do not stabilize $CO_2^{\bullet-}$. Moreover, the recent developments in the cathode electrode using metal oxides-based materials and carbon-based materials enable the decrease in the required over potential for the electrochemical reduction of CO_2 [7]. On the other hand, the advanced metal cathode electrodes in combination with the light-to-current conversion devices have been also developed, which can drive the electrochemical reduction of CO_2 using light energy. For example, Panasonic Corp. released the artificial photosynthesis system consisting of GaN-based photoelectrode (photoanode) and indium metal plate cathode, that produces formic acid with high solar light conversion efficiency comparable to the photosynthesis of natural plants. In addition, Toshiba Corp. also found the combination system of Au nanoparticle cathode and multi-conjugated semiconductor which evolved CO as a reduction product of CO_2 with excellent efficiency. In this wise, the electrochemical CO_2 reduction system coupled with the sufficiently advanced photon utilizing techniques cultivated in the field of solar cell is considered to be one of the most promising process to achieve the artificial photosynthesis.

Homogeneous Photocatalyst for CO_2 Reduction: Generally, photocatalytic reduction of CO_2 using homogeneous catalyst such as metal complex can achieve high selectivity for the reduction products of CO_2 because the intermediate species including CO_2 as one of the ligands are formed during the reactions. In the primary period, the photocatalytic systems consisting of the metal complex homogeneous catalysts for CO_2 reduction (e.g. $[Ru(bpy)_2(CO)_2]^{2+}$) and the photosensitizer

metal complex (e.g. $[Ru(bpy)_3]^{2+}$) were reported [8, 9]. For the mixture system of two components (photosensitizer and catalyst), the electron transfer from a photosensitizer to a CO_2 reduction catalyst determines the efficiency of the whole photocatalytic reaction. The optimization of both components and the reaction conditions enabled to achieve the quantum efficiency $\Phi = 0.59$ (quantum efficiency: number of the consumed electrons for products formation per number of the adsorbed photons to the photocatalytic system) [3]. Moreover, Ishitani et al. reported the supramolecular photocatalyst including ruthenium complex for the photosensitizer and rhenium complex for the CO_2 reduction catalyst showed much higher photocatalytic activity than the corresponding mixed system with mononuclear Ru and Re complexes [10]. However, strong reducing reagents such as trimethylamine (TEA), triethanolamine (TEOA), or 1-benzyl-1,4-dihydronicotinamide (BNAH) are necessary to drive the photocatalytic reduction of CO_2 over these homogeneous catalysts, indicating that these systems are not capable of using H_2O as a proton source and an electron donor. What is more, almost the homogeneous complex catalysts were poisoned by the presence of H_2O molecules. In the immediate past, water tolerance homogeneous system for the reduction of CO_2 was developed which can work in an aqueous solution with copresence of water-soluble sacrificial reductant [11]. High selectivity, high quantum efficiency, and easy tuning of catalyst design are considered to the excellent points for constructing the photocatalytic system. Others advance in the field of homogeneous catalysts for the CO_2 reduction is summarized in the review article [12].

Heterogeneous Photocatalyst for CO_2 Reduction: Many researches on the photocatalytic conversion of CO_2 using heterogeneous photocatalyst have been conducted in parallel with those on the photocatalytic water splitting [13]. Photocatalytic reactions are categorized into two types from the point of view of thermodynamics; one is the uphill reactions and the other is the downhill reactions. The conversion of CO_2 into CO, HCHO, HCOOH, CH_3OH, or hydrocarbons and the H_2O splitting into H_2 and O_2 are regarded as the former because photon energy is transformed to chemical energy through these reactions. In other words, the change in Gibbs free energy of these reactions are positive ($\Delta G > 0$), as seen in the photosynthesis by green plants in nature. In contrast, the photo-induced degradation (mineralization) of organic compounds such as dyes, alcohols, and aldehydes etc. using O_2 are considered as the downhill reactions. These photoaccelerating reactions

proceed in the same direction in which it takes place spontaneously in the dark condition ($\Delta G < 0$). In that sense, the constructing of the photocatalytic system which involves the uphill reaction may enable the artificial photosynthesis induced by solar light [14]. As Andrew Bocarsly et al. summarized the latest review [1], kinds of semiconductor-based materials were reported as photocatalysts for the conversion of CO_2. We always check the reported photocatalytic systems for the conversion of CO_2 in accordance with three points.

(1) Selectivity toward the CO_2 reduction products among total reduction products is above 50%.

(2) Evolution of the stoichiometric amounts of oxidation products.

(3) Isotopic experiment for determining the carbon source of CO evolved.

Although many literatures insisted that the photocatalytic conversions of CO_2 in the presence of H_2O (or in H_2O solution) were driven, the main reduction product was sometimes H_2; a reduction product of proton (H^+) derived from H_2O. In those cases, the photoexcited electrons are dominantly consumed to reduce H^+, indicating that the photocatalytic water splitting progresses in preference to the photocatalytic conversion of CO_2. The selectivity toward CO_2 reduction products should be above 50% for the photocatalytic reactions intended to the conversion of CO_2. Moreover, it is necessary to detect the oxidation products accompanied with the evolution of reduction products; for the case of the reduction of CO_2 into CO in an aqueous media, O_2 should be evolved as an oxidation product of H_2O in accordance with following equations. The formation of the stoichiometric amount of O_2 indicates that H_2O acts as a proton source and an electron donor in the photocatalytic reaction.

<u>Reduction</u>

$$CO_2 + 2H^+ + 2e^- \longrightarrow CO + H_2O$$

$$2H^+ + 2e^- \longrightarrow H_2$$

<u>Oxidation</u>

$$2H_2O + 4h^+ \longrightarrow O_2 + 4H^+$$

In addition, the isotopic experiment using ^{13}C-labeled CO_2 ($^{13}CO_2$) as a substrate is essential to confirm the carbon source of the CO_2 reduction products because organic residues might be decomposed into CO or CH_4 under the illumination. The literatures which satisfy the above mentioned three points are totally limited. Ag-loaded $BaLa_4Ti_4O_{15}$ photocatalyst reported by Kudo et

al. [15], Ag-loaded Ga_2O_3-based mixed oxides [16-18] and Ta_2O_5-based photocatalysts [19] found by our research group are good examples.

Hybrid Photocatalyst for CO_2 Reduction: In order to overcome the critical issues; low stability and necessity to use strong reducing reagent for the homogeneous system, and low selectivity toward CO_2 reduction products and low quantum efficiency for the heterogeneous systems, hybrid photocatalysts between semiconductors and metal complexes were developed. In 2010, Morikawa et al. reported visible light-driven hybrid photocatalyst consisting of *p*-type nitrogen-doped Ta_2O_5 (N-Ta_2O_5) and $[Ru(dcbpy)_2(CO)_2]^{2+}(Cl^-)_2$ for the selective conversion of CO_2 into HCOOH [20]. The photoexcited electrons on the conduction band of N-Ta_2O_5 would transfer to ruthenium complex, and then that complex drove the reduction of CO_2 into HCOOH electrochemically. Based on the above result, two steps excitation type (Z-scheme type) hybrid photocatalyst which contains Pt/TiO_2 photoanode and ruthenium complexes polymer-deposited InP photocathode was constructed, and this system achieved 0.04% of solar light conversion efficiency for HCOOH production [21]. In addition, ruthenium complexes fixed on TaON or C_3N_4 hybrid photocatalyst were developed by Maeda et al. [22-24], which enables the photocatalytic conversion of CO_2 under visible light irradiation in the presence of sacrificial reagents. Although the photocatalytic activity for CO_2 conversion deeply depends on the combination of three components; semiconductor, photosensitizer (light harvesting), and CO_2 reduction catalyst, the advance in this field might lead us to a practical level for the artificial photosynthesis.

Strategy for the New Photocatalyst: Our research group has reported that various metal oxides show the photocatalytic activity for the conversion of CO_2 in the presence of H_2 as a reductant. ZrO_2 [25-28], MgO [29, 30], and Ga_2O_3 [31], which have basic sites on their surface, exhibited relatively high activity for CO evolution as a reduction product of CO_2 under UV light irradiation. On the other hand, Al_2O_3, TiO_2, and Nb_2O_5 did not show the activity for the photocatalytic conversion of CO_2 because these oxides might not be favorable for the adsorption of CO_2. In the case of MgO, a new acceptor level derived from adsorbed CO_2 species (bidentate carbonate-MgO) was formed between the valence band and the conduction band levels of MgO. Photoexcitation of electron from the

valence band of MgO (O 2p) to the new acceptor level might induce the photocatalytic reaction; we call this phenomenon as *in situ doping*. In contrast, the adsorbed species of CO_2 on the surface of Ga_2O_3 was reduced into bidentate formate species by the photogenerated electron via the band excitation of Ga_2O_3, and then the decomposition of formate resulted in the CO evolution. Hence, we regard the photocatalyst materials which permit CO_2 molecules adsorbed on as promising candidates for the photocatalytic conversion of CO_2. On the other hand, the use of H_2O as a reductant in the photocatalytic reaction is desired in the point of view of environment because H_2O is abundant, safe, and easily available proton source. Typical metal oxide photocatalysts such as ZrO_2, MgO, and Ga_2O_3, unfortunately, did not active in an aqueous media for the photocatalytic conversion of CO_2, indicating that basic sites covered with H_2O molecules did not approve the adsorption of CO_2. In that sense, photocatalyst materials which have high water tolerance basic sites should be suitable for the photocatalytic conversion of CO_2 in the presence of H_2O (as a proton source and an electron donor).

Fundamentals of Layered Double Hydroxides (LDHs)

Layered double hydroxides (LDHs), also called hydrotalcite-like compounds, are natural and/or synthetic anionic clay materials. The term LDH was coined in the early works of Feithnecht, who named them "Doppelschichtstruktruren" (i.e., double layer structures), presuming a structure with intercalated hydroxide layers. This hypothesis was refuted many years later on the basis of single-crystal X-ray diffraction (XRD) analysis, which showed that LDHs consist of positively charged two-dimensional (2D) sheets, with all the cations located in the same layer, and the charge-compensating anions and water molecules in the interlayer region [32, 33]. It is known that the parent material of these anionic clays is the natural mineral hydrotalcite, which has the formula $Mg_6Al_2(OH)_{16}CO_3 \cdot 4H_2O$. The general formula of LDHs is

$$[M^{2+}_{1-x}M^{3+}_{x}(OH)_2]^{x+}(A^{n-}_{x/n}) \cdot mH_2O$$

where M^{2+} and M^{3+} are divalent and trivalent cations, respectively. The value of x represents the molar ratio of $M^{3+}/(M^{2+} + M^{3+})$, while A^{n-} is the interlayer anion of valence n. The characters of M^{2+}, M^{3+}, x, and A^{n-} can alter over a wide range, thus giving rise to a large number of isostructural materials with various physical and chemical properties. The range of x which enables the formation a pure LDH phase is reported from 0.2 to 0.4. When the x value is outside of this range, hydroxides

or other compounds are formed as impurity phases. The divalent cations (M^{2+} = Fe^{2+}, Co^{2+}, Ni^{2+}, Cu^{2+}, Zn^{2+}, Mn^{2+}, Cd^{2+}, and Ca^{2+}) and the trivalent cations (M^{3+} = Co^{3+}, Fe^{3+}, Mn^{3+}, Ga^{3+}, Cr^{3+}, In^{3+}, V^{3+}, Y^{3+}, La^{3+}) take part in LDHs by through fully or partially replacing Mg^{2+} or Al^{3+} of the brucite-like layer of hydrotalcite [34]. Multi-metal cations can be simultaneously incorporated into the brucite-like layer to prepare multi-component LDHs, provided *x* is in the correct range. The most common anion found in naturally occurring LDHs is carbonate (CO_3^{2-}), which shows a high affinity for the interlayer in a series of LDHs. In fact, various kinds of charge-compensating anions may be incorporated into the interlayer, namely inorganic anions (NO_3^-, SO_4^{2-}, halides, oxyanions, silicates etc.), polyoxometalate anions ($Mo_7O_{24}^{6-}$, $W_7O_{24}^{6-}$, $V_{10}O_{28}^{6-}$, $PMo_{12}O_{40}^{3-}$, $PW_{12}O_{40}^{3-}$ etc.), complex anions (porphyrin complexes, phthalocyanine complexes, $Fe(CN)_6^{4-}$/$Fe(CN)_6^{3-}$), and organic anions (carboxylates, dicarboxylates, alkylsulfates, alkanesulfates etc. [34]

LDHs are widely used as basic materials for CO_2 capture and storage [35], removal of organic and inorganic anions from the aqueous solution [36-38], and base-catalyzed reactions [39]. Ebitani et al. reported that Mg−Al LDHs catalyze the aldol condensation of carbonyl compounds in an aqueous solution because their surface base sites show the property of high water tolerance [40], indicating that basic sites of LDHs and their derivatives may function in the presence of water.

Preparation Techniques of LDHs

As reviewed by Reichle [41] and Cavani et al. [32], various preparation methods of LDHs have been developed. The optimum conditions, e.g., atmosphere, temperature, pH during the preciptation, concentration of precursor solution, aging procedure, etc. should be chosen in accordance with the kinds of metal components constituting the hydroxide sheets.

Co-precipitation Method: LDHs are traditionally synthesized by co-precipitation from aqueous solution. The most common procedure is the constant-pH co-precipitation process, wherein the mixed aqueous solution of the metal components and the base solution (normally, an aqueous solution of NaOH) are added simultaneously to an aqueous solution of Na_2CO_3 to maintain the suspension at a stable pH. In the so-called variable pH co-precipitation process, LDHs containing CO_3^{2-} as interlayer anions are prepared by gradually adding the aqueous solution containing the

metal cations to the aqueous solution of Na_2CO_3 until the suspension reaches a specified pH. As necessary, the aqueous solution of NaOH is then used to maintain the pH until the precipitation is completed. In both processes, the resulting suspension is stirred at a certain temperature as an aging for varying periods of time, and then collected by filtration. The filter cake is washed with pure water and is then dried.

Hydrothermal Synthesis: Hydrothermal treatment is usually applied to obtain well-crystallized LDHs with large platelets. Homogeneous co-precipitation method under hydrothermal conditions is an advanced technique to synthesize well-defined LDHs particles. Ogawa et al., for example, reported the following procedure: an aqueous solution containing urea and salts of the metal components mixed in a certain ratio were transferred into an autoclave and heated at 393 K for 24 h. After cooling to room temperature, the solid precipitate was collected and washed with deionized water. We generally synthesized various kinds of LDHs via co-precipitation method combined with hydrothermal treatment as follows: after constant pH co-precipitation process at room temperature, the resulting suspension is transferred to a stainless steel autoclave with an inner Teflon vessel, and aged under hydrothermal conditions at 383 K. The resultant solid is collected by filtration and washed with 1.0 L of ultra-pure water, and then dried at 383 K in air.

Rehydration: Since atmospheric CO_2 is incorporated into the structure of LDH with high affinity, most synthesized LDHs contain CO_3^{2-} as interlayer anions or as surface-adsorbed species. The rehydration process (also called the reconstruction process), based on the "memory effect," is necessary to obtain carbonate-free LDHs. As-prepared LDH is calcined at over 773 K in air or in an inert gas atmosphere to produce the mixed oxide via decomposition of its characteristic layered structure. The resulting mixed oxide is immersed in decarbonated water at room temperature for several hours under an inert gas atmosphere to yield rehydrated LDH, during which the layer structures of the hydroxide sheets are reconstructed and the charge-compensating CO_3^{2-} anions are replaced by OH^- anions [42]. Medina et al. argued that the rehydrated Mg−Al LDH that have active hydroxyl groups located near the edges of the platelets exhibit high performance in aldol condensations [43].

Application of LDHs to Photocatalytic Reactions

Degradation of Organic Compounds: The photocatalytic elimination of toxic organic pollutants using visible light has been extensively studied for two decades. From the perspectives of environmental concerns and energy shortages, it is necessary to develop a novel photocatalyst, which can effectively utilize renewable and clean solar energy. Although the band edge of TiO_2-based materials (such as $TiO_{2-x}N_x$) significantly shifts towards the visible region, their photoelectronic transition efficiencies are low due to inherent light absorption properties of these materials. Aiming to obtain a novel photocatalyst with large surface area and high crystallinity, ordered layer photocatalysts have been paid great attentions [44]. Zn-containing LDHs (Zn−M LDHs) are widely used as photocatalysts for the degradation of organic compounds. Shao et al. reported that as-prepared Zn−Ti LDH, with a low band gap of ca. 3.1 eV exhibited significant photocatalytic activity for the degradation of methylene blue under visible light irradiation; a level of activity was much higher than those of ZnO and TiO_2. Furthermore, Zn−Ti LDH is stable through five repeated application cycles with nearly constant photodecomposition percentage, indicating that Zn−Ti LDH does not deactivate during the photocatalytic process [45]. Xia et al. demonstrated the photocatalytic degradation of rhodamine B (RB) under visible light irradiation using a series of Zn−M LDH (M = Al, Fe, Ti, and FeTi). The degradation rates of RB for all four of the LDHs are over 50% after the photoirradiation for 60 min, in the following order: Zn−Ti ≈ Zn−Al > Zn−Fe−Ti > Zn−Fe LDHs. Thermal regeneration of the Zn−Ti LDH utilized for RB degradation was feasible for at least three cycles, indicating that the structural stability of this material is sufficient to use it repeatedly as a photocatalyst for the degradation of RB [46]. In addition, various Zn−M LDHs, such as Zn−Cr [47], Ag-loaded Zn−Cr [48], Pt-loaded Zn−Ti [49], Zn−Bi [50], and Mg−Zn−In LDH [44] have been reported as photocatalysts for the decomposition of organic compounds. On the other hand, metal oxides/LDH composites have been also reported to show similar activity for these photocatalytic reactions. Valente et al. presented the preparation of CeO_2 supported by Mg−Al LDH and their photocatalytic activities for the degradation of phenol and phenol-derivatives [51]. The photocatalytic systems for the degradation of organic dyes and compounds using TiO_2/Mg−Al LDH [52], ZnO/Mg−Al LDH [53], SnO_2/Mg−Al LDH [54], and Fe_3O_4/Zn−Cr LDH [55] were also demonstrated.

Water Splitting: Since Honda and Fujishima found the photoelectrochemical water-splitting system using TiO_2 as a photoanode, various inorganic materials have been applied to catalyze the photocatalytic splitting of water. As brucite-like hydroxide sheets of LDHs can incorporate various kinds of metal cations to achieve the characteristic light absorption properties, some LDHs have recently attracted attention for their potential as new visible-light-responsive photocatalysts. LDHs are sometimes fabricated via a homogeneous precipitation method using urea and/or other amine compounds, as mentioned above. Organic residues cannot be removed by the mild heat treatment that enables LDHs to maintain their characteristic layered structure. Hence, it should be noted that such organic contaminants might influence photocatalytic activities. García et al. reported that semiconductor materials based on three kinds of Zn^{2+}-containing LDHs (Zn−Cr, Zn−Ti, and Zn−Ce LDH) show photocatalytic activity for O_2 evolution from water under visible light irradiation, in the presence of $AgNO_3$ as a sacrificial reagent. A certain amount of O_2 was evolved under visible light irradiation using Zn−Cr LDH as the photocatalyst; furthermore, once the photocatalytic reaction rate tends to slow down, addition of $AgNO_3$ reactivates the formation of O_2. It is indicated that the reason for the cessation in the O_2 evolution is the lack of the sacrificial reagent, and not deactivation or corrosion of the catalyst. It should also be noted that the overall efficiency of the Zn−Cr LDH for the O_2 evolution under visible light irradiation is 1.6 times higher than that of a WO_3 photocatalyst under the same reaction conditions [56]. Wei et al. published a visible-light-responsive photocatalyst fabricated by anchoring Ni−Ti LDH to the surface of reduced graphene oxide sheets (RGO) that displays good activity for the photocatalytic O_2 evolution. The generation rates of O_2 over Ni−Ti LDH/RGO composites are much larger compared to bare Ni−Ti LDH and RGO, respectively; that is, the combination of Ni−Ti LDH and RGO significantly enhances the photocatalytic activity [57]. Wei et al. also reported a photocatalytic H_2 production system using various LDHs as photocatalysts that contain highly dispersed TiO_6 units. Ni−Ti, Zn−Ti, and Mg−Al−Ti LDH show photocatalytic activity for H_2 evolution using lactic acid as a sacrificial electron donor. In particular, Zn−Ti LDH, which contains highly dispersed TiO_6 units, displays a production rate 18 times higher than that of $K_2Ti_4O_9$, which contains highly aggregated TiO_6 octahedra [58]. On the other hand, Xu et al. demonstrated photocatalytic H_2 evolution with the Rose bengal (Rbg) and Pt nanoparticles (photosensitizers) fixed on Mg−Al LDH (co-catalyst). A

self-assembled Rbg–LDH–Pt system produces H_2 from water that contains triethanolamine (TEOA) as a sacrificial reagent; the amount is a few times greater than that of the Rbg–Pt (without LDH) system. Pt nanoparticles on Mg−Al LDH can be used repeatedly, and the total turnover number after six runs for the Rbg–LDH–Pt system is calculated to be 304, based on Pt. Photocatalytic water splitting has many advantages: (i) immobilizing the dye photosensitizer for suppressed self-quenching, (ii) close arrangement between photosensitizer molecules and co-catalyst nanoparticles for efficient electron transfer, (iii) formation of well-dispersed co-catalyst nanoparticles on the support surface, and (iv) easy recycling of the expensive co-catalyst [59].

CO_2 Conversion: Photocatalytic conversion of CO_2 to valuable compounds is one of the promising methods to create a sustainable carbon-cycling system. The CO_2 molecules adsorbed on the surface of photocatalysts should be converted into active species that can be easily reduced by photogenerated electrons. Therefore, solid base materials are suitable candidates to construct the photocatalytic system for CO_2 conversion, as mentioned above. In the last five years, several research groups have demonstrated the photocatalytic conversion of CO_2 using synthetic LDHs. Izumi et al. reported that Cu^{2+}-containing LDH photocatalysts show activity for CO_2 conversion using H_2 as the reductant, and CO and methanol are evolved as the reduction products of CO_2. In their system, $[Zn_3Ga(OH)_8]^+{}_2[Cu(OH)_4]^{2-} \cdot mH_2O$ and $[Zn_{1.5}Cu_{1.5}Ga(OH)_8]^+{}_2(CO_3)^{2-} \cdot mH_2O$ are used as photocatalysts, and the former shows higher activity than the latter for methanol formation as the reduction product of CO_2. Cu^{2+} species, in the interlayer for the former and in the inlayer for the latter, are considered active sites for CO_2 conversion under the irradiation [60-62]. Katsumata et al. also exhibited that noble-metal (Pt, Pd, and Au)-loaded Zn−Cr LDHs are active for the photocatalytic conversion of CO_2 to CO under UV irradiation. Since CO is not detected under visible light irradiation, it is concluded that photocatalytic conversion of CO_2 does not occur by absorption of the 410- and 570-nm peaks attributed to d−d transition [63].

Outline of the Present Thesis

This thesis focused on the photocatalytic conversion of CO_2 in an aqueous solution using layered double hydroxides (LDHs) as photocatalysts. CO was evolved as a reduction product of CO_2

with high selectivity under UV light irradiation in all cases. This thesis consists of six chapters.

Chapter 1 describes that various kinds of M^{2+}–M^{3+} LDHs (M^{2+} = Mg^{2+}, Ni^{2+}, and Zn^{2+}; M^{3+} = Al^{3+}, Ga^{3+}, and In^{3+}) synthesized via co-precipitation method exhibited the photocatalytic activity for the conversion of CO_2 in pure water. The use of Ni–Al LDH as a photocatalyst enabled us to achieve maximum conversion of CO_2 into CO with high selectivity, because it produced less H_2 as a reduction product of H^+ derived from water than other LDHs. Mass spectrometry revealed that the carbon source of CO evolved was not the organic residues on the surface of LDHs photocatalysts bu the introduced CO_2 gas as a substrate.

Chapter 2 shows the effect of NaCl additive on the photocatalytic conversion of CO_2 in an aqueous solution using Ni–Al LDH as a photocatalyst. The addition of Cl^- to the reaction solution clearly improved the photocatalytic activity for the conversion of CO_2 into CO, and simultaneously suppressed the H_2 evolution as a reduction product of H^+. *N*,*N'*-dimethyl-*p*-phenylenediamin (DPD) test suggested that the Cl^- present in the reaction solution functions as an effective hole scavenger and that it would be oxidized to Cl_2, which immediately converts into hypochlorous acid (HClO).

In chapter 3, the influence of the fluorination of Mg–Al LDH and Ni–Al LDH on the photocatalytic conversion of CO_2 in water was investigated. The fluorination of Mg–Al LDH led to an enhancement in both the amount of CO evolved and the selectivity towards CO formation. The author conclude that the fluorination of LDH by incorporation of AlF_6^{3-} units in the hydroxide sheets affords surface properties suitable for the photocatalytic conversion of CO_2 in the presence of Cl^-, which acts as a hole scavenger.

Chapter 4 presents the photocatalytic activities of transition metals-containing M^{2+}–M^{3+} LDHs (M^{2+} = Co^{2+}, Ni^{2+}, Cu^{2+}, and Zn^{2+}; M^{3+} = V^{3+}, Cr^{3+}, Mn^{3+}, and Fe^{3+}) for the conversion of CO_2 in an aqueous NaCl solution. The author found that Ni–V LDH showed the high photocatalytic activity for the conversion of CO_2, and over 200 μmol of CO was evolved as a reduction product of CO_2 after 8 h of photoirradiation. The existence of V^{3+} afforded good performance for the conversion of CO_2 into CO in an aqueous solution of NaCl because the combination of V^{3+} and Cl^- play a significant role in the photocatalytic conversion of CO_2 to CO in an aqueous solution.

In Chapter 5, electrochemical and photoelectrochemical properties of Ni–Al LDH were investigated. Ni–Al LDH showed the electrochemical properties corresponding to the *n*-type material,

that is, cathodic dark current under a cathodic polarization and anodic photocurrent under an anodic polarization were respectively found in the electrochemical measurements. The potential of the photogenerated electrons for Ni−Al LDH photocatalyst was estimated to −0.40 V vs. NHE (pH = 0) via impedance measurements, which is enough to induce the two-electron reduction of CO_2 into CO.

Chapter 6 shows the photocatalytic activity of Mg−Al LDH-Ga_2O_3 composite photocatalyst for the conversion of CO_2 in an aqueous $NaHCO_3$ solution. Composite photocatalyst achieved the excellent activity for CO evolution in the presence of 0.25 wt.% Ag cocatalyst. The stoichiometric formation of O_2 as an oxidation product of H_2O suggested that H_2O acts as an electron donor and a proton source. Both the increase in the specific surface area by Mg−Al LDH modification and the high ability of Mg−Al LDH as an adsorbent for CO_2, which preserves CO_2 molecules near from the Ag cocatalyst, approved the selective conversion of CO_2 into CO under UV light irradiation.

References

1. J. L. White, M. F. Baruch, J. E. Pander Iii, Y. Hu, I. C. Fortmeyer, J. E. Park, T. Zhang, K. Liao, J. Gu, Y. Yan, T. W. Shaw, E. Abelev and A. B. Bocarsly, *Chemical Reviews*, 2015, DOI: 10.1021/acs.chemrev.5b00370.
2. *Standard Potentials in Aqueous Solution*, Marcel Dekker, 1985.
3. H. Takeda and O. Ishitani, *Coordination Chemistry Reviews*, 2010, **254**, 346-354.
4. W. Wang, S. Wang, X. Ma and J. Gong, *Chemical Society Reviews*, 2011, **40**, 3703-3727.
5. H. Arakawa *et al., Chemical Reviews*, 2001, **101**, 953-996.
6. Y. Hori, H. Wakebe, T. Tsukamoto and O. Koga, *Electrochimica Acta*, 1994, **39**, 1833-1839.
7. J. Cheng, M. Zhang, G. Wu, X. Wang, J. Zhou and K. Cen, *Environmental Science & Technology*, 2014, **48**, 7076-7084.
8. H. Ishida, T. Terada, K. Tanaka and T. Tanaka, *Inorganic Chemistry*, 1990, **29**, 905-911.
9. H. Ishida, K. Tanaka and T. Tanaka, *Organometallics*, 1987, **6**, 181-186.
10. B. Gholamkhass, H. Mametsuka, K. Koike, T. Tanabe, M. Furue and O. Ishitani, *Inorganic Chemistry*, 2005, **44**, 2326-2336.
11. A. Nakada, K. Koike, K. Maeda and O. Ishitani, *Green Chem.*, 2016, DOI: 10.1039/c5gc01720c.

12. Y. Yamazaki, H. Takeda and O. Ishitani, *Journal of Photochemistry and Photobiology C: Photochemistry Reviews*, 2015, DOI: 10.1016/j.jphotochemrev.2015.09.001.

13. S. Navalon, A. Dhakshinamoorthy, M. Alvaro and H. Garcia, *ChemSusChem*, 2013, **6**, 562-577.

14. A. Kudo and Y. Miseki, *Chemical Society Reviews*, 2009, **38**, 253-278.

15. K. Iizuka, T. Wato, Y. Miseki, K. Saito and A. Kudo, *Journal of the American Chemical Society*, 2011, **133**, 20863-20868.

16. K. Teramura, Z. Wang, S. Hosokawa, Y. Sakata and T. Tanaka, *Chemistry - A European Journal*, 2014, **20**, 9906-9909.

17. Z. Wang, K. Teramura, S. Hosokawa and T. Tanaka, *Journal of Materials Chemistry A*, 2015, **3**, 11313-11319.

18. Z. Wang, K. Teramura, Z. Huang, S. Hosokawa, Y. Sakata and T. Tanaka, *Catalysis Science & Technology*, 2015, DOI: 10.1039/C5CY01280E.

19. K. Teramura, H. Tatsumi, Z. Wang, S. Hosokawa and T. Tanaka, *Bulletin of the Chemical Society of Japan*, 2015, **88**, 431-437.

20. S. Sato, T. Morikawa, S. Saeki, T. Kajino and T. Motohiro, *Angewandte Chemie International Edition*, 2010, **49**, 5101-5105.

21. S. Sato, T. Arai, T. Morikawa, K. Uemura, T. M. Suzuki, H. Tanaka and T. Kajino, *Journal of the American Chemical Society*, 2011, **133**, 15240-15243.

22. R. Kuriki, K. Sekizawa, O. Ishitani and K. Maeda, *Angewandte Chemie International Edition*, 2015, **54**, 2406-2409.

23. K. Maeda, R. Kuriki, M. Zhang, X. Wang and O. Ishitani, *Journal of Materials Chemistry A*, 2014, **2**, 15146-15151.

24. K. Sekizawa, K. Maeda, K. Domen, K. Koike and O. Ishitani, *Journal of the American Chemical Society*, 2013, **135**, 4596-4599.

25. Y. Kohno, T. Tanaka, T. Funabiki and S. Yoshida, *Chemical Communications*, 1997, 841-842.

26. Y. Kohno, T. tanaka, T. Funabiki and S. Yoshida, *Chemistry Letters*, 1997, **26**, 993-994.

27. Y. Kohno, T. Tanaka, T. Funabiki and S. Yoshida, *Journal of the Chemical Society, Faraday Transactions*, 1998, **94**, 1875-1880.

28. Y. Kohno, T. Tanaka, T. Funabiki and S. Yoshida, *Physical Chemistry Chemical Physics*, 2000, **2**, 2635-2639.

29. Y. Kohno, H. Ishikawa, T. Tanaka, T. Funabiki and S. Yoshida, *Physical Chemistry Chemical Physics*, 2001, **3**, 1108-1113.

30. K. Teramura, T. Tanaka, H. Ishikawa, Y. Kohno and T. Funabiki, *The Journal of Physical Chemistry B*, 2004, **108**, 346-354.

31. H. Tsuneoka, K. Teramura, T. Shishido and T. Tanaka, *The Journal of Physical Chemistry C*, 2010, **114**, 8892-8898.

32. F. Cavani, F. Trifirò and A. Vaccari, *Catalysis Today*, 1991, **11**, 173-301.

33. C. Delhoyo, *Applied Clay Science*, 2007, **36**, 103-121.

34. Z. P. Xu, J. Zhang, M. O. Adebajo, H. Zhang and C. Zhou, *Applied Clay Science*, 2011, **53**, 139-150.

35. M. K. Ram Reddy, Z. P. Xu, G. Q. Lu and J. C. Diniz da Costa, *Industrial & Engineering Chemistry Research*, 2006, **45**, 7504-7509.

36. J. Das, B. S. Patra, N. Baliarsingh and K. M. Parida, *Applied Clay Science*, 2006, **32**, 252-260.

37. K. H. Goh, T. T. Lim and Z. Dong, *Water Research*, 2008, **42**, 1343-1368.

38. R. L. Goswamee, P. Sengupta, K. G. Bhattacharyya and D. K. Dutta, *Applied Clay Science*, 1998, **13**, 21-34.

39. B. F. Sels, D. E. De Vos and P. A. Jacobs, *Catalysis Reviews*, 2001, **43**, 443-488.

40. K. Ebitani, K. Motokura, K. Mori, T. Mizugaki and K. Kaneda, *The Journal of Organic Chemistry*, 2006, **71**, 5440-5447.

41. W. T. Reichle, *Solid State Ionics*, 1986, **22**, 135-141.

42. C. Xu, Y. Gao, X. Liu, R. Xin and Z. Wang, *RSC Advances*, 2013, **3**, 793-801.

43. S. Abelló, F. Medina, D. Tichit, J. Pérez-Ramírez, J. C. Groen, J. E. Sueiras, P. Salagre and Y. Cesteros, *Chemistry – A European Journal*, 2005, **11**, 728-739.

44. L. Huang, S. Chu, J. Wang, F. Kong, L. Luo, Y. Wang and Z. Zou, *Catalysis Today*, 2013, **212**, 81-88.

45. M. Shao, J. Han, M. Wei, D. G. Evans and X. Duan, *Chemical Engineering Journal*, 2011,

168, 519-524.

46. S. J. Xia, F. X. Liu, Z. M. Ni, J. L. Xue and P. P. Qian, *Journal of Colloid and Interface Science*, 2013, **405**, 195-200.
47. L. Mohapatra and K. M. Parida, *Separation and Purification Technology*, 2012, **91**, 73-80.
48. J. Sun, Y. Zhang, J. Cheng, H. Fan, J. Zhu, X. Wang and S. Ai, *Journal of Molecular Catalysis A: Chemical*, 2014, **382**, 146-153.
49. G. Chen, S. Qian, X. Tu, X. Wei, J. Zou, L. Leng and S. Luo, *Applied Surface Science*, 2014, **293**, 345-351.
50. L. Mohapatra and K. M. Parida, *Physical Chemistry Chemical Physics*, 2014, **16**, 16985-16996.
51. J. S. Valente, F. Tzompantzi and J. Prince, *Applied Catalysis B: Environmental*, 2011, **102**, 276-285.
52. S. Pausova, J. Krysa, J. Jirkovsky, G. Mailhot and V. Prevot, *Environmental Science and Pollution Research (international)*, 2012, **19**, 3709-3718.
53. S. Yuan, Y. Li, Q. Zhang and H. Wang, *Colloids and Surfaces A: Physicochemical and Engineering Aspects*, 2009, **348**, 76-81.
54. E. Dvininov, M. Ignat, P. Barvinschi, M. A. Smithers and E. Popovici, *Journal of Hazardous Materials*, 2010, **177**, 150-158.
55. D. Chen, Y. Li, J. Zhang, J.-z. Zhou, Y. Guo and H. Liu, *Chemical Engineering Journal*, 2012, **185-186**, 120-126.
56. C. G. Silva, Y. Bouizi, V. Fornés and H. García, *Journal of the American Chemical Society*, 2009, **131**, 13833-13839.
57. B. Li, Y. Zhao, S. Zhang, W. Gao and M. Wei, *ACS Applied Materials & Interfaces*, 2013, **5**, 10233-10239.
58. Y. Zhao, P. Chen, B. Zhang, D. S. Su, S. Zhang, L. Tian, J. Lu, Z. Li, X. Cao, B. Wang, M. Wei, D. G. Evans and X. Duan, *Chemistry A Europian Journal*, 2012, **18**, 11949-11958.
59. J. Hong, Y. Wang, J. Pan, Z. Zhong and R. Xu, *Nanoscale*, 2011, **3**, 4655-4661.
60. N. Ahmed, Y. Shibata, T. Taniguchi and Y. Izumi, *Journal of Catalysis*, 2011, **279**, 123-135.
61. M. Morikawa, N. Ahmed, Y. Yoshida and Y. Izumi, *Applied Catalysis B: Environmental*, 2014,

144, 561-569.

62. M. Morikawa, Y. Ogura, N. Ahmed, S. Kawamura, G. Mikami, S. Okamoto and Y. Izumi, *Catalysis Science & Technology*, 2014, **4**, 1644-1651.

63. K. Katsumata, K. Sakai, K. Ikeda, G. Carja, N. Matsushita and K. Okada, *Materials Letters*, 2013, **107**, 138-140.

Chapter 1

Photocatalytic Conversion of CO_2 in an Aqueous Solution Using Various Kinds of Layered Double Hydroxides

Abstract

We found that various layered double hydroxides (LDHs) showed good activity for the photocatalytic conversion of CO_2 in an aqueous solution. Isotope experiments using $^{13}CO_2$ as a substrate clearly revealed that CO was generated as a main reduction product of CO_2. Ni-Al LDH (Ni/Al = 4) exhibited the largest amount of CO evolved among the various kinds of LDHs. Especially, Ni-Al LDHs fabricated from chlorides showed the higher conversion of CO_2 to CO than those from nitrates. The amount of CO evolved was increased by the addition of chloride ions into the reaction solution, on the other hand, the addition of carbonate and hydrocarbonate ions did not enhance the conversion of CO_2 but promoted the selectivity to H_2 evolution for water splitting.

Introduction

Over the past a few decades, the amount of CO_2 in air has been increased to a critical level owing to high consumption rates of fossil fuels such as coal, oil, and natural gas. The fixation of CO_2 in a chemical process is attracted by many scientists and engineers because the increasing atmospheric concentration of CO_2 would cause the global warming. The conversion of CO_2 into valuable chemicals such as CO and CH_4 using solar energy is one of the most suitable ways from the point of view of energy problem. The photocatalytic conversion of CO_2 using several kinds of heterogeneous photocatalysts including TiO_2 were first reported by Honda and his co-workers in 1979 [1]. However, TiO_2 possesses a fetal weak point that the conduction band is located at the more positive potential than that required to reduce CO_2. For this reason, it is of interest to explore other photocatalysts which show the activity for the photocatalytic conversion of CO_2 [2]. Some research groups have been trying to apply non-titanium metal oxides to the photocatalytic conversion of CO_2 [2], such as CdS[3], $NiO/InTaO_4$ [4], $ZnGa_2O_4$ [5], Bi_2WO_6 [6], ZnO [7], etc. Recently, Kudo et al. reported that Ag cocatalyst-modified $ALa_4Ti_4O_{15}$ (A = Ca, Sr, and Ba) exhibits the photocatalytic activity for the conversion of CO_2 into CO and HCOOH[8]. It was the first report that O_2 gas was also evolved stoichiometrically, indicating that H_2O functions as a reductant (an electron donor) for the photocatalytic conversion of CO_2.

Our group found that CO was generated as a result of the photocatalytic conversion of CO_2 over ZrO_2 [9-12], MgO[13,14], $ATaO_3$ (A = Li, Na, and K) [15], and Ga_2O_3 [16], which are known as solid base materials, in the presence of H_2 or CH_4 as a reductant. It is known that CO_2, which is one of acidic substrates, can be easily adsorbed and then, monodentate, bidentate, and bridging carbonates are generated together with surface oxygen atoms on the surface of the solid base materials. These nonlinear CO_2 molecules formed on the surface of the photocatalysts are more destabilized than the typical linear CO_2 molecule, which indicates that the distorted CO_2 molecules are expected to be activated under photoirradiation easily in the conversion of CO_2. Those photocatalysts, however, did not work in an aqueous solution because the base sites were poisoned by H_2O. Layered double hydroxides (LDHs) are well known as natural or synthetic crystalline clays. Ebitani et al. reported that Mg−Al LDH (hydrotalcite) catalyzed the aldol condensation of carbonyl compounds in an

aqueous solution because their surface base sites show high water tolerance property[17]. This result indicates that the LDHs including Mg−Al LDH can function as solid base catalysts and CO_2 can be adsorbed on the surface of LDHs in an aqueous solution. If CO_2 is first adsorbed on the photocatalyst surface and then activated under photoirradiation, most LDHs would function as photocatalysts in water. Although LDHs are well-known catalyst supports (e.g. Mg-Al hydrotalcite), they have rarely been used as photocatalysts. LDHs show photocatalytic activity for the degradation of organic compounds [18] and O_2 evolution from water in the presence of $AgNO_3$ sacrificial reagent [19]. Subsequently, Hwang and co-workers developed visible-light-responsive nanohybrids of LDHs and a layered metal oxide [20]. A copper-modified LDH was reported to show activity for the photocatalytic conversion of CO_2 in the presence of H_2 gas as a reductant [21]. In that study, LDH was used only as a CO_2 adsorbent because the Cu species acted as active sites, as is the case for Cu/TiO_2, a photocatalyst for CO_2 conversion [22]. It is well-known that LDHs can be fabricated using not only nitrates but also chlorides, and that their surface properties and morphology would be changed by residual anions derived from the precursors. We expect that the photocatalytic activity of LDHs should be also affected by their precursors. In this study, we have tried to apply various kinds of LDHs synthesized from nitrates and chlorides to the photocatalytic conversion of CO_2 in an aqueous solution, and the effect of anions existing in the reaction solution on the selectivity of products evolved was investigated.

Experimental

Various LDHs ($[M^{2+}_{1-x}–M^{3+}_{x}(OH)_2]^{x+}(A^{n-})_{x/n} \cdot mH_2O$); ($M^{2+} = Mg^{2+}$, Zn^{2+}, Ni^{2+}; $M^{3+} = Al^{3+}$, Ga^{3+}, and In^{3+}), were synthesized by the following coprecipitation method; an aqueous solution of nitrates or chlorides of M^{2+} and M^{3+} was slowly added to an aqueous Na_2CO_3 solution at room temperature with vigorously stirring. The pH was kept constant at 10 by adding an aqueous NaOH solution. The resulting suspension was transferred into a stainless steel autoclave with an inner Teflon vessel and aged at 383 K for 20 h under hydrothermal condition. The solid was collected by filtration and washed with ultra-pure water, and dried at 383 K in air atmosphere. $M^{2+}–M^{3+}$ LDH(NO_3^-) and $M^{2+}–M^{3+}$ LDH(Cl^-) mean $M^{2+}–M^{3+}$ LDH prepared from nitrates and chlorides as

precursors of hydroxide sheets, respectively. For example, Mg_3−Al_1 LDH(Cl^-) presents the layered double hydroxide consisting of magnesium and aluminum with the ratio Mg^{2+} : Al^{3+} = 3 : 1, which was synthesized from chloride salts.

The powder X-ray diffraction (XRD) patterns of various LDHs were collected on an X-ray diffractometer (Rigaku, Multiflex), using Cu K_α radiation (λ = 0.154 nm) at a scan speed of 4.0 degree min^{-1}. The thermo gravimetric analysis for LDHs was performed using Rigaku, Thermo Plus 2. The certain amount of sample was set in the furnace, and the temperature was increased by 3 K min^{-1} under flow condition of dried air. Temperature programmed desorption profiles were obtained using TPD-1-AT (BEL Japan, Inc.) equipped with Q-Mass (ANELVA, M-QA100F) as a detector. 50 mg of sample powder was set in a quartz glass tube and the temperature was increased by 5 K min^{-1} under He flow. Q-Mass profile in m/z = 44 and 45 were monitored during increasing temperature to confirm the desorption of $^{12}CO_2$ and $^{13}CO_2$ gases, respectively.

Photocatalytic conversion of CO_2 in H_2O was carried out in a closed circulating system connected to a vacuum line. Two types of reactors were utilized for the photocatalytic activity tests in the present study. For an outer irradiation type reactor, 100 mg of the photocatalyst powder was dispersed in 4 mL of water, and 500 μmol of pure CO_2 gas was introduced into the dead space. After circulation for certain minutes, the suspension was illuminated under a 200 W Hg-Xe lamp (San-Ei Electric Co., Ltd.). The other type was an inner irradiation type reactor equipped with a cooling water system made by a quartz glass. 500 mg of photocatalyst (LDH) powder was dispersed in 350 mL of ultra-pure water in the glass reactor, and the suspension was degassed. Gaseous CO_2 purified by vacuum distillation at liquid-N_2 temperature was introduced into the free gas space, and the circulating was performed for 1 hour before photoirradiation. Then, the suspension was illuminated from within the reactor with a 400 W high pressure Hg lamp through the quartz water jacket. The products were analyzed by thermal conductivity detector gas chromatography (TCD-GC) using a GC-8A chromatograph (Shimadzu Corporation, Japan) equipped with an Active Carbon column or a MS-5A column. A quadruple-type mass spectrometer (BEL Japan, Inc., BEL Mass) was used for isotope experiments.

Results and discussion

Figure 1 shows X-ray diffraction (XRD) patterns of various kinds of M^{2+}–M^{3+} LDHs(NO_3^-); $M^{2+}/M^{3+} = 3$, $M^{2+} = Mg^{2+}$, Zn^{2+}, Ni^{2+}; $M^{3+} = Al^{3+}$, Ga^{3+}, and In^{3+}. Each sample, except that prepared using Zn^{2+} and In^{3+}, showed a characteristic XRD pattern. Two sharp diffraction peaks at 11 and 23 degree are assigned to (0 0 3) and (0 0 6) planes reflections, which are characteristic reflection for a series of LDHs [23]. It was considered that LDH structure was not formed in the precipitated sample synthesized from Zn^{2+} and In^{3+}. Because the (0 0 3) reflections for Mg_3–Ga_1, Ni_3–Ga_1, and Zn_3–Ga_1 LDHs were sharp, the layer structure of LDHs which contain Ga^{3+} as a metal component of hydroxide sheets would be advanced in *c*-axis direction. As presented in **Figure 2**, diffraction peaks corresponding to LDH-like compounds were found in the XRD patterns of M^{2+}–M^{3+} LDHs(Cl^-); Mg_3–Al_1, Ni_3–Al_1, Zn_3–Al_1, Mg_3–In_1, and Ni_3–In_1 LDHs [23]. As for Ni_3–Al_1 LDH(Cl^-) (**pattern *a***), two sharp diffraction peaks at 11.4 and 23.1 degree are assigned to (0 0 3) and (0 0 6) planes reflections, which are related to interval of each hydroxide sheets and distance from hydroxide sheets to interlayer anions, respectively. The other intense peak at 60.8 degree is indexed as a (1 1 0) plane reflection with respect to hexagonal axes. The parameter ***a*** of layered double hydroxides corresponding to the cation-cation distance within the hydroxide sheet can be calculated

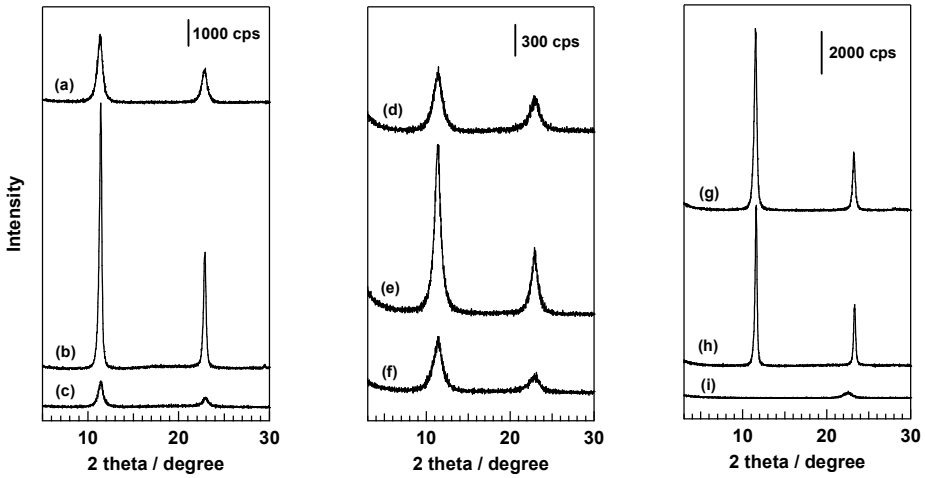

Figure 1 XRD patterns of various M^{2+}–M^{3+} LDHs(NO_3^-); (a) Mg_3–Al_1, (b) Mg_3–Ga_1, (c) Mg_3–In_1, (d) Ni_3–Al_1, (e) Ni_3–Ga_1, (f) Ni_3–In_1, (g) Zn_3–Al_1, and (h) Zn_3–Ga_1 LDH, and the precipitated sample of (i) Zn–In.

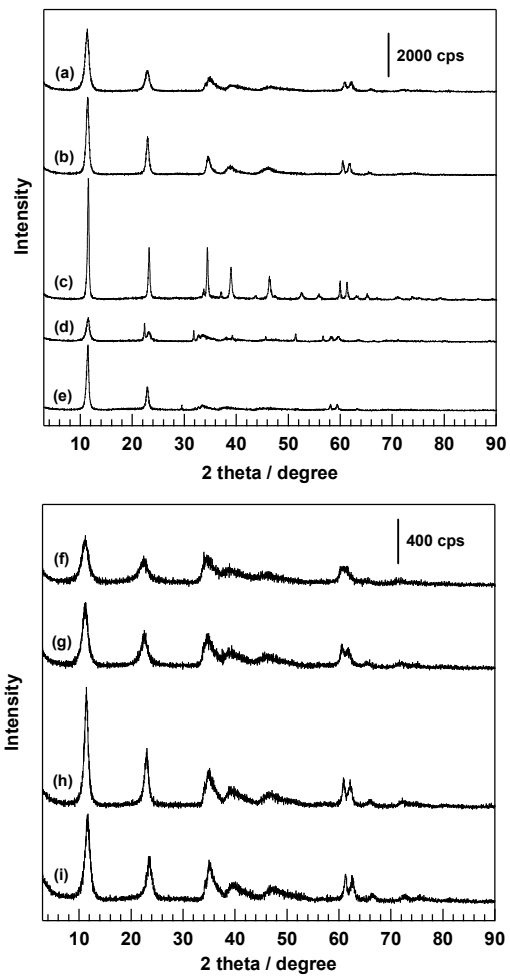

Figure 2 XRD patterns of various M^{2+}–M^{3+} LDHs(Cl^-); (a) Ni_3–Al_1, (b) Mg_3–Al_1, (c) Zn_3–Al_1, (d) Ni_3–In_1, (e) Mg_3–In_1, (f) Ni_5–Al_1, (g) Ni_4–Al_1, (h) Ni_3–Al_1, and (i) Ni_2–Al_1 LDH.

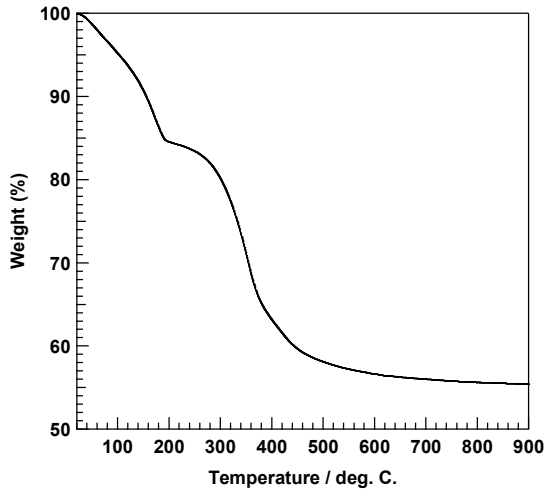

Figure 3 The weight loss curve of Ni_3–Al_1 LDH(Cl^-) in TG analysis.

as follow: $\boldsymbol{a} = 2\boldsymbol{d}_{(1\,1\,0)}$. The (1 1 0) reflection of Mg_3–In_1 LDH(Cl^-) appeared at lower angle than that of Mg_3–Al_1 LDH(Cl^-), indicating that the cation-cation distance of Mg_3–In_1 LDH(Cl^-) was longer than that of Mg_3–Al_1 LDH(Cl^-). This peak shift is due to the difference of ionic radii of trivalent cation, Al^{3+}: 53.5 pm and In^{3+}: 80.0 pm [24], existing in the hydroxide sheet of LDHs. On the other hand, the position of these sharp diffraction peaks were not changed with Ni/Al ratio in Ni–Al LDH(Cl^-) (**pattern *f*–*i***). The value of full width at half maximum (FWHM) of (0 0 3) plane reflection was the smallest at Ni/Al = 3, indicating that the stacking of hydroxide sheets along with ***c*** axis has been advanced at Ni/Al = 3. **Figure 3** shows the weight loss curve of Ni_3–Al_1 LDH(Cl^-) recorded by thermal gravimetric analysis. It was known that LDHs exhibit the characteristic two

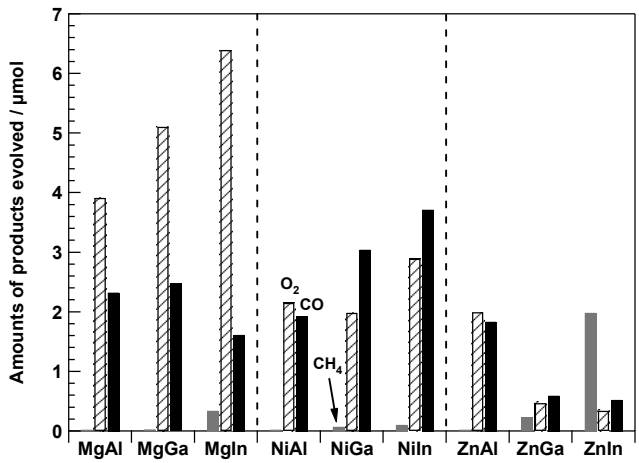

Figure 4(a) Amounts of products evolved in the photocatalytic conversion of CO_2 in water using various M^{2+}–M^{3+} LDHs(NO_3^-). Photoirradiation time: 10 h. Reactor: outer irradiation type. Black: CO, gray: CH_4, and slash: O_2.

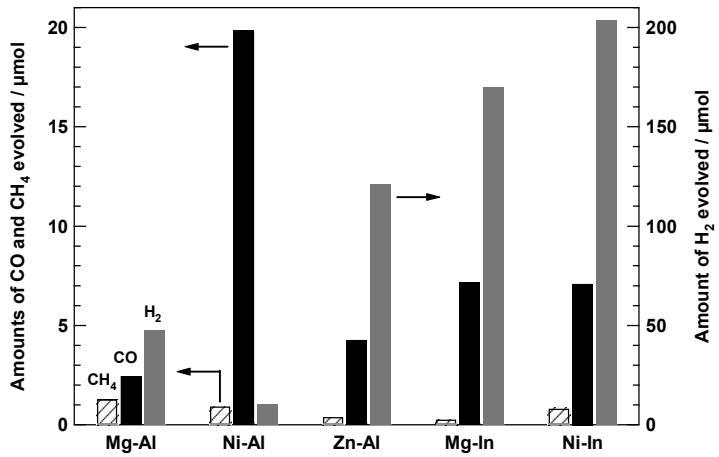

Figure 4(b) Amounts of products evolved in the photocatalytic conversion of CO_2 in water using various M^{2+}–M^{3+} LDHs(Cl^-). Photoirradiation time: 8 h. Reactor: outer irradiation type. Black: CO, gray: H_2, and slash: CH_4.

steps weight loss with increasing temperature in the TG curve [23]. The first step at less than 473 K is due to desorption of water molecules kept on the surface and in the interlayer. The second step between 473－673 K is caused by collapse of the layer structure accompanied with the dehydration of hydroxyl groups and the decomposition of charge compensating interlayer anions.

Figure 4(a) shows the amounts of products evolved for the photocatalytic conversion of CO_2 in H_2O over various M^{2+}–M^{3+} LDHs(NO_3^-) after 10 h of photoirradiation conducted by using the outer irradiation type reactor. All M^{2+}–M^{3+} LDHs(NO_3^-), including Zn-In precipitate, showed activity for the photocatalytic conversion of CO_2 in water under UV light irradiation. In these cases,

the CO_2 conversion afforded only CO formation as a reduction product of CO_2. Interestingly, H_2 was not formed, indicating the non-occurrence of overall water splitting. When a photocatalyst that shows suitable activity for overall water splitting is used for the photocatalytic conversion of CO_2 in water, H_2 would be formed as main reduction product. However, the photocatalytic conversion of CO_2 over the prepared LDHs did not proceed stoichiometrically, as shown in **Figure 4(a)**. We estimated that the residual inorganic anions derived from precursors of LDHs caused the excess amount of O_2 evolution (the details would be discussed later part). On the other hand, we achieved the improvement in the amount of CO evolved in the photocatalytic conversion of CO_2 in water by using the inner irradiation type reactor and the use of LDHs(Cl^-) instead of LDHs(NO_3^-), as displayed in **Figure 4(b)**. All kinds of M^{2+}–M^{3+} LDHs(Cl^-) were simultaneously active for the photocatalytic conversion of CO_2 and the photocatalytic H_2 evolution from water, and CO was evolved as a main reduction product of CO_2. No product was evolved without the photoitrradiation and in the absence of LDHs, respectively. The selectivity toward CO evolution obviously depended on the metal components of hydroxide sheets of LDHs. Ni_3–Al_1 LDH(Cl^-) showed the highest selectivity to CO among various LDHs(Cl^-). Mg_3–In_1 LDH(Cl^-) and Ni_3–In_1 LDH(Cl^-), which contained indium as trivalent cation in the hydroxide sheet, exhibited the high efficiency for the H_2 production, but the amount of CO evolved was small. In the case of Ni_3–Al_1 LDH(Cl^-), the amount of H_2 evolved was much lower than those of others LDHs. It is important to suppress the formation of H_2 in order to obtain more high selectivity to the conversion of CO_2 because the photocatalytic reduction of H^+ derived from H_2O into H_2 competitively takes place in the photocatalytic conversion of CO_2 in H_2O.

Table 1 Amounts of products evolved in the photocatalytic conversion of CO_2 in water using Ni–Al LDHs(Cl^-) with different Ni/Al ratio, and $Ni(OH)_2$. Photoirradiation time: 10 h. Reactor: inner irradiation type. Additive: 0.1 M NaCl.

Ni/Al ratio	Ni content (%)	Amounts of products evolved / μmol			Selectivity $(CO+CH_4) / (CO+CH_4+H_2)$
		CO	CH_4	H_2	
2	67	20.6	4.4	18.8	0.57
3	75	21.0	1.2	12.3	0.64
4	80	36.6	0.7	12.2	0.75
5	83	29.5	0.7	0.0	1.00
$Ni(OH)_2$	100	13.0	3.1	22.0	0.42

We expect that Ni species in Ni_3−Al_1 LDH(Cl^-) which might function like a cocatalyst cause the selective formation of CO. After 8 h of photoirradiation, the amounts of CO, CH_4, and H_2 evolved were 21.0, 1.2, and 12.3 μmol for Ni_3−Al_1 LDH(Cl^-), respectively, and the selectivity toward CO evolution (%) = 100 × (CO / (CO + CH_4 + H_2)) was 67%. **Table 1** shows the amounts of CO, H_2, and CH_4 evolved in the photocatalytic conversion of CO_2 in water over Ni−Al LDH(Cl^-) with different Ni/Al ratio. The largest amount of CO was evolved at Ni/Al = 4 after 10 h of photoirradiation, and the photocatalytic H_2 production proceeded well over Ni−Al LDH(Cl^-) with smaller Ni/Al ratio (Al rich). It is known that the ratio of metal components affects the surface property of LDHs, for example, Ebitani et al. insisted that the surface basic property of Mg−Al LDH depends on the Mg/Al ratio, and Mg−Al LDH (Mg/Al = 3) showed the highest activity for the aldol condensation [17]. In our case, the photocatalytic activity was also affected by the Ni/Al ratio of Ni−Al LDH(Cl^-), and Ni/Al = 4 was the most effective ratio for the evolution of CO as mentioned above. The amounts of CO evolved over $Ni(OH)_2$ and $Al(OH)_3$, which does not have typical structure of LDHs, were less than that over Ni−Al LDH(Cl^-) (Ni/Al = 2, 3, 4, and 5), indicating that mixed hydroxide containing Ni^{2+} and Al^{3+} gives surface properties suitable for the photocatalytic conversion of CO_2 in water.

Table 2 shows the difference of the activity between Ni_4−Al_1 LDH(Cl^-) and Ni_4−Al_1 LDH(NO_3^-) for the photocatalytic conversion of CO_2 in an aqueous solution. Larger amounts of CO and H_2 were evolved over Ni−Al LDH(Cl^-) than those over Ni−Al LDH(NO_3^-). On the other hand, Ni−Al LDH(NO_3^-) showed the high efficiency for the formation of CH_4 and O_2. To investigate the origin of CO evolved in the reaction, the isotopic experiment using ^{13}C-labeled CO_2 as a substrate was conducted over Ni_4−Al_1 LDH(Cl^-). The GC-MS chromatogram for this isotope experiment is

Table 2 The difference of the photocatalytic activity for the conversion of CO_2 in an aqueous solution between Ni_3−Al_1 LDH(Cl^-) and Ni_3−Al_1 LDH(NO_3^-). Photoirradiation time: 10 h. Reactor: inner irradiation type.

Photocatalyst	Amounts of products evolved / μmol			
	H_2	O_2	CH_4	CO
Ni_4−Al_1 LDH (NO_3^-)	trace	25.5	5.7	8.1
Ni_4−Al_1 LDH (Cl^-)	12.3	trace	1.2	21.0

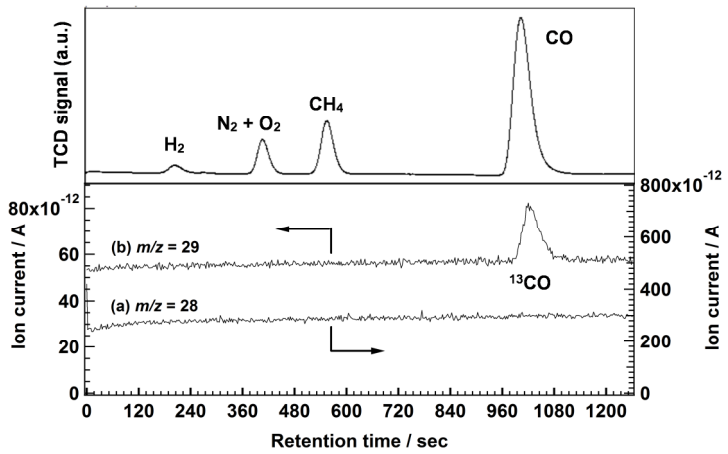

Figure 5 GC-MS chromatogram for the isotopic experiment; photocatalytic conversion of $^{13}CO_2$ in an aqueous solution over Ni_4–Al_1 LDH(Cl^-). Reactor: inner irradiation type. Photoirradiation time: 26 h. Additive: 0.1 M NaCl.

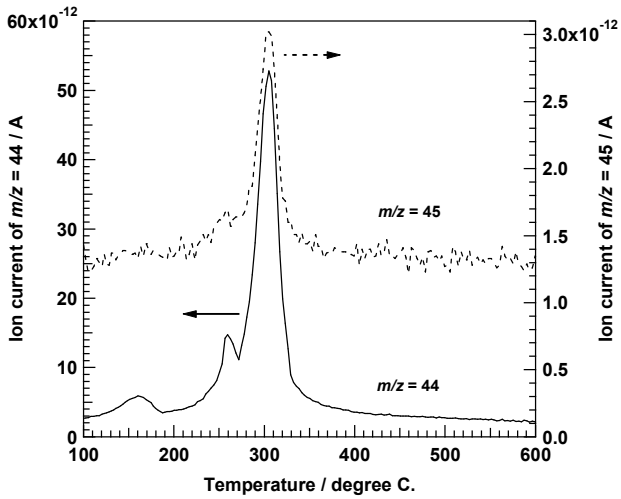

Figure 6 Temperature programed desorption profiles of Ni-Al LDH(Cl^-) which was used for the isotopic experiment using $^{13}CO_2$ as substrate. Solid line: m/z = 44 ($^{12}CO_2$), dot line: m/z = 45 ($^{13}CO_2$)

shown in **Figure 5**. The peak at 1000 second in GC chromatogram is assigned to CO in this case. There was a clear peak in the profile of m/z = 29 at the same retention time with GC chromatogram, and no peak was observed in the profile of m/z = 28. Therefore, only ^{13}CO (m/z = 29) was evolved in the photocatalytic conversion of $^{13}CO_2$ over Ni_4–Al_1 LDH(Cl^-). This result clearly indicated that the carbon sources of CO evolved were introduced CO_2; therefore, carbon species such as carbonate ions kept in the interlayer of LDH and contaminated organics did not decompose into CO. **Figure 6** shows the temperature programed desorption profile of Ni_4–Al_1 LDH(Cl^-) which was used for the

isotope experiment using $^{13}CO_2$ as described above. $^{12}CO_2$ (m/z = 44) and $^{13}CO_2$ (m/z = 45) were desorbed from the used photocatalyst at around 573 K, indicating that adsorbed $^{13}CO_2$ species such as carbonate or hydrocarbonate species existed on the surface and the interlayer of LDH. This result showed that parts of the introduced CO_2 molecules were adsorbed on Ni_4–Al_1 LDH(Cl^-) during the photocatalytic conversion of CO_2 in an aqueous solution. Accordingly, we concluded that the adsorbed CO_2 species on the surface of LDH, which are derived from the introduced gaseous CO_2 in the gas phase, are reduced into CO under UV light photoirradiation.

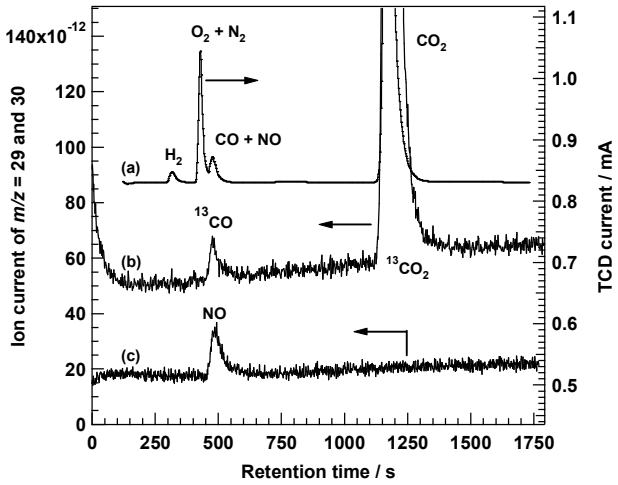

Figure 7 GC-MS chromatogram in the photocatalytic conversion of $^{13}CO_2$ in H_2O over Mg_3–In_1 LDH(NO_3^-) after 26 h of photoirradiation. (a) TCD-GC chromatogram, (b) m/z = 29 profile, (c) m/z = 30 profile. Reactor: outer irradiation type.

The elemental analysis revealed that 1.2 wt% of chlorine atoms and 0.6 wt% of nitrogen atoms derived from precursors of hydroxide sheets existed on Ni_4–Al_1 LDH(Cl^-) and Ni_4–Al_1 LDH(NO_3^-), respectively. As shown in **Figure 4(a)**, Mg_3–In_1 LDH(NO_3^-) showed high activity for the CO and O_2 evolution in the photocatalytic conversion of CO_2 in water, 1.6 μmol of CO as a reduction product of CO_2 and 6.4 μmol of O_2 were evolved after 10 h of photoirradiation. **Figure 7** shows (a) TCD-GC chromatogram, Q-Mass profiles of (b) m/z = 29 and (c) m/z = 30, in the photocatalytic conversion of $^{13}CO_2$ in water over Mg_3–In_1 LDH(NO_3^-). In the profile of m/z = 29, the peak at 480 second was assigned to ^{13}CO, and the large peak attributed to a fragment ion of $^{13}CO_2$ appeared at around 1200 second. Whereas, there was a peak in the m/z = 30 profile at the same retention time as that of CO, which can be ascribed to NO based on the reference experiments. This

result indicates that residual nitrate ions existed on Mg_3–In_1 LDH(NO_3^-) were decomposed into NO and O_2 under UV light photoirradiation. Accordingly, the unpreventable photodecomposition of the residual nitrate ions into NO and O_2 proceeded together with the photocatalytic conversion of CO_2 into CO over LDHs fabricated using nitrates. The photodecomposition of nitrate ions during the photocatalytic reaction caused the evolution of excess amount (nonstoichiometric amount) of O_2, resulting in the formation of larger amount of O_2 over Ni_4–Al_1 LDH(NO_3^-) than that over Ni_4–Al_1 LDH(Cl^-) as shown in **Table 2**.

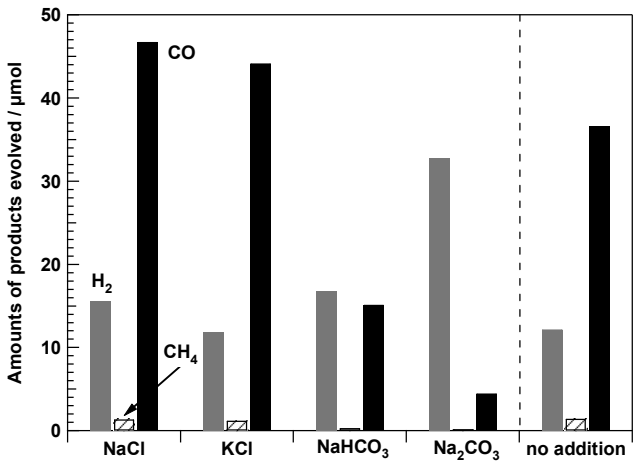

Figure 8 Amounts of products evolved in the photocatalytic conversion of CO_2 in an aqueous solution containing various inorganic salts using Ni_4–Al_1 LDH(Cl^-). Photoirradiation time: 10 h. Reactor: inner irradiation type. Black: CO, gray: H_2, and slash: CH_4.

It is generally known that carbonate ions are preserved in the interlayer of LDHs as charge compensating anions. Our fabricating LDHs in this study also keep large amount of carbonate ions with small amount of residual chloride ions derived from the precursor of hydroxide sheets. **Figure 8** shows the effect of anion addition to the reaction solution on the photocatalytic conversion of CO_2 in an aqueous solution over Ni_4–Al_1 LDH(Cl^-). The amount of H_2 evolved as a reduction product of H^+ derived from H_2O was increased by the addition of $NaHCO_3$ or Na_2CO_3, although the formation of CO was drastically suppressed. Sayama and Arakawa reported that the addition of carbonate ions or hydrocarbonate ions to an aqueous solution enhance the evolution of H_2 for water splitting [26]. In our case, on the other hand, the amount of CO evolved was increased in the presence of NaCl and KCl in an aqueous solution as compared to that in a pure water. The formation of O_2 was not observed in all

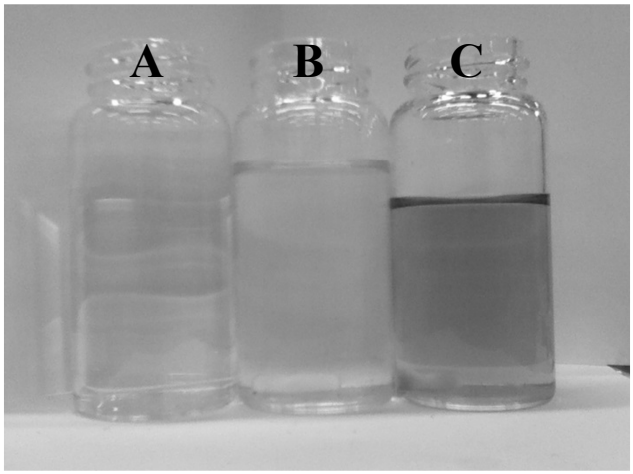

Figure 9 Results of starch-iodine reaction for (A) pure water, (B) solution before the reaction, and (C) solution after the reaction. Photocatalyst: Ni_4−Al_1 LDH(Cl^-). Photoirradiation time: 8 h. Reactor: inner irradiation type. Additive: 0.1 M NaCl.

cases. This results indicated that chloride ions in the reaction solution promoted the photocatalytic conversion of CO_2 into CO over Ni_4−Al_1 LDH(Cl^-). We expect that chloride ion in an aqueous solution act as a hole scavenger in the photocatalytic reaction. Chloride ions should be oxidized by holes generated with the photoexicitation of electrons through two processes. One is that chloride ion is oxidized into chlorine (Eq.1), and chlorine (Cl_2) is disproportionately decomposed into chloride ion (Cl^-) and hypochlorite ion (ClO^-) (Eq. 2).

(Eq.1) $2Cl^- + 2h^+ \rightarrow Cl_2$

(Eq.2) $Cl_2 + H_2O \rightarrow 2H^+ + Cl^- + ClO^-$

The other is that chloride ion is oxidized into hypochlorite ion directly (Eq. 3).

(Eq.3) $Cl^- + 2h^+ + 2OH^- \rightarrow ClO^- + H_2O$

Standard redox potential of (Cl_2/Cl^-) and (ClO^-/Cl^-) are known as + 1.40 V and + 0.89 V (vs. NHE at pH = 0), respectively [27]. In both cases, hypochlorite ion which can act as a strong oxidizing reagent in an aqueous solution would be formed finally. In addition, chlorate ion (ClO_3^-) and perchlrate ion (ClO_4^-) might be generated through the disproportionation of hypochlorite ions in an aqueous solution. It is possible that the oxidation products of chloride ions such as ClO^-, ClO_3^-, or ClO_4^- are produced instead of O_2 as an oxidation product of H_2O. The solution after the reaction was positive for the starch-iodine reaction, while the solution before the reaction (an 0.1 M aqueous solution of NaCl) and pure water were negative as shown in **Figure 9**. This result indicated that ClO^-,

ClO_3^-, and ClO_4^- whose redox potential are positive enough to oxidize iodide ion into iodine were formed in the aqueous solution during the photocataytic conversion of CO_2. We concluded that chloride ion in an aqueous solution act as a hole scavenger under UV light photoirradiation and is oxidized into ClO^-, ClO_3^-, and ClO_4^- in our system using Ni−Al LDH(Cl^-) as a photocatalyst, while the photodecomposition of the residual nitrate ion in Ni−Al LDH(NO_3^-) resulted in the evolution of O_2 and NO in the gas phase.

Conclusion

LDHs in which the surface base sites have high water tolerance show superior activity than does a simple metal hydroxide for the photocatalytic conversion of CO_2 into CO in water (this process is similar to photosynthesis). We found that Ni_4−Al_1 LDH(Cl^-) exhibited the highest efficiency for the photocatalytic conversion of CO_2 into CO in an aqueous solution among various kinds of LDHs. LDHs which contain In^{3+} as a trivalent cation in the hydroxide sheet, exhibited the high efficiency for the H_2 production, while the amount of CO evolved was totally small. CO_2 introduced in the gas phase was adsorbed on the surface of LDHs, and then reduced into CO under photoirradiation because only ^{13}CO was formed in the isotope experiment using $^{13}CO_2$ as a substrate. The residual nitrate ions (NO_3^-) in LDHs derived from precursors of metal components influenced the photocatalytic activity for the conversion of CO_2, and NO and O_2 were evolved via photodecomposition under the illumination. The addition of chloride ions to the reaction solution enhanced the selectivity to CO. Chloride ions (Cl^-) in an aqueous solution act as a hole scavenger under UV light photoirradiation and it might be oxidized into ClO^-, ClO_3^-, or ClO_4^-.

References

1. T. Miyasaka, T. Watanabe, A. Fujishima, K. Honda, *Nature*, 1979, **277**, 638-638.
2. S. Navalon, A. Dhakshinamoorthy, M. Alvaro, and H. Garcia, *ChemSusChem.*, 2013, **6**, 562-577.
3. B.-J. Liu, T. Torimoto, H. Yoneyama, *Journal of Photochemistry and Photobiology A:*

Chemistry, 1998, **113**, 93-97.

4. P.-W. Pan, Y.-W. Chen, *Catalysis Communications*, 2007, **8**, 1546-1549.
5. S. C. Yan, S. X. Ouyang, J. Gao, M. Yang, J. Y. Feng, X. X. Fan, L. J. Wan, Z. S. Li, J. H. Ye, Y. Zhou, Z. Zou, *Angewandte Chemie International Edition*, 2010, **49**, 6400-6404.
6. J. Pan, X. Wu, L. Wang, G. Liu, G. Q. Lu, H.-M. Cheng, *Chemical Communications*, 2011, **47**, 8361-8363.
7. L. Wan, X. Wang, S. Yan, H. Yu, Z. Li, Z. Zou, *CrystEngComm.*, 2012, **14**, 154-159.
8. K. Iizuka, T. Wato, Y. Miseki, K. Saito, A. Kudo, *Journal of the American Chemical Society*, 2011, **133**, 20863-20868.
9. Y. Kohno, T. Tanaka, T. Funabiki and S. Yoshida, *Chemistry Letters*, 1997, **26**, 993-994.
10. Y. Kohno, T. Tanaka, T. Funabiki and S. Yoshida, *Journal of the Chemical Society, Faraday Transactions*, 1998, **94**, 1875-1880.
11. Y. Kohno, T. Tanaka, T. Funabiki and S. Yoshida, *Physical Chemistry Chemical Physics*, 2000, **2**, 5302-5307.
12. Y. Kohno, T. Tanaka, T. Funabiki and S. Yoshida, *Physical Chemistry Chemical Physics*, 2000, **2**, 2635-2639.
13. Y. Kohno, H. Ishikawa, T. Tanaka, T. Funabiki and S. Yoshida, *Physical Chemistry Chemical Physics*, 2001, **3**, 1108-1113.
14. K. Teramura, T. Tanaka, H. Ishikawa, Y. Kohno and T. Funabiki, *The Journal of Physical Chemistry B*, 2004, **108**, 346-354.
15. K. Teramura, S. Okuoka, H. Tsuneoka, T. Shishido, T. Tanaka, *Applied Catalysis B: Environmental*, 2010, **96**, 565-568.
16. H. Tsuneoka, K. Teramura, T. Shishido, T. Tanaka, *The Journal of Physical Chemistry C*, 2010, **114**, 8892-8898.
17. K. Ebitani, K. Motokura, K. Mori, T. Mizugaki and K. Kaneda, *The Journal of Organic Chemistry*, 2006, **71**, 5440-5447.
18. a) E. M. Seftel, E. Popovici, M. Mertens, E. A. Stefaniak, R. Van Grieken, P. Cool, E. F. Vansant, *Applied Catalysis B: Environmental*, 2008, **84**, 699-705; b) J. S. Valente, F. Tzompantzi, J. Prince, J. G. H. Cortez, R. Gomez, *Applied Catalysis B: Environmental*,

2009, **90**, 330-342; c) M. Shao, J. Han, M. Wei, D. G. Evans, X. Duan, *Chemical Engineering Journal*, 2011, **168**, 519-524.

19. C. Gomes Silva, Y. Bouizi, V. Fornes, H. Garcia, *Journal of the American Chemical Society*, 2009, **131**, 13833-13839.
20. J. L. Gunjakar, T.W. Kim, H.N. Kim, I.Y. Kim, S.J. Hwang, *Journal of the American Chemical Society*, 2011, **133**, 14998-15007.
21. N. Ahmed, Y. Shibata, T. Taniguchi, Y. Izumi, *Journal of Catalysis*, 2011, **279**, 123-135.
22. C.C. Yang, Y.H. Yu, B. van der Linden, J. C. S. Wu, G. Mul, *Journal of the American Chemical Society*, 2010, **132**, 8398-8406.
23. F. Cavani, F. Trifiro, A.Vaccari, *Catalysis Today*, 1991, **11**, 173-302.
24. R. D. Shannon, *Acta Crystallographica*, 1976, **A32**, 751-767.
25. L. Moberg, B. Karlberg, *Analytica Chimica Acta*, **2007**, 127-133.
26. K. Sayama and H. Arakawa, *The Journal of Physical Chemistry*, 1993, **97**, 531-533.
27. Steven G. Bratsch, *Journal of Physical and Chemical Reference Data*, 1989, **18**, 1.

Chapter 2

Effect of the Chloride Ion as a Hole Scavenger on the Photocatalytic Conversion of CO_2 in an Aqueous Solution over Ni−Al Layered Double Hydroxides

Abstract

The photocatalytic conversion of CO_2 into useful chemical compounds in water without using organic sacrificial reagents is a promising method to overcome environmental and energy problems. Various synthesized layered double hydroxides (LDHs) are capable of reducing CO_2 to CO in an aqueous solution under UV light irradiation. However, it is difficult to oxidize H_2O to O_2 in a photocatalytic system using LDHs as photocatalysts. In this study, we investigated the photocatalytic conversion of CO_2 using a Ni−Al LDH in an aqueous solution of NaCl. Hypochlorous acid (HClO) was produced as an oxidation product of Cl^- with the formation of reduction products such as CO and H_2 under photoirradiation. We propose the inclusion of Cl^- in the reaction solution to be one of the most promising ways for obtaining a hole scavenger, an approach that would enable the construction of an artificial photosynthesis system for the conversion of CO_2.

Introduction

The use of photocatalytic reactions to convert CO_2 into valuable chemicals such as CO, HCHO, HCOOH, CH_3OH, and CH_4 is one of the most promising methods to develop a sustainable carbon cycling system. We previously reported the photocatalytic activity of ZrO_2 [1-4], MgO [5, 6], and Ga_2O_3 [7], which have basic sites on their surface, for the conversion of CO_2 in the presence of H_2 as a reductant. This requires the conversion of CO_2 molecules, which are adsorbed on the surface of these photocatalysts, into active species to enable their facile reduction by the photogenerated electrons. Therefore, solid state basic materials are suitable candidates to construct photocatalytic systems required for the conversion of CO_2.

Layered double hydroxides (LDHs, $[M^{2+}_{1-x}M^{3+}_{x}(OH)_2]^{x+}[A_{x/n}]^{n-}\cdot mH_2O$) are known as natural and/or synthetic clays that contain highly ordered two-dimensional hydroxide sheets [8]. Their structures are based on edge-sharing octahedral units centred around a metal ion, which is coordinated to OH groups ($M^{2+}(OH)_6$), in which the divalent metal cations are partially substituted by trivalent metal cations. The LDH interlayer is known to be capable of retaining various kinds of anions to compensate for the positive charge of the hydroxide sheets. LDHs are widely used as basic materials for CO_2 capture and storage [9], removal of organic and inorganic anions from water [10-12], and base-catalysed reactions [13]. We reported a series of synthetic M^{2+}–M^{3+} LDHs (M^{2+} = Mg, Ni, and Zn; M^{3+} = Al, Ga, and In) that show activity toward the photocatalytic conversion of CO_2 in water [14]. In particular, the use of Ni−Al layered double hydroxide (Ni−Al LDH) as a photocatalyst enabled us to achieve the maximum conversion of CO_2 to CO with high selectivity, because it produces lesser H_2 as a reduction product of H^+ derived from water than other LDHs [15]. On the other hand, other LDHs such as Mg−In LDH and Ni−In LDH, both of which contain In^{3+} as a trivalent cation, increase the H_2 production, a less preferable result. This led us to conclude that Ni−Al LDHs offer suitable surface properties for the selective photocatalytic conversion of CO_2 in water. During previous research efforts, we used isotopic experiments to demonstrate that the CO_2 gas that was introduced as a substrate was indeed the origin of the CO evolved. Lately, LDHs have attracted considerable attention as photocatalysts for CO_2 conversion [16-20], water splitting using sacrificial reagents [21-23], and decomposition of organic compounds [24-26] due to their environmentally friendly properties,

characteristic layer structures, large specific surface areas, and remarkable adsorption capacities [27]. Izumi et al. [16-18], Katsumata et al. [19], and Xu et al. [20] have reported the photocatalytic conversion of CO_2 using synthetic LDHs.

Of late, many approaches to the overall photocatalytic water splitting reaction using reversible redox mediators such as I_3^-/I^- [28, 29], IO_3^-/I^- [30, 31], Fe^{3+}/Fe^{2+} [32-34], and Co^{3+}/Co^{2+} [35] have been explored. Matsumura et al. reported the reduction of H_2O to H_2 by using Br^-, which was oxidized to Br_2, and the oxidation of H_2O to O_2 using Fe^{3+}, which was reduced to Fe^{2+} using a photoelectrochemical cell with two separate compartments. In their system, Br_2 (or Br_3^-) was produced as an oxidation product of Br^- with the evolution of H_2 [36]. It is known that halide anions in photocatalytic systems can scavenge holes formed by the photoexcitation of electrons from the valence band to the conduction band of the photocatalysts. In this regard, both Krivec et al. [37] and Pelizzetti et al. [38] focused on the inhibition effects of Cl^- during the photocatalytic degradation of organic compounds. Both these groups insisted that the Cl^- that exists in the photocatalytic system can react with the photogenerated holes and consequently reduce the number of active oxidizing species capable of decomposing organic molecules. However, the oxidation product of Cl^- was not observed in either of these studies. In recent days, Li and co-workers reported that a small amount of Cl^- in the reaction solution affected the photocatalytic activity for an overall water splitting to H_2 and O_2, through the photocatalytic oxidation of Cl^- by the photogenerated holes [39]. In this study, we attempted to detect the stoichiometric formation of the oxidation products of Cl^- in the photocatalytic conversion of CO_2 using Ni−Al LDH in an aqueous solution of Cl^-, which was added as a hole scavenger.

Experimental

Ni−Al LDHs with various Ni/Al ratios (Ni/Al = 2, 3, 4, and 5) were fabricated by using the typical coprecipitation method provided hereafter. A mixed aqueous solution of $NiCl_2 \cdot 6H_2O$ (Wako Pure Chemical Industries, Ltd., 99.9%) and $AlCl_3$ (Wako Pure Chemical Industries, Ltd., 98.0%) was slowly dropped into an aqueous solution of Na_2CO_3 (Wako Pure Chemical Industries, Ltd., 99.5%) at room temperature. The pH value was maintained between 9.9 and 10.1 by adding an aqueous

solution of NaOH (Wako Pure Chemical Industries, Ltd., 97.0%) during the precipitation using a liquid feeding pump (NRP−76, NISSHIN RIKA, Japan) connected to a pH controller (NPH−660NDE, NISSHIN RIKA, Japan). The resulting suspension was transferred to a stainless steel autoclave equipped with an inner Teflon vessel, and aged under hydrothermal conditions at 383 K for periods ranging from 0 to 120 h. The solid precipitate was collected by filtration, washed with 1.0 L of ultra-pure water, and then dried at 383 K in air.

The powder XRD patterns of the Ni−Al LDHs were measured by using an X-ray diffractometer (Ultime IV, Rigaku), using Cu K_α radiation (λ = 0.154 nm) at a scan speed of 4.0° min^{-1}. The Brunauer-Emmett-Teller (BET) specific surface areas of the Ni−Al LDHs were estimated from their N_2 adsorption isotherms at 77 K using an adsorption analyser (BELSORP-miniII, BEL Japan, Inc.), prior to which each sample was evacuated at 383 K for 1 h using a pretreatment system (BELPREP-vacII, BEL Japan, Inc.). SEM images of Ni−Al LDHs were captured by using a Field Emission Scanning Electron Microscope (FE-SEM, SU-8220, Hitachi High-Technologies) at the acceleration voltage of 3.0 kV. X-ray photoelectron spectroscopy (XPS) measurement of as-prepared Ni−Al LDH was performed by using an X-ray photoelectron spectrometer (ESCA 3400, Shimadzu Corp.). The Ni 2p spectra of Ni−Al LDH and reference samples were collected using Mg K_α X-ray source, and calibrated by the peak that can be assigned to C 1s absorption. Ni K-edge XAFS spectrum of Ni−Al LDH was measured at the BL01B1 of SPring-8 with the approval of the Japan Synchrotron Radiation Research Institute (JASRI) (Proposal No. 2013A1615). The spectrum was recorded in a transmittance mode at room temperature, using Si(111) double crystal monochromator. The photon energy was calibrated by using Ni foil.

The photocatalytic conversion of CO_2 was carried out in an aqueous solution by using a quartz inner-irradiation type reaction vessel in a quasi-flowing batch system. The photocatalyst powder was dispersed in 1.0 L of an aqueous solution, which was subsequently degassed using a stream of He gas. Following this, high purity CO_2 gas (99.999%) was bubbled into the aqueous solution containing the photocatalyst at a flow rate of 15 mL min^{-1}. The suspension was irradiated under a 400 W high-pressure mercury lamp via a quartz filter equipped with a cooling water system. The resulting products, namely CO, H_2, and O_2, were analysed by using a barrier discharge ionization detector gas chromatography (BID-GC) system using a gas chromatograph (GC-2010

Tracera, Shimadzu Corp.) equipped with a MICROPACKED ST column using He gas as a carrier. The selectivity toward CO evolution among the reduction products was given by Formula (1).

Formula (1) Selectivity toward CO (%) = 100 × (CO / μmol) / ((CO / μmol) + (H_2 / μmol))

The formation of hypochlorous acid (HClO) in aqueous solutions during the photocatalytic reactions can be confirmed by using a DPD method [40, 41], which is one of the most popular techniques to observe HClO in water, based on the oxidation potential of HClO. The most commonly used is a colorimetric method, based on addition of the *N,N'*-diethyl-*p*-phenylenediamine (DPD) reagent. If HClO is present in the sample solution, a red oxidized form of DPD yields rapidly through the stoichiometric reaction. The DPD solution was prepared by dissolving 0.06 g of the DPD reagent (Wako pure chemical, Japan), which is a mixture of DPD sulphate and Na_2SO_4, in 3.0 mL of phosphate buffer solution (pH = 6.5). Following this, 1.0 mL of the prepared DPD solution was added to 5.0 mL of the sample solution, and was shaken for 20 s. The transmittance spectrum was measured immediately using a multiscan UV–vis spectrometer (MCPD-7700, Ohtsuka, Japan). The concentration of HClO in the aqueous solution was estimated from the absorbance at 515 nm.

Results and discussion

Figure 1(a−f) shows the XRD patterns of Ni−Al LDHs (Ni/Al = 4) aged under hydrothermal conditions at 383 K for various treating times (0−120 h). All the patterns corresponded to the typical structure of LDHs. The sharp diffraction peaks at 11.1° and 22.5°, which are marked with asterisks (*), can be assigned to the (0 0 3) and (0 0 6) planes reflections, respectively. The positions of these diffraction peaks depend on the size of the interlayer anions, i.e., the intercalation of large anions is responsible for the peak shift of these reflections. The XRD patterns revealed that the interlayer distance of Ni−Al LDH remained unchanged owing to aging under hydrothermal conditions, indicating that the anions that were present before the hydrothermal aging procedure are retained in the interlayer between the hydroxide sheets [8]. In addition, the two diffraction peaks at around 60°, which are marked with daggers (†), can be attributed to the (1 1 0) and (1 1 3) planes, respectively. No change was observed in the position of these reflection peaks. Moreover, the broadened peaks between 30−40° might be caused by the (0 0 9) plane reflection overlapped with the

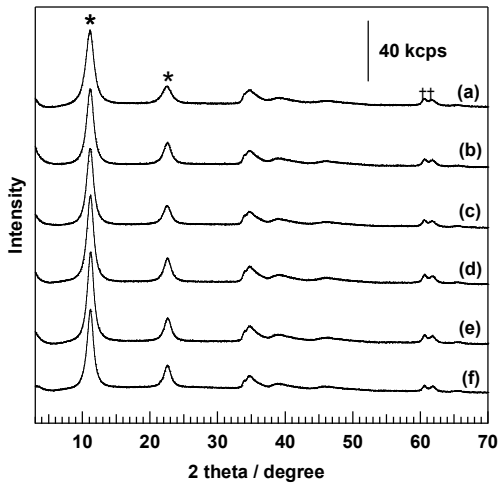

Figure 1 XRD patterns of synthesized Ni−Al LDHs (Ni/Al = 4) via aging under hydrothermal condition at 383 K for **(a)** 0 h, **(b)** 5 h, **(c)** 10 h, **(d)** 20 h, **(e)** 60 h, and **(f)** 120 h.

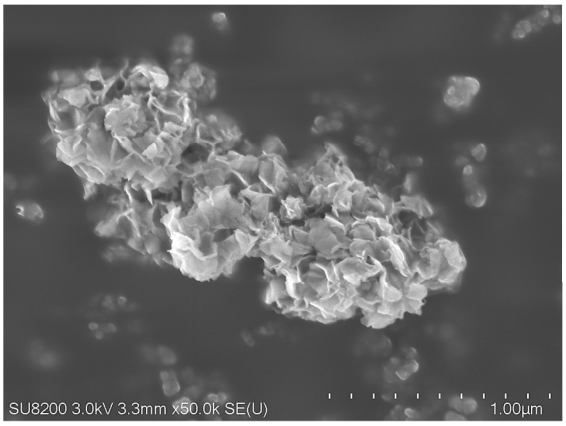

Figure 2 SEM image of synthesized Ni−Al LDH (Ni/Al = 4) via aging under hydrothermal condition at 383 K for 20 h.

(0 1 2) and (0 1 5) phases. The morphology of the as-synthesized Ni−Al LDH (Ni/Al = 4) was examined with scanning electron microscopy (SEM) as shown in **Figure 2**. It can be seen that many platelets are stacked according to the so-called the card-house type sheet aggregation. **Table 1** lists the full width at half maximum of the (0 0 3) phase reflection (hereafter referred to as $FWHM_{(0\,0\,3)}$) and the specific surface area estimated from the N_2 adsorption isotherm using the BET method at liquid N_2 temperature (77 K). The $FWHM_{(0\,0\,3)}$ was found to decrease gradually as the hydrothermal aging time was increased, indicating that stacking of the layer structure advanced in the direction of the *c*-axis owing to the hydrothermal treatment. Moreover, the specific surface area of Ni−Al LDH was also found to depend on the aging time, and a maximum specific surface area was achieved after a hydrothermal aging treatment of 20 h. As reported by Jasra and coworkers, it is generally known that the crystallinity of hydrotalcite-like compounds is advanced by the hydrothermal treatment in accordance with the decrease in the specific surface area [42]. The reason why the specific surface area of Ni−Al LDH was improved after hydrothermal treatment within 20 h is not clear, whereas the $FWHM_{(0\,0\,3)}$ monotonously decreased with the aging time. As shown in **Figure 3**, the Ni 2p XPS spectrum of as-synthesized Ni−Al LDH was almost the same as the spectra of $Ni(OH)_2$ and $NiCO_3$, and partially different from that of NiO. With reference to the previous reports, the binding energy (BE) value of the main Ni $2p_{3/2}$ peak, at around 856.0 eV, was assigned to the Ni^{2+} ion by comparison

Table 1 Effect of the aging time under hydrothermal condition on the $FWHM_{(003)}$ and the specific area of Ni−Al LDH (Ni/Al =4). [a] Aging: hydrothermal treatment at 383 K, [b] full width at half maximum of (003) phase diffraction peak, [c] specific surface area determined by N_2 adsorption isotherm.

Aging [a] time / h	$FWHM_{(003)}$ [b] / degree	SSA [c] / $m^2\ g^{-1}$
0	1.52	62.9
5	1.32	64.5
10	1.26	67.9
20	1.23	97.2
60	1.17	94.3
90	1.08	61.1
120	1.07	47.2

with the known BE value for the Ni $2p_{3/2}$ photoelectrons of $Ni(OH)_2$ [43-45]. The Ni K-edge XANES spectrum of Ni−Al LDH which is shown in **Figure 4**, was not inconsistent with the result of the XPS measurement. The position of the absorption edge (E_0) and the intensity of the white line of Ni−Al LDH were very similar to those of $Ni(OH)_2$. It is indicated that the oxidation state and the coordination environment of Ni species in as-prepared Ni−Al LDH correspond to $Ni(OH)_2$; it is known that LDH group materials have a similar structure to the brucite ($Mg(OH)_2$) where octahedral of Mg^{2+} (six-fold coordination to OH^-) share edges to form infinite sheets [46, 47].

Figure 5(a) shows the formation rates of CO and H_2, both of which were reduction products of CO_2 dissolved in the solution and H^+ derived from H_2O, respectively, in the photocatalytic conversion of CO_2 in an aqueous solution of NaCl (0.1 M) using Ni−Al LDH (Ni/Al = 4) as a

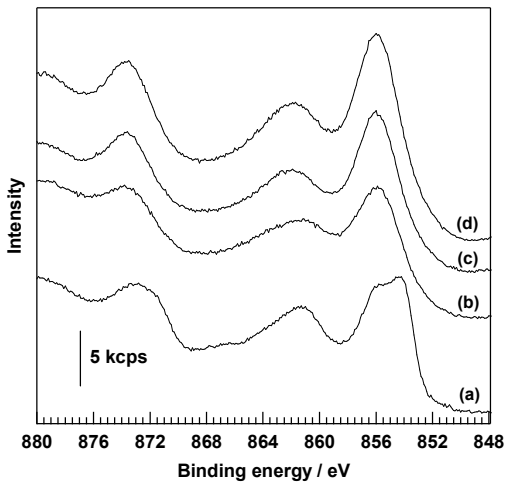

Figure 3 Ni 2p XPS profiles of (a) NiO, (b) $NiCO_3$, (c) $Ni(OH)_2$, and (d) synthesized Ni−Al LDH.

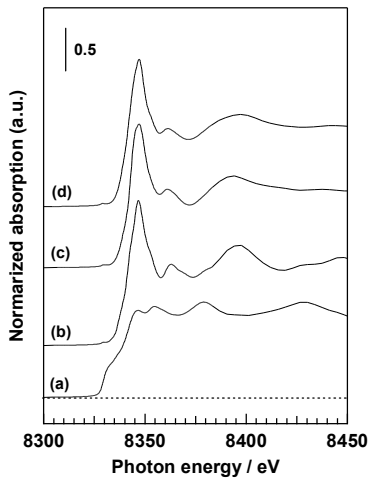

Figure 4 Ni K-edge XANES spectra of (a) Ni foil, (b) NiO, (c) $Ni(OH)_2$, and (d) as-prepared Ni−Al LDH.

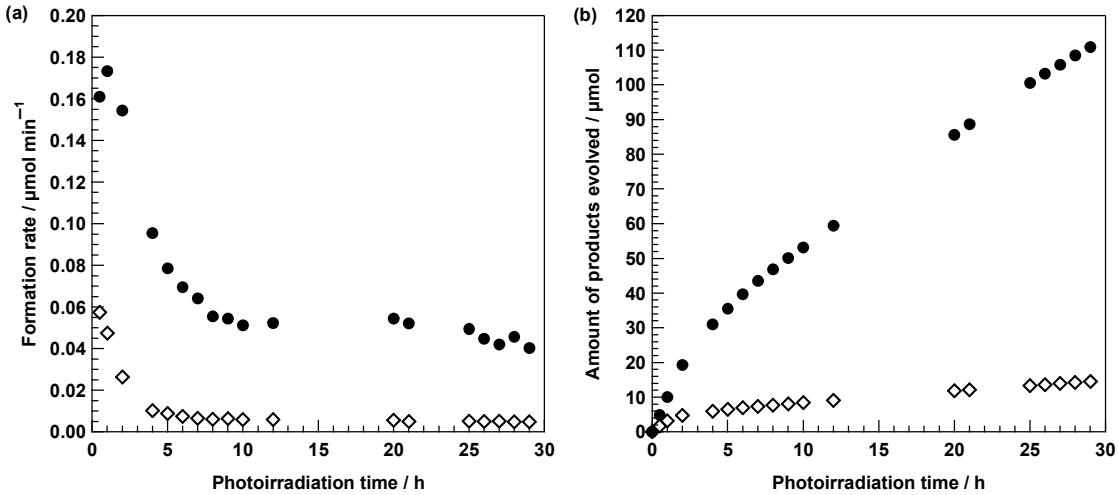

Figure 5 (a) Formation rates of CO (●) and H_2 (◊), and **(b)** total amounts of CO (●) and H_2 (◊) evolved in the photocatalytic conversion of CO_2 in an aqueous solution using Ni−Al LDH (Ni/Al = 4). Additive: 0.1 M NaCl. Photocatalyst weight: 0.3 g.

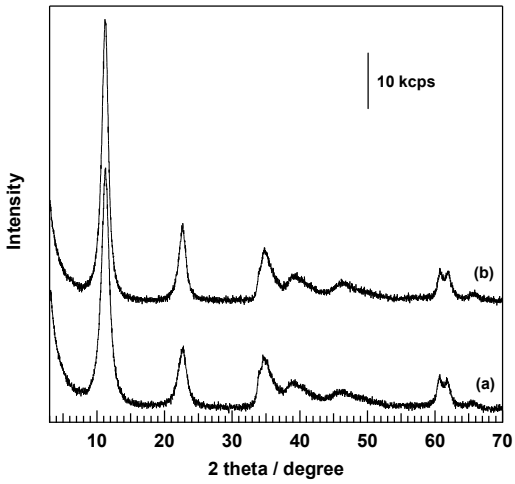

Figure 6 XRD patterns of Ni−Al LDHs (a) before and (b) after the photocatalytic reaction in an aqueous solution of NaCl.

photocatalyst. The formation rate of CO after 1 h of photoirradiation was 1.7×10^{-1} μmol min^{-1}, which was 3.4 times higher than that of H_2. No other reduction products of CO_2, such as formic acid, methane, and methanol, were obtained. Measurements confirmed that the oxidation of H_2O did not lead to the formation of any O_2 in our photocatalytic system. Meanwhile, the formation rates of CO and H_2 decreased during the first 10 h of photoirradiation, stabilizing at ca. 5.0×10^{-2} μmol min^{-1} and ca. 6.0×10^{-3} μmol min^{-1}, respectively. **Figure 5(b)** shows the total amounts of the products, which were estimated from the formation rates through integration with time. The total amount of CO evolved as a reduction product of CO_2 increased with photoirradiation time and was 110.9 μmol after

29 h of photoirradiation. The structural changes in Ni−Al LDH through the photocatalytic reaction for 29 h were not observed in the XRD patterns that are shown in **Figure 6**. The value of $FWHM_{(0\,0\,3)}$ and the positions of the reflection peaks of Ni−Al LDH after the reaction were not changed as compared to those of as-synthesized one, indicating that the structural properties of Ni−Al LDH are not altered during the photocatalytic conversion of CO_2 in an aqueous solution of NaCl. As shown in **Figure 7**, on the other hand, the total amount of CO and H_2 evolved were gradually decreased with an increasing number of repetitions. This seems to indicate that the photocatalytic activity of the Ni−Al LDH photocatalyst is not as stable in our reaction system. Therefore, the cause of the changes in Ni−Al LDH during photoirradiation and how this might cause its deactivation for the photocatalytic conversion of CO_2 have not been clarified.

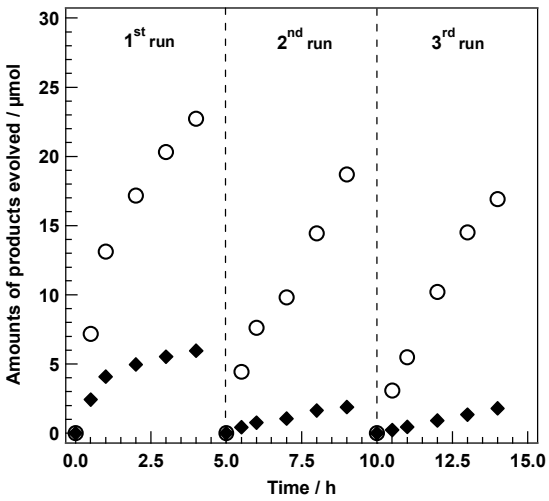

Figure 7 The result of repeat test for the photocatalytic conversion of CO_2 in an aqueous solution of NaCl using Ni−Al LDH photocatalyst. Circle: CO, diamond: H_2. Photocatalyst weight: 0.3 g.

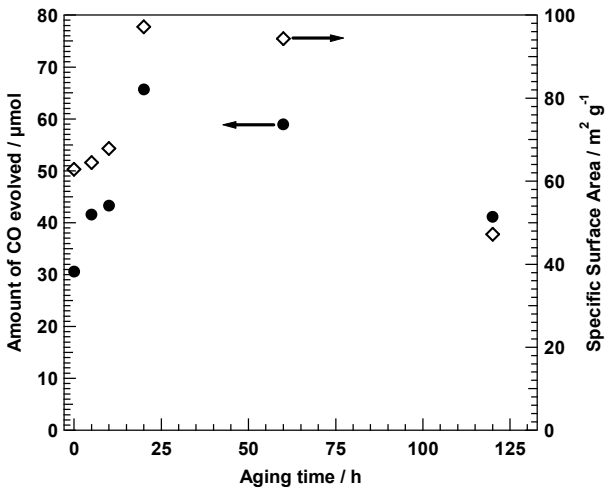

Figure 8 Effect of the aging time under hydrothermal condition on the total amount of CO evolved in the photocatalytic conversion of CO_2 (left axis) after 8 h of photoirradiation and the specific surface area (right axis). Photocatalyst weight: 1.0 g.

The effect of hydrothermal aging on the specific surface area of Ni−Al LDH (Ni/Al = 4), which is shown in **Table 1**, is represented again as a function of time in **Figure 8**. Ni−Al LDH (Ni/Al = 4), which was aged under hydrothermal conditions for a relatively short time, exhibited a larger specific surface area than when prepared without aging. The specific surface area of Ni−Al LDH (Ni/Al = 4) gradually decreased after prolonged hydrothermal aging. This result is not inconsistent with the fact that extending the aging time causes Ni−Al LDH (Ni/Al = 4) to develop a high

crystallinity in the direction of the *c*-axis, as shown in **Table 1**. On the other hand, **Figure 8** also shows that the total amount of CO evolved from the photocatalytic conversion of CO_2 using Ni−Al LDH (Ni/Al = 4) is influenced by the aging time. The effect of the hydrothermal treating time on the change in the total amount of CO yielded after 8 h of photoirradiation was in good agreement with the specific surface area after the same length of hydrothermal treatment, indicating that the amount of CO evolved strongly depended on the magnitude of the surface area. In other words, Ni−Al LDH with a large specific surface area can achieve high photocatalytic activity for the conversion of CO_2 to CO, as shown in **Figure 9**. In contrast, the selectivity toward CO, which is given by Formula (1) in the experimental section, did not depend on the specific surface area, indicating that the selectivity is controlled by the surface properties corresponding to the Ni/Al ratio as described below. It should be noted that the adsorption of a CO_2 molecule on LDH is not a negligible step in the photocatalytic conversion of CO_2 in an aqueous solution, considering the results we previously published [15] in this regard, which revealed that the introduced CO_2 molecules existed on the surface and/or in the interlayer of Ni−Al LDH, as was shown via a temperature-programmed desorption experiment using isotopic ^{13}C-labled CO_2 as a substrate.

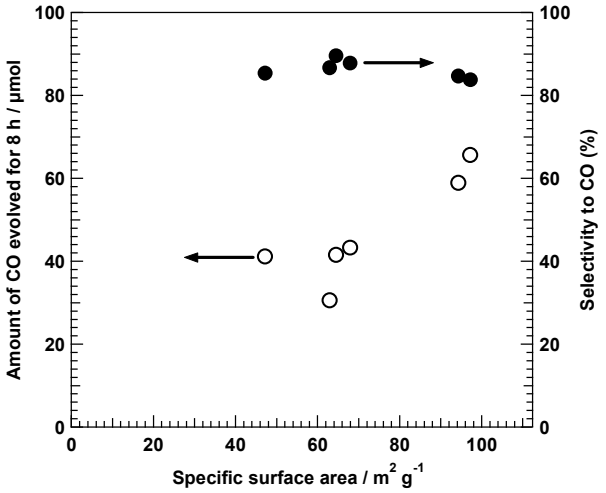

Figure 9 Amount of CO evolved (white circle) and selectivity toward CO (black circle) with the change of specific surface area of Ni−Al LDH photocatalyst in the photocatalytic conversion of CO_2 in an aqueous solution of NaCl. Photocatalyst weight: 1.0 g, photoirradiation time: 8 h.

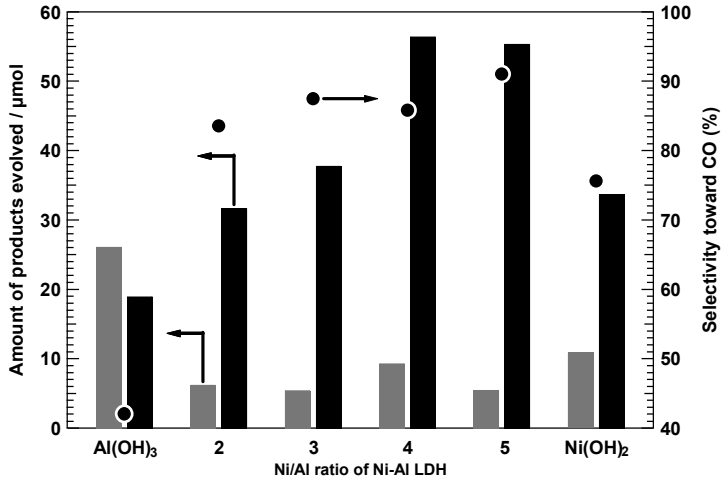

Figure 10 Total amounts of products evolved and selectivity toward CO for the photocatalytic conversion of CO_2 in an aqueous solution using $Al(OH)_3$, Ni−Al LDH (Ni/Al = 2, 3, 4, and 5), and $Ni(OH)_2$. Black bar: CO, grey bar: H_2, circle: selectivity toward CO. Photocatalyst weight: 1.0 g, photoirradiation time: 8 h.

Figure 10 shows the total amounts of CO and H_2 evolved during the photocatalytic conversion of CO_2 in an aqueous solution of NaCl (0.1 M) using Ni−Al LDH with various Ni/Al ratios (Ni/Al = 2, 3, 4, and 5) after 8 h of photoirradiation. The total amounts of CO and H_2 evolved were influenced by the Ni/Al ratio of Ni−Al LDH, indicating that the selectivity toward CO evolution depended on the Ni/Al ratio. The Ni−Al LDH with Ni/Al = 4 exhibited the highest conversion of CO_2 for the photocatalytic conversion of CO_2 using the various Ni/Al ratios. The Ni−Al LDH with Ni/Al = 5, which contains 83 mol% of nickel in the hydroxide sheet, showed a much higher activity for CO evolution and selectivity toward CO than $Ni(OH)_2$, indicating that the incorporation of Al^{3+} into $Ni(OH)_2$ to construct the LDH structure significantly enhanced the photocatalytic activity for the conversion of CO_2 in an aqueous solution. In addition, Ni−Al LDHs (Ni/Al = 2, 3, 4, and 5) exhibited a higher selectivity to CO formation than $Al(OH)_3$ and $Ni(OH)_2$ as shown in **Figure 10**. Ebitani et al. demonstrated that the properties of basic sites of Mg−Al LDHs were changed as their Mg/Al ratio was changed [48]. It is suspected that the introduction of Al^{3+} into the $Ni^{2+}(OH)_6$ octahedral unit affects the surface basicity, and that mixed hydroxides containing both Ni^{2+} and Al^{3+} in a certain ratio possess surface properties that are conducive to the photocatalytic conversion of CO_2.

Table 2 Effect of inorganic additives on the amounts of products evolved in the photocatalytic conversion of CO_2 in an aqueous solution using Ni−Al LDH (Ni/Al = 4). Concentration of additive: [anion] = 0.1 M. Photoirradiation time: 8 h. Photocatalyst weight: 1.0 g.

Additive	Amount of products evolved		Selectivity to CO (%)
	H_2 / μmol	CO / μmol	
Non	21.0	25.2	54
$NaHCO_3$	83.6	21.8	21
Na_2CO_3	99.8	34.3	26
Na_2SO_4	4.5	34.0	88
$NaNO_3$	0.0	0.5	100
NaCl	9.3	56.4	86

It is well known that inorganic anions contained in a reaction solution are able to critically influence the photocatalytic activity. In 1992, Sayama and Arakawa demonstrated the effect of $NaHCO_3$ addition on the photocatalytic decomposition of H_2O and the photocatalytic reduction of CO_2 using ZrO_2 as a photocatalyst [49]. Recently, several researchers insisted that the addition of $NaHCO_3$ to the reaction solution is essential for achieving the photocatalytic conversion of CO_2 in water, because it improves the selectivity toward CO production [50, 51]. **Table 2** presents the effect of the addition of anions to the reaction solution on the amounts of CO and H_2 evolved and the selectivity toward CO during the photocatalytic conversion of CO_2 in an aqueous solution using Ni−Al LDH (Ni/Al = 4) as a photocatalyst after 8 h of photoirradiation. The addition of $NaHCO_3$ or Na_2CO_3 promoted H_2 production via the reduction of H^+ derived from H_2O, whereas the amount of CO evolved was not affected by these additives. On the other hand, neither Na_2SO_4 nor $NaNO_3$ could positively affect product formation in our photocatalytic system. The presence of $NaNO_3$ led to the formation of O_2 under photoirradiation due to the photodecomposition of NO_3^-. In contrast to the other inorganic salts, the addition of NaCl clearly enhanced the photocatalytic conversion of CO_2 to CO. The amount of CO evolved in a 0.1 M aqueous solution of NaCl after 8 h of photoirradiation was more than twice the amount that was found to evolve when pure water was used. Simultaneously, the addition of NaCl suppressed the formation of H_2 as a reduction product of H^+. Accordingly, the selectivity toward CO evolution was advanced by the addition of NaCl to the reaction solution. **Figure 11** shows the amounts of CO and H_2 evolved and the selectivity toward CO during the photocatalytic conversion of CO_2 in an aqueous solution containing various kinds of halogenides,

using Ni−Al LDH as a photocatalyst after 5 h of photoirradiation. It can be seen that NaCl was no exception, and that other chloride salts such as KCl, CsCl, $MgCl_2$, and $CaCl_2$ influenced the selectivity toward CO evolution to a similar extent. This suggested that the presence of Cl^- in the reaction solution promoted the photocatalytic conversion of CO_2 regardless of the nature of the counter cations. However, the addition of iodide ions (I^-) decreased the photocatalytic activity of the Ni−Al LDH for the evolution of CO and H_2. Abe et al. reported the overall water splitting system by using I^- as a redox mediator, which is oxidized by a hole generated by the photoexcitation of an electron from the valence band to the conduction band of a TaON photocatalyst under visible light irradiation [31]. In our case, on the other hand, the colour change of the reaction solution to yellow during the reaction indicated that I^- might be converted into triiodine (I_3^-) under UV light irradiation by capturing the photogenerated holes; hence, the photocatalytic reaction over Ni−Al LDH was prevented by the presence of I_3^- in the reaction suspension. We therefore propose Cl^- in the reaction solution as one of the most promising candidates for a hole scavenger capable of functioning under UV light irradiation.

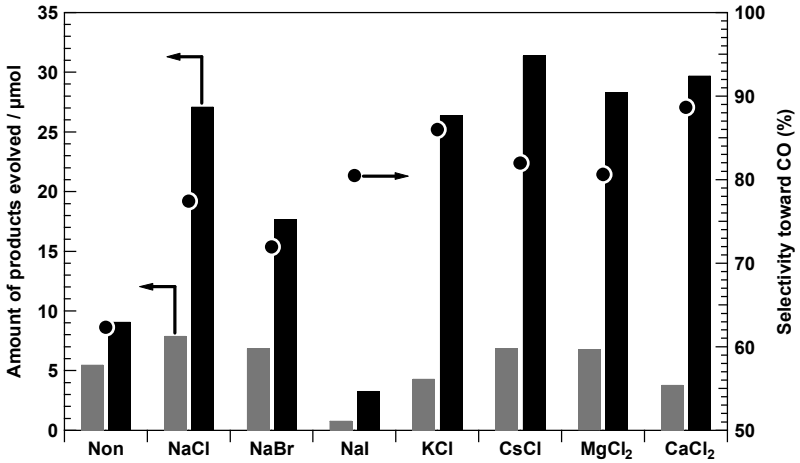

Figure 11 Total amounts of products evolved and selectivity toward CO for the photocatalytic conversion of CO_2 in an aqueous solution of various halogenide salts using Ni−Al LDH (Ni/Al = 4). Black bar: CO, grey bar: H_2, circle: selectivity toward CO. Concentration of additive: [halide anion] = 0.1 M. Photoirradiation time: 5 h. Photocatalyst weight: 0.5 g.

In addition, it is also necessary to discuss the stoichiometric formation of reduction and oxidation products for the photocatalytic conversion of CO_2. Iizuka et al. [50] and Teramura et al. [51] reported a photocatalytic system for the conversion of CO_2 with H_2O as a reducing reagent using

$ALa_4Ti_4O_{15}$ (A = Ca, Sr, and Ba) and Zn-doped Ga_2O_3 photocatalysts, respectively, and determined that a stoichiometric amount of O_2 was evolved as an oxidation product of H_2O via the capturing of the photogenerated holes. In our system, in which Ni−Al LDH is used as a photocatalyst, however, O_2 was not formed at all during the photocatalytic reaction. **Figure 12(a−h)** shows the absorption spectra for the DPD test to confirm HClO in the reaction solution after the reaction for each photoirradiation time, which contains a certain amount of photocatalyst powder. Two intense absorption peaks around 515 nm and 555 nm were observed, and these peaks can be assigned to the oxidized form of DPD. In this study, the absorbance at 515 nm was used to estimate the concentration of HClO that was produced during the reaction as referred to in the previous report [40, 41]. The amount of HClO plotted versus the photoirradiation time is shown in **Figure 12(i)** with the amounts of reduction products such as CO and H_2. In the photocatalytic conversion of CO_2 using Ni−Al LDH (Ni/Al = 4) in an aqueous solution of NaCl (0.1 M), the products CO, H_2, and HClO were formed under photoirradiation as a reduction product of CO_2 and H^+, and as an oxidation product of Cl^-, respectively. It should be possible to detect HClO selectively by using a DPD (*N,N*-dimethyl-*p*-phenylenediamine) test due to the strong oxidation power of HClO, i.e., the oxidation potentials of the other oxyanions of chlorine, ClO_2^-, ClO_3^-, and ClO_4^-, are insufficient to allow them to react with DPD. In the reaction solution, Cl^- is considered to play the role of a reducing reagent and to be oxidized to HClO by the photogenerated holes during the photocatalytic reaction. Previous studies have attempted to use Cl^- as a hole scavenger in a photocatalytic system; nevertheless, no oxidation product was observed for this anion [37, 38]. To the best of our knowledge, this is the first report to confirm the formation of HClO as an oxidation product of Cl^- during a photocatalytic reaction. **Figure 13** shows the influence of the NaCl concentration of the reaction solution on the total amounts of products formed after 8 h of photoirradiation. It can be seen that the total amounts of both the reduction (CO + H_2) and oxidation (HClO) products were affected by the NaCl concentration, and that the largest amount of these products was produced at a concentration of NaCl: 0.20 mol L^{-1}. The evolution of certain amounts of CO, H_2, and HClO in the absence of additional Cl^- in the reaction solution was ascribed to the presence of residual Cl^- on the Ni−Al LDHs. An elemental analysis revealed that more than 0.4 mmol g^{-1} of Cl^- derived from the precursors of the hydroxide sheets was contained in the Ni−Al LDHs, indicating that these Cl^- ions

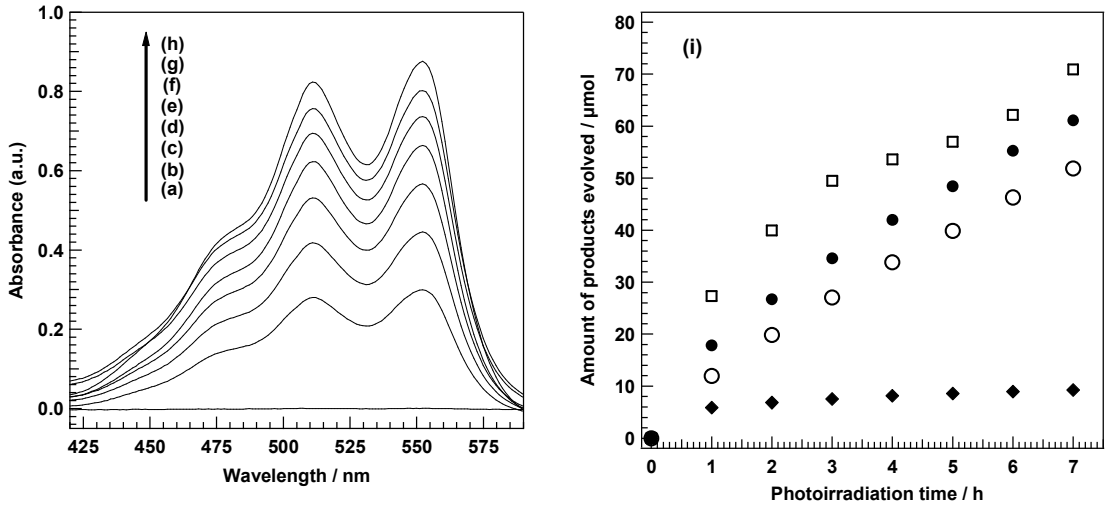

Figure 12 Absorption spectra for the DPD test to confirm HClO in the reaction solution after each photoirradiation time. **(a)** before the reaction and after the photoirradition for **(b)** 1 h, **(c)** 2 h, **(d)** 3 h, **(e)** 4 h, **(f)** 5 h, **(g)** 6 h, and **(h)** 7 h. Sample solution including photocatalyst powder: 5.0 mL, DPD solution: 1.0 mL; **(i)** total amounts of products evolved for the photocatalytic conversion of CO_2 in an aqueous solution using Ni−Al LDH (Ni/Al = 4). Diamond: H_2, white circle: CO, black circle: total amounts of reduction products (H_2 + CO), square: hypochlorous acid (HClO). Additive: 0.1 M NaCl, photocatalyst weight: 1.0 g.

might perform the same function as those in the reaction solution, in that they are partially oxidized to HClO. In this regard, one could speculate that Cl^- is oxidized to chlorine (Cl_2) by capturing the photogenerated holes as shown in Formula (2), whereupon Cl_2 in the water would be expected to immediately undergo conversion to HClO and HCl via a disproportionation reaction (Formula (3)).

Formula (2) $2Cl^- + 2h^+ \rightarrow Cl_2$

Formula (3) $Cl_2 + H_2O \rightarrow HClO + HCl$

Formula (4) $CO_2 + 2H^+ + 2e^- \rightarrow CO + H_2O$

Formula (5) $2H^+ + 2e^- \rightarrow H_2$

Taking these reaction formulae into account, HClO could be regarded as a two-electron oxidation product of Cl^-; thus, 2 μmol of holes should be consumed to form 1 μmol of HClO. Besides, it is known that CO and H_2 are the two-electron reduction products of CO_2 and H^+, respectively (Formula (4) and (5)). An estimated ratio of the total number of consumed holes to electrons for 8 h of photoirradiation, plotted versus the concentration of NaCl, is shown in **Figure 13**. Below NaCl concentrations of 0.1 M, the value of the product ratio was approximately 1.0, indicating that the stoichiometric formation of reduction products and the oxidation product was achieved in this

photocatalytic reaction. On the other hand, the ratio gradually decreased as the NaCl concentration increased. A high concentration of NaCl is considered to prevent the adsorption of HClO, which is produced during the reaction, on the surface of the Ni−Al LDH. HClO species that are not dissolved in the reaction solution, but are instead adsorbed on the surface of the Ni−Al LDH, can be detected by the DPD test, because HClO in an aqueous solution is known to be readily decomposed into HCl photochemically under UV light irradiation. Hence, the observed decrease in the ratio of the number of consumed holes to electrons may have been caused by the partial photodecomposition of HClO formed in the reaction solution at a high NaCl concentration. Accordingly, we concluded that stoichiometric amounts of CO and H_2, as reduction products, and adsorbed HClO on Ni−Al LDH, as an oxidation product, evolved during the photocatalytic conversion of CO_2 using Ni−Al LDH as a photocatalyst in an aqueous solution of 0.1 M NaCl under UV light irradiation.

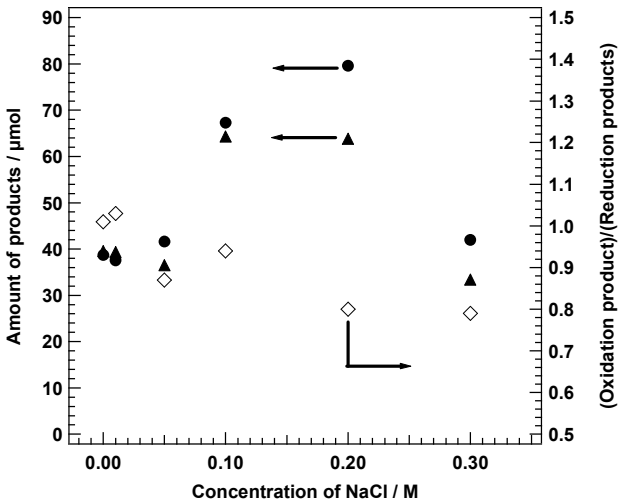

Figure 13 Influence of NaCl concentration on the photocatalytic conversion of CO_2 in an aqueous solution using Ni−Al LDH (Ni/Al = 4). Black circle: total amounts of reduction products (H_2 + CO), black triangle: amount of hypochlorous acid (HClO), white rhombus: ratio of oxidation product to reduction products. Additive: NaCl, photocatalyst weight: 1.0 g, photoirradiation time: 8 h.

Conclusion

The photocatalytic conversion of CO_2 in an aqueous solution was achieved by using synthetic Ni−Al LDH as a photocatalyst. After exposing the solution to photoirradiation for 29 h, the amount of CO (as a reduction product of CO_2) and the selectivity of the reduction products toward CO evolution were 110.9 μmol and 88.4%, respectively. The addition of Cl^- to the reaction solution clearly improved the photocatalytic activity for the conversion of CO_2 to CO, and simultaneously suppressed the formation of H_2 as a reduction product of H^+. A DPD test revealed that, under photoirradiation, HClO is stoichiometrically formed as an oxidation product of Cl^-, together with reduction products such as CO and H_2. It is suggested that the Cl^- present in the reaction solution functions as an effective hole scavenger and that it would be oxidized to Cl_2, which would immediately be converted into HClO in the presence of water.

References

1. Y. Kohno, T. tanaka, T. Funabiki and S. Yoshida, *Chemical Communications*, 1997, 841-842.
2. Y. Kohno, T. tanaka, T. Funabiki and S. Yoshida, *Chemistry Letters*, 1997, **26**, 993-994.
3. Y. Kohno, T. Tanaka, T. Funabiki and S. Yoshida, *Journal of the Chemical Society, Faraday Transactions*, 1998, **94**, 1875-1880.
4. Y. Kohno, T. Tanaka, T. Funabiki and S. Yoshida, *Physical Chemistry Chemical Physics*, 2000, **2**, 2635-2639.
5. Y. Kohno, H. Ishikawa, T. Tanaka, T. Funabiki and S. Yoshida, *Physical Chemistry Chemical Physics*, 2001, **3**, 1108-1113.
6. K. Teramura, T. Tanaka, H. Ishikawa, Y. Kohno and T. Funabiki, *The Journal of Physical Chemistry B*, 2004, **108**, 346-354.
7. H. Tsuneoka, K. Teramura, T. Shishido and T. Tanaka, *The Journal of Physical Chemistry C*, 2010, **114**, 8892-8898.
8. F. Cavani, F. Trifirò and A. Vaccari, *Catalysis Today*, 1991, **11**, 173-301.

9. M. K. Ram Reddy, Z. P. Xu, G. Q. Lu and J. C. Diniz da Costa, *Industrial & Engineering Chemistry Research*, 2006, **45**, 7504-7509.

10. K. H. Goh, T. T. Lim and Z. Dong, *Water Research*, 2008, **42**, 1343−1368.

11. J. Das, B. S. Patra, N. Baliarsingh and K. M. Parida, *Applied Clay Science*, 2006, **32**, 252-260.

12. R. L. Goswamee, P. Sengupta, K. G. Bhattacharyya and D. K. Dutta, *Applied Clay Science*, 1998, **13**, 21-34.

13. B. F. Sels, D. E. De Vos and P. A. Jacobs, *Catalysis Reviews*, 2001, **43**, 443-488.

14. K. Teramura, S. Iguchi, Y. Mizuno, T. Shishido and T. Tanaka, *Angewandte Chemie International Edition*, 2012, **51**, 8008-8011.

15. S. Iguchi, K. Teramura, S. Hosokawa and T. Tanaka, *Catal. Today*, 2015, **251**, 140-144.

16. N. Ahmed, Y. Shibata, T. Taniguchi and Y. Izumi, *Journal of Catalysis*, 2011, **279**, 123-135.

17. M. Morikawa, N. Ahmed, Y. Yoshida and Y. Izumi, *Applied Catalysis B: Environmental*, 2014, **144**, 561-569.

18. M. Morikawa, Y. Ogura, N. Ahmed, S. Kawamura, G. Mikami, S. Okamoto and Y. Izumi, *Catalysis Science & Technology*, 2014, **4**, 1644-1651.

19. K. Katsumata, K. Sakai, K. Ikeda, G. Carja, N. Matsushita and K. Okada, *Materials Letters*, 2013, **107**, 138-140.

20. J. Hong, W. Zhang, Y. Wang, T. Zhou and R. Xu, *ChemCatChem*, 2014, **6**, 2315-2321.

21. J. Hong, Y. Wang, J. Pan, Z. Zhong and R. Xu, *Nanoscale*, 2011, **3**, 4655-4661.

22. C. G. Silva, Y. Bouizi, V. Fornés and H. García, *Journal of the American Chemical Society*, 2009, **131**, 13833-13839.

23. S. Cho, J.-W. Jang, Y. B. Park, J. Y. Kim, G. Magesh, J. H. Kim, M. Seol, K. Yong, K.-H. Lee and J. S. Lee, *Energy & Environmental Science*, 2014, **7**, 2301-2307.

24. Y. Zhao, M. Wei, J. Lu, Z. L. Wang and X. Duan, *ACS Nano*, 2009, **3**, 4009-4016.

25. S.-J. Xia, F.-X. Liu, Z.-M. Ni, W. Shi, J.-L. Xue and P.-P. Qian, *Applied Catalysis B: Environmental*, 2014, **144**, 570-579.

26. G. Chen, S. Qian, X. Tu, X. Wei, J. Zou, L. Leng and S. Luo, *Applied Surface Science*, 2014, **293**, 345-351.

27. J. Liu and G. Zhang, *Physical Chemistry Chemical Physics*, 2014, **16**, 8178-8192.

28. R. Abe, K. Shinmei, N. Koumura, K. Hara and B. Ohtani, *Journal of the American Chemical Society*, 2013, **135**, 16872-16884.

29. T. Ohno, S. Saito, K. Fujihara and M. Matsumura, *Bulletin of the Chemical Society of Japan*, 1996, **69**, 3059-3064.

30. K. Maeda, M. Higashi, D. Lu, R. Abe and K. Domen, *Journal of the American Chemical Society.*, 2010, **132**, 5858-5868.

31. R. Abe, M. Higashi and K. Domen, *ChemSusChem*, 2011, **4**, 228-237.

32. H. Kato, M. Hori, R. Konta, Y. Shimodaira and A. Kudo, *Chemistry Letters*, 2004, **33**, 1348-1349.

33. K. Sayama, R. Yoshida, H. Kusama, K. Okabe, Y. Abe and H. Arakawa, *Chemical Physics Letters*, 1997, **277**, 387-391.

34. Y. Sasaki, A. Iwase, H. Kato and A. Kudo, *Journal of Catalysis*, 2008, **259**, 133-137.

35. Y. Sasaki, H. Kato and A. Kudo, *Journal of the American Chemical Society*, 2013, **135**, 5441-5449.

36. K. Fujihara, T. Ohno and M. Matsumura, *Journal of the Chemical Society, Faraday Transactions*, 1998, **94**, 3705-3709.

37. M. Krivec, R. Dillert, D. W. Bahnemann, A. Mehle, J. Strancar and G. Drazic, *Physical Chemistry Chemical Physics*, 2014, **16**, 14867-14873.

38. P. Calza and E. Pelizzetti, *Pure and Applied Chemistry*, 2001, **73**, 1839-1848.

39. L. Huang, R. Li, R. Chong, G. Liu, J. Han and C. Li, *Catalysis Science & Technology*, 2014, **4**, 2913-2918.

40. K. Carlsson, L. Moberg and B. Karlberg, *Water Research*, 1999, **33**, 375-380.

41. L. Moberg and B. Karlberg, *Analytica Chimica Acta*, 2000, **407**, 127-133.

42. S. K. Sharma, P. K. Kushwaha, V. K. Srivastava, S. D. Bhatt and R. V. Jasra, *Industrial & Engineering Chemistry Research*, 2007, **46**, 4856-4865.

43. A. P. Grosvenor, M. C. Biesinger, R. S. C. Smart and N. S. McIntyre, *Surface Science*, 2006, **600**, 1771-1779.

44. B. P. Payne, M. C. Biesinger and N. S. McIntyre, *Journal of Electron Spectroscopy and*

Related Phenomena, 2009, **175**, 55-65.

45. H. Park, J. Chae, S.-M. Park, K.-B. Kim and K. Roh, *Metals and Materials International*, 2013, **19**, 887-894.

46. M. Wei, X. Xu, X. Wang, F. Li, H. Zhang, Y. Lu, M. Pu, D. G. Evans and X. Duan, *European Journal of Inorganic Chemistry*, 2006, **2006**, 2831-2838.

47. A. Mignani, B. Ballarin, M. Giorgetti, E. Scavetta, D. Tonelli, E. Boanini, V. Prevot, C. Mousty and A. Iadecola, *The Journal of Physical Chemistry C*, 2013, **117**, 16221-16230.

48. K. Ebitani, K. Motokura, K. Mori, T. Mizugaki and K. Kaneda, *The Journal of Organic Chemistry*, 2006, **71**, 5440-5447.

49. K. Sayama and H. Arakawa, *The Journal of Physical Chemistry,* 1993, **97**, 531-533.

50. K. Iizuka, T. Wato, Y. Miseki, K. Saito and A. Kudo, *Journal of the American Chemical Society*, 2011, **133**, 20863-20868.

51. K. Teramura, Z. Wang, S. Hosokawa, Y. Sakata and T. Tanaka, *Chemistry - A European Journal*, 2014, **20**, 9906-9909.

Chapter 3

Photocatalytic Conversion of CO_2 in Water Using Fluorinated Layered Double Hydroxides as Photocatalysts

Abstract

The photocatalytic conversion of CO_2, which can convert CO_2 into useful chemicals, such as CH_4, CH_3OH, HCOOH, HCHO, and CO, is attractive process for creating an artificial carbon cycling system. It was found that the synthetic Ni−Al layered double hydroxide (Ni−Al LDH) can reduce CO_2 into CO in an aqueous solution of NaCl under UV light irradiation, and chloride ions (Cl^-) in the reaction solution scavenge the photogenerated holes. In this study, we prepared fluorinated Mg−Al LDH and Ni−Al LDH for altering the chemical and/or physical properties of the LDH as a solid base, and investigated the effect of fluorination on the photocatalytic activity for the conversion of CO_2 in an aqueous solution. We found that the fluorination of LDH by incorporation of hexafluoroaluminate (AlF_6^{3-}) units in the hydroxide sheets clearly improved the amount of CO evolved as a reduction product of CO_2.

Introduction

The development of a chemical process that can fix CO_2 using natural energy sources is necessary for creating an artificial carbon cycling system. The photocatalytic conversion of CO_2 is considered one of the most attractive processes for converting CO_2 into useful chemicals, such as CH_4, CH_3OH, HCOOH, HCHO, and CO, because, in future, it might be able to use solar energy as the driving source. Our research group has previously reported the photocatalytic conversion of CO_2 using H_2 as a reductant over metal oxides such as ZrO_2 [1-4], MgO [5, 6], $ATaO_3$ (A = Li, Na, and K) [7], and Ga_2O_3 [8]. The results showed that the adsorbed CO_2 species on the surface of these photocatalysts play an important role in the photocatalytic conversion of CO_2. This indicates that solid base materials that have the ability to provide suitable surface properties for CO_2 adsorption should be promising candidates for this photocatalytic reaction. However, because their basic sites are easily poisoned by water, these metal oxide photocatalysts do not show promising results for the conversion of CO_2 in aqueous solutions. The development of a highly stable photocatalytic system, capable of functioning in water, for the selective conversion of CO_2 is required for the construction of a photocatalytic carbon cycling system.

Layered double hydroxides (LDHs) [9-11], which can function as solid base materials in the presence of water [12], are presented by the general formula $[M^{2+}_{1-z}–M^{3+}_{z}(OH)_2](A^{n-})_{z/n}\cdot mH_2O$. M^{2+} and M^{3+} are the divalent and trivalent cations, respectively. A^{n-} is the interlayer anion of valence n and compensates for the positive charge of the hydroxide sheets. The value z represents the molar ratio of $M^{3+}/(M^{2+} + M^{3+})$ within the hydroxide sheets, and it has been reported that the LDH structure can exist for z values in the 0.1−0.5 range [9]. The nature of M^{2+}, M^{3+}, z, and A^{n-} can be altered over a wide range of values; therefore, by referring to published reports, various isostructural materials with varied chemical properties can be successfully synthesized [13-28]. In recently years, the application of various LDHs to photocatalytic reactions, including the degradation of organic compounds [17, 29-33] and water splitting [23, 34, 35], has been studied. For example, the photocatalytic evolution of H_2 from water using Ni−Ti LDH as the photocatalyst was achieved in the presence of a sacrificial reagent under visible light irradiation [35]. Previously, we applied a series of synthetic LDHs to the photocatalytic conversion of CO_2 in water and found that Ni−Al LDH exhibited high activity for the

CO evolution under UV light irradiation [36, 37]. The use of Ni−Al LDH enabled the selective formation of CO, because the amount of H_2 evolved by the reduction of H^+ derived from water was much smaller than that of other LDHs. Moreover, in the presence of Ni−Al LDH, the addition of chloride ion (Cl^-) to the reaction solution enhanced the conversion of CO_2 to CO, and a stoichiometric amount of hypochlorous acid (HClO) was produced by the oxidation of Cl^- [38].

Many attempts have been made to modify the chemical and/or physical properties of LDHs. A series of noble metal particles loaded on the surface of Mg−Al LDH exhibited excellent catalytic activities for dehydrogenation [39], oxidation [40], and reforming [41] processes. The intercalations of different kinds of functional compounds, such as polyoxometalates (POM) [42-44], metal complexes [45, 46], and organic dyes [47, 48], into the interlayer space of LDHs were presented by many researchers. Moreover, some composite materials with metal oxides, such as TiO_2/Mg−Al LDH [49, 50] and CeO_2/Mg−Al LDH [51], have also been reported to improve the photocatalytic activity. In 2012, Lima *et al.* developed the fluorinated Mg−Al LDH using Na_3AlF_6 as a fluorine source, wherein some $(Al(OH)_6)^{3-}$ octahedral structures within the hydroxide sheets were partially substituted by AlF_6^{3-} units [52]. The fluorination of LDH via intercalation of fluoride anions (F^-) in the interlayer space has also been reported previously [53-55]. It is expected that F^- should ultimately be exchanged with other selective anions such as CO_3^{2-}, because F^- is not stable as a charge compensating anion of LDH. Therefore, the incorporation of fluorine, by substituting the OH groups, as part of the brucite-like hydroxide layer is a new strategy for altering the chemical and/or physical properties of the LDH material as a solid base. In fact, Lima *et al.* have suggested that, because of its high electronegativity, the incorporation of fluorine as AlF_6^{3-} units into the hydroxide sheets greatly influences the basicity of the LDH [52]. We predict that the CO_2 adsorption on the surface of the LDH is enhanced by the fluorination. Thus, the selectivity toward CO_2 reduction should be improved. In this study, we prepared fluorinated Mg−Al LDH and Ni−Al LDH with different fluorine contents by following the previously reported procedures and investigated the effect of fluorination on the photocatalytic activity for the conversion of CO_2 in an aqueous solution.

Experimental

Fluorinated layered double hydroxides (***F(x)***M^{2+}−Al LDH, M^{2+} = Mg^{2+} and Ni^{2+}) were synthesized by a typical coprecipitation method. Precursors of metal components, such as $MgCl_2 \cdot 6H_2O$ or $NiCl_2 \cdot 6H_2O$, $AlCl_3$, and Na_3AlF_6, were dissolved in 1.0 L of ultra-pure water. The value of ***x*** in ***F(x)***M^{2+}−Al LDH means a ratio of Na_3AlF_6 in the total Al species ($AlCl_3$ + Na_3AlF_6) when preparing it. The aqueous solution of precursors was dropped into an aqueous solution of Na_2CO_3 at room temperature with vigorous stirring. The pH of the suspension was strictly kept between 9.9 to 10.1 by using a pH controller (NPH-660NDE, Nissin Rika) equipped with a liquid feeding pump for an aqueous solution of NaOH. The resulting suspension was aged at 333 K for 12 h, and then collected by filtration. The solid precipitate was washed with 1.0 L of ultra-pure water and dried at 383 K in air atmosphere. The atomic ratio of M^{2+} to Al^{3+} (M^{2+}/Al^{3+}, M^{2+} = Mg^{2+} and Ni^{2+}) was fixed at 3 in all samples. ***F(7.5)imp-***Ni−Al LDH was prepared as a reference sample via an impregnation method. ***F(0)***Ni−Al LDH powder was dispersed in an aqueous solution which contains a required amount of Na_3AlF_6, and the suspension was dried up at 353 K under air atmosphere.

The powder XRD patterns of a series of prepared LDHs were measured by an X-ray diffractometer (MultiFlex, Rigaku) using Cu $K_{\alpha 1}$ radiation (λ = 0.154 nm) at a scan rate of 4.0 ° min^{-1}. UV/Vis diffuse reflection spectra of LDHs were collected on a UV-Visible Spectrometer (V-650, JASCO) equipped with an integrated sphere accessory. Thermal analysis for the synthesized LDHs were carried out using a thermobalance (Thermo Plus 2, Rigaku) under dried air atmosphere at a flow rate of 80 mL min^{-1}. The specific surface areas of samples were estimated from the N_2 adsorption isotherms at 77 K using a surface area analyzer (BELSORP-miniII, BEL Japan, Inc.). Prior to the measurements, LDHs were evacuated at 383 K for 1 h using a pretreatment instrument (BELPREP-vacII, BEL Japan, Inc.). X-ray photoelectron spectra (XPS) profiles of the synthesized LDHs were collected by an X-ray photoelectron spectrometer (ESCA 3400, Shimadzu Corp.). The narrow range scans for Ni 2p and F 1s spectra were performed using an Mg K_α X-ray source, and the peak positions were calibrated by the peak that can be attributed to C 1s. The peak intensity of F 1s spectra was normalized with that of Ni $2p_{3/2}$ peak.

The photocatalytic activity of synthesized ***F(x)***M^{2+}−Al LDHs (M^{2+} = Mg^{2+} or Ni^{2+}) for the

conversion of CO_2 in water were evaluated by using a quartz inner-irradiation type reaction vessel connected to the closed circulation system. 0.5 g of photocatalyst powder was dispersed in 350 mL of ultra-pure water, and the suspension was degassed at room temperature. 7.6 mmol of CO_2 gas, which was purified by a vacuum distillation at liquid N_2 temperature, was introduced into the free gas space. The suspension was irradiated under a 400 W high-pressure Hg lamp (HL400BH-9, SEN LIGHTS Corp.) through a quartz filter equipped with a cooling water system. The gas phase products were analyzed by a thermal conductivity detector gas chromatography (TCD-GC) using a GC-8A chromatograph (GC-8AIT, Shimadzu Corp.) fitted out a MS-5A packed column. GC-MS analysis was performed using a quadruple-type mass spectrometer (BEL Mass, BEL Japan, Inc.) in the case of an isotopic experiment. The selectivity toward CO evolution among reduction products was calculated by following equation.

$$\text{Selectivity toward CO evolution (\%)} = 100 \times \mathbf{A}_{CO} / (\mathbf{A}_{CO} + \mathbf{A}_{H2})$$

$\mathbf{A}_{CO}$: amount of CO evolved / μmol

$\mathbf{A}_{H2}$: amount of H_2 evolved / μmol

The amount of HClO produced in the reaction solutions was determined by a DPD (*N,N*'-dimethyl-*p*-phenylenediamine) method [56, 57], which is one of the most popular techniques to observe HClO in water. The DPD solution was prepared by dissolving 0.06 g of the DPD reagent, which is a mixture of DPD sulphate and Na_2SO_4, in 3.0 mL of phosphate buffer solution (pH = 6.5). Following this, 1.0 mL of the prepared DPD solution was added to 5.0 mL of the sample solution, and was shaken for 20 s. The transmittance spectrum was measured immediately using a multiscan UV-vis spectrometer (MCPD-7700, Otsuka Electronics Co., Ltd). The concentration of HClO in the aqueous solution was estimated from the absorbance at 515 nm.

Results and discussion

Figure 1 displays the XRD patterns of ***F(0)***Mg−Al LDH and ***F(5)***Mg−Al LDH collected over (a) a wide and (b) a narrow range of angles, respectively. Both diffraction patterns corresponded with the typical structure of the LDH group; i.e., the layered structure of the hydroxide sheets grew along the *c*-axis with respect to the hexagonal crystalline units. As reported by Lima *et al.* [52], three

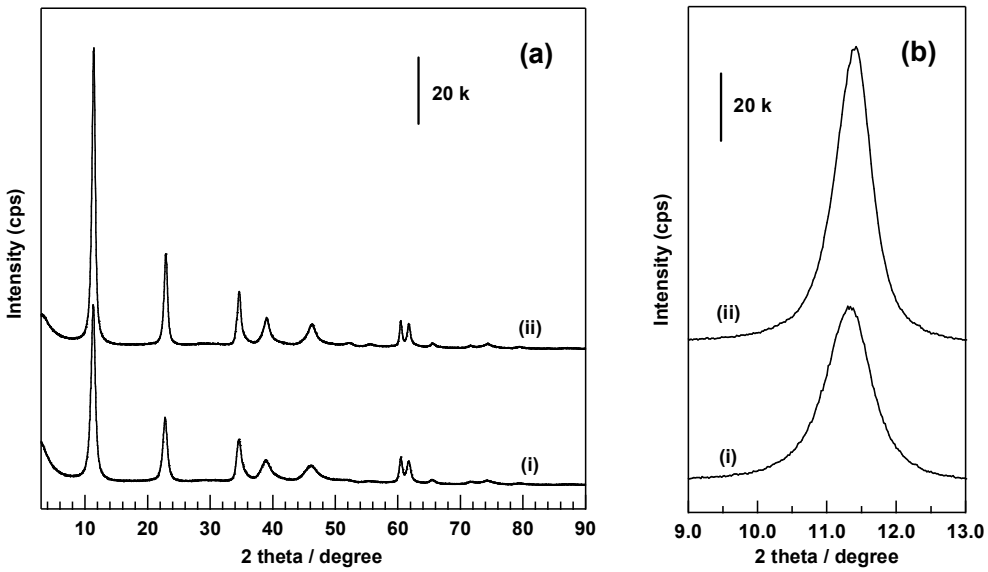

Figure 1 XRD patterns of (i) ***F(0)***Mg−Al LDH and (ii) ***F(5)***Mg−Al LDH collected over (a) a wide and (b) a narrow range of angles.

sharp reflection peaks observed at around 11.4°, 22.9°, and 34.6° in the XRD pattern of the fluorinated Mg−Al LDH were assigned to the (0 0 3), (0 0 6), and (0 0 9) planes, respectively. These reflections are related to the thickness of the layer structure, especially the d-spacing of the (0 0 3) plane ($d_{(0\,0\,3)}$), which corresponds to the interval of adjacent hydroxide sheets. It is well known that the intercalation of anions, which have large ionic radii, results in an increase in the layer distance in the LDH structure. For example, the peak position of the (0 0 3) plane was shifted to a lower angle by the incorporation of organic dye anions or metal oxy anions. Carriazo *et al.* reported that Mg−Al LDH, which contains $(H_2W_{12}O_{40})^{6-}$ as an interlayer charge compensating anion, shows (0 0 3) plane diffraction peak at around 6.1° (2θ, Cu $K_{\alpha 1}$) [43]. Taking this into account, the presence of AlF_6^{3-} anion in the interlayer space of LDH should shift the peak of the (0 0 3) plane reflection to a lower angle because of the bulky structure of AlF_6^{3-}; in contrast, the ionic radius of CO_3^{2-} is 178 pm [58]. The fluorination of LDH via the incorporation of the AlF_6^{3-} unit into hydroxide sheets did not change the interlayer distance, which indicated that AlF_6^{3-} units were not present in the interlayer space. On the other hand, the peak position of the (0 0 3) plane diffraction peak was shifted slightly to a higher angle, as shown in **Figure 1(b)**. This change indicated that the decrease in interlayer distance was caused by fluorination. Lima *et al.* proposed that the enhancement of hydrogen-bonding between the hydroxide sheets and interlayer water molecules decreased the interval between hydroxide sheets,

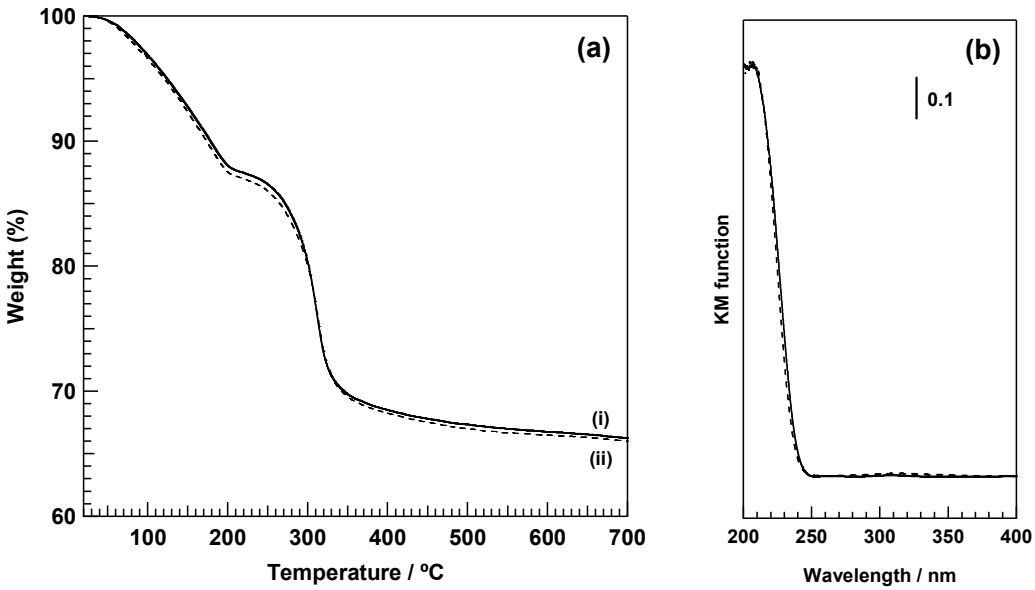

Figure 2 (a) Weight loss curves in thermal gravimetric analysis and (b) UV/Vis diffuse reflectance spectra of (i) ***F(0)***Mg−Al LDH and (ii) ***F(5)***Mg−Al LDH.

because fluorine is one of the most electronegative elements [52]. Other intense peaks located above 60° are attributed to the (1 1 0) and (1 1 3) planes reflections. The cation-to-cation distance within the hydroxide sheet (parameter *a*) can be calculated using the d-spacing of the (1 1 0) plane reflection ($a = 2d_{(1\,1\,0)}$). The peak position of the (1 1 0) plane diffraction was not influenced by the fluorination of hydroxide sheets, indicating that parameter *a* remained unchanged. Lima *et al.* presented the MAS NMR results of ^{27}Al and ^{19}F and reported that the AlF_6^{3-} units should be incorporated randomly in the hydroxide sheets [52]. Weight loss curves of ***F(0)***Mg−Al LDH and ***F(5)***Mg−Al LDH, obtained using thermal gravimetric analysis are presented in **Figure 2(a)**. The LDH group structure shows weight loss in two steps. The first weight loss happens below 473 K and is attributed to the desorption of water molecules from the interlayer. The second loss takes place between 473 and 673 K and is attributed to two phenomena, viz. the decomposition of interlayer charge-compensating anions and the dehydration of hydroxide sheets accompanied by the collapse of the layer structure. Both ***F(0)*** and ***F(5)***Mg−Al LDHs exhibited similar weight loss curves. No changes were observed with regards to the weight loss temperature and the extent of weight loss. These results indicated that the fluorination of Mg−Al LDH influenced neither the stability of hydroxide sheets nor the amount of carbonate ions preserved in the interlayer space. **Figure 2(b)** shows the UV/Vis diffuse reflectance spectra of ***F(0)*** and ***F(5)***Mg−Al LDHs. Both the shape of the spectrum and the absorption edge were

not changed by the fluorination of Mg−Al LDH. On the other hand, Na_3AlF_6 powder exhibited no absorption peak in the 200−800 nm range. The fluorination of Mg−Al LDH via incorporation of AlF_6^{3-} units into the hydroxide sheets did not change the absorption spectrum. In the present study, the fluorination of LDH is not considered "doping", but is considered a "solid solution". This is because fluorine atoms are present as a component of the AlF_6^{3-} units in the brucite-like hydroxide sheets.

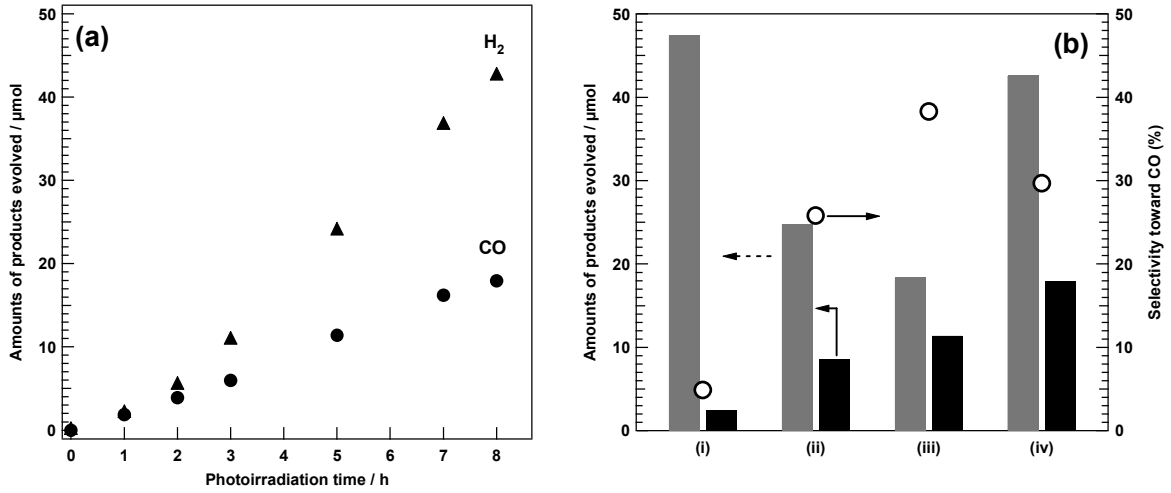

Figure 3 (a) Time courses of H_2 and CO evolution in the photocatalytic conversion of CO_2 in an aqueous NaCl solution (0.1 M) using ***F(5)***Mg−Al LDH photocatalyst. (b) Total amounts of H_2 and CO after 8 h of photoirradiation in the photocatalytic conversion of CO_2 in water. (i) ***F(0)***Mg−Al LDH photocatalyst with no additive, (ii) ***F(0)***Mg−Al LDH photocatalyst with 0.1 M of NaCl additive, (iii) ***F(5)***Mg−Al LDH photocatalyst with no additive, and (iv) ***F(5)***Mg−Al LDH photocatalyst with 0.1 M of NaCl additive. The selectivity toward CO among reduction products is presented with circles in Figure 3(b).

Figure 3(a) displays the time courses of CO evolution in the photocatalytic conversion of CO_2 in an aqueous NaCl solution using ***F(5)***Mg−Al LDH photocatalyst. ***F(5)***Mg−Al LDH photocatalyst could reduce CO_2 under UV light irradiation, and CO and H_2 were evolved with high stability as the reduction product of CO_2 and proton (H^+), respectively. Other reduction products, such as methane, methanol, formaldehyde, and formic acid were not produced in this photocatalytic reaction system. We previously reported that the addition of Cl^- in the reaction solution improves the activity for the photocatalytic conversion of CO_2 into CO over Ni−Al LDH because Cl^- acts as a hole scavenger [38] and hence advances the conversion. It is proposed that Cl^- in the reaction solution

enhances CO formation based on the same mechanism as in the case of Ni−Al LDH; i.e., Cl^- captures the photogenerated holes and it should be oxidized to Cl_2. As shown in **Figure 3(b)**, the photocatalytic activity for CO formation over ***F(0)***Mg−Al LDH was also enhanced by the addition of Cl^-. Moreover, the fluorination of Mg−Al LDH obviously increases the amount of CO evolved in the photocatalytic conversion of CO_2 in an aqueous NaCl solution (see difference between (ii) and (iv)). In this case, the amount of CO produced for ***F(5)***Mg−Al LDH was twice that for ***F(0)***Mg−Al LDH. On the other hand, the amount of H_2 evolved was also affected by both Cl^- addition and the fluorination of Mg−Al LDH (by comparing (i) and (ii) in **Figure 3(b)**). It is well known that selective CO_2 reduction is one of the most important indices of photocatalytic activity for CO_2

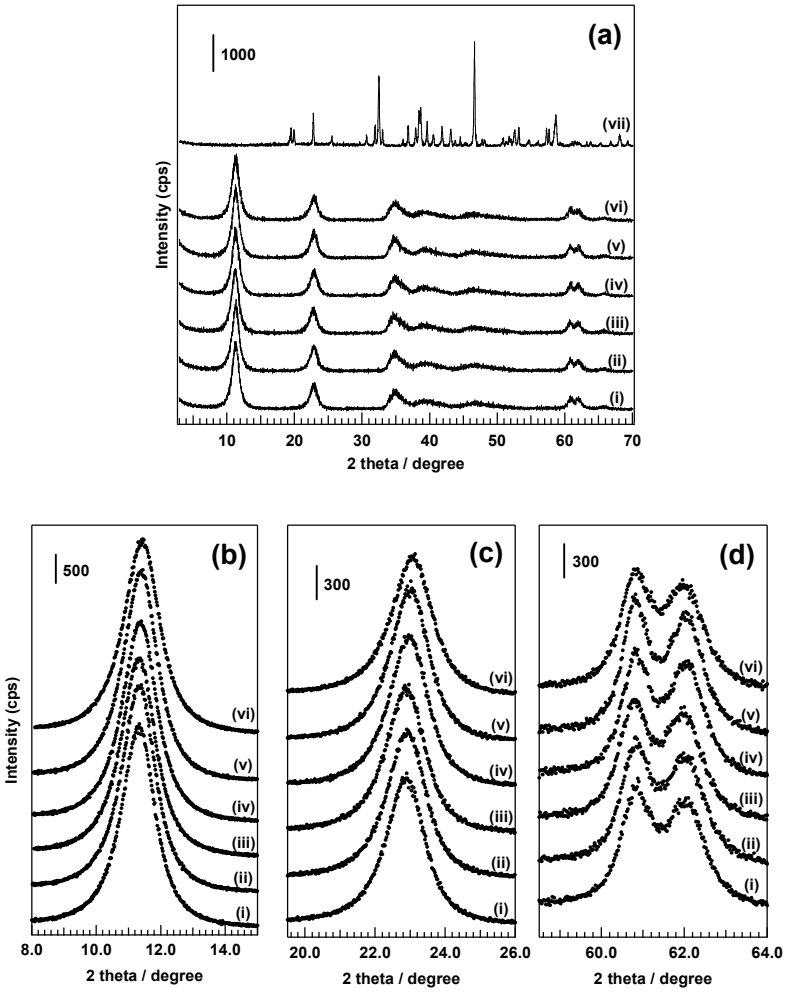

Figure 4 XRD patterns of ***F(x)***Ni−Al LDH and Na_3AlF_6 collected over (a) a wide range and a narrow ranges of angles for (b) (0 0 3) plane, (c) (0 0 6) plane, and (d) (1 1 0) plane reflections. ***x*** = (i) 0, (ii) 2.5, (iii) 5.0, (iv) 7.5, (v) 10, (vi) 20, and (vii) Na_3AlF_6.

conversion in water, because the reduction of protons (H^+) takes place competitively in this reaction. In this regard, ***F(5)***Mg−Al LDH enabled the improvement in selectivity towards CO formation in an aqueous NaCl solution. Hence, we propose that the fluorination of Mg−Al LDH leads to an enhancement in both the amount of CO evolved and the selectivity towards CO formation.

As described in our previous work, the amount of CO evolved for Ni−Al LDH is larger than that for Mg−Al LDH, and the use of Ni−Al LDH as a photocatalyst particularly suppresses the H_2 evolution. Therefore, Ni−Al LDH is considered one of the most favorable photocatalysts for selective CO_2 in an aqueous solution [37]. **Figure 4(a)** shows the XRD patterns of ***F(x)***Ni−Al LDH (***x*** = 0, 2.5, 5.0, 7.5, 10 and 20) and Na_3AlF_6, which was used as a precursor for the AlF_6^{3-} unit. The typical diffraction patterns corresponding to the LDH structure were observed over the entire range of ***x*** values without any impurity phases such as $Ni(OH)_2$, $Al(OH)_3$, NaF, and Na_3AlF_6. This indicated that the fluorinated Ni−Al LDHs were successfully synthesized via the co-precipitation method. **Figures 4(b), (c), and (d)** show the XRD patterns of ***F(x)***Ni−Al LDH (***x*** = 0, 2.5, 5.0, 7.5, 10 and 20) collected in a narrow range to observe details of the (0 0 3), (0 0 6), and (1 1 0) planes reflections, respectively. As discussed above, the intercalation of AlF_6^{3-} in the interlayer of the hydroxide sheets should cause an increase in the interlayer distance ($d_{(0\,0\,3)}$). However, the (0 0 3) and (0 0 6) planes diffraction peaks of Ni−Al LDH, which are related to the thickness of the layer structures, shifted to slightly higher angles with an increase in the fluorination rate. This result indicated that the marginal decrease in layer distance was caused by the incorporation of fluorine species in the hydroxide sheets of Ni−Al LDH, which was consistent with the results obtained by Lima *et al.* [52]. **Table 1** lists the position of the (0 0 6) and (1 1 0) planes reflections in the XRD

Table 1 Peak positions of (0 0 6) and (1 1 0) phase reflections in the XRD patterns, the calculated value of $d_{(003)}$, the specific surface area (S_{BET}), and the result of the photocatalytic activity test for ***F(x)***Ni−Al LDH (***x*** = 0, 2.5, 5.0, 7.5, 10, and 20).

F content (x)	Position / degree		$d_{(003)}$ / Å	S_{BET} / $m^2\ g^{-1}$	Amounts of products / μmol		Selectivity (%)
	(006)	(110)			CO	H_2	
0	22.90	60.88	7.76	75.1	18.8	20.6	47
2.5	22.92	60.82	7.75	83.4	30.0	8.0	79
5.0	22.95	60.80	7.75	113	36.8	7.0	84
7.5	22.97	60.80	7.74	113	47.3	12.0	80
10	23.00	60.82	7.73	120	31.7	14.1	69
20	23.10	60.82	7.70	86.3	18.5	12.6	59

patterns, the calculated value of $d_{(0\ 0\ 3)}$, the specific surface area (S_{BET}), and the results of the photocatalytic activity test for ***F(x)***Ni−Al LDH (***x*** = 0, 2.5, 5.0, 7.5, 10, and 20). The distance between adjacent hydroxide sheets ($d_{(0\ 0\ 3)}$), which was calculated from the position of the (0 0 6) plane reflection in this study, gradually decreased with an increase in the amount of AlF_6^{3-} units in the hydroxide sheets. However, the position of the (1 1 0) phase diffraction peak was not influenced by fluorination. The amount of CO evolved after 8 h of photoirradiation was affected by the fluorination of Ni−Al LDH, and ***F(7.5)***Ni−Al LDH exhibited the highest activity for CO formation. In particular, 47.3 μmol of CO was produced after 8 h of photoirradiation using ***F(7.5)***Ni−Al LDH in the photocatalytic conversion of CO_2 in an aqueous NaCl solution. It was found that the excess AlF_6^{3-} incorporation (***x*** = 10 and 20) caused a decrease in the photocatalytic conversion of CO_2 to CO. On the other hand, ***F(2.5)***Ni−Al LDH produced less H_2 than ***F(0)***Ni−Al LDH, indicating that fluorination altered the selectivity towards CO formation among the reduction products. In fact, after 8 h of photoirradiation, the selectivity towards CO clearly changed with the extent of fluorination (as shown in **Table 1**). By comparing with the results previously reported from our group [37], the photocatalytic activity of Ni−Al LDH was clearly improved by the tuning of the reaction condition (addition of NaCl) and the chemical properties of photocatalyst itself (fluorination). Furthermore, the actual amount of CO_2 reduction product, 47.3 μmol of CO after 8 h of photoirradiation in this study, is much largervalue than others reports using LDHs photocatalysts for the conversion of CO_2 [59-62]. As presented in **Table 1**, the specific surface area of ***F(x)***Ni−Al LDH was also influenced by the value of ***x***. For ***x*** = 5.0, 7.5, and 10, the results showed relatively larger surface areas. We have already reported that the amount of CO evolved in the photocatalytic conversion of CO_2 in an aqueous NaCl solution using Ni−Al LDH strongly depends on the surface area. This means that Ni−Al LDH with a large specific surface area can achieve higher photocatalytic activity for the conversion of CO_2 to CO because the adsorption of CO_2 molecules on the surface of photocatalyst materials is an innegligible step to convert CO_2 [38]. Therefore, an increase in the specific surface area is one of the reasons for the enhanced formation of CO upon fluorination of Ni−Al LDH. Meanwhile, another change in the physical and/or chemical properties because of fluorination would cause the difference in selectivity towards CO formation. Lima *et al.* suggested that fluorine incorporation into LDH hydroxide sheets leads to the formation of strong basic sites [52]. We presume that the change in surface properties has a

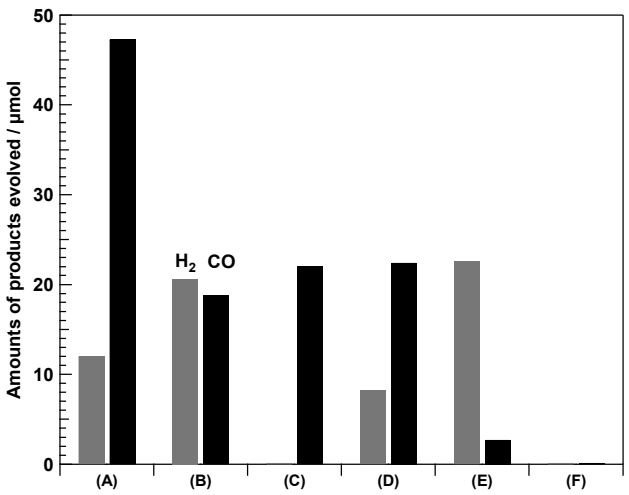

Figure 5 Total amounts of H_2 (blue) and CO (red) after 8 h of photoirradiation in the photocatalytic conversion of CO_2 in an aqueous solution of NaCl. (A) ***F(7.5)***Ni−Al LDH, (B) ***F(0)***Ni−Al LDH, (C) ***F(0)***Ni−Al LDH (Na_3AlF_6 was dissolved into the reaction solution as a second additive), (D) ***F(7.5)imp-***Ni−Al LDH, (E) ***F(7.5)***Ni−Al LDH without CO_2 (Ar was introduced instead of CO_2), and (F) ***F(7.5)***Ni−Al LDH without irradiation.

critical influence on the adsorption features of CO_2 molecules and the selectivity towards CO formation is therefore improved via suppression of H_2 evolution by the fluorination of Ni−Al LDH. In other words, the fluorination of the hydroxide sheets would impart surface properties that facilitate the conversion of CO_2 to CO in aqueous solution. This is because the adsorbed CO_2 species on the surface of LDH are considered responsible for this reaction. More detailed information, such as changes in the amount of adsorbed CO_2, the heat of adsorption for CO_2 upon fluorination and the adsorbed CO_2 species under the reaction conditions, is now being obtained in further investigations.

Figure 5 presents the results of various blank tests for the photocatalytic conversion of CO_2 in an aqueous solution using ***F(7.5)***Ni−Al LDH as the photocatalyst. No photocatalytic activity was observed without photoirradiation (see Figure 5(F)). **Table 1** shows that the fluorination of Ni−Al LDH (x = 7.5) clearly improved CO formation, while simultaneously suppressing the H_2 evolution (see Figures 5(A) and (B)). The addition of Na_3AlF_6, which was used as a precursor to AlF_6^{3-} units, did not improve the activity for CO formation over ***F(0)*** Ni−Al LDH (see Figure (C)). The use of ***F(7.5)imp-***Ni−Al LDH, which is prepared via an impregnation method and wherein all AlF_6^{3-} units are present on the surface of ***F(0)***Ni−Al LDH, did not result in the enhancement of CO evolution. These results indicated that the incorporation of AlF_6^{3-} units in the hydroxide sheets significantly

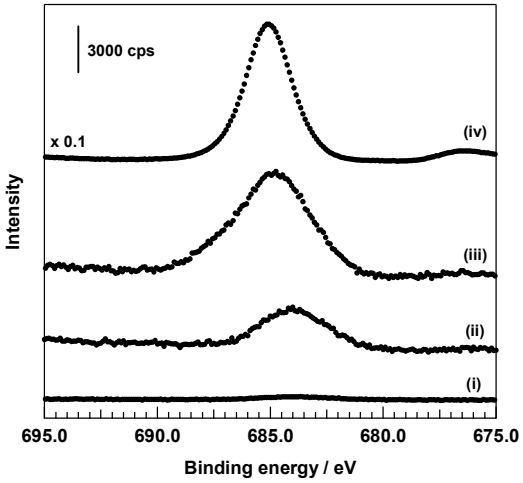

Figure 6 F 1s XPS profiles of (i) ***F(0)***Ni−Al LDH, (ii) ***F(7.5)***Ni−Al LDH, (iii) ***F(7.5)imp-***Ni−Al LDH, and (iv) Na_3AlF_6. The intensities of (i), (ii), and (iii) were normalized with that of Ni $2p_{3/2}$ peak.

improved the photocatalytic conversion of CO_2 to CO. To confirm the existence of AlF_6^{3-} units on the surface of ***F(7.5)***Ni−Al LDH and ***F(7.5)imp-***Ni−Al LDH, F 1s X-ray photoelectron spectroscopy was performed (as shown in **Figure 6)**. The peak at around 684.0 eV in the profile of ***F(7.5)***Ni−Al LDH suggested that fluorine atoms were present on the surface of this material. However, no peak was observed in the profile of ***F(0)***Ni−Al LDH. Furthermore, the normalized intensity of ***F(7.5)imp-***Ni−Al LDH was larger than that of ***F(7.5)***Ni−Al LDH, indicating that the concentration of AlF_6^{3-} units on the surface was higher in ***F(7.5)imp-***Ni−Al LDH than it was in ***F(7.5)***Ni−Al LDH. The peak position of ***F(7.5)***Ni−Al LDH shifted to a slightly lower binding energy in comparison to that of ***F(7.5)imp-***Ni−Al LDH, while the peak of ***F(7.5)imp-***Ni−Al LDH was found at almost the same position as Na_3AlF_6. This result provides strong evidence in support of the hypothesis stating that AlF_6^{3-} units are randomly incorporated in the hydroxide sheets, because the fluorine atoms of the AlF_6^{3-} units that constitute the hydroxide sheets are negatively charged. In other words, fluorine atoms that participate in the structure of Ni^{2+}−F−Al^{3+} within the hydroxide sheets have a higher negative charge than those in bare AlF_6^{3-} units (Al^{3+}−F−Al^{3+}). The F 1s XPS profile results reflect this change in the environment of fluorine atoms along with the incorporation of AlF_6^{3-} units in the $Ni(OH)_2$ structure.

Figure 5(E) shows that a certain amount of H_2 and a small amount of CO were produced when, instead of CO_2, Ar was introduced. The CO evolved in this experiment originated from the

naturally adsorbed CO_2 species and/or the CO_3^{2-} preserved in the interlayer space. **Figure 7(a)** shows the results of GC-MS analysis for the photocatalytic conversion of ^{13}C-labeled CO_2 (99 atom% of the isotopic purity) in an aqueous NaCl solution using ***F(7.5)***Ni−Al LDH as the photocatalyst. GC-MS analysis was conducted to reveal the carbon source of the product. The peak at 600 s in GC chromatogram is assigned to CO. The sharp peak in the profile of *m/z* = 29, which can be found at the same retention time, is attributed to ^{13}C-labeled CO. This indicated that the carbon source of CO evolved in this photocatalytic system is the CO_2 gas that was introduced as a substrate. In addition, **Figure 7(b)** displays the amounts of products produced after 20 h of photoirradiation for the photocatalytic conversion of ^{13}C-labeled CO_2 using ***F(7.5)***Ni−Al LDH. The total amount of CO evolved (^{12}CO + ^{13}CO), which was evaluated by TCD-GC, was 93.3 μmol, whereas the amount of H_2 evolved was 24.7 μmol. These results indicated that the selectivity towards CO among the reduction products was around 80% after 20 h of photoirradiation. By determination of peak area in the profile of *m/z* = 29, it was estimated that almost 94% of the CO evolved was ^{13}C-labled CO. Since it is difficult to detect small amount of unlabeled CO because of the high base level of the *m/z* = 28 peak, which is attributed to the contaminated air in the Q-Mass apparatus, the quantification of ^{13}CO using the profile of *m/z* = 29 is necessary for confirming the actual origin of CO. Additionally, a certain amount of HClO was produced as an oxidation product in the reaction solution. As previously

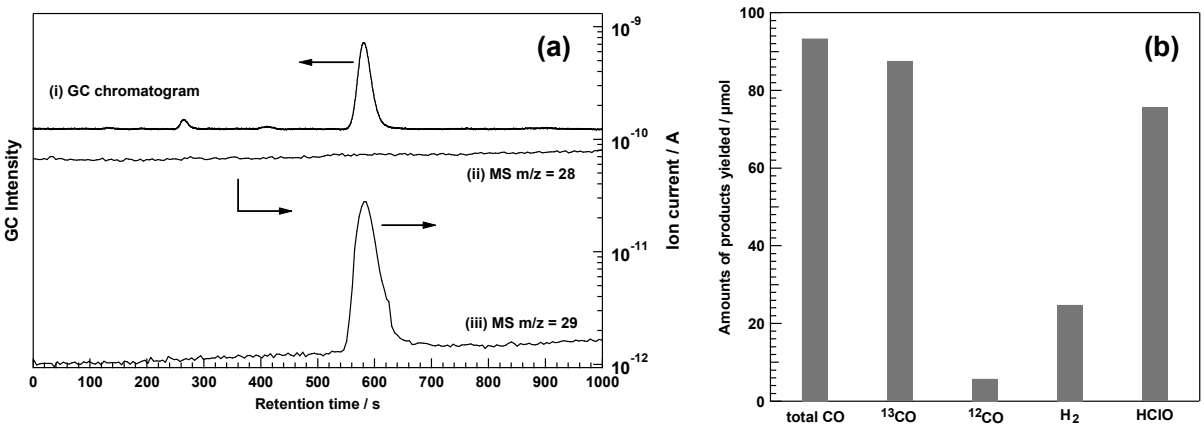

Figure 7 (a) GC-MS chromatogram for the photocatalytic conversion of ^{13}C-labeled CO_2 in an aqueous solution of NaCl using ***F(7.5)***Ni−Al LDH as a photocatalyst. (i) GC chromatogram detected by TCD, ion current profile of (ii) *m/z* = 28, and (iii) *m/z* = 29. (b) Amounts of products yielded after 20 h of photoirradiation quantified by using the TCD-GC for "total CO" and "H_2", the Q-Mass for "^{13}CO", and the DPD test for "HClO".

reported by our group, HClO is formed via disproportionation of Cl_2 in water, which is formed by the oxidation of Cl^- [38]. We previously confirmed the stoichiometric formation of HClO via two-electron oxidation of Cl^-, which can be detected by the DPD test [56, 57], with the evolution of reduction products such as CO and H_2 over Ni−Al LDH. In the present study, the amount of HClO produced in the reaction solution was less than the stoichiometric amount, which indicated that some of the photogenerated holes have been scavenged by another process. The photocatalytic activity clearly decreased in the absence of NaCl additive. Therefore, we conclude that the photocatalytic conversion of CO_2 to CO over fluorinated Ni−Al LDH (***F(x)***Ni−Al LDH) in an aqueous NaCl solution proceeds using Cl^- as a hole scavenger. The results also show that the fluorination of LDH by incorporation of AlF_6^{3-} units in hydroxide sheets affords surface properties suitable for the photocatalytic conversion of CO_2 in the presence of Cl^-. Moreover, the structural change was not observed in ***F(7.5)***Ni−Al LDH which was used in the photocatalytic conversion of CO_2 for 20 h as compared to that before the reaction, indicating that the stability of the fluorinated Ni−Al LDH photocatalyst is considered to be sufficient for the use in the photocatalytic reactions.

Conclusion

We found that the fluorination of Mg−Al LDH and Ni−Al LDH improved the photocatalytic conversion of CO_2 to CO in an aqueous NaCl solution under UV light irradiation. After 20 h of photoirradiation over ***F(7.5)***Ni−Al LDH, the amount of CO evolved via reduction of CO_2 and the selectivity towards CO among the reduction products were 93.3 μmol and 80%, respectively. When compared to ***F(7.5)imp-***Ni−Al LDH, the incorporation of AlF_6^{3-} units in the hydroxide sheets causes significant improvement in the photocatalytic conversion of CO_2 to CO. The isotopic experiment revealed that almost all of the evolved CO originated from the CO_2 gas that was introduced as a substrate. In addition, a certain amount of hypochlorous acid (HClO) was produced as an oxidation product in the reaction solution. We conclude that the fluorination of LDH by incorporation of AlF_6^{3-} units in the hydroxide sheets affords surface properties suitable for the photocatalytic conversion of CO_2 in the presence of Cl^-, which acts as a hole scavenger.

References

1. Y. Kohno, T. Tanaka, T. Funabiki and S. Yoshida, *Chemical Communications*, 1997, 841-842.
2. Y. Kohno, T. tanaka, T. Funabiki and S. Yoshida, *Chemistry Letters*, 1997, **26**, 993-994.
3. Y. Kohno, T. Tanaka, T. Funabiki and S. Yoshida, *Journal of the Chemical Society, Faraday Transactions*, 1998, **94**, 1875-1880.
4. Y. Kohno, T. Tanaka, T. Funabiki and S. Yoshida, *Physical Chemistry Chemical Physics*, 2000, **2**, 2635-2639.
5. Y. Kohno, H. Ishikawa, T. Tanaka, T. Funabiki and S. Yoshida, *Physical Chemistry Chemical Physics*, 2001, **3**, 1108-1113.
6. K. Teramura, T. Tanaka, H. Ishikawa, Y. Kohno and T. Funabiki, *The Journal of Physical Chemistry B*, 2004, **108**, 346-354.
7. K. Teramura, S. Okuoka, H. Tsuneoka, T. Shishido and T. Tanaka, *Applied Catalysis B: Environmental*, 2010, **96**, 565-568.
8. H. Tsuneoka, K. Teramura, T. Shishido and T. Tanaka, *The Journal of Physical Chemistry C*, 2010, **114**, 8892-8898.
9. F. Cavani, F. Trifirò and A. Vaccari, *Catalysis Today*, 1991, **11**, 173-301.
10. B. F. Sels, D. E. De Vos and P. A. Jacobs, *Catalysis Reviews*, 2001, **43**, 443-488.
11. C. Delhoyo, *Applied Clay Science*, 2007, **36**, 103-121.
12. K. Ebitani, K. Motokura, K. Mori, T. Mizugaki and K. Kaneda, *The Journal of Organic Chemistry*, 2006, **71**, 5440-5447.
13. G. Abellan, E. Coronado, C. Marti-Gastaldo, J. Waerenborgh and A. Ribera, *Inorganic Chemistry*, 2013, **52**, 10147-10157.
14. F. Giovannelli, M. Zaghrioui, C. Autret-Lambert, F. Delorme, A. Seron, T. Chartier and B. Pignon, *Materials Chemistry and Physics*, 2012, **137**, 55-60.
15. M. Gong, Y. Li, H. Wang, Y. Liang, J. Z. Wu, J. Zhou, J. Wang, T. Regier, F. Wei and H. Dai, *Journal of the American Chemical Society*, 2013, **135**, 8452-8455.
16. Y. Guo, Z. Zhu, Y. Qiu and J. Zhao, *Journal of Hazardous Materials*, 2012, **239–240**,

279-288.

17. L. Huang, S. Chu, J. Wang, F. Kong, L. Luo, Y. Wang and Z. Zou, *Catalysis Today*, 2013, **212**, 81-88.

18. T. Iwasaki, H. Yoshii, H. Nakamura and S. Watano, *Applied Clay Science*, 2012, **58**, 120-124.

19. B. Li, Y. Zhao, S. Zhang, W. Gao and M. Wei, *ACS Applied Materials & Interfaces*, 2013, **5**, 10233-10239.

20. H. Lin, Y. Zhang, G. Wang and J.-B. Li, *Frontiers of Materials Science*, 2012, **6**, 142-148.

21. J. Prince, F. Tzompantzi, G. Mendoza-Damián, F. Hernández-Beltrán and J. S. Valente, *Applied Catalysis B: Environmental*, 2015, **163**, 352-360.

22. F. B. Saiah, B. L. Su and N. Bettahar, *Journal of Hazardous Materials*, 2009, **165**, 206-217.

23. C. G. Silva, Y. Bouizi, V. Fornés and H. García, *Journal of the American Chemical Society*, 2009, **131**, 13833-13839.

24. F. Song and X. Hu, *Journal of the American Chemical Society*, 2014, **136**, 16481-16484.

25. T. Takei, A. Miura, N. Kumada and K. Okada, *Journal of Porous Materials*, 2012, **20**, 777-783.

26. L. Tian, Y. Zhao, S. He, M. Wei and X. Duan, *Chemical Engineering Journal*, 2012, **184**, 261-267.

27. X. Xu, R. Lu, X. Zhao, S. Xu, X. Lei, F. Zhang and D. G. Evans, *Applied Catalysis B: Environmental*, 2011, **102**, 147-156.

28. X. Zhang, Z. Wang, N. Qiao, S. Qu and Z. Hao, *ACS Catalysis*, 2014, **4**, 1500-1510.

29. L. Mohapatra and K. M. Parida, *Separation and Purification Technology*, 2012, **91**, 73-80.

30. L. Mohapatra and K. M. Parida, *Physical Chemistry Chemical Physics*, 2014, **16**, 16985-16996.

31. M. Shao, J. Han, M. Wei, D. G. Evans and X. Duan, *Chemical Engineering Journal*, 2011, **168**, 519-524.

32. J. Sun, Y. Zhang, J. Cheng, H. Fan, J. Zhu, X. Wang and S. Ai, *Journal of Molecular Catalysis A: Chemical*, 2014, **382**, 146-153.

33. S. J. Xia, F. X. Liu, Z. M. Ni, J. L. Xue and P. P. Qian, *Journal of Colloid and Interface*

Science, 2013, **405**, 195-200.

34. J. Hong, Y. Wang, J. Pan, Z. Zhong and R. Xu, *Nanoscale*, 2011, **3**, 4655-4661.
35. Y. Zhao, P. Chen, B. Zhang, D. S. Su, S. Zhang, L. Tian, J. Lu, Z. Li, X. Cao, B. Wang, M. Wei, D. G. Evans and X. Duan, *Chemistry A Europian Journal*, 2012, **18**, 11949-11958.
36. K. Teramura, S. Iguchi, Y. Mizuno, T. Shishido and T. Tanaka, *Angewandte Chemie International Edition*, 2012, **51**, 8008-8011.
37. S. Iguchi, K. Teramura, S. Hosokawa and T. Tanaka, *Catalysis Today*, 2015, **251**, 140-144.
38. S. Iguchi, K. Teramura, S. Hosokawa and T. Tanaka, *Physical Chemistry Chemical Physics*, 2015, **17**, 17995-18003.
39. T. Mitsudome, Y. Mikami, H. Funai, T. Mizugaki, K. Jitsukawa and K. Kaneda, *Angewandte Chemie International Edition*, 2008, **47**, 138-141.
40. T. Mitsudome, A. Noujima, T. Mizugaki, K. Jitsukawa and K. Kaneda, *Advanced Synthesis & Catalysis*, 2009, **351**, 1890-1896.
41. C. Pendem, P. Gupta, N. Chaudhary, S. Singh, J. Kumar, T. Sasaki, A. Datta and R. Bal, *Green Chemistry*, 2012, **14**, 3107-3113.
42. E. A. Gardner, S. K. Yun, T. Kwon and T. J. Pinnavaia, *Applied Clay Science*, 1998, **13**, 479-494.
43. D. Carriazo, S. Lima, C. Martín, M. Pillinger, A. A. Valente and V. Rives, *Journal of Physics and Chemistry of Solids*, 2007, **68**, 1872-1880.
44. S. Omwoma, W. Chen, R. Tsunashima and Y. Song, *Coordination Chemistry Reviews*, 2014, **258–259**, 58-71.
45. A. Corma, V. Fornes, F. Rey, A. Cervilla, E. Llopis and A. Ribera, *Journal of Catalysis*, 1995, **152**, 237-242.
46. M. Elena Pérez-Bernal, R. Ruano-Casero and T. Pinnavaia, *Catalysis Letters*, 1991, **11**, 55-61.
47. E. P. Giannelis, D. G. Nocera and T. J. Pinnavaia, *Inorganic Chemistry*, 1987, **26**, 203-205.
48. U. Costantino, N. Coletti, M. Nocchetti, G. G. Aloisi and F. Elisei, *Langmuir*, 1999, **15**, 4454-4460.
49. S. Pausova, J. Krysa, J. Jirkovsky, G. Mailhot and V. Prevot, *Environmental Science and*

Pollution Research, 2012, **19**, 3709-3718.

50. Z. Huang, P. Wu, Y. Lu, X. Wang, N. Zhu and Z. Dang, *Journal of Hazardous Materials*, 2013, **246-247**, 70-78.
51. J. S. Valente, F. Tzompantzi and J. Prince, *Applied Catalysis B: Environmental*, 2011, **102**, 276-285.
52. E. Lima, M. d. J. Martínez-Ortiz, R. I. G. Reyes and M. Vera, *Inorganic Chemistry*, 2012, **51**, 7774-7781.
53. G. Wu, X. Wang, B. Chen, J. Li, N. Zhao, W. Wei and Y. Sun, *Applied Catalysis A: General*, 2007, **329**, 106-111.
54. G. Wu, X. Wang, W. Wei and Y. Sun, *Applied Catalysis A: General*, 2010, **377**, 107-113.
55. M. G. Álvarez, R. J. Chimentão, F. Figueras and F. Medina, *Applied Clay Science*, 2012, **58**, 16-24.
56. L. Moberg and B. Karlberg, *Analytica Chimica Acta*, 2000, **407**, 127-133.
57. K. Carlsson, L. Moberg and B. Karlberg, *Water Research*, 1999, **33**, 375-380.
58. H. D. B. Jenkins and K. P. Thakur, *Journal of Chemical Education*, 1979, **56**, 576-577.
59. N. Ahmed, Y. Shibata, T. Taniguchi, Y. Izumi, *Journal of Catalysis*, 2011, **279**, 123-135.
60. M. Morikawa, N. Ahmed, Y. Yoshida, Y. Izumi, *Applied Catalysis B: Environmental*, 2014, **144**, 561-569.
61. M. Morikawa, Y. Ogura, N. Ahmed, S. Kawamura, G. Mikami, S. Okamoto, Y. Izumi, *Catalysis Science & Technology*, 2014, **4**, 1644-1651.
62. K. Katsumata, K. Sakai, K. Ikeda, G. Carja, N. Matsushita, K. Okada, *Materials Letters*, 2013, **107**, 138-140.

Chapter 4

Preparation of Transition Metal-containing Layered Double Hydroxides and Application to the Photocatalytic Conversion of CO_2 in Water

Abstract

Layered double hydroxides (LDHs) have been paid great attention in the field of the photocatalysis due to their interesting physicochemical properties such as positively charged hydroxide sheet, compositional flexibilities, and large surface area. We previously reported that the use of Ni−Al LDH as a photocatalyst enabled us to achieve the maximum conversion of CO_2 to CO with high selectivity among a series of synthesized LDHs, and chloride ions (Cl^-) in the reaction solution enhanced the amount of CO evolved. In this study, we attempted to prepare 16 different kinds of transition metal containing M^{2+}−M^{3+} LDHs (M^{2+} = Co^{2+}, Ni^{2+}, Cu^{2+}, and Zn^{2+}; M^{3+} = V^{3+}, Cr^{3+}, Mn^{3+}, and Fe^{3+}) and applied them to the photocatalytic conversion of CO_2 in an aqueous solution of NaCl. Ni−V LDH, which has large specific surface area, exhibited the highest activity for the CO evolution among these LDHs; however the formation of H_2 as a reduction product of protons (H^+) was totally suppressed. It is estimated that a combination of V^{3+} and Cl^- plays a significant role for the high photocatalytic activity and the high selectivity toward CO formation.

Introduction

Layered double hydroxides (LDHs) with a general formula of $[M^{2+}_{1-x}–M^{3+}_{x}(OH)_2](A^{n-})_{x/n}\cdot mH_2O$ are known as anionic clays that have highly ordered layer structures in the *c*-axis direction, where M^{2+} and M^{3+} are divalent and trivalent cations, respectively [1,2]. The value of *x* represents the molar ratio of $M^{3+}/(M^{2+} + M^{3+})$, whereas A^{n-} is the interlayer anion of valence *n*. Generally, the value of *m* indicates the extent of hydration, which is highly influenced by the surrounding environment such as atmosphere, temperature, and humidity. The natures of M^{2+}, M^{3+}, *x*, and A^{n-} can vary over a wide range; hence, a series of isostructural materials with various chemical properties can be synthesized [3]. When the *x* value is outside of the 0.2−0.4 range, hydroxides or other compounds can form as impurity phases. The best-known LDH material is hydrotalcite, which has a structural formula of $Mg_6Al_2(OH)_{16}CO_3\cdot 4H_2O$. Various LDHs can be formed by fully or partially replacing Mg^{2+} or Al^{3+} with divalent (M^{2+} = Fe^{2+}, Co^{2+}, Ni^{2+}, Cu^{2+}, Zn^{2+}, Mn^{2+}, Cd^{2+}, and Ca^{2+}) or trivalent cations (M^{3+} = Co^{3+}, Fe^{3+}, Mn^{3+}, Ga^{3+}, Cr^{3+}, In^{3+}, V^{3+}, Y^{3+}, and La^{3+}), respectively [4-20]. Moreover, tetravalent cations (M^{4+} = Ti^{4+}, Zr^{4+}, and Sn^{4+}) are also reported to form LDH structures [21-28]; however, M^{4+} cations sometimes form amorphous oxides instead of incorporating within the hydroxide sheets. Recently, various LDHs have been applied to photocatalytic reactions such as degradation of organic compounds, water splitting, and conversion of CO_2. For example, García et al. reported that various Zn^{2+}-containing LDHs (Zn−Cr, Zn−Ti, and Zn−Ce LDHs) exhibited photocatalytic activity for O_2 evolution from an aqueous solution of $AgNO_3$ under visible light irradiation [18]. On the other hand, photocatalytic H_2 production from water, with lactic acid as a sacrificial electron donor, was demonstrated using Ni−Ti, Zn−Ti, and Mg−Al−Ti LDHs under visible light irradiation [26]. In addition, photocatalytic degradations of dyes and organic compounds using a series of LDHs as photocatalysts have also been recently introduced [9,24,25,29-37].

Photocatalytic conversion of CO_2 into valued chemicals such as CO, HCHO, HCOOH, CH_3OH, and CH_4 is one of the most promising methods to construct a sustainable carbon cycling system. We have previously reported that ZrO_2 [38-41], MgO [42,43], and Ga_2O_3 [44], on which basic surface sites were suitable for the adsorption of CO_2 molecules, showed photocatalytic activity for the conversion of CO_2 to CO in gas phase using H_2 as a reductant. CO_2 molecules that are adsorbed on

the basic sites of these materials can be altered into active species, which is necessary for the photocatalytic conversion of CO_2, as shown in previous literature [43,44]. Accordingly, solid base materials are promising candidates to develop a photocatalytic system for the conversion of CO_2. From this view point, we attempted to apply synthesized LDHs to the photocatalytic conversion of CO_2 into CO in water, and found that various M^{2+}–M^{3+} LDHs (M^{2+} = Mg^{2+}, Ni^{2+}, and Zn^{2+}; M^{3+} = Al^{3+}, Ga^{3+}, and In^{3+}) exhibited photocatalytic activity [45]. Similarly, Izumi et al. and Katsumata et al. also reported the photocatalytic conversion of CO_2 using Cu-containing LDHs [46-48] and noble metal-loaded LDHs [49], respectively. In our previous study, Ni−Al LDH, in particular, showed high activity and selectivity for CO formation among a series of LDHs; the amount of H_2 evolved as a reduction product of protons (H^+) derived from water was much smaller than those of the other LDHs [50]. Isotopic experiments using $^{13}CO_2$ as a substrate revealed that the CO evolved in the photocatalytic reaction over these LDHs originated from the introduced CO_2 substrate. The addition of chloride ions (Cl^-) to the reaction solution promoted the conversion of CO_2 to CO, and we confirmed that during the photocatalytic reaction, a stoichiometric amount of hypochlorous acid (HClO) was produced as an oxidation product of Cl^- in the reaction solution, which was quantified by *N,N'*-diethyl-*p*-phenylenediamine (DPD) tests [51,52]. This indicated that Cl^- can act as a hole scavenger and is oxidized into chlorine (Cl_2), which is immediately transformed into HClO in water [53]. In this study, we synthesized various transition metal-containing M^{2+}–M^{3+} LDHs (M^{2+} = Co^{2+}, Ni^{2+}, Cu^{2+}, and Zn^{2+}; M^{3+} = V^{3+}, Cr^{3+}, Mn^{3+}, and Fe^{3+}) and investigated their photocatalytic activities for the conversion of CO_2 in an aqueous NaCl solution under UV light irradiation.

Experimental

Various M^{2+}–M^{3+} layered double hydroxides (M^{2+}–M^{3+} LDHs, M^{2+} = Co^{2+}, Ni^{2+}, Cu^{2+}, and Zn^{2+}; M^{3+} = V^{3+}, Cr^{3+}, Mn^{3+}, and Fe^{3+}) were synthesized by a typical co-precipitation method, unless otherwise noted, with that the ratio of M^{2+} to M^{3+} (M^{2+}/M^{3+}) was fixed at 2. A mixed aqueous solution of precursors ($M^{2+}Cl_2$ and $M^{3+}Cl_3$) was slowly dropped to an aqueous solution of Na_2CO_3 at room temperature with a vigorous stirring. The pH was kept stable by adding an aqueous solution of NaOH during the precipitation using a liquid feeding pump (NRP-76, Nissin Rika) connected to a pH

controller (NPH-660NDE, Nissin Rika). The resulting suspension was aged at 333 K for 24 h with the stirring. The solid was collected by the suction filtration and rinsed with 1.0 L of ultra-pure water, and then dried at 333 K in a vacuum oven. Organic chemicals and solvents were not used throughout each step of the LDH preparation procedure to prevent a contamination of carbon residue in the photocatalytic reaction.

The powder X-ray diffraction (XRD) patterns of prepared M^{2+}–M^{3+} LDHs were measured by an X-ray diffractometer (Ultime IV, Rigaku), using Cu K_α radiation (λ = 0.154 nm) at a scan rate of 4.0° min^{-1}. The morphology of these as-synthesized samples were investigated from SEM images, which were captured by using a field emission scanning electron microscope (SU-8220, Hitachi High-Technologies) at an acceleration voltage of 3.0 kV. The specific surface areas of LDHs were estimated from their N_2 adsorption isotherms at 77 K via BET method using an adsorption analyzer (BELSORP-miniII, BEL Japan). Prior to the measurements, each sample was evacuated at 383 K for 1 h using a pretreatment system (BELPREP-vacII, BEL Japan). The thermal analysis for the prepared LDHs were performed using a thermobalance (Thermo Plus 2, Rigaku). A certain amount of sample powder was set in the furnace, and the change of sample weight was recorded with the increasing temperature under a dried air flowing at a flow rate of 80 mL min^{-1}. UV/Vis diffuse reflectance spectra of LDHs were obtained using a UV-Vis Spectrometer (V-670, JASCO) equipped with an integrated sphere accessory.

The photocatalytic conversion of CO_2 in an aqueous solution of NaCl was carried out using an inner-irradiation type reaction vessel under CO_2 gas flow. 0.5 g of as-synthesized photocatalyst powder was dispersed in 1.0 L of an aqueous solution of NaCl (0.1 M), and He or CO_2 gas was bubbled into the suspension to degas the dissolved air. The suspension was illuminated with a 400 W high-pressure mercury lamp through a quartz filter equipped with a cooling water system under a flow of CO_2 gas at a flow rate of 15 mL min^{-1}. The products such as CO, H_2, and O_2 were analyzed by a barrier discharge ionization detector (BID) gas chromatograph (GC-2010 Tracera, Shimadzu Corp.,), which was connected to the reactor online, equipped with a MICROPACKED ST column using He gas as a carrier. Amount of metal ions in the reaction solution which were eluted from the photocatalyst powder during the photocatalytic reaction was estimated by the elemental analysis using an ICP-OES (iCAP7400 Duo, Thermo Fisher Scientific, Inc.).

Results and discussion

Figure 1 shows the X-ray diffraction (XRD) patterns of powder samples synthesized via the coprecipitation method using each of the metal chlorides as precursors (M^{2+}/M^{3+} = 2, if not otherwise specified). A series of LDHs (Co−Cr, Co−Fe, Ni−V, Ni−Cr, Ni−Mn, Ni−Fe, Zn−Cr, Zn−Mn, and Zn−Fe LDH) exhibited characteristic diffraction peaks corresponding to the LDH structure [1], which are presented as asterisks (*) in **Figure 1(a-d)**. Two sharp diffraction peaks assigned to (0 0 3) and (0 0 6) planes reflections, were located around 11−12° and 22−24°, respectively. The broadened (0 0 9) diffraction peak around 33−35° was difficult to separate from the (0 1 2) plane. The (0 0 3), (0 0 6), and (0 0 9) diffraction peaks are related to the structure layered toward the *c*-axis direction. The

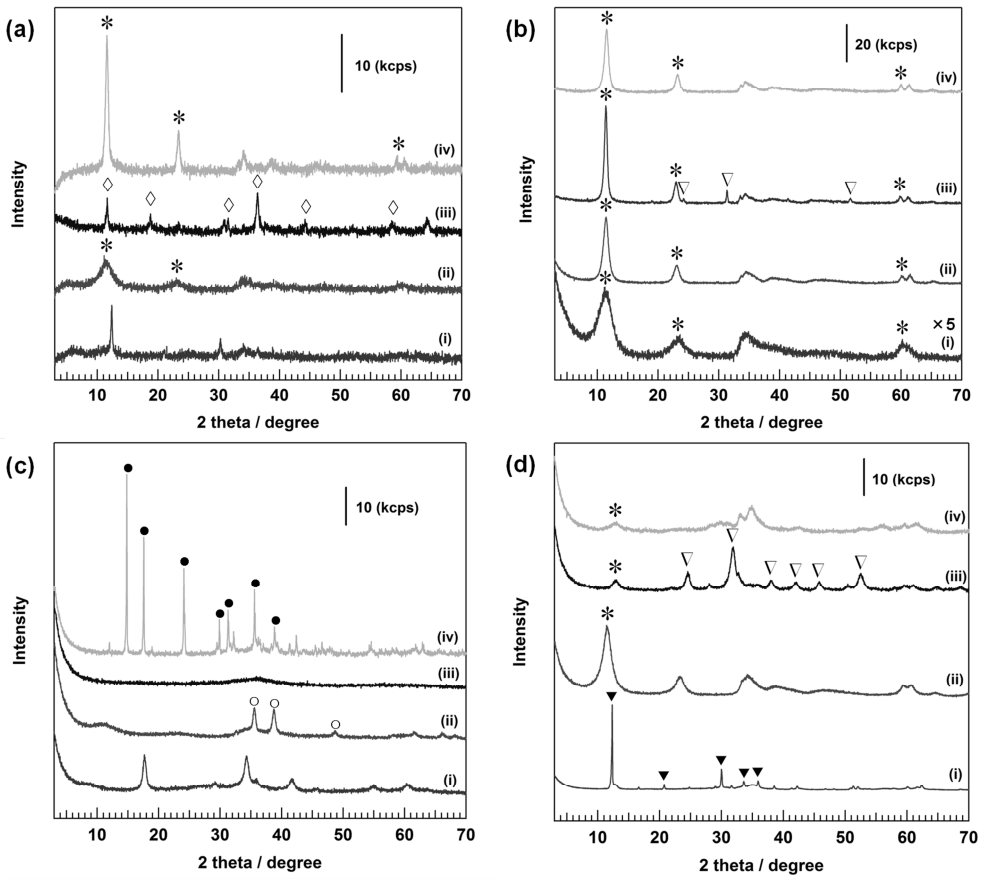

Figure 1 XRD patterns of **(a)** Co−M^{3+} LDHs, **(b)** Ni−M^{3+} LDHs, **(c)** Cu−M^{3+} LDHs, and **(d)** Zn−M^{3+} LDHs. M^{3+} = (i) V^{3+}, (ii) Cr^{3+}, (iii) Mn^{3+}, and (iv) Fe^{3+}. The characteristic peaks are marked with asterisk (*), diamond (◊), white triangle (Δ), black circle (●), white circle (○), and black triangle (▼), which are respectively assigned to LDH structure, Co_3O_4, rhodochrosite ($MnCO_3$), $CuFeO_2$, CuO, and $Zn_3(OH)_2V_2O_7 \cdot 2H_2O$.

existence of a layer structure is commonly determined by the reflection peak of the (0 0 3) plane. The other two intense peaks around 60−63°, which sometimes occur as a single broad peak, are indexed as (1 1 0) and (1 1 3) planes with respect to the hexagonal unit. These reflections can be utilized for calculating parameter a ($a = 2d_{(1\,1\,0)}$); the value of a depends on the nature of the metal cations of the hydroxide sheets and the ratio of the metal components. These results indicated that Ni−M^{3+} (M^{3+} = V^{3+}, Cr^{3+}, Mn^{3+}, and Fe^{3+}), Co−Cr, Co−Fe, and Zn−Cr LDHs have relatively advanced layer structures along the c-axis direction, whereas Zn−Mn, and Zn−Fe LDHs have layer structures with impurity phases. On the other hand, the other precipitated samples in this study, Cu−M^{3+} (M^{3+} = V^{3+}, Cr^{3+}, Mn^{3+}, and Fe^{3+}), Co−V, Co−Mn, and Zn−V, did not form LDH structures. Diffraction peaks assigned to Co_3O_4 (◊) were found in the Co−Mn sample, as shown in **Figure 1(a)**. In addition, $CuFeO_2$ (●) and CuO (○) phases were confirmed in the XRD patterns of Cu−Fe and Cu−Cr precipitates, respectively, which are presented in **Figure 1(c)**. The impurity phases, as marked with white triangles (▽) and black triangles (▼) in **Figure 1(d)**, correspond to rhodochrosite ($MnCO_3$) and $Zn_3(OH)_2V_2O_7{\cdot}2H_2O$, respectively. Moreover, the $MnCO_3$ phase reflection (▽) was also confirmed in the diffraction pattern of Ni−Mn LDH, as shown in **Figure 1(b)**, indicating that $MnCO_3$ crystals formed as an impurity phase in the Ni−Mn LDH structure. None of the peaks in the XRD patterns of Co−V and Cu−V precipitates could be assigned to any reported crystal phases.

Table 1 summarizes the existence of the LDH structure determined from the XRD patterns, specific surface area (S_{BET}), and full width at half maximum of the (0 0 3) plane reflection ($FWHM_{(0\,0\,3)}$) for each of the synthesized samples in this study. As mentioned above, the characteristic layer structure of Co−Cr, Co−Fe, Ni−V, Ni−Cr, Ni−Mn, Ni−Fe, Zn−Cr, Zn−Mn, and Zn−Fe LDHs were confirmed using the XRD patterns. On the other hand, Co−V, Co−Mn, Cu−M^{3+} (M^{3+} = V^{3+}, Cr^{3+}, Mn^{3+}, and Fe^{3+}), and Zn−V precipitates had no LDH structure, although it was previously reported that Co−Mn [11,14], Cu−Cr [10], and Cu−Fe [19] LDHs were successfully synthesized. In order to achieve the LDH structure for these precipitates, it is necessary to optimize the detailed preparation procedure, such as the precursor concentration in the solution, the conditions during co-precipitation (pH, temperature, and atmosphere), and the conditions of aging, rinsing, and drying. In this study, all samples were prepared via a unified procedure, as presented in the experimental section. Among the successfully synthesized LDHs, Ni−M^{3+} (M^{3+} = V^{3+}, Cr^{3+}, Mn^{3+}, and Fe^{3+}) LDHs exhibited relatively

Table 1 Summary of the characterizations and the photocatalytic activity test for the synthesized 16 different kinds of M^{2+}–M^{3+} LDHs (M^{2+} = Co^{2+}, Ni^{2+}, Cu^{2+}, and Zn^{2+}; M^{3+} = V^{3+}, Cr^{3+}, Mn^{3+}, and Fe^{3+}). [a] LDH structure was judged from the XRD patterns. [b] S_{BET} was estimated from the N_2 absorption isotherms at 77 K. [c] Amounts of products evolved were evaluated by the photocatalytic reaction. [d] Selectivity to CO_2 reduction was calculated by using the formula; Selectivity to CO_2 reduction (%) = 100 × ((CO + CH_4) / (CO + CH_4 + H_2)).

Components		LDH structure	S_{BET} / m^2 g^{-1}	$FWHM_{(003)}$ / degree	Amounts of products evolved / μmol			Selectivity to CO_2 reduction (%)
divalent	trivalent				CO	CH_4	H_2	
Co	V	—	12	—	3.3	1.4	0.2	96
	Cr	○	140	3.1	40.2	1.0	3.0	93
	Mn	—	52	—	59.8	trace	2.0	97
	Fe	○	110	0.6	109.1	5.2	6.6	95
Ni	V	○	200	2.2	147.1	trace	4.2	97
	Cr	○	75	1.1	4.6	0.0	2.8	62
	Mn	○	27	0.6	4.6	0.0	17.0	21
	Fe	○	30	0.9	29.0	1.3	7.9	79
Cu	V	—	48	—	9.4	0.0	4.3	69
	Cr	—	60	—	2.0	trace	4.1	33
	Mn	—	39	—	2.4	0.0	0.2	92
	Fe	—	55	—	5.3	0.0	0.8	87
Zn	V	—	70	—	3.8	0.0	0.0	100
	Cr	○	260	1.7	34.0	0.0	7.1	83
	Mn	○	81	2.5	24.0	0.0	30.0	44
	Fe	○	140	—	3.3	0.0	27.0	11

small $FWHM_{(0\ 0\ 3)}$ values, indicating that Ni–M^{3+} LDHs have an advanced characteristic layer stacking along the *c*-axis. Co–Cr, Co–Fe, Ni–V, Zn–Cr, and Zn–Fe LDHs exhibited particularly large specific surface areas, whereas it was known that the specific surface areas of a series of LDH materials were less than 100 m^2 g^{-1} [1,50]. Previously, we have reported that Ni–Al LDH, which has a large surface area, can produce large amounts of CO as a reduction product of CO_2 in an aqueous solution under UV light irradiation. This indicates that the adsorption of CO_2 molecules on the surface of the Ni–Al LDH photocatalyst is a significant process for the selective conversion of CO_2. **Table 1** also lists the amounts of products evolved in the gas phase and the selectivity toward CO_2 reduction in the photocatalytic conversion of CO_2 in an aqueous NaCl solution using 16 different precipitated samples as photocatalysts for 5 h of photoirradiation. Each sample showed photocatalytic activity without pretreatment or modification. Reduction products such as CO, CH_4, and H_2 were produced in the gas phase. The photocatalytic activities presented in this study did not

correspond with the magnitude of the specific surface areas of the LDH photocatalysts. Ni−V LDH, Co−Fe LDH, and Co−Mn precipitate (no LDH structure) evolved larger amounts of CO than that evolved by Ni−Al LDH, which was previously reported by our group as a good photocatalyst for this reaction [53]. The amount of H_2 produced over these photocatalysts as a reduction product of H^+ was less than that of CO, indicating that these photocatalysts achieved a selective reduction of CO_2 to CO and CH_4 under UV light irradiation. In particular, Ni−V LDH evolved 147.1 μmol of CO after 5 h of photoirradiation, and the selectivity toward CO formation among the reduction products was 97%. Moreover, Co−Cr LDH, Co−Fe LDH, Ni−Fe LDH, and Co−V precipitate enabled the production of a certain amount of CH_4, which is known as an eight-electron reduction product of CO_2.

Figure 2 exhibits the weight loss profiles of Ni−M^{3+} (M^{3+} = V^{3+}, Cr^{3+}, Mn^{3+}, and Fe^{3+}) LDHs measured by thermogravimetric analysis (TGA), which is typically used to characterize the LDH structure in the prepared samples. Several weight losses were present in the TGA profiles of these as-prepared LDHs. It has been reported that LDHs show characteristic two-step weight losses with increasing temperature [1]. The initial step at < 473 K was caused by the desorption of water molecules preserved on the surface and in the interlayer. The second step above 473 K was caused by the collapse of the layer structure, accompanied by dehydration of the hydroxyl groups and decomposition of the charge compensating interlayer anions. As shown in **Figure 2**, Ni−V, Ni−Cr, and Ni−Fe LDHs exhibited two-step weight loss curves with the increase in temperature. It is

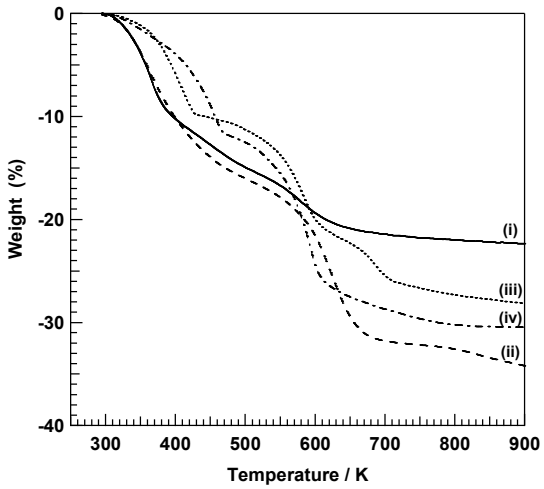

Figure 2 Weight loss profiles of Ni−M^{3+} LDHs (M^{3+} = (i) V^{3+}, (ii) Cr^{3+}, (iii) Mn^{3+}, and (iv) Fe^{3+}) in a thermal gravimetric analysis. Atmosphere: dried air flow at a rate of 80 mL min^{-1}, temperature increasing rate: 5 K min^{-1}.

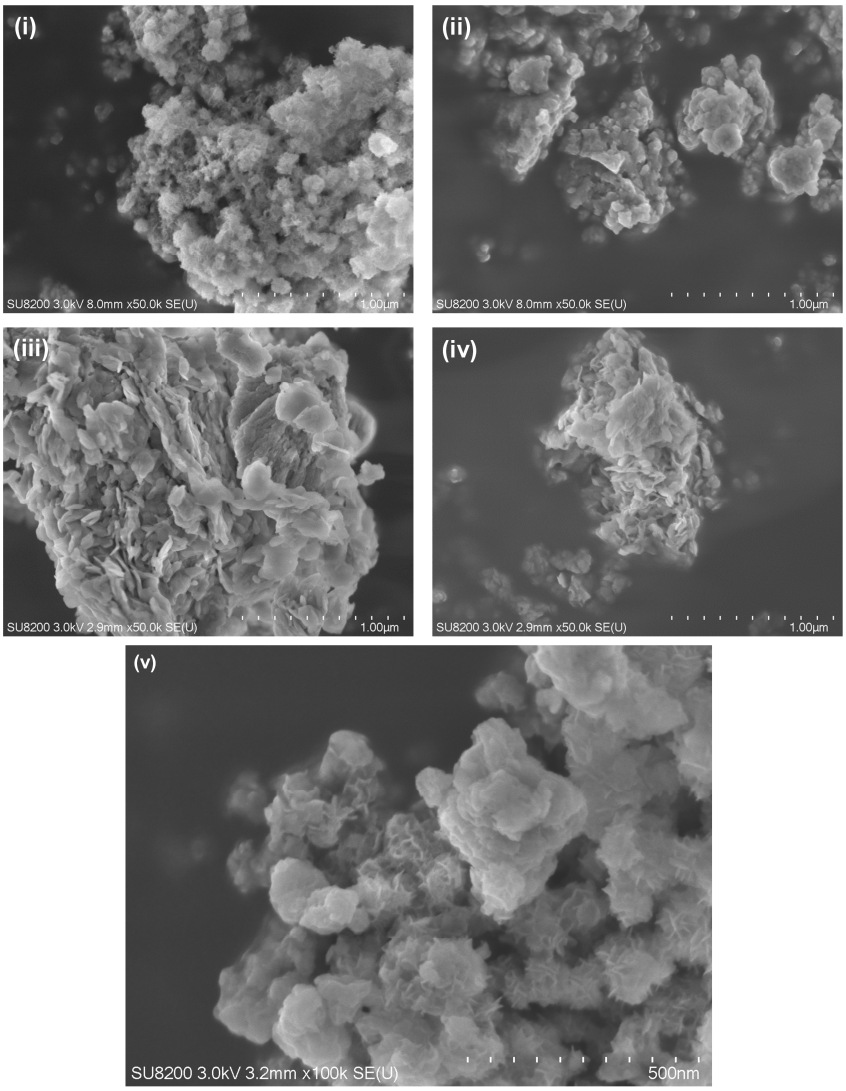

Figure 3 SEM images of the synthesized Ni−M^{3+} (M^{3+} = (i) V^{3+}, (ii) Cr^{3+}, (iii) Mn^{3+}, (iv) Fe^{3+}) LDHs, and (v) enlarged view of the SEM image of Ni−V LDH.

expected that the LDH structures of these samples were converted into mixed oxide phases above 700 K. In the case of Ni−Mn LDH, however, another weight loss occured after the second step. It is presumed that this third weight loss was due to the decomposition of $MnCO_3$ into Mn_2O_3 [54], indicating that the layer structure of Ni−Mn LDH would collapse at the second step to form $MnCO_3$, and then became a mixed oxide phase at the third step. The morphologies of the synthesized Ni−M^{3+} (M^{3+} = V^{3+}, Cr^{3+}, Mn^{3+}, and Fe^{3+}) LDHs were investigated using scanning electron microscopy (SEM) images, as displayed in **Figure 3**. The assembly of many platelet structures was observed in the SEM images of Ni−Fe, Ni−Mn, and Ni−V LDHs. Ni−Cr LDH did not show the sheet structure, although characteristic diffraction peaks due to the layer structure were clearly confirmed in the XRD

pattern. The platelet structure of the Ni−V LDH was much smaller than those of the other LDHs, which is consistent with the BET surface area results showing that the Ni−V LDH has the largest specific surface area among the Ni−M^{3+} (M^{3+} = V^{3+}, Cr^{3+}, Mn^{3+}, and Fe^{3+}) LDHs.

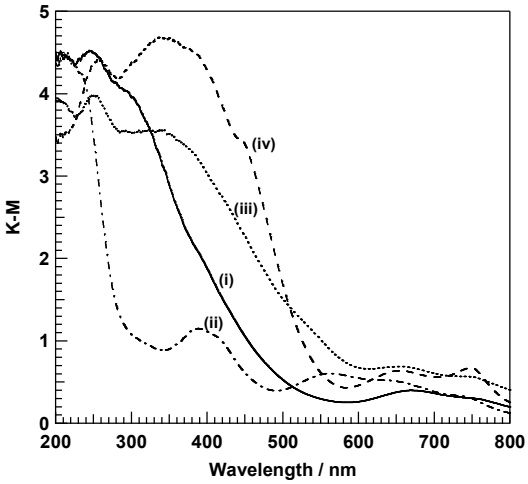

Figure 4 UV/Vis diffuse reflectance spectra of Ni−M^{3+} LDHs (M^{3+} = (i) V^{3+}, (ii) Cr^{3+}, (iii) Mn^{3+}, and (iv) Fe^{3+}).

UV/Vis diffuse reflectance spectra of Ni−M^{3+} (M^{3+} = V^{3+}, Cr^{3+}, Mn^{3+}, and Fe^{3+}) LDHs are presented in **Figure 4**. Absorption peaks due to the d-d transition of Ni^{2+} and each M^{3+} were found in the visible region. The photocatalytic reaction did not proceed thoroughly using a Pyrex jacket equipped with a cooling system, whereas the use of a quartz jacket helped achieve suitable photocatalytic activity. It can be speculated that UV light irradiation < 280 nm is necessary to induce the photocatalytic reaction over Ni−M^{3+} LDHs.

Figure 5(a) displays the formation rates of CO and H_2 evolved in the photocatalytic conversion of CO_2 in an aqueous NaCl solution after 1 h of photoirradiation using Ni−M^{3+} (M^{3+} = V^{3+}, Cr^{3+}, Mn^{3+}, and Fe^{3+}) LDHs, Ni−Al LDH, and $Ni(OH)_2$ as photocatalysts. The amount of H_2 evolved was less than that of CO in all cases, indicating that selective CO_2 reduction was achieved under UV light irradiation. Ni−Cr and Ni−Mn LDHs showed lower CO evolution activities than $Ni(OH)_2$, which has no characteristic LDH structure. On the other hand, the CO formation rates for Ni−V, Ni−Fe, and Ni−Al LDH were higher than that of $Ni(OH)_2$. This result is consistent with the previous assertion that incorporation of M^{3+} into $Ni(OH)_2$ to construct the LDH structure clearly enhances the photocatalytic activity for the conversion of CO_2 in an aqueous NaCl solution. In

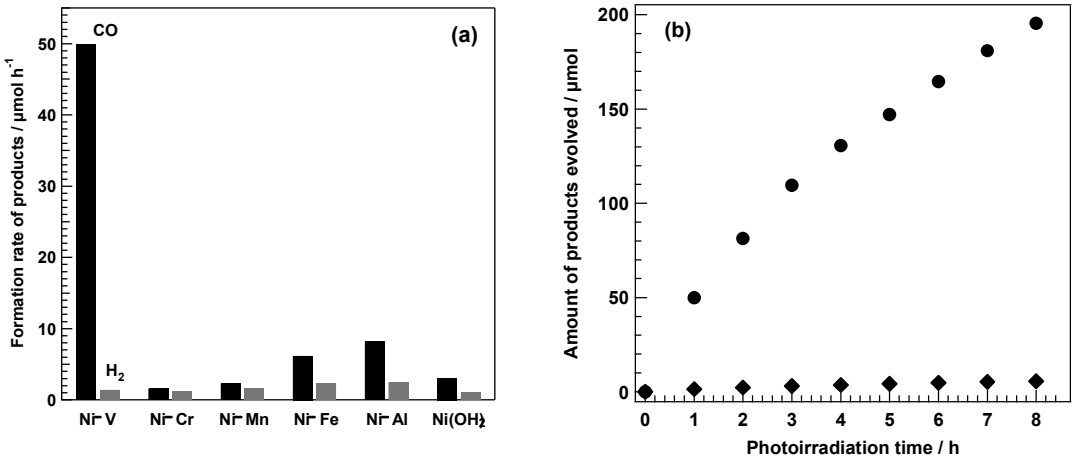

Figure 5 (a) Formation rates of CO (black) and H_2 (gray) evolved in the photocatalytic conversion of CO_2 in an aqueous solution of NaCl after 1 h of photoirradiation using Ni−M^{3+} LDHs (M^{3+} = V^{3+}, Cr^{3+}, Mn^{3+}, and Fe^{3+}), Ni−Al LDH, and $Ni(OH)_2$. **(b)** Time course of the total amounts of products evolved (accumulated) in the photocatalytic conversion of CO_2 in an aqueous solution of NaCl using Ni−V LDH. Circle: CO and diamond: H_2.

particular, the CO formation rate over Ni−V LDH was 49.9 μmol h^{-1} after 1 h of photoirradiation, which is much greater than that of the other Ni−M^{3+} (M^{3+} = Cr^{3+}, Mn^{3+}, Fe^{3+}, and Al^{3+}) LDHs and $Ni(OH)_2$. The time course of the products evolved in the photocatalytic conversion of CO_2 in an aqueous NaCl solution using Ni−V LDH as a photocatalyst is shown in **Figure 5(b)**. CO was continuously produced as a reduction product of CO_2 during the 8 h of photoirradiation, and the total (accumulated) amount of CO evolved was ~200 μmol, whereas the amount of H_2 formed was < 10 μmol. Accordingly, the Ni−V LDH is considered a promising material for the photocatalytic selective conversion of CO_2 to CO in an aqueous NaCl solution. In addition, none of the Ni−M^{3+} (M^{3+} = V^{3+}, Cr^{3+}, Mn^{3+}, Fe^{3+}, and Al^{3+}) LDHs showed photocatalytic activity without NaCl in the reaction solution. We have previously reported that Cl^- in the reaction solution can act as a hole scavenger and improves the photocatalytic conversion of CO_2 into CO over Ni−Al LDH photocatalysts [53]. We presume that Cl^- promotes the selective conversion of CO_2 for the photocatalytic system using Ni−M^{3+} (M^{3+} = V^{3+}, Cr^{3+}, Mn^{3+}, and Fe^{3+}) LDHs via the same mechanism as that of Ni−Al LDH. In other words, Cl^- is oxidized by the photogenerated holes into Cl_2, which is immediately converted into HClO in water.

Figure 6 displays the XRD patterns of (a) Ni−V LDH with various Ni/V ratios (Ni/V = 2, 3, 4, and 5) and (b) Ni_2−V_x−Al_{1-x} LDH (x = 0, 0.1, 0.5, 0.7, 1.0). The positions of the characteristic diffraction peaks around 11° (black circle), 23° (white circle), and 61° (triangle), which are assigned to the (0 0 3), (0 0 6), and (1 1 0) planes reflections, respectively, did not alter with the change in the Ni/V ratio of Ni−V LDH, as shown in **Figure 6(a)**. This result indicates that the hydroxide sheet thickness and the cation to cation distance within the hydroxide sheets is not influenced by the ratio of Ni^{2+} to V^{3+} since there is little difference in the reported ionic radii of the 6-fold coordinated Ni^{2+} and V^{3+} (69.0 pm and 64.0 pm, respectively) [55]. However, the specific surface areas of the Ni−V LDHs were affected by the Ni/V ratio within the hydroxide sheets; the observed S_{BET} values of Ni/V = 2, 3, 4, and 5 were 200, 120, 130, and 87 m^2 g^{-1}, respectively. On the other hand, **Figure 6(b)** shows that the XRD patterns were obviously influenced by the V/Al ratio in the Ni_2−V_x−Al_{1-x} LDH (the ratio of Ni/M^{3+} is fixed at 2, x = 0, 0.1, 0.5, 0.7, and 1.0). The intense peaks > 60° are attributed to the (1 1 0) and (1 1 3) planes reflections. These peaks, which sometimes overlap because of broadening, shifted to a higher angle with a decrease in the V/Al ratio. This change can be explained by the incorporation of Al^{3+}, which has a much smaller ionic radii (53.5 pm [55]) than V^{3+}, that decreases the average cation-to-cation distance within hydroxide sheets. In addition, the peak intensity and FWHM value of the (0 0 3) plane reflection were altered by the V/Al ratio; the increase in the (0 0 3) peak intensity and the

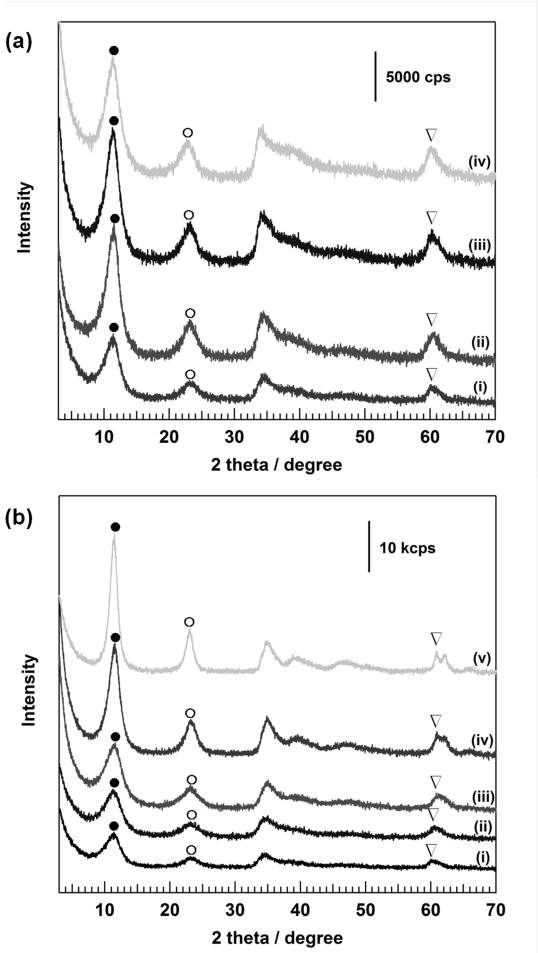

Figure 6 (a) XRD patterns of Ni−V LDH with Ni/V = (i) 2, (ii) 3, (iii) 4, and (iv) 5). **(b)** XRD patterns of Ni_2−V_x−Al_{1-x} (x = (i) 0, (ii) 0.1, (iii) 0.5, (iv) 0.7, and (v) 1.0). The characteristic peaks which are marked with black circle (●), white circle (○), and triangle (Δ) are attributed to (0 0 3), (0 0 6), and (1 1 0) phase reflections of LDH structure.

decrease in the $FWHM_{(0\,0\,3)}$ indicated that the layer stacking along the *c*-axis direction was advanced by the substitution of V^{3+} with Al^{3+} within the hydroxide sheets.

Table 2 Formation rates of products evolved in the photocatalytic conversion of CO_2 in an aqueous solution of NaCl using Ni−V LDHs with various Ni/V ratio after 1 h and 5 h of photoirradiation.

Photocatalyst	Formation rate / μmol h^{-1}			
	CO		H_2	
	1 h	5 h	1 h	5 h
Ni/V = 2	49.9	16.5	1.4	0.5
Ni/V = 3	23.0	7.6	1.3	0.2
Ni/V = 4	15.6	4.6	0.9	0.1
Ni/V = 5	12.9	8.4	0.0	0.1
$Ni(OH)_2$	3.1	4.6	1.1	0.5
V_2O_5	0.2	Trace	Trace	Trace

Table 2 displays the amount of products evolved in the photocatalytic conversion of CO_2 in an aqueous NaCl solution using Ni−V LDHs with various Ni/V ratios, $Ni(OH)_2$, and V_2O_5. Ni−V LDHs exhibited much higher CO formation activities than $Ni(OH)_2$ and V_2O_5, which were used as reference photocatalysts. On the other hand, none of the photocatalysts showed H_2 evolution activity via the reduction of H_2O. The CO formation rate was clearly affected by the Ni/V ratio in the Ni−V LDH, with Ni/V = 2 showing the largest amount of CO evolution. The incorporation of V^{3+} into $Ni(OH)_2$ to construct the LDH structure obviously enhanced the CO formation activity. Furthermore, high V^{3+} content in the Ni−V LDH (which is synonymous with a small Ni/V ratio) afforded good photocatalytic activity for the conversion of CO_2 in an aqueous NaCl solution. However, the formation rate of CO gradually decreased with the photoirradiation time, and dropped to about a third of the initial rate after 5 h of photoirradiation. It can be estimated that the Ni−V LDH photocatalyst is deactivated during the photocatalytic reaction, as is described later. **Figure 7** exhibits the CO formation rate in the photocatalytic conversion of CO_2 in an aqueous NaCl solution using Ni_2−V_x−Al_{1-x} LDHs (x = 0, 0.1, 0.5, 0.7, and 1.0). The photocatalytic activities were clearly influenced by the V^{3+} to Al^{3+} ratio, and the increase in the V^{3+} concentration improved the CO formation rate under UV light irradiation. This result is consistent with that of Ni−V LDH case; the use of a low Ni/V ratio achieved the high photocatalytic activity for CO_2 conversion in an aqueous

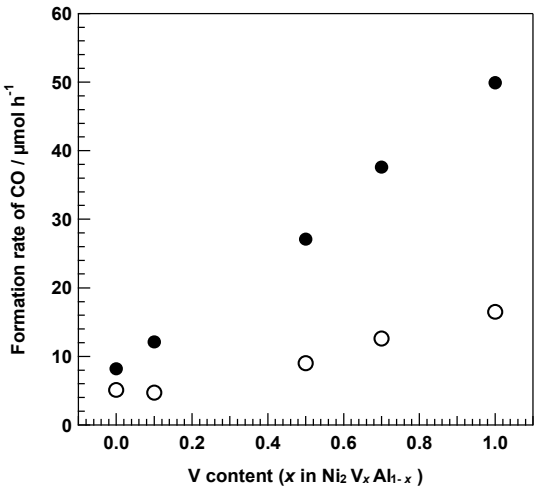

Figure 7 Formation rate of CO in the photocatalytic conversion of CO_2 in an aqueous solution of NaCl using $Ni_2{-}V_x{-}Al_{1-x}$ (x = 0, 0.1, 0.5, 0.7, and 1.0) after 1 h (black circle) and 5 h (white circle) of photoirradiation.

NaCl solution. The V^{3+} specie in the LDH hydroxide sheets is expected to play an important role in this reaction. However, the low Ni−V LDH stability during the photocatalytic reaction was not restituted by the incorporation of Al^{3+} into the Ni−V LDH to assemble the $Ni_2{-}V_x{-}Al_{1-x}$ LDH, which was found to have an relatively advanced layer structure.

Figure 8(a) shows the time course of the products evolved and the amount of metal ions in the reaction solution eluted from the Ni−V LDH photocatalyst during the photocatalytic conversion of CO_2 in an aqueous NaCl solution. As mentioned previously, the CO formation rate gradually decreased with the photoirradiation time: 49.9 μmol h^{-1} after 1 h of photoirradiation diminished to 14.5 μmol h^{-1} after 8 h of photoirradiation. The H_2 formation rate also declined from 1.4 μmol h^{-1} after 1 h of photoirradiation to 0.3 μmol h^{-1} after 8 h of photoirradiation. In contrast, the amount of Ni ions in the reaction solution increased with the photocatalytic reaction time. Furthermore, amorphous $Ni(OH)_2$ was completely eluted into the reaction solution within 5 h of photoirradiation under the same reaction conditions, whereas the Ni−Al LDH, which forms a rigid layer structure, was sufficiently stable. Accordingly, the pregnable layer structure of the Ni−V LDH and the existence of the amorphous $Ni(OH)_2$ phase would facilitate elution during the photocatalytic reaction. After 8 h of photoirradiation, no change was observed in the XRD pattern as compared with the as-prepared Ni−V LDH; nevertheless, over 40% of the Ni ions in the Ni−V LDH have been eluted into the reaction solution, indicating that the non-crystalline phase, e.g., $Ni(OH)_2$ was preferentially

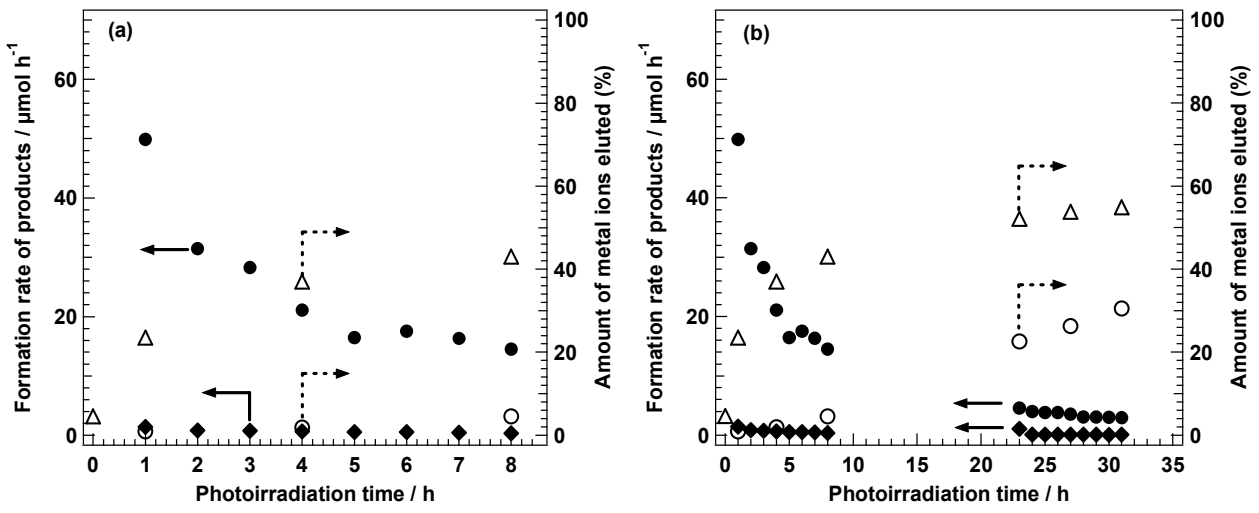

Figure 8 Time courses of the formation rates of gas phase products (left axis) and the amounts of metal ions eluted from Ni−V LDH into the reaction solution (right axis) in the photocatalytic conversion of CO_2 in an aqueous solution of NaCl for **(a)** 8 h and **(b)** 30 h of photoirradiation. Black circle: CO, diamond: H_2, triangle: nickel ions, and white circle: vanadium ions.

dissolved in the reaction solution. Hence, after 8 h of photoirradiation, the amount of V ions in the reaction solution was much lower than that of Ni ions. As shown in **Figure 8(b)**, which represents an elongated time course, V ions in the Ni−V LDH began elution into the reaction solution after almost half of the Ni ions have leached out. The formation rates of CO and H_2 continuously decreased, and less than 0.3 μmol h^{-1} of CO was evolved after 200 h of photoirradiation. Almost all of the Ni−V LDH powder has disappeared during that time; in other words, all of the Ni and V ions eluted into the reaction solution. In addition, the leaching of Ni−V LDH was clearly suppressed under a flow of He instead of CO_2 gas. These results indicated that Ni−V LDH consisting of mixed hydroxide sheets afforded surface properties suitable for the photocatalytic conversion of CO_2 in an aqueous solution; however, this photocatalyst easily leached under UV light irradiation in a CO_2 atmosphere. When Ni−Al LDH was used as a photocatalyst, as described in previous literature, a stoichiometric amount of HClO was produced in the reaction solution as an oxidation product of Cl^- during the photocatalytic conversion of CO_2 in an aqueous NaCl solution [53]. In contrast, the amount of HClO produced in the photocatalytic reaction using Ni−V LDH, as demonstrated in this study, was much lower than the stoichiometric amount. Although the reason why the incorporation of V^{3+} enhanced the photocatalytic activity for CO_2 conversion is not clear, we estimate the oxidation reaction pass as

presented below.

(1) $2Cl^- + 2h^+ \rightarrow Cl_2$

(2) $Cl_2 + H_2O \rightarrow HClO + HCl$

(3) $2HClO + 2H^+ + 2e^- \rightarrow Cl_2 + 2H_2O$

(4) $V^{3+} + H_2O \rightarrow VO^{2+} + 2H^+ + e^-$

Cl^- was oxidized to chlorine (Cl_2) by capturing the photogenerated holes, as shown in formula (1). This reaction is considered to trigger the subsequent process, because the photocatalytic activity of Ni−V LDH is completely diminished in the absence of NaCl. It is known that Cl_2 is immediately converted to HClO and HCl via disproportionation reaction in water (formula (2)). It can be approximated that HCl produced in the reaction solution causes Ni−V LDH to be more easily leached. Meanwhile, HClO has strong oxidation power due to the reaction shown in formula (3), according to the reported value of $E°(HClO/Cl_2)$ = 1.630 V vs. SHE [56], indicating that HClO can oxidize the V^{3+} present in the hydroxide sheets and/or in the reaction solution. Considering the oxidation potential from V^{3+} to VO^{2+} ($E°(VO^{2+}/V^{3+})$ = 0.337 V vs. SHE [56]), the formula for HClO consumption in the reaction solution is described by formula (5).

(5) $2\,HClO + 2V^{3+} \rightarrow Cl_2 + 2VO^{2+} + 2H^+$

VO^{2+} is sufficiently soluble and shows light blue color in aqueous solution. The filtrate solution after the photocatalytic reaction actually exhibited a slightly blue color. It might be presumed that the reason why HClO, which was considered to be an oxidation product of Cl^-, was not detected at all by DPD test is that HClO produced in the reaction solution was continuously consumed by the oxidation of the V^{3+} species. Regeneration of Cl_2 via the oxidation of V^{3+} (formula (5)) is considered to be converted to HClO and HCl again, as shown in formula (2), indicating that a combination of V^{3+} and Cl^- might plays significant roles like a redox couple in the consumption of photogenerated holes during the photocatalytic conversion of CO_2 into CO. On the other hand, the addition of Na_2CO_3 to the reaction solution as a second additive (0.1 M NaCl + 0.1 M Na_2CO_3) improved the stability of the Ni−V LDH photocatalyst for the conversion of CO_2 to CO in an aqueous solution, as shown in **Figure 9**. The increase of pH from 5.0 to 7.0 by adding Na_2CO_3 to the aqueous NaCl solution effectively suppressed the leaching of Ni−V LDH during the photocatalytic reaction. We conclude that the Ni−V LDH photocatalyst is substantially active for the conversion of CO_2 in an aqueous

NaCl solution, though its stability under the reaction conditions is insufficient because of the oxidation of V^{3+} induced by HClO. The co-presence of V^{3+} and Cl^- might make it possible to achieve high photocatalytic activity for the conversion of CO_2 into CO in an aqueous solution.

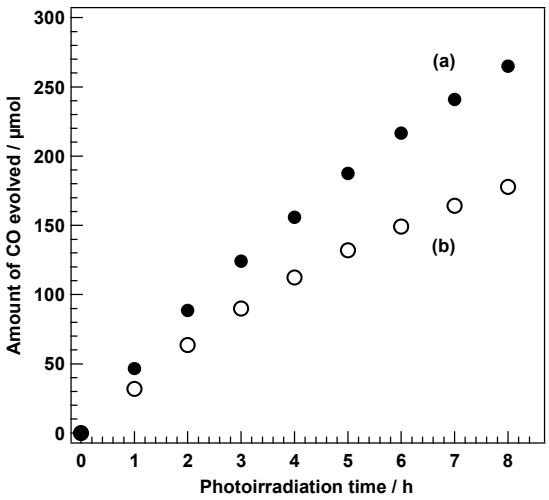

Figure 9 Time course of the total amounts of CO evolved (accumulated) in the photocatalytic conversion of CO_2 using Ni−V LDH in an aqueous solution of (a) NaCl (0.1 M) + Na_2CO_3 (0.1 M) and (b) NaCl (0.1 M).

Conclusion

We found that Ni−V LDH showed the high photocatalytic activity for the conversion of CO_2 in an aqueous solution of NaCl. Over 200 μmol of CO was evolved as a reduction product of CO_2 after 8 h of photoirradiation when Ni−V LDH (Ni/V = 2) was used as a photocatalyst. Through the investigation of photocatalytic activities for different V^{3+} content of Ni−V LDH and Ni−V−Al LDH, the existence of V^{3+} afforded good performance for the conversion of CO_2 into CO in an aqueous solution of NaCl. The stability of Ni−V LDH was insufficient due to the leaching into the reaction solution. It can be noted that the combination of V^{3+} and Cl^- play a significant role in the photocatalytic conversion of CO_2 to CO in an aqueous solution.

References

1. F. Cavani, F. Trifirò and A. Vaccari, *Catalysis Today*, 1991, **11**, 173-301.
2. C. Delhoyo, *Applied Clay Science*, 2007, **36**, 103-121.
3. Z. P. Xu, J. Zhang, M. O. Adebajo, H. Zhang and C. Zhou, *Applied Clay Science*, 2011, **53**, 139-150.
4. B. Li, Y. Zhao, S. Zhang, W. Gao and M. Wei, *ACS Applied Materials & Interfaces*, 2013, **5**, 10233-10239.
5. X. Zhang, Z. Wang, N. Qiao, S. Qu and Z. Hao, *ACS Catalysis*, 2014, **4**, 1500-1510.
6. J. Prince, F. Tzompantzi, G. Mendoza-Damián, F. Hernández-Beltrán and J. S. Valente, *Applied Catalysis B: Environmental*, 2015, **163**, 352-360.
7. X. Xu, R. Lu, X. Zhao, S. Xu, X. Lei, F. Zhang and D. G. Evans, *Applied Catalysis B: Environmental*, 2011, **102**, 147-156.
8. T. Iwasaki, H. Yoshii, H. Nakamura and S. Watano, *Applied Clay Science*, 2012, **58**, 120-124.
9. L. Huang, S. Chu, J. Wang, F. Kong, L. Luo, Y. Wang and Z. Zou, *Catalysis Today*, 2013, **212**, 81-88.
10. L. Tian, Y. Zhao, S. He, M. Wei and X. Duan, *Chemical Engineering Journal*, 2012, **184**, 261-267.
11. H. Lin, Y. Zhang, G. Wang and J.-B. Li, *Frontiers of Materials Science*, 2012, **6**, 142-148.
12. G. Abellan, E. Coronado, C. Marti-Gastaldo, J. Waerenborgh and A. Ribera, *Inorganic Chemistry*, 2013, **52**, 10147-10157.
13. M. Gong, Y. Li, H. Wang, Y. Liang, J. Z. Wu, J. Zhou, J. Wang, T. Regier, F. Wei and H. Dai, *Journal of the American Chemical Society*, 2013, **135**, 8452-8455.
14. F. Song and X. Hu, *Journal of the American Chemical Society*, 2014, **136**, 16481-16484.
15. F. B. Saiah, B. L. Su and N. Bettahar, *Journal of Hazardous Materials*, 2009, **165**, 206-217.
16. T. Takei, A. Miura, N. Kumada and K. Okada, *Journal of Porous Materials*, 2012, **20**, 777-783.
17. F. Giovannelli, M. Zaghrioui, C. Autret-Lambert, F. Delorme, A. Seron, T. Chartier and B.

Pignon, *Materials Chemistry and Physics*, 2012, **137**, 55-60.

18. C. G. Silva, Y. Bouizi, V. Fornés and H. García, *Journal of the American Chemical Society*, 2009, **131**, 13833-13839.
19. Y. Guo, Z. Zhu, Y. Qiu and J. Zhao, *Journal of Hazardous Materials*, 2012, **239–240**, 279-288.
20. J. M. Fernández, C. Barriga, M. A. Ulibarri, F. M. Labajos and V. Rives, *Chemistry of Materials*, 1997, **9**, 312-318.
21. E. M. Seftel, E. Popovici, M. Mertens, E. A. Stefaniak, R. Van Grieken, P. Cool and E. F. Vansant, *Applied Catalysis B: Environmental*, 2008, **84**, 699-705.
22. S.-J. Xia, F.-X. Liu, Z.-M. Ni, W. Shi, J.-L. Xue and P.-P. Qian, *Applied Catalysis B: Environmental*, 2014, **144**, 570-579.
23. X. Wang, P. Wu, Z. Huang, N. Zhu, J. Wu, P. Li and Z. Dang, *Applied Clay Science*, 2014, **95**, 95-103.
24. G. Chen, S. Qian, X. Tu, X. Wei, J. Zou, L. Leng and S. Luo, *Applied Surface Science*, 2014, **293**, 345-351.
25. M. Shao, J. Han, M. Wei, D. G. Evans and X. Duan, *Chemical Engineering Journal*, 2011, **168**, 519-524.
26. Y. Zhao, P. Chen, B. Zhang, D. S. Su, S. Zhang, L. Tian, J. Lu, Z. Li, X. Cao, B. Wang, M. Wei, D. G. Evans and X. Duan, *Chemistry*, 2012, **18**, 11949-11958.
27. O. Saber, *Journal of Materials Science*, 2007, **42**, 9905-9912.
28. X. Shu, W. Zhang, J. He, F. Gao and Y. Zhu, *Solid State Sciences*, 2006, **8**, 634-639.
29. S. J. Xia, F. X. Liu, Z. M. Ni, J. L. Xue and P. P. Qian, *Journal of Colloid and Interface Science*, 2013, **405**, 195-200.
30. L. Mohapatra and K. M. Parida, *Separation and Purification Technology*, 2012, **91**, 73-80.
31. J. Sun, Y. Zhang, J. Cheng, H. Fan, J. Zhu, X. Wang and S. Ai, *Journal of Molecular Catalysis A: Chemical*, 2014, **382**, 146-153.
32. L. Mohapatra and K. M. Parida, *Physical Chemistry Chemical Physics*, 2014, **16**, 16985-16996.
33. J. S. Valente, F. Tzompantzi and J. Prince, *Applied Catalysis B: Environmental*, 2011, **102**,

276-285.

34. S. Pausova, J. Krysa, J. Jirkovsky, G. Mailhot and V. Prevot, *Environmental Science and Pollution Research*, 2012, **19**, 3709-3718.

35. S. Yuan, Y. Li, Q. Zhang and H. Wang, *Colloids and Surfaces A: Physicochemical and Engineering Aspects*, 2009, **348**, 76-81.

36. E. Dvininov, M. Ignat, P. Barvinschi, M. A. Smithers and E. Popovici, *Journal of Hazardous Materials*, 2010, **177**, 150-158.

37. D. Chen, Y. Li, J. Zhang, J.-z. Zhou, Y. Guo and H. Liu, *Chemical Engineering Journal*, 2012, **185-186**, 120-126.

38. Y. Kohno, T. Tanaka, T. Funabiki and S. Yoshida, *Chemical Communications*, 1997, 841-842.

39. Y. Kohno, T. tanaka, T. Funabiki and S. Yoshida, *Chemistry Letters*, 1997, **26**, 993-994.

40. Y. Kohno, T. Tanaka, T. Funabiki and S. Yoshida, *Journal of the Chemical Society, Faraday Transactions*, 1998, **94**, 1875-1880.

41. Y. Kohno, T. Tanaka, T. Funabiki and S. Yoshida, *Physical Chemistry Chemical Physics*, 2000, **2**, 2635-2639.

42. Y. Kohno, H. Ishikawa, T. Tanaka, T. Funabiki and S. Yoshida, *Physical Chemistry Chemical Physics*, 2001, **3**, 1108-1113.

43. K. Teramura, T. Tanaka, H. Ishikawa, Y. Kohno and T. Funabiki, *The Journal of Physical Chemistry B*, 2004, **108**, 346-354.

44. H. Tsuneoka, K. Teramura, T. Shishido and T. Tanaka, *The Journal of Physical Chemistry C*, 2010, **114**, 8892-8898.

45. K. Teramura, S. Iguchi, Y. Mizuno, T. Shishido and T. Tanaka, *Angewandte Chemie International Edition*, 2012, **51**, 8008-8011.

46. N. Ahmed, Y. Shibata, T. Taniguchi and Y. Izumi, *Journal of Catalysis*, 2011, **279**, 123-135.

47. M. Morikawa, N. Ahmed, Y. Yoshida and Y. Izumi, *Applied Catalysis B: Environmental*, 2014, **144**, 561-569.

48. M. Morikawa, Y. Ogura, N. Ahmed, S. Kawamura, G. Mikami, S. Okamoto and Y. Izumi, *Catalysis Science & Technology*, 2014, **4**, 1644-1651.

49. K. Katsumata, K. Sakai, K. Ikeda, G. Carja, N. Matsushita and K. Okada, *Materials Letters*, 2013, **107**, 138-140.

50. S. Iguchi, K. Teramura, S. Hosokawa and T. Tanaka, *Catalysis Today*, 2015, **251**, 140-144.

51. K. Carlsson, L. Moberg and B. Karlberg, *Water Research*, 1999, **33**, 375-380.

52. L. Moberg and B. Karlberg, *Analytica Chimica Acta*, 2000, **407**, 127-133.

53. S. Iguchi, K. Teramura, S. Hosokawa and T. Tanaka, *Physical Chemistry Chemical Physics*, 2015, **17**, 17995-18003.

54. Lianyi Shao, Jie Shu, Rui Ma, Miao Shui, Lu Hou, Kaiqiang Wu, Dongjie Wang and Y. Ren, *International Journal of Electrochemical Science*, 2013, **8**, 1170-1180.

55. R. D. Shannon, *Acta Crystallographica Section A*, 1976, **32**, 751-767.

56. *Standard Potentials in Aqueous Solution*, Marcel Dekker, 1985.

Chapter 5

Investigation on Electrochemical and Photoelectrochemical Properties of Ni−Al LDH Photocatalyst

Abstract

Recently, layered double hydroxides (LDHs) have attracted considerable attention in the field of photocatalysis because of their characteristic layered structure, adsorption properties, and large specific surface areas. Previously, we reported the photocatalytic activity of Ni−Al LDH for the conversion of CO_2 into CO in water. Most of the investigations on LDHs have focused on their photocatalytic activities. In contrast, very few studies have investigated their electrochemical properties such as energy gap, potentials of photogenerated electron and hole, and the efficiency of charge separation induced by photoirradiation. In this study, we demonstrate the photocurrent characteristics of a series of LDH photocatalysts. Also, we estimated the potentials of photogenerated electrons and holes, which are responsible for the photocatalytic reaction, using electrochemical techniques. Ni−Al LDH showed an anodic photocurrent under UV light irradiation. The flat band potential of the Ni−Al LDH photocatalyst was estimated to be −0.40 V vs NHE (pH = 0), which is sufficient to reduce CO_2 to CO. Moreover, we revealed that the flat band potentials of M^{2+}−M^{3+} LDH are clearly influenced by the type of trivalent metal (M^{3+}) components.

Introduction

Layered double hydroxides (LDHs), also known as anionic clays[1–3], have the general formula $[M^{2+}_{1-x}–M^{3+}_{x}(OH)_2](A^{n-})_{x/n}\cdot mH_2O$, where M^{2+} and M^{3+} are divalent and trivalent cations, respectively; A^{n-} is an interlayer anion of valence n; and x denotes the molar ratio of $M^{3+}/(M^{2+} + M^{3+})$. The metal cations occupy the centers of edge-sharing octahedra, whose vertexes contain hydroxide ions that connect to form infinite two-dimensional sheets. Currently, many advanced applications for LDHs have been developed; for example, anion conductive materials[4–7], capacitors[8–11], electrocatalysts[12], and photocatalysts[13–15]. Some reactions carried out using these photocatalysts are photocatalytic degradation of organic compounds using a series of Zn-containing LDHs (Zn−Al, Zn−Bi, and Zn−Ti LDH)[14, 16, 17] and a CeO_2/Mg−Al LDH composite[18], half-reactions of photocatalytic water splitting in the presence of sacrificial reagents using Ti-containing LDHs (Ni−Ti and Zn−Ti LDH)[19–20] and Zn−Cr LDH[21], and photocatalytic conversion of CO_2[22–25]. We developed a photocatalytic system for the conversion of CO_2 in aqueous solution using Ni−Al LDH[26, 27], which enables the selective formation of CO (as the reduction product of CO_2) because of the complete suppression of H_2 evolution via reduction of protons (H^+). In such a case, photoirradiation through pyrex glass did not induce any photocatalytic reaction over Ni−Al LDH, whereas the use of quartz glass allowed the photocatalytic conversion of CO_2, indicating that UV light irradiation ($\lambda < 300$ nm) is necessary for this photocatalytic reaction[28]. In contrast, García et al. reported that Zn−Cr LDH was an active photocatalyst for the oxidation of H_2O into O_2 under visible light irradiation[21]. Because LDHs show photocatalytic activities for several kinds of reactions as reported by us and others (as cited above), there must be an energy gap that can induce photocatalytic reactions under illumination. However, only a few studies have investigated the electrochemical properties of these LDHs, such as energy gap measurement, charge separation induced by photoirradiation, and potentials of photogenerated electrons and holes. Concerning the reduction of CO_2 in aqueous media, the relationship between the standard potential for CO_2 (i.e., $E^{o}(CO_2/CO) = -0.11$ V vs. NHE)[29] and the potential of the photoexcited electron in the photocatalyst material must be considered carefully because it is difficult to reduce CO_2, one of the most stable molecules, particularly in comparison with the reduction of a proton ($E^{o}(H^+/H_2) = 0.0$ V vs. NHE)[29].

Electrochemical and photoelectrochemical measurements are useful techniques that are widely used in the field of photocatalysis to understand the photocatalytic properties of materials, such as the distinction between *n*-type and *p*-type semiconductors, photon-to-current conversion efficiencies, energy levels of the bottom of conduction band (hereinafter "$\boldsymbol{E_{CB}}$") and the top of valence band (hereinafter "$\boldsymbol{E_{VB}}$"), and the energy gap of the band structure (hereinafter "$\boldsymbol{E_{BG}}$")[30]. Electrochemical properties can be investigated by observing the interface between the semiconductor electrode and the electrolyte solution while applying an external bias to the former[31, 32]. When a certain potential is applied, the Fermi level of the semiconductor lies at the same energy as the redox potential of the electrolyte solution, and there is no charge transfer between them; thus, no band bending occurs. This potential is referred to as the flat band potential (hereinafter "$\boldsymbol{E_{FB}}$")[33, 34]. For *n*-type semiconductors[31], the cathodic dark current is detected when the applied potential is more negative than $\boldsymbol{E_{FB}}$ because the accumulation layer, which appears under cathodic polarization, enables electron transfer from the electrode to the electrolyte solution, similar to that of a metallic electrode. In contrast, *n*-type semiconductors can act as photoanodes under anodic polarization. The photogenerated hole (h^+) in the depletion layer can move toward the interface, in accordance with band bending, and can easily receive electrons from the electrolyte solution. This permits electron transfer from the semiconductor to the counter electrode through a conductor cable, which is regarded as the anodic photocurrent. The values of $\boldsymbol{E_{FB}}$ and $\boldsymbol{E_{BG}}$ for semiconductor photocatalysts can be determined experimentally by using the Mott-Schottky and Davis-Mott equations; the details are presented in the Experimental section.

In the present study, we estimated the photoelectrochemical properties such as photocurrent character, energy gap, potentials of the photogenerated electrons and holes for Ni−Al LDH and other LDHs with reference to the cases of TiO_2 and Ta_2O_5.

Experimental

Ni−Al LDH was synthesized by a typical coprecipitation method. An aqueous solution containing $NiCl_2{\cdot}6H_2O$ (99.9%, Wako) and $AlCl_3$ (98.0%, Wako) was slowly dropped into an aqueous Na_2CO_3 (99.5%, Wako) solution at room temperature. The pH of the solution was kept stable between 9.9 and 10.1 by adding an aqueous NaOH (97.0%, Wako) solution using a liquid feed

pump (NRP-76, NISSHIN RIKA). The resulting suspension was aged at 383 K under hydrothermal condition using a stainless steel autoclave equipped with an inner Teflon vessel. The solid cake was collected by filtration and washed with ultra-pure water, and then dried at 383 K in air. Others combination of metal components in LDH, such as Mg−Al, Zn−Al, Ni−Ga, and Ni−In were fabricated via same procedure to Ni−Al LDH using chloride salts as precursors.

For an electrochemical and a photoelectrochemical measurements, LDH electrodes were prepared on a fluorine doped tin oxide (FTO) glass via an electrophoresis deposition method. 100 mg of LDH powder was added into 50 mL of an acetone solution containing 10 mg of iodine as an electrolyte, and then the LDH powder was dispersed thoroughly by an ultrasonication. Prior to use, FTO glass (AGC fabritech Co., Ltd) was washed with aceton and 2-propanol solution in turn. Two FTO glasses were immersed in the solution with facing each other, and direct current (DC) was applied between the two FTO glasses by using an electrochemical measurement system (HZ-5000, Hokuto Denko Corp.), at 0.1 mA stable current (2 min) for measurements in an aqueous solution, and at 10.0 V stable voltage (5 min) for those in an organic solution. After drying at room temperature in air, prepared LDH electrode (hereinafter, called X LDH/FTO electrode, X = Ni−Al, Mg−Al, Zn−Al, Ni−Ga, and Ni−In) was heated at 473 K for 2 h in order to remove the residual iodine. As reference electrodes, TiO_2/FTO and Ta_2O_5/FTO electrode were prepared via a same procedure using TiO_2 (ST-01, Ishihara Sangyo Kaisha, Ltd.) and Ta_2O_5 (Kojundo Chemical Laboratory Co., Ltd.) as powder samples.

X-ray diffraction (XRD) patterns of the prepared electrodes were collected by using an X-ray diffractometer (Multiflex, Rigaku) using Cu K_α radiation at an acceleration voltage of 40 kV with 0.02° per a step. Scanning electron microscopy images for a sectioned view of the electrodes were captured by using a Field Emission Scanning Electron Microscope (SU-8220, Hitachi High-Technologies) at an acceleration voltage of 3.0 kV. UV/Vis diffuse reflectance spectra of LDHs powder samples were measured by a UV-Visible Spectrometer (V-670, JASCO) equipped with an integrated sphere accessory. The energy gap (hereinafter "$\boldsymbol{E_g}$") of a series of LDHs and $\boldsymbol{E_{BG}}$ of TiO_2 and Ta_2O_5 were determined by the Davis-Mott equation[35] using the Kubelka-Munk function $\boldsymbol{F(R_\infty)}$ obtained from diffuse reflectance spectrum,

(Eq. 1) $$[\boldsymbol{F}(\boldsymbol{R}_\infty)\boldsymbol{h\nu}]^{-\boldsymbol{n}} = \mathbf{A}(\boldsymbol{h\nu}-\boldsymbol{E_g})$$

where: h, v, and **A** are Plank's constant, frequency of vibration, and proportional constant, respectively.

Electrochemical measurements were performed using a three-electrode electrochemical cell consisting of the prepared LDH/FTO electrode, Ag/AgCl electrode, and Pt wire as working electrode, reference electrode, and counter electrode, respectively. Prior to the measurements, the dissolved air in the electrolyte solution was completely removed by He gas flow. For a cyclic voltammetry, acetonitrile solution was used as a solvent, which contains 0.05 M of $LiClO_4$ as an electrolyte. The current value was recorded as the applied voltage was varied from −2.0 to 1.0 V vs. Ag/AgCl with a sweep rate of 10 mV s^{-1} using an electrochemical measurement system (HZ-5000, Hokuto Denko Corp.). For an impedance measurement, an aqueous Na_2SO_4 solution (0.1 M) was used as an electrolyte solution. The imaginary component of the impedance (Z'') of the equivalent circuit including X LDH/FTO electrode (X = Ni−Al, Mg−Al, Zn−Al, Ni−Ga, or Ni−In) was evaluated at an alternating current frequency of 72.0, 52.0, and 37.3 kHz with a sweeping applied voltage from 0.5 to −0.5 V vs. Ag/AgCl by an electrochemical measurement system (HZ-5000, Hokuto Denko Corp.). The capacitance (C) of the circuit was calculated from the imaginary component of the impedance (Z'') using the relationship,

(Eq. 2) $$|Z''| = 1/(2\pi f C)$$

where π and f means the circumference ratio and the frequency of the alternating current. The value of E_{FB} for the working electrode was estimated by using the resulted value of C in accordance with Mott-Schottky equation,

(Eq. 3) $$C^{-2} = (2/\varepsilon\varepsilon_0 A^2 e N_D)\,(E - E_{FB} - k_B T/e)$$

where: C and A are the interfacial capacitance and area, respectively, N_D the number of donors, E the applied potential, k_B Boltzmann's constant, T the absolute temperature, ε the dielectric constant of the semiconductor, ε_0 the permittivity of free space, and e is the electronic charge. Therefore, the value of E_{FB} should be obtained from the intercept on x-axis in the plot of C^{-2} versus the applied potential E. In the present study, the energy gap, the potential of photogenerated electron and hole are hereinafter presented as E_g, E_e and E_h for a series of LDHs, and the band gap energy, the potential of the bottom of conduction band and the top of valence band are called as E_{BG}, E_{CB} and E_{VB} for TiO_2 and Ta_2O_5; typical semiconductor photocatalysts. The difference of potential (E)

derived from the value of pH of the electrolyte solution was revised in accordance with Nernst equation as below,

(Eq. 4) $\boldsymbol{E}_{(\mathbf{pH}=\boldsymbol{a})} = \boldsymbol{E}_{(\mathbf{pH}=\boldsymbol{b})} - 0.059 \times (\boldsymbol{a}-\boldsymbol{b})$

where: $\boldsymbol{E}_{(\mathbf{pH}=\boldsymbol{a})}$ and $\boldsymbol{E}_{(\mathbf{pH}=\boldsymbol{b})}$ are the value of potential at pH = ***a*** and ***b***. For example, 0.00 V at pH = 0.0 should be converted into 0.41 V at pH = 7.0. Furthermore, the difference of potential with kinds of standard electrodes was converted to the normal hydrogen electrode (NHE) by using relationships as presented below for the silver-silver chloride standard electrode (Ag/AgCl) [36-37] and the standard calomel electrode (SCE) [36-37].

(Eq. 5) $\boldsymbol{E}$ **(vs. NHE)** − $\boldsymbol{E}$ **(vs. Ag/AgCl)** = 0.199 V

(Eq. 6) $\boldsymbol{E}$ **(vs. NHE)** − $\boldsymbol{E}$ **(vs. SCE)** = 0.244 V

Photoelectrochemical measurements were conducted using a three-electrode electrochemical cell equipped with a quartz window. The prepared LDH/FTO electrode, Ag/AgCl electrode, and Pt wire were used as working electrode, reference electrode, and counter electrode, respectively. For the measurement in an organic solvent, $LiClO_4$ acetonitrile solution (0.05 M) containing 5 vol.% methanol was used as an electrolyte solution. In contrast, an aqueous Na_2SO_4 solution which contains 5 vol.% methanol was used for the measurement in an aqueous solution. In both cases, the solution was thoroughly degassed by He gas flow. The working electrode (X LDH/FTO, X = Ni−Al, Mg−Al, and Zn−Al) was irradiated by a 200 W Hg-Xe lamp (SAN-EI Electric Co., Ltd.) through the quartz window. The photocurrent value was collected by an electrochemical measurement system (HZ-5000, Hokuto Denko Corp.) without external bias. For an linear sweep voltammetry under the photoirradiation, the applied bias was swept from −1.5 to 1.0 V vs. Ag/AgCl.

Results and discussion

Figure 1A shows the X-ray diffraction (XRD) pattern of the prepared Ni−Al LDH/FTO composite. Compared to those of the Ni−Al LDH powder sample (a) and bare FTO glass (c), the XRD pattern of Ni−Al LDH/FTO (b) shows mixed diffraction peaks of the above two samples. Two low angle peaks, 11° and 23°, in the powder sample are indexed as (0 0 3) and (0 0 6) planes, respectively, which define the characteristic layer structure of the LDH powders[1]. The peak positions

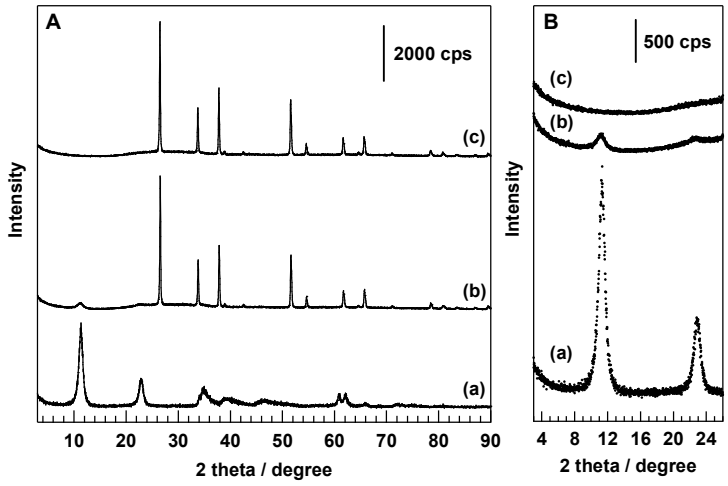

Figure 1 XRD patterns of **(a)** Ni−Al LDH powder sample, **(b)** Ni−Al LDH/FTO, and **(c)** FTO collected in **(A)** wide range scan and **(B)** narrow range scan.

of these reflections correspond to the layer-to-layer thickness; that is, the interlayer distance is equal to $d_{(0\,0\,3)}$ with respect to hexagonal axes. As shown in **Figure 1B**, Ni−Al LDH/FTO exhibited small peaks around the same position as those in the powder sample, indicating that Ni−Al LDH is fixed on the FTO glass and retains its layer structure. Moreover, the interlayer distance was conserved after the deposition onto FTO, because the positions of the (0 0 3) and (0 0 6) reflections were unchanged. **Figure 2A** shows the SEM images of Ni−Al LDH/FTO prepared by the electrophoresis deposition method. Regions X and Y mark the deposited Ni−Al LDH region and the FTO glass, respectively. We found that Ni−Al LDH particles with a thickness of several micrometers were deposited on the FTO glass. Regarding the enlarged views shown in **Figure 2B**, flower-petal-like morphologies, which are characteristic of LDH-type materials[1, 38], were also maintained. These SEM images are consistent with the results of XRD measurements of Ni−Al LDH/FTO. Based on the XRD patterns and SEM images, the state of the Ni−Al LDH deposited on FTO glass is considered to be similar to that of the powder sample, which shows photocatalytic activity for the conversion of CO_2 in aqueous solution[26, 28].

Figure 3 shows the cyclic voltammogram recorded using a three-electrode electrochemical cell. The prepared Ni−Al LDH/FTO was used as the working electrode under He atmosphere. When the working electrode was set under cathodic polarization, the cathodic dark current was determined, indicating that electron transfer from the working electrode to the electrolyte solution occurred because of the formation of an accumulation layer at the interface of the electrode, making the

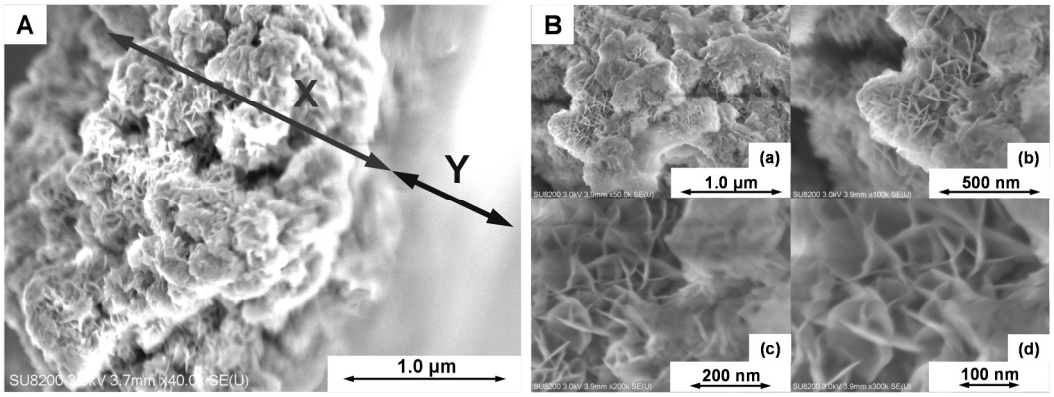

Figure 2 Sectioned view of SEM images for Ni−Al LDH/FTO captured at magnification of **(A)** 40.0 k, **(B-a)** 50.0 k, **(B-b)** 100 k, **(B-c)** 200 k, and **(B-d)** 300 k. The region **X** and **Y** in an image **(A)** indicate deposited Ni−Al LDH layer and FTO substrate, respectively.

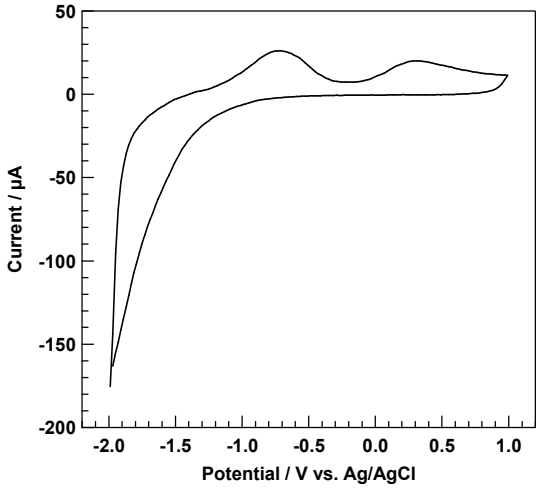

Figure 3 Cyclic voltammogram of Ni−Al LDH/FTO. Electrochemical cell: Ni−Al LDH/FTO working electrode, Ag/AgCl reference electrode, Pt wire counter electrode, and 0.05 M $LiClO_4$ acetonitrile electrolyte solution. Atmosphere: He. Sweep range: from −2.0 to 1.0 V, and return to −2.0 V. Sweep rate: 10 mV s^{-1}.

electron flow possible without an electric barrier. The cathodic dark current under cathodic polarization is known as a characteristic feature of *n*-type semiconductor materials. In contrast, anodic current should not be found under the dark condition for *n*-type electrodes because of the band bending in the depletion layer. However, two anodic current peaks were found. Because the standard potential was reported as $E°(IO_3^-/I^-)$ = 1.08 V vs. NHE (pH = 0)[29], the first peak, at ca. 0.4 V vs. Ag/AgCl, was assigned to the oxidation of I^- to IO_3^-, derived from I_2 that was used in the electrophoresis process. However, we were unable to assign the other peak, at ca. −0.2 V, to any reaction.

Figure 4A shows the photocurrent values of the Ni−Al LDH/FTO working electrode under illumination cycling through the quartz window with no applied external bias. The anodic photocurrent rose on illumination and diminished when the illumination stopped. The use of acetonitrile solution containing $LiClO_4$ resulted in a higher photocurrent than the use of an aqueous Na_2SO_4 solution. In both cases, the addition of methanol into the electrolyte solution was necessary to induce the anodic photocurrent, indicating that photogenerated holes (h^+) can oxidize methanol in the electrolyte solution and photoexcited electrons (e^-) can transfer to the counter electrode as an anodic current. As shown in **Figure 4B**, the substitution of Ni^{2+} in Ni−Al LDH by either Mg^{2+} or

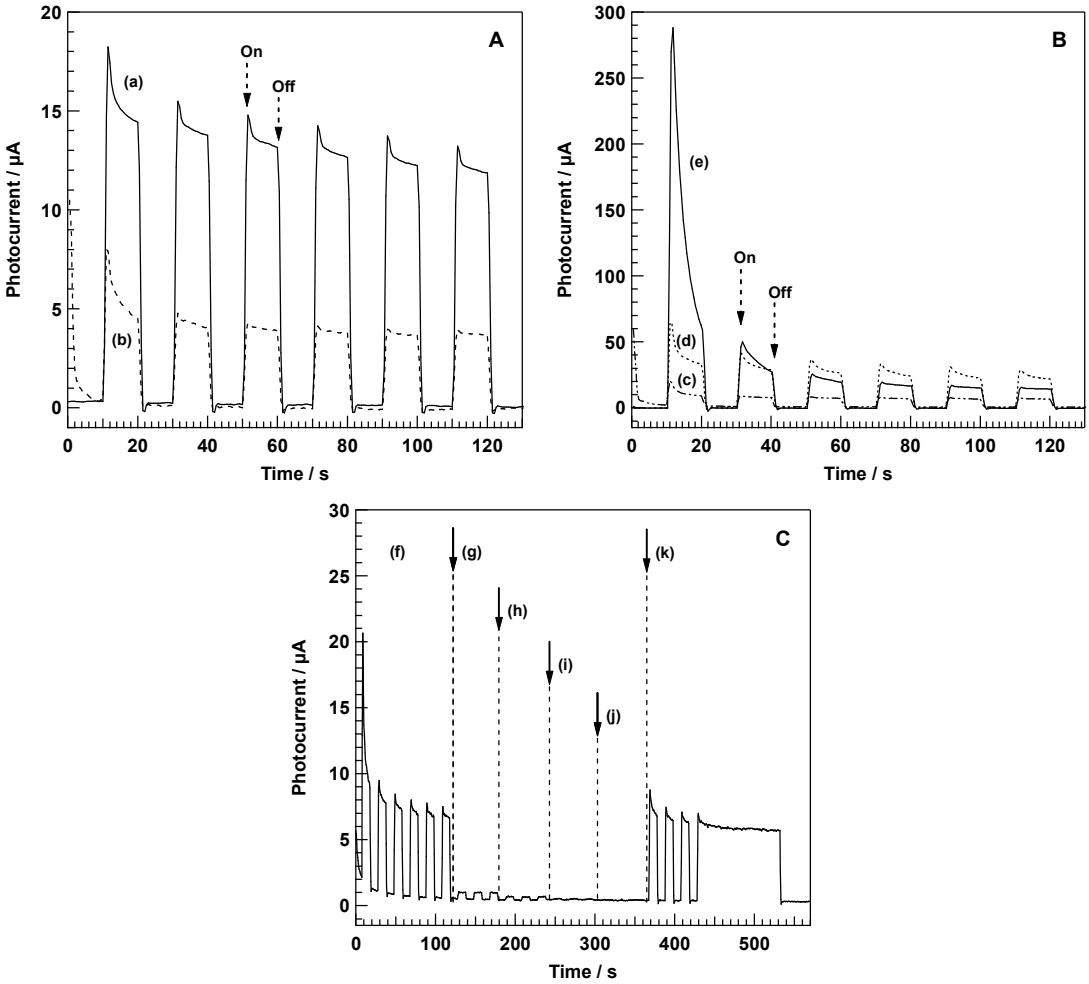

Figure 4 Photocurrent values under illumination cycling for X LDH/FTO (X = Ni−Al, Mg−Al, and Zn−Al). **(A)**: Ni−Al LDH/FTO measured in **(a)** 0.05 M $LiClO_4$ acetonitrile (5 vol.% methanol) and **(b)** 0.1 M Na_2SO_4 *aq.* (5 vol.% methanol). **(B) (c)** Ni−Al LDH/FTO, **(d)** Mg−Al LDH/FTO, and **(e)** Zn−Al LDH/FTO measured in 0.05 M $LiClO_4$ acetonitrile (5 vol.% methanol). **(C)** Ni−Al LDH/FTO measured in 0.05 M $LiClO_4$ acetonitrile (5 vol.% methanol) under the photoirradiation through **(f)** quartz glass, **(g)** UV-29, **(h)** UV-31, **(i)** UV-33, **(j)** UV-35, and **(k)** quartz glass. Atmosphere: He.

Zn^{2+} affected the photocurrent value, and the order of the initial photocurrent intensity was (e) Zn−Al LDH > (d) Mg−Al LDH > (c) Ni−Al LDH. This agrees with the quantity of electrons consumed in the photocatalytic conversion of CO_2 in water using these LDHs (powder samples) as previously shown[28]; specifically, the amount of electrons used to reduce CO_2 and H^+ (CO, CH_4, and H_2 were produced as reduction products) during 8 h of photoirradiation were 254, 110, and 68 μmol for Zn−Al LDH, Mg−Al LDH, and Ni−Al LDH, respectively. Although Ni−Al LDH evolved the largest amount of CO and showed the highest selectivity among these M^{2+}−Al LDHs, the total amounts of reduction products was greatest in the Zn−Al LDH because, in that case, a large amount of H_2 was evolved. The photocurrent values measured in the present study are considered to reflect the total photocatalytic activities of the LDH samples; that is, the metal components of the hydroxide sheets alter the photocatalytic activity of a series of LDH materials, and Zn−Al LDH is a good photocatalyst based on the results of the photoelectrochemical measurements and the photocatalytic reaction. However, it is possible that self-oxidation of Zn−Al LDH by the photogenerated holes led to a rapid decrease in the photocurrent intensity, as reported for the case of ZnO[39]. **Figure 4C** shows the photocurrent value of Ni−Al LDH/FTO under cycled illumination in a photoelectrochemical cell using an aqueous Na_2SO_4 solution as the electrolyte. In regions (f) and (k), photoirradiation was performed using a Hg-Xe lamp through a quartz window. For regions (g), (h), (i), and (j), long-pass cut-off filters UV-29, UV-31, UV-33, and UV-35, respectively, were set to control the photoirradiation wavelengths. The photocurrent intensity under photoirradiation through the UV-29 filter was much smaller than that through the quartz window. Moreover, the use of UV-31, UV-33, or UV-35 significantly diminished the photocurrent value during illumination. This result indicates that UV light irradiation of <270 nm is necessary to induce photocatalytic reactions over Ni−Al LDH, because a very low percentage of light at 270 nm can be transmitted through the UV-29 filter. Based on a Davis-Mott plot of Ni−Al LDH shown in **Figure 5**, the band gap energy of Ni−Al LDH is estimated at 4.8 eV (= 258 nm). This value is consistent with the results of the wavelength dependence measurements on the photocurrent intensity.

Figure 6 shows the linear sweep voltammogram measured while the light source was cycled on and off under He atmosphere. Under anodic polarization, the anodic photocurrent flowed when photoirradiation started. The presence of a depletion layer at the interface of the electrode under

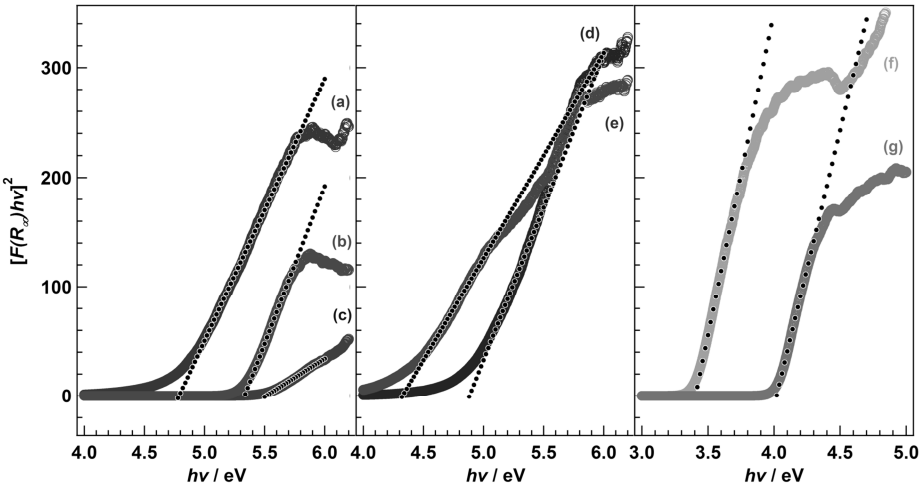

Figure 5 Davis-Mott plot of **(a)** Ni−Al LDH, **(b)** Mg−Al LDH, **(c)** Zn−Al LDH, **(d)** Ni−Ga LDH, **(e)** Ni−In LDH, **(f)** TiO_2, and **(g)** Ta_2O_5 based on the results of UV/Vis diffused reflection spectra.

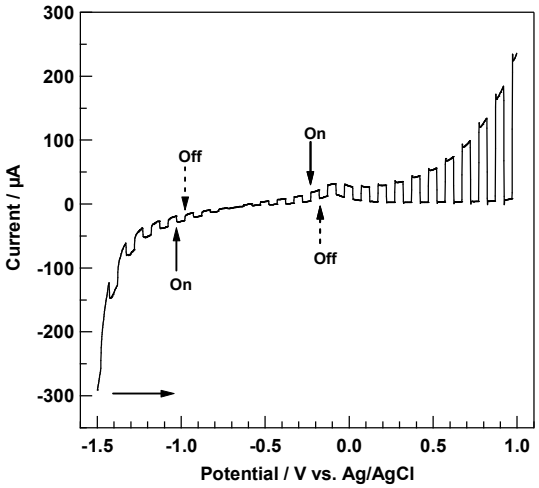

Figure 6 Linear sweep voltammogram of Ni−Al LDH/FTO measured with the repetition of turning on and off the illumination. Electrolyte: 0.05 M $LiClO_4$ acetonitrile (5 vol.% methanol). Atmosphere: He. Sweep range: from −1.5 to 1.0 V. Sweep rate: 10 mV s^{-1}. Photoirradiation: through quartz glass window.

anodic polarization enables the separation of the photogenerated charge carriers. Accordingly, for an *n*-type material at the positive potential, the band edges curve upwards, the hole moves toward the interface, and the electron moves to the interior of the material[31, 32]. Holes are high-energy species that can extract an electron from the electrolyte solution; that is, the *n*-type material acts as a photoanode under anodic polarization. Based on this, it can be inferred that Ni−Al LDH has electrochemical properties corresponding to an *n*-type material. In contrast, a small cathodic photocurrent was observed under cathodic polarization, which generally results from the *p*-type

character. We presumed that the cathodic photocurrent was due to the self-reduction of Ni species in Ni−Al LDH: from Ni^{2+} to Ni^{0} ($E°(Ni^{2+}/Ni)$ = −0.26 V vs. NHE (pH = 0))[29] or from NiOOH to $Ni(OH)_2$ ($E°(NiOOH/Ni(OH)_2)$ = 0.52 V vs. NHE (pH = 0))[29]. Moreover, the onset potential for the anodic photocurrent, based on the shape of the photocurrent profile during photoirradiation cycling, was estimated to ca. −0.75 V vs. Ag/AgCl in this study.

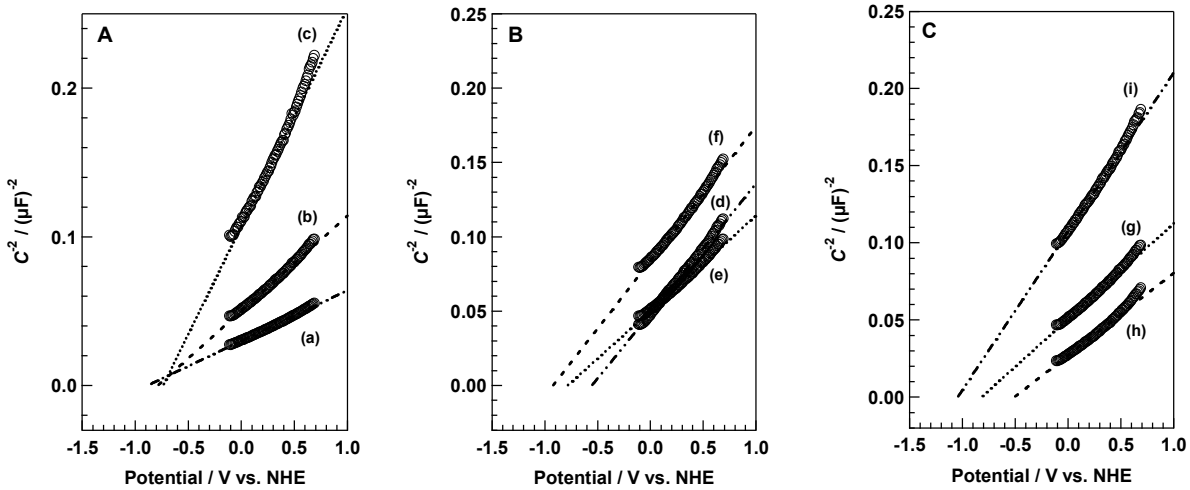

Figure 7 Mott-Schottky plots based on the results of the impedance measurements. **(A)** Plots for Ni−Al LDH/FTO at a frequency of **(a)** 37.3, **(b)** 52.0, and **(c)** 72.0 kHz. **(B)** Plots for **(d)** TiO_2/FTO, **(e)** Ni−Al LDH/FTO, and **(f)** Ta_2O_5/FTO at a frequency of 52.0 kHz. **(C)** Plots for **(g)** Ni−Al LDH/FTO, **(h)** Ni−Ga LDH/FTO, and **(i)** Ni−In LDH/FTO at a frequency of 52.0 kHz. Electrolyte solution: 0.1 M Na_2SO_4 *aq*. Atmosphere: He.

Figure 7A, B, and C show the Mott-Schottky plots of X LDH/FTO (X = Ni−Al, Mg−Al, Zn−Al, Ni−Ga, and Ni−In), TiO_2/FTO, and Ta_2O_5/FTO determined with the help of impedance measurements obtained by using these materials as working electrodes. As mentioned above, the flat band potential ($\boldsymbol{E_{FB}}$) can be determined by extrapolation to $\boldsymbol{C}^{-2} = 0$ ($\boldsymbol{C}$: capacitance), in accordance with the Mott-Schottky equation. When impedance measurements were conducted at variable frequencies, the fitted line for each Mott-Schottky plot should converge at $\boldsymbol{E_{FB}}$ ($\boldsymbol{C}^{-2} = 0$). In the case of Ni−Al LDH/FTO, actually, the fitting lines of the Mott-Schottky plots for frequencies of 37.3, 52.0, and 72.0 kHz crossed at a point shifted along the *x*-axis intercept, as shown in **Figure 7A**. Despite that, $\boldsymbol{E_{FB}}$ of Ni−Al LDH/FTO was estimated to range from −0.9 to −0.7 V vs. NHE (pH = 6.2). Moreover, the incline of the fitting line for the Mott-Schottky plot was positive (rightward inclining), indicating that the Ni−Al LDH has an *n*-type semiconductor-like property[31], as we

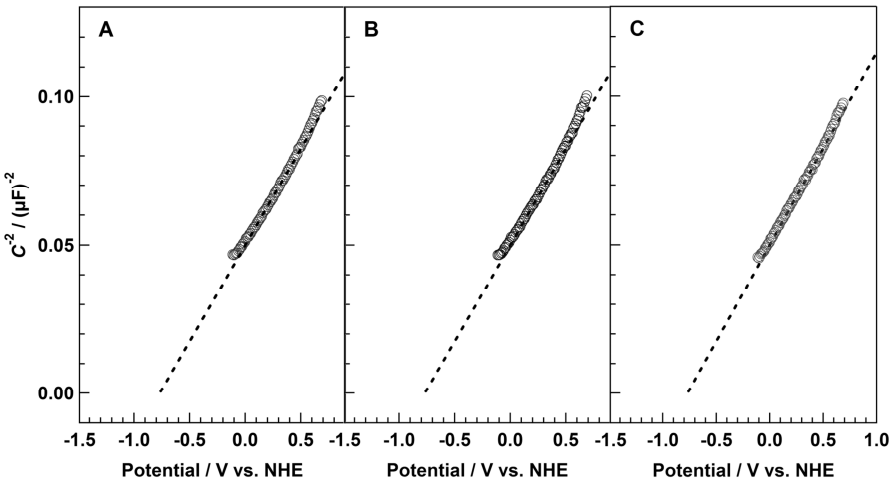

Figure 8 Mott-Schottky plot for **(A)** Ni−Al LDH/FTO, **(B)** Mg−Al LDH/FTO, and **(C)** Zn−Al LDH/FTO based on the results of the impedance measurements at a frequency of 52.0 kHz. Electrolyte solution:0.1 M Na_2SO_4 *aq*. Atmosphere: He.

determined before from the photoelectrochemical measurements. **Figure 7B** displays the Mott-Schottky plots of (d) TiO_2/FTO, (e) Ni−Al LDH/FTO, and (f) Ta_2O_5/FTO, recorded using an aqueous Na_2SO_4 solution (pH = 6.2) as an electrolyte under 52.0 kHz of the alternating current frequency. From this result, $\boldsymbol{E_{FB}}$ of anatase TiO_2 was considered as −0.55 V vs. NHE, and the value of $\boldsymbol{E_{FB}}$ matched with those of previous reports that described the energy position of the flat band for anatase TiO_2[40–41]. Similarly, the estimated value of $\boldsymbol{E_{FB}}$ of Ta_2O_5 in this study was −0.92 V vs. NHE (pH = 6.2), similar to those reported in previous literature[42]. Compared to these reference samples, the position of $\boldsymbol{E_{FB}}$ in Ni−Al LDH was between those of TiO_2 and Ta_2O_5, and was determined to be −0.77 V vs. NHE (pH = 6.2). This value was slightly shifted from the onset potential obtained from the photocurrent observation by sweeping the applied bias (**Figure 6**). Hans et al. have pointed out the dependence of the onset potential of photocurrent on experimental conditions such as surface coverage with reducible adsorbates, illumination intensity, wavelength, and pH of the electrolyte solution[43–44]. Concerning the present study, the results of the impedance measurements in accordance with the Mott-Schottky equation were used to determine the value of $\boldsymbol{E_{FB}}$. Generally, the difference in the value of $\boldsymbol{E_{FB}}$ for *n*-type metal oxide semiconductors is considered to be due to the metal components, which form the conduction band. The conduction band of TiO_2 and Ta_2O_5 mainly comprise the Ti 3d and Ta 5d orbitals, respectively. As shown in **Figure 7C**, a change in the estimated $\boldsymbol{E_{FB}}$ value was found with substitution of metal species of hydroxide sheets within the

LDH structure. The incorporation of Ga^{3+} or In^{3+} instead of Al^{3+} in the Ni−Al LDH for the formation of Ni−Ga LDH or Ni−In LDH clearly influenced on the value of $\boldsymbol{E_{FB}}$, whereas the substitution of Ni^{2+} with Mg^{2+} or Zn^{2+} did not affect the value of $\boldsymbol{E_{FB}}$, as shown in **Figure 8**. Based on these results, we concluded that the potential of the photogenerated electrons for a series of M^{2+}−M^{3+} LDH group materials are regulated by M^{3+} species within the hydroxide sheets, rather than M^{2+} species. Moreover, the Mott-Schottky plot for Ni−Al LDH shifted to negative potential with increasing pH of the electrolyte solution in accordance with the Nernst equation (Eq. 4), as shown in **Figure 9**.

Figure 10 summarizes the results of investigation on the electrochemical properties for X LDHs (X = Ni−Al, Mg−Al, Zn−Al, Ni−Ga, and Ni−In) and reference samples (TiO_2 and Ta_2O_5). Unless otherwise noted, the units of potential in this paragraph are quoted vs. NHE (pH = 0). Because the Fermi level for electrons of *n*-type character materials is considered to merge with the lowest potential of the conduction band[30], the value of $\boldsymbol{E_{FB}}$ obtained through the impedance measurements in this study is read as that of $\boldsymbol{E_e}$ for the LDH photocatalysts, and that of $\boldsymbol{E_{CB}}$ for the TiO_2 and Ta_2O_5 typical semiconductor photocatalysts. The value of energy gap ($\boldsymbol{E_g}$) between $\boldsymbol{E_e}$ and $\boldsymbol{E_h}$ for a series of LDHs, and the band gap ($\boldsymbol{E_{BG}}$) between $\boldsymbol{E_{CB}}$ and $\boldsymbol{E_{VB}}$ for TiO_2 and Ta_2O_5 were estimated from UV/vis diffuse reflectance spectra based on the Davis-Mott plot, as shown in **Figure 5**. In addition, the potential of the top of the valence band ($\boldsymbol{E_{VB}}$) was calculated using the values of

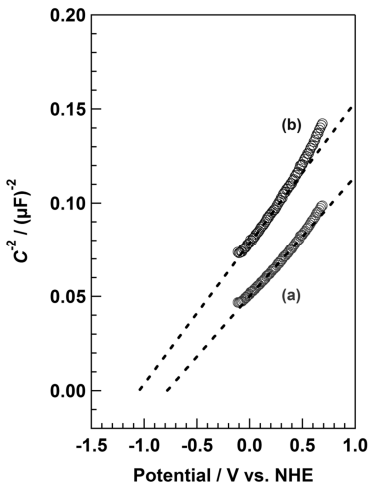

Figure 9 Change of Mott-Schottky plot of Ni−Al LDH/FTO in accordance with the value of pH of the electrolyte solution. pH of the electrolyte solution: **(a)** 6.2 or **(b)** 12.7. Frequency: 52.0 kHz. Atmosphere: He.

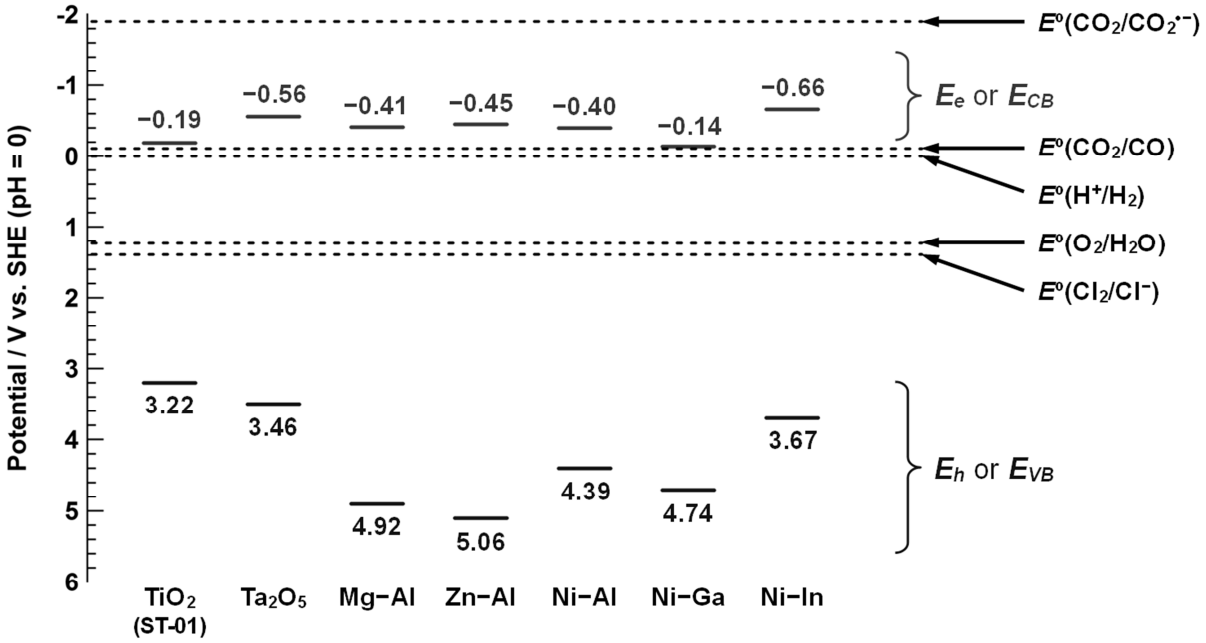

Figure 10 Summary of the investigation on the electrochemical properties for X LDH (X = Ni−Al, Mg−Al, Zn−Al, Ni−Ga, and Ni−In), and references (TiO_2 and Ta_2O_5). Standard potentials of redox couples are cited from the literature[29, 45]. Potentials of the photogenerated electrons and holes are respectively presented in upper and lower side of numbers.

$\boldsymbol{E_{CB}}$ and $\boldsymbol{E_{BG}}$. For the case of TiO_2, $\boldsymbol{E_{CB}}$ and $\boldsymbol{E_{BG}}$ were estimated to be −0.19 eV and 3.4 eV, respectively. The value of $\boldsymbol{E_{CB}}$ was adapted to that previously reported because −0.40 V vs. SCE (pH = 0) in the literature presented by Grätzel et al. [41] must be converted to −0.16 V vs. NHE (pH = 0) in accordance with the (Eq. 6). The $\boldsymbol{E_{BG}}$ value determined in this study was slightly larger than the general value. For Ta_2O_5, the estimated values of $\boldsymbol{E_{CB}}$ and $\boldsymbol{E_{VB}}$ were respectively −0.56 V and 3.46 V, which are consistent with the result of electrochemical measurement in the literature[42]. Based on these results for the reference samples, we suggest that the electrochemical character of X LDH (X = Ni−Al, Mg−Al, Zn−Al, Ni−Ga, and Ni−In) photocatalysts is as follows. For Ni−Al LDH, which has been reported as a photocatalyst for selective conversion of CO_2 into CO in our previous studies[26, 28], $\boldsymbol{E_e}$ was −0.40 V, thereby satisfying the required potential for the reduction of CO_2 to CO; however, it was not enough for the one-electron reduction of CO_2 ($E°(CO_2/CO_2^{\bullet-}) \approx -2.0$ V vs. NHE) [45]. From this result, it can be inferred that Ni−Al LDH photocatalyst can reduce CO_2 into CO in a two-electron process. On the other hand, $\boldsymbol{E_h}$ of Ni−Al LDH was found to be 4.39 V, significantly more positive than the value of $\boldsymbol{E_{VB}}$ for typical oxides such as TiO_2 and Ta_2O_5. This potential is

sufficient to oxidize Cl^- into Cl_2, as shown in **Figure 10** ($E°$ (Cl_2/Cl^-) = 1.39 V) [29]. We previously insisted that Cl^- in the reaction solution can act as an effective hole scavenger for the photocatalytic conversion of CO_2 in an aqueous solution and Cl^- should be oxidized into Cl_2, which is immediately converted into hypochlorous acid (HClO)[28]. By carrying out electrochemical investigations, we inferred that photogenerated electrons and holes in Ni−Al LDH are capable of reducing CO_2 into CO and oxidizing Cl^- into Cl_2. The changes in the value of $\boldsymbol{E_h}$ were determined by substituting Ni^{2+} in Ni−Al LDH with Mg^{2+} or Zn^{2+}, whereas the position of $\boldsymbol{E_e}$ was not influenced by the type of divalent metal in M^{2+}−Al LDH, as mentioned above. In contrast, the change of trivalent metal clearly affected the position of $\boldsymbol{E_e}$; for example, the incorporation of In^{3+} shifted to a negative value compared to Al^{3+}, while $\boldsymbol{E_e}$ of Ni−Ga LDH was found to have a positive potential, similar to the value of $\boldsymbol{E_{CB}}$ for TiO_2. By considering thermodynamic aspects, the reduction of protons to H_2 ($E°$ (H^+/H_2) = 0.0 V) [29], which competitively takes place in the photocatalytic conversion of CO_2 in an aqueous media, is relatively favorable in comparison to reduction of CO_2 into CO ($E°$ (CO_2/CO) = −0.11 V) [29, 45] because of their reduction potentials. The overpotential of the photoexcited electron toward the reduction of CO_2 into CO ($\Delta\boldsymbol{E_{OP}}$) is presented in accordance with (Eq. 7), as shown below.

(Eq. 7) $\Delta\boldsymbol{E_{OP}} = E°\ (CO_2/CO) - \boldsymbol{E_e}$

where $E°$ (CO_2/CO) and $\boldsymbol{E_e}$ are the standard potential of CO_2 reduction to CO and the potential of the photogenerated electron, estimated from $\boldsymbol{E_{FB}}$, respectively. Hence, Ni−In LDH, whose photoexcited electron has a large overpotential in the reduction of CO_2 into CO ($\Delta\boldsymbol{E_{OP}}$ = 0.55 V), should be more advantageous for the selective reduction of CO_2 than Ni−Al LDH ($\Delta\boldsymbol{E_{OP}}$ = 0.29 V). However, the photocatalytic conversion of CO_2 in water using powder samples[26] shows that Ni−Al LDH, whose $\boldsymbol{E_e}$ is more positive than that of Ni−In LDH, shows a higher selectivity toward CO_2 reduction among the reduction products (ca. 70% of the selectivity toward CO_2 reduction among the total reduction products; CO, CH_4, and H_2) rather than Ni−In LDH (ca. 4.8%). In such as case, Ni−In LDH evolved large amounts of H_2 as the reduction product of H^+, indicating that the photogenerated electrons were mainly consumed in the reduction of H^+. In other words, Ni−Al LDH enabled the selective conversion of CO_2 in spite of its relatively positive $\boldsymbol{E_e}$. This correlation clearly indicates that the selectivity toward CO_2 reduction and the inhibition of proton reduction to H_2 were determined by not only the overpotential of photogenerated electron but also by the chemical properties and

morphologies. Herein, we have clarified the photocurrent character and electrochemical properties such as potentials of photogenerated electrons and holes for a series of LDHs, including Ni−Al LDH, through electrochemical and photoelectrochemical measurements.

Conclusion

A series of LDHs (Ni−Al, Mg−Al, and Zn−Al LDH) were found to produce anodic photocurrent under no external bias, and the order of the initial photocurrent intensities were in accordance with the amount of electrons consumed in the photocatalytic conversion of CO_2 in water using these LDH powder samples. Ni−Al LDH had electrochemical properties corresponding to *n*-type materials; that is, cathodic dark current under cathodic polarization and anodic photocurrent under anodic polarization were determined by electrochemical measurements. The value of $\boldsymbol{E_e}$ for the Ni−Al LDH photocatalyst was estimated to be −0.40 V vs. NHE (pH = 0), which is enough to induce the two-electron reduction of CO_2 into CO. The change of M^{3+} metal in Ni−M^{3+} LDH clearly influenced $\boldsymbol{E_e}$; $\boldsymbol{E_e}$ changed from negative to positive in the following order: Ni−In LDH, Ni−Al LDH, and Ni−Ga LDH. We concluded that the photogenerated electrons consumed in the reduction of CO_2 into CO or H^+ into H_2 is determined by not only by the overpotential but also by the chemical properties of LDH photocatalysts.

References

1. F. Cavani, F. Trifirò and A. Vaccari, *Catalysis Today*, 1991, **11**, 173-301.
2. C. Delhoyo, *Applied Clay Science*, 2007, **36**, 103-121.
3. B. F. Sels, D. E. De Vos and P. A. Jacobs, *Catalysis Reviews*, 2001, **43**, 443-488.
4. Y. Arishige, D. Kubo, K. Tadanaga, A. Hayashi and M. Tatsumisago, *Solid State Ionics*, 2014, **262**, 238-240.
5. D. Kubo, K. Tadanaga, A. Hayashi and M. Tatsumisago, *Journal of Electroanalytical Chemistry*, 2012, **671**, 102-105.
6. D. Kubo, K. Tadanaga, A. Hayashi and M. Tatsumisago, *Journal of Power Sources*, 2013,

222, 493-497.

7. K. Tadanaga, Y. Furukawa, A. Hayashi and M. Tatsumisago, *Journal of The Electrochemical Society*, 2012, **159**, B368-B370.
8. J. Fang, M. Li, Q. Li, W. Zhang, Q. Shou, F. Liu, X. Zhang and J. Cheng, *Electrochimica Acta*, 2012, **85**, 248-255.
9. Z. Gao, J. Wang, Z. Li, W. Yang, B. Wang, M. Hou, Y. He, Q. Liu, T. Mann, P. Yang, M. Zhang and L. Liu, *Chemistry of Materials*, 2011, **23**, 3509-3516.
10. A. Malak-Polaczyk, C. Vix-Guterl and E. Frackowiak, *Energy & Fuels*, 2010, **24**, 3346-3351.
11. T. Stimpfling and F. Leroux, *Chemistry of Materials*, 2010, **22**, 974-987.
12. D. H. Youn, Y. B. Park, J. Y. Kim, G. Magesh, Y. J. Jang and J. S. Lee, *Journal of Power Sources*, 2015, **294**, 437-443.
13. W. He, R. Wang, L. Zhang, J. Zhu, X. Xiang and F. Li, *Journal of Materials Chemistry A*, 2015, **3**, 17977-17982.
14. L. Mohapatra and K. M. Parida, *Physical Chemistry Chemical Physics*, 2014, **16**, 16985-16996.
15. L. Wang, F. Dionigi, N. T. Nguyen, R. Kirchgeorg, M. Gliech, S. Grigorescu, P. Strasser and P. Schmuki, *Chemistry of Materials*, 2015, **27**, 2360-2366.
16. M. Shao, J. Han, M. Wei, D. G. Evans and X. Duan, *Chemical Engineering Journal*, 2011, **168**, 519-524.
17. S. J. Xia, F. X. Liu, Z. M. Ni, J. L. Xue and P. P. Qian, *Journal of Colloid and Interface Science*, 2013, **405**, 195-200.
18. J. S. Valente, F. Tzompantzi and J. Prince, *Applied Catalysis B: Environmental*, 2011, **102**, 276-285.
19. B. Li, Y. Zhao, S. Zhang, W. Gao and M. Wei, *ACS Applied Materials & Interfaces*, 2013, **5**, 10233-10239.
20. Y. Zhao, P. Chen, B. Zhang, D. S. Su, S. Zhang, L. Tian, J. Lu, Z. Li, X. Cao, B. Wang, M. Wei, D. G. Evans and X. Duan, *Chemistry*, 2012, **18**, 11949-11958.
21. C. G. Silva, Y. Bouizi, V. Fornés and H. García, *Journal of the American Chemical Society*,

2009, **131**, 13833-13839.

22. N. Ahmed, Y. Shibata, T. Taniguchi and Y. Izumi, *Journal of Catalysis*, 2011, **279**, 123-135.
23. K.-i. Katsumata, K. Sakai, K. Ikeda, G. Carja, N. Matsushita and K. Okada, *Materials Letters*, 2013, **107**, 138-140.
24. M. Morikawa, N. Ahmed, Y. Yoshida and Y. Izumi, *Applied Catalysis B: Environmental*, 2014, **144**, 561-569.
25. M. Morikawa, Y. Ogura, N. Ahmed, S. Kawamura, G. Mikami, S. Okamoto and Y. Izumi, *Catalysis Science & Technology*, 2014, **4**, 1644-1651.
26. S. Iguchi, K. Teramura, S. Hosokawa and T. Tanaka, *Catalysis Today*, 2015, **251**, 140-144.
27. K. Teramura, S. Iguchi, Y. Mizuno, T. Shishido and T. Tanaka, *Angewandte Chemie International Edition*, 2012, **51**, 8008-8011.
28. S. Iguchi, K. Teramura, S. Hosokawa and T. Tanaka, *Physical Chemistry Chemical Physics*, 2015, **17**, 17995-18003.
29. A. J. B. Ed., R. Parsons, J. Jordan, *Standard Potentials in Aqueous Solution*, Marcel Dekker, 1985.
30. R. Beranek, *Advances in Physical Chemistry*, 2011, **2011**, 1-20.
31. A. W. Bott, *Current Separations*, 1998, **17**, 87-91.
32. L. L. K. Gelderman, and S. W. Donne, *Journal of Chemical Education*, 2007, **84**, 685-688.
33. W. G. F. Cardon, *Journal of Physics D: Applied Physics*, 1978, **11**, L63-67.
34. W. J. Albery, G. J. O'Shea and A. L. Smith, *Journal of the Chemical Society, Faraday Transactions*, 1996, **92**, 4083-4085.
35. E. A. Davis and N. F. Mott, *Philosophical Magazine*, 1970, **22**, 0903-0922.
36. R. G. Bates, *Determination of pH: theory and practice*, John Wiley & Sons, 1973.
37. D. T. Sawyer, A. Sobkowiak and J. L. Roberts, *Electrochemistry for Chemists*, Wiley, 1995.
38. J. Zhang, X. Xie, C. Li, H. Wang and L. Wang, *RSC Advances*, 2015, **5**, 29757-29765.
39. L. N. Elaziouti and B. Ahmed, *Journal of Chemical Engineering & Process Technology*, 2011, **2**, 106.
40. L. Kavan, M. Grätzel, S. E. Gilbert, C. Klemenz and H. J. Scheel, *Journal of the American Chemical Society*, 1996, **118**, 6716-6723.

41. G. Rothenberger, D. Fitzmaurice and M. Graetzel, *The Journal of Physical Chemistry*, 1992, **96**, 5983-5986.

42. W.-J. Chun, A. Ishikawa, H. Fujisawa, T. Takata, J. N. Kondo, M. Hara, M. Kawai, Y. Matsumoto and K. Domen, *The Journal of Physical Chemistry B*, 2003, **107**, 1798-1803.

43. J. M. Bolts and M. S. Wrighton, *The Journal of Physical Chemistry*, 1976, **80**, 2641-2645.

44. H. R. Sprunken, R. Schumacher and R. N. Schindler, *Faraday Discussions of the Chemical Society*, 1980, **70**, 55-66.

45. J.-M. Lehn and R. Ziessel, *Proceedings of the National Academy of Sciences of the United States of America*, 1982, **79**, 701-704.

Chapter 6

Improvement in the Photocatalytic Activity for the Conversion of CO_2 in Water by Modification of Ga_2O_3 with Mg−Al Layered Double Hydroxide

Abstract

Photocatalytic conversion of CO_2 into useful chemicals is one of the promising countermeasures against the increasing concentrations of CO_2 in our atmosphere. This is because photocatalytic reactions can drive a thermodynamically uphill reaction, the so called "artificial photosynthesis." We previously reported that Ag cocatalyst-loaded Ga_2O_3 photocatalysts show high activity in the conversion of CO_2 into CO in water, and their further modification with $ZnGa_2O_4$ helped improve the selectivity toward CO evolution among the reduction products by suppressing H_2 evolution. In this study, we report that modification of a Ga_2O_3 photocatalyst with Mg−Al layered double hydroxide (LDH) clearly enhanced the photocatalytic activity for the conversion of CO_2. The formation rate of CO and the selectivity toward CO evolution were 245.6 μmol h^{-1} and 59.8%, respectively, when 1.0 g of Mg−Al LDH-Ga_2O_3 composite photocatalyst was used in the presence of 0.25 wt.% Ag cocatalyst. Moreover, the turnover number (TON) of electrons, which are used to reduce CO_2 into CO, was 88.6 per Ag atom for 5 h of photoirradiation.

Introduction

Photocatalysis is a growing field of interest in the scientific community due to the ability to convert light energy into chemical energy in a storable form. This has implications in the critical environmental issues that we face today. Photocatalytic overall splitting of water into H_2 and O_2 under sunlight illumination has been previously reported,[1-3] and H_2 can be used as an energy source in various applications. Photocatalytic artificial photosynthesis involves several steps such as photoabsorption (light harvesting), charge separation, oxidation of H_2O, and consumption of the photogenerated electron for the reduction reaction.[4,5] As there is some interest in removing CO_2 (a greenhouse gas) from our atmosphere, a photocatalytic reaction that can reduce CO_2 via an uphill process ($\Delta G > 0$) should be a promising technique.[5-7] We have previously reported the photocatalytic activity of Ga_2O_3, Zn-modified Ga_2O_3, and $ZnGa_2O_4$ for the conversion of CO_2 into CO in an aqueous $NaHCO_3$ solution in the presence of a Ag cocatalyst.[8-10] Although the Ag-loaded Ga_2O_3 photocatalyst showed high photocatalytic performance, the selectivity toward CO evolution among the reduction products was disappointingly low, and H_2 evolution was predominantly observed.[8] Because H_2 formation competes for electrons that are required for the reduction of CO_2, further optimization is necessary for suppressing this process. The modification of the Ga_2O_3 photocatalyst with a Zn species led to a drastic increase in the selectivity toward CO evolution by suppressing H_2 evolution.[10] X-ray diffraction (XRD) and X-ray absorption fine structure (XAFS) revealed that $ZnGa_2O_4$ was formed on the surface of Ga_2O_3 modified with Zn species after calcination at 1223 K.[8,10] The formation of $ZnGa_2O_4$, which itself can act as a photocatalyst,[10] clearly suppresses H_2 production and improves the selectivity toward CO evolution among the reduction products. While we were successful in improving the selectivity of our catalyst via modification with $ZnGa_2O_4$, unfortunately the rate of CO_2 evolution (110 μmol h^{-1} for 1.0 g of Ag/$ZnGa_2O_4$/Ga_2O_3) was deemed insufficient.

The modification of a photocatalyst with the solid base material that can supply adsorption sites for CO_2 molecules is a promising technique to regulate the selectivity in the photocatalytic conversion of CO_2 in water. MgO-modified TiO_2,[11,12] magnesium/aluminum layered double oxide (LDO)-grafted TiO_2,[13] and self-assembly of carbon nitride (C_3N_4) and different types of LDH

(LDH-C_3N_4)[14] have been shown to exhibit photocatalytic activity for the conversion of CO_2. Moreover, our group also reported that the modification of the Ta_2O_5 photocatalyst with alkaline earth metal oxides, especially with SrO, drastically improved the selectivity toward CO evolution for the photocatalytic conversion of CO_2 in an aqueous $NaHCO_3$ solution.[15] Layered double hydroxides (LDHs) are known as anionic clays consisting of highly ordered two-dimensional hydroxide sheets and charge-compensating interlayer anions.[16,17] The general formula of LDHs is $[M^{2+}_{1-x}M^{3+}_{x}(OH)_2]^{x+}(A^{n-}_{x/n})\cdot mH_2O$, where M^{2+} and M^{3+} are divalent and trivalent cations, respectively; x represents the molar ratio of $M^{3+}/(M^{2+} + M^{3+})$, while A^{n-} is the interlayer anion of valence n.[18] Mg−Al LDH ($Mg_6Al_2(OH)_{16}(CO_3)\cdot 4H_2O$) is the most well-known LDH, and it is widely used as the solid base material for removing a variety of anions from wastewater,[19-21] for base-catalyzed reactions,[22-24] and for CO_2 capture and storage (CCS).[25] Moreover, the Mg−Al LDH can catalyze the aldol condensation of carbonyl compounds in an aqueous solution, as reported by Ebitani *et al.*,[26] indicating that the Mg−Al LDH and its derivatives can be used as solid base catalysts in the presence of water because their surface basic sites show high water tolerance. The photocatalytic conversion of CO_2 in water using a series of LDHs as photocatalysts, whose surface properties can drive the selective reduction of CO_2 into CO by suppressing H_2 evolution, has also been reported by our research group.[27-29] In this study, we demonstrated that the modification of the Ga_2O_3 photocatalyst with Mg−Al LDH improved both the amount of CO evolved as a reduction product of CO_2 and the selectivity toward CO evolution among the other reduction products.

Experimental

Gallium oxide (Ga_2O_3, 99.99%, Kojundo Chemical Laboratory Co., Ltd.) was used without any treatment in this study. An aqueous solution of metal components ($MgCl_2\cdot 6H_2O$ and $AlCl_3$) was slowly dropped onto an aqueous Na_2CO_3 solution which contains Ga_2O_3 powder with keeping pH value between 9.9 and 10.1 by adding an aqueous NaOH solution. The ratio of metal components in Mg−Al LDH was fixed at Mg/Al = 3. The resulting suspension was aged at 333 K for 24 h under ambient pressure with vigorous stirring. The solid precipitate was washed with ultra-pure water, and collected by suction filtration. The cake was dried at 333 K under vacuum condition. Amount of the

modified Mg−Al LDH (***x***) was varied from 30 to 95 mol% in accordance with an equation presented below (formula (1)).

$$\boldsymbol{x}\ (\text{mol\%}) = 100 \times (\boldsymbol{A}_{\mathbf{Mg}} + \boldsymbol{A}_{\mathbf{Al}}) / (\boldsymbol{A}_{\mathbf{Mg}} + \boldsymbol{A}_{\mathbf{Al}} + \boldsymbol{A}_{\mathbf{Ga}}) \qquad (1)$$

where; $\boldsymbol{A}_{\mathbf{Mg}}$, $\boldsymbol{A}_{\mathbf{Al}}$, and $\boldsymbol{A}_{\mathbf{Ga}}$ show numbers (mol unit) of Mg atoms, Al atoms, and Ga_2O_3 in the prepared photocatalyst. For example, the value of ***x*** = 50 means that the molar ratio of (Mg + Al) / Ga_2O_3 = 1.0. Hereinafter, ***x***-MgAl/Ga_2O_3 represents Mg−Al LDH-modified Ga_2O_3 with the molar ratio of ***x***. The reference composite samples; ***x***-Mg/Ga_2O_3 and ***x***-Al/Ga_2O_3, which are respectively $Mg(OH)_2$ and $Al(OH)_3$-modified Ga_2O_3, were prepared via same procedure to the case of ***x***-MgAl/Ga_2O_3.

Silver cocatalyst was loaded to photocatalysts by the typical impregnation method. The required amount of as-synthesized ***x***-MgAl/Ga_2O_3 powder was dispersed in an aqueous solution containing a certain amount of $AgNO_3$, and then evaporated at 353 K. The resulting powder was calcined at 723 K for 2 h in air atmosphere. In this paper, ***y***Ag/***x***-MgAl/Ga_2O_3 means ***y*** wt.% Ag cocatalyst-loaded ***x***-MgAl/Ga_2O_3 photocatalyst.

Ag cocatalyst-loaded Mg−Al LDH (Ag/MgAl): Mg−Al LDH was synthesized via typical co-precipitation method as presented above with the exception of Ga_2O_3 powder in an aqueous Na_2CO_3 solution. 1.0 wt.% Ag cocatalyst was loaded on the prepared Mg−Al LDH by the impregnation method as with the case described previously.

Ag cocatalyst-loaded bare Ga_2O_3 (***y***Ag/Ga_2O_3): ***y*** wt.% of Ag cocatalyst was introduced on the commercial Ga_2O_3 (99.99%, Kojundo Chemical Laboratory Co., Ltd.) by the impregnation method as mentioned above.

Mg−Al LDH-modified ***y***Ag/Ga_2O_3 (***x***-MgAl/***y***Ag/Ga_2O_3): An aqueous solution of precursors ($MgCl_2 \cdot 6H_2O$ and $AlCl_3$) was slowly dropped onto an aqueous Na_2CO_3 solution which contains the ***y***Ag/Ga_2O_3 powder via the same procedure to that for ***x***-MgAl/Ga_2O_3.

Physical mixture of Mg−Al LDH and ***y***Ag/Ga_2O_3 (***x***-MgAl + ***y***Ag/Ga_2O_3): The calculated amounts of prepared Mg−Al LDH powder and ***y***Ag/Ga_2O_3 powder were sufficiently mixed in an agate mortar.

Ag cocatalyst-loaded SiO_2-modified Ga_2O_3 (***y***Ag/***x***-Si/Ga_2O_3): The required amounts of Ga_2O_3 powder (99.99%, Kojundo Chemical Laboratory Co., Ltd.), tetraethyl orthosilicate (TEOS),

and urea were mixed in a ultra-pure water, and resulting suspension was aged at 373 K for 24 h under hydrothermal condition using a stainless steel autoclave equipped with an inner Teflon vessel. The impregnation of Ag cocatalyst and the calcination at 723 K resulted in ***y***Ag/***x***-Si/Ga_2O_3 composite.

The powder XRD patterns of the prepared samples were collected by using an X-ray diffractometer (Ultime IV, Rigaku), using Cu K_α radiation. UV/Vis diffuse reflectance spectra of the photocatalysts were measured using a UV-VIS Spectrophotometer (V-650, JASCO) equipped with an integrated sphere. The Brunauer-Emmett-Teller (BET) specific surface areas of the samples were estimated from their N_2 adsorption isotherms at 77 K (liquid N_2 temperature) using a volumetric adsorption measurement instrument (BELSORP-miniII, MicrotracBEL). Prior to the measurement, the powder sample was evacuated at 373 K for 1 h using a pretreatment instrument (BELPREP-vacII, MicrotracBEL). SEM images of the synthesized samples were captured by using a Field Emission Scanning Electron Microscope (FE-SEM, SU-8220, Hitachi High-Technologies) at an acceleration voltage of 3.0 kV.

Photocatalytic activity for the conversion of CO_2 in an aqueous solution was evaluated by using an inner-irradiation type quasi-flowing batch system. Photocatalyst powder was dispersed in 1.0 L of an aqueous $NaHCO_3$ solution, and the dissolved air in this suspension was thereafter degassed by flowing high-purity CO_2 gas (99.999%). CO_2 gas was continuously bubbled into the reaction solution at a flow rate of 30 mL min^{-1}. The suspension was irradiated by a 400 W high-pressure Hg lamp through a quartz filter equipped with a cooling water system. The resulting products in the gas phase, such as CO, H_2, O_2, were analyzed by an on-line barrier discharge ionization detector (BID) gas chromatography (GC-2010 Tracera, Shimadzu Corp.) using a MICROPACKED ST column. The formation rates of these products (μmol h^{-1}) were calculated by using a 1.0 mL of volumetric pipe. The selectivity toward CO evolution in CO and H_2, and the balance between consumed electrons (e^-) and holes (h^+) were given by formula (2) and (3), respectively.

$$\text{Selectivity toward CO evolution (\%)} = 100 \times \boldsymbol{R}_{\mathbf{CO}} / (\boldsymbol{R}_{\mathbf{CO}} + \boldsymbol{R}_{\mathbf{H2}}) \quad (2)$$

$$\text{Consumed } e^-/h^+ = (\boldsymbol{R}_{\mathbf{CO}} + \boldsymbol{R}_{\mathbf{H2}}) / \boldsymbol{R}_{\mathbf{O2}} \quad (3)$$

where $\boldsymbol{R}_{\mathbf{CO}}$, $\boldsymbol{R}_{\mathbf{H2}}$, and $\boldsymbol{R}_{\mathbf{O2}}$ represents the formation rates of CO, H_2, and O_2, respectively.

Results and discussion

Figure 1 shows the XRD patterns of the synthesized composite photocatalysts and reference samples. Bare Ga_2O_3 **(a)** showed the typical reflection pattern corresponding to β-phase Ga_2O_3.[30] The sharp diffraction peaks, which are assigned to the (0 0 3), (0 0 6), and (0 0 9) planes reflections, respectively, were found at 11.5°, 23.2°, and 34.8°, respectively, in the XRD pattern of bare Mg−Al LDH **(b)**.[16] The positions of these peaks should be determined by the interlayer distance between each hydroxide sheet; a literature review shows that the carbonate ion (CO_3^{2-}) is mainly intercalated in the interlayer space.[31] Moreover, the two diffraction peaks around 60º corresponded to the (1 1 0) and (1 1 3) planes reflections respectively. As compared to bare Ga_2O_3 and Mg−Al LDH, the XRD pattern of ***95***-MgAl/Ga_2O_3 **(c)** showed a mixed phase comprising Ga_2O_3 and Mg−Al LDH. The peak position of the (0 0 3) plane reflection was the same as that of bare Mg−Al LDH, indicating that CO_3^{2-}-intercalated Mg−Al LDH was formed in the ***95***-MgAl/Ga_2O_3 composite sample. It was expected that the position of the (1 1 0) plane reflection should be shifted to a lower angle when Ga^{3+} was incorporated into the hydroxide sheet within the LDH structure, because the ionic radii of six-fold coordinated Al^{3+} and Ga^{3+} are 53.5 and 62.0 pm, respectively.[32] Based on this consideration, a slight peak shift to a lower angle in the (1 1 0) plane reflection (from 60.7° to 60.4°) suggests that

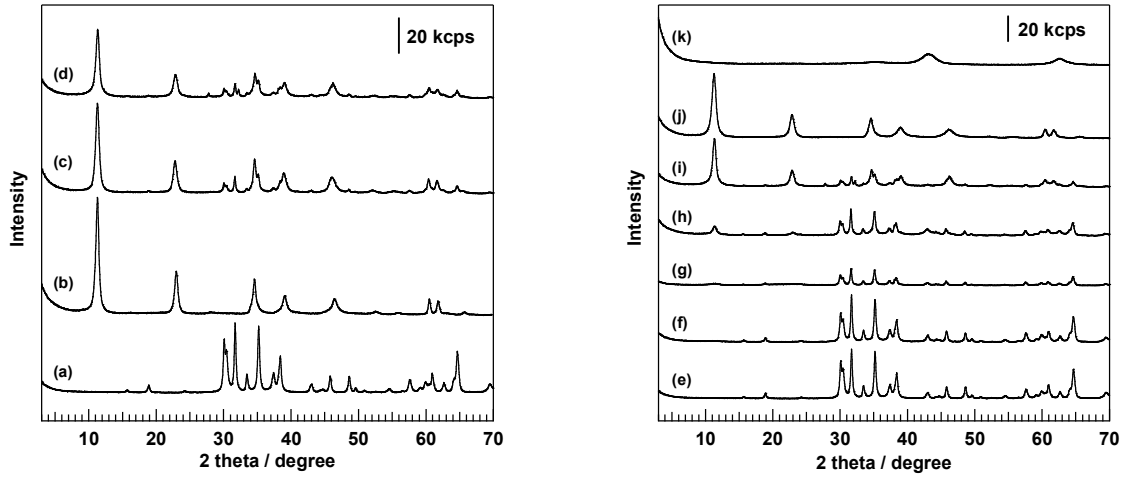

Figure 1 XRD patterns of (a) Ga_2O_3 (commercial), (b) and (j) Mg−Al LDH, (c) ***95***-MgAl/Ga_2O_3, (d) ***0.25***Ag/***95***-MgAl/Ga_2O_3, (e) ***1.0***Ag/***30***-MgAl/Ga_2O_3, (f) ***1.0***Ag/***50***-MgAl/Ga_2O_3, (g) ***1.0***Ag/***70***-MgAl/Ga_2O_3, (h) ***1.0***Ag/***85***-MgAl/Ga_2O_3, (i) ***1.0***Ag/***95***-MgAl/Ga_2O_3, and (k) Mg−Al LDH calcined at 723 K.

the LDH structure comprised a very small amount of Ga^{3+} derived from Ga_2O_3. In other words, this analysis of our XRD pattern leads us to conclude that this Mg-Al LDH contains primarily Mg^{2+}, Al^{3+} and a small amount of Ga^{3+} within the hydroxide sheets, and the chemical connection was formed between Ga_2O_3 and Mg−Al LDH through these hydroxide sheets. The characteristic layered structure of Mg−Al LDH was retained after Ag cocatalyst loading, as shown in **(d)**. **Figure 1(e−i)** shows the XRD patterns of ***1.0***Ag/***x***-MgAl/Ga_2O_3 (where ***x*** = 30, 50, 70, 85, and 95). The (0 0 3) plane reflection was not found in ***1.0***Ag/***30***-MgAl/Ga_2O_3 and ***1.0***Ag/***50***-MgAl/Ga_2O_3, whereas ***1.0***Ag/***x***-MgAl/Ga_2O_3 (***x*** = 70, 85, and 95) showed an XRD pattern containing diffraction peaks corresponding to the layer structure of the LDH despite the calcination at 723 K in the procedure for Ag cocatalyst loading. However, It is known that bare Mg−Al LDH decomposes into an amorphous mixed oxide when calcined at 723 K, accompanied with the collapse of the layered structure[16], as shown in **Figure 1(k)**. This result indicates that the thermal stability of Mg−Al LDH in the ***1.0***Ag/***x***-MgAl/Ga_2O_3 composite was better than that of bare Mg−Al LDH, probably because of the chemical interaction between LDH and Ga_2O_3.

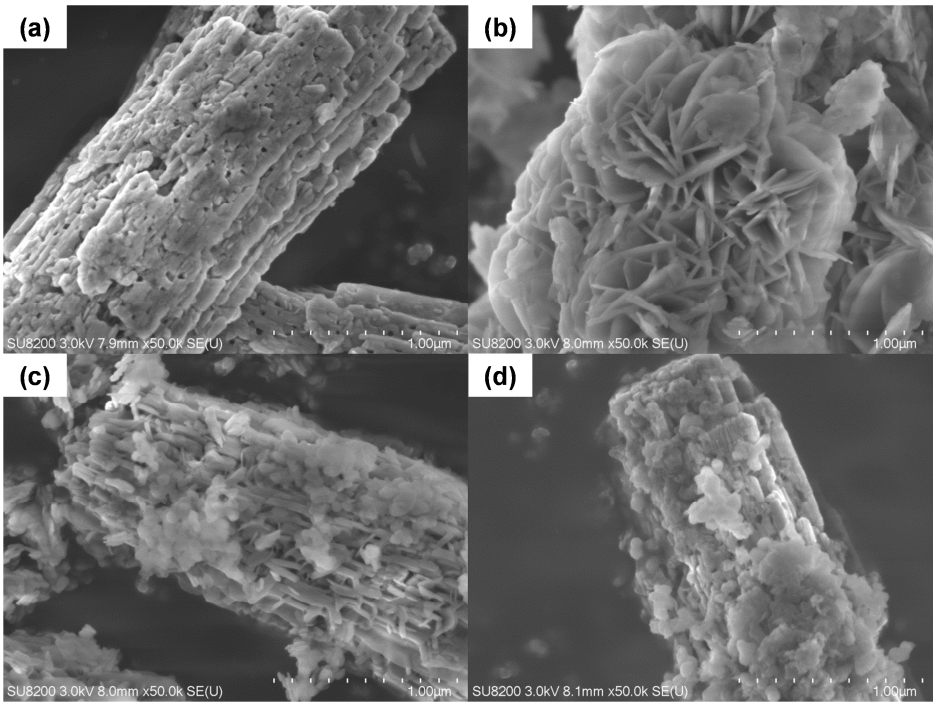

Figure 2 SEM images of (a) Ga_2O_3 (commercial), (b) Mg−Al LDH, (c) ***50***-MgAl/Ga_2O_3, and (d) ***95***-MgAl/Ga_2O_3.

The morphology of the composite photocatalyst was confirmed by SEM images, as shown in **Figure 2**. Several micrometer-sized pillar-shaped particles containing many cracks and pore structures were observed in the SEM images of Ga_2O_3. Mg−Al LDH showed many platelet structures shaped like flower petals, which is the characteristic of LDHs. In the composite photocatalyst, a part of Ga_2O_3 particles was covered with the platelet-like Mg−Al LDH particles. In fact, the surface of Ga_2O_3 was practically covered with Mg−Al LDH in the case of ***95***-MgAl/Ga_2O_3 composite sample (**Figure 2(d)**). The absorption edge of the ***95***-MgAl/Ga_2O_3 composite photocatalyst in its UV/Vis DR spectrum (**Figure 3**) was almost the same to that of bare Ga_2O_3, indicating that the modification of Ga_2O_3 with Mg−Al LDH did not affect its absorption properties. When the Ag cocatalyst was loaded on to the ***x***-MgAl/Ga_2O_3 composite, a broad absorption band appeared around 330 nm, which can be attributed to the plasmonic absorption of Ag metal particles or *d-d* transition of Ag_2O.

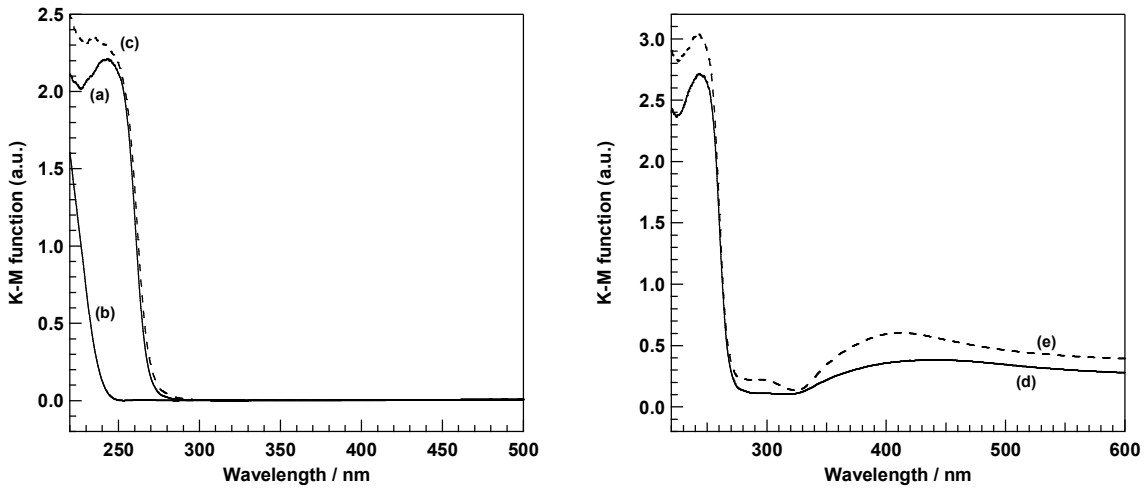

Figure 3 UV/Vis diffuse reflectance spectra of (a) ***95***-MgAl/Ga_2O_3, (b) Mg−Al LDH, (c) Ga_2O_3, (d) ***1.0***Ag/***95***-MgAl/Ga_2O_3, and (e) ***1.0***Ag/***95***-MgAl/Ga_2O_3 (after reaction).

Table 1 summarizes the specific surface area, content of Ga_2O_3 in the composite photocatalyst, and the result of the photocatalytic reaction for the ***1.0***Ag/***x***-MgAl/Ga_2O_3 composite (where ***x*** = 30, 50, 70, 75, and 95), Ag//Ga_2O_3, and Ag/Mg−Al LDH. It was considered that only Ga_2O_3 could act as a photocatalyst in this composite material because Ag-loaded bare Mg−Al LDH did not show any photocatalytic activity. Therefore, the amount of photocatalyst that can generate photoexcited electrons and holes should be varied with the value of ***x***; for example, 500 mg of

Table 1 The specific surface area and the result of photocatalytic conversion of CO_2 in water for ***x***-MgAl/Ga_2O_3 composite photocatalyst (***x*** = 30, 50, 70, 75, and 95), bare Ga_2O_3, and bare Mg−Al LDH. Amount of Ag cocatalyst: 1.0 wt.%. Total amount of photocatalyst: 0.5 g. Additive: 0.1 M $NaHCO_3$. Photoirradiation time: 1 h.

Photocatalyst	S_{BET} / $m^2\ g^{-1}$	Weight / g		Formation rate of products / μmol h^{-1}			Selectivity to CO (%)	e^-/h^+ balance
		Total	Ga_2O_3	H_2	O_2	CO		
bare Ga_2O_3	13	0.50	0.50	182.3	117.9	78.6	30.1	1.11
30-MgAl/Ga_2O_3	16	0.50	0.46	203.5	152.7	141.4	41.0	1.13
50-MgAl/Ga_2O_3	22	0.50	0.42	237.3	180.9	178.2	42.9	1.15
70-MgAl/Ga_2O_3	35	0.50	0.35	205.8	164.1	173.5	45.7	1.16
75-MgAl/Ga_2O_3	47	0.50	0.30	138.6	140.9	173.3	55.6	1.11
95-MgAl/Ga_2O_3	92	0.50	0.09	31.4	47.2	67.6	68.2	1.05
bare Mg−Al LDH	59	0.50	0.00	trace	trace	trace	–	–

50-MgAl/Ga_2O_3 composite comprises 420 mg of Ga_2O_3 photocatalyst and 80 mg of Mg−Al LDH. The Ag-loaded bare Ga_2O_3 (***x*** = 0) evolved certain amounts of H_2, O_2, and CO in the stoichiometric balance of e^- to h^+ (e^-/h^+ = 1.11). The selectivity toward CO evolution among the reduction products was 30.1% for bare Ga_2O_3, indicating that the photogenerated electrons were largely consumed for the reduction of protons (H^+) into H_2. When the value of ***x*** was increased (***x*** = 30 and 50), the photocatalytic activity (determined from the amount of O_2 evolved) improved in spite of the decrease in the amount of Ga_2O_3. The balance of e^-/h^+ was kept approximately stoichiometric by varying the value of ***x***. With a focus on the reduction products, Mg−Al LDH modification of Ga_2O_3 enabled us to achieve an increase in the amount of CO evolved as a reduction product of CO_2. In particular, the formation rate of CO was 178.4 μmol h^{-1} for ***x*** = 50, twice as large as that for bare Ga_2O_3. When the value of ***x*** was above 50, the photocatalytic activity, and hence, the amount of CO evolved, gradually decreased on increasing the extent of Mg−Al LDH modification (i.e., ***x***). The decrease in the amount of Ga_2O_3 present in the composite photocatalyst should decrease the photocatalytic activity. For example, the formation rate of O_2 for ***x*** = 95, which reflects the total photocatalytic activity, was less than half of that for bare Ga_2O_3. In contrast, the selectivity toward CO evolution was increased on increasing the value of ***x***. The suppression of H_2 evolution is considered to be particularly important because the reduction of H^+ into H_2 easily takes place in the photocatalytic conversion of CO_2 in water. The ***95***-MgAl/Ga_2O_3 composite photocatalyst showed 68.2% selectivity toward CO evolution, i.e., Mg−Al LDH modification of Ga_2O_3 can effectively suppress H_2 evolution. Based on the result

for bare Mg−Al LDH, which itself was not active for this reaction, we conclude that the composite photocatalyst comprising Ga_2O_3 and Mg−Al LDH is necessary for achieving the selective reduction of CO_2 into CO.

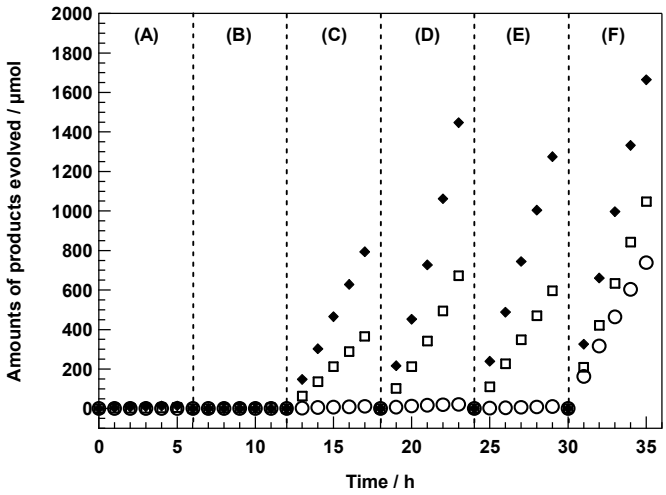

Figure 4 Amounts of products evolved in the various control experiments for the photocatalytic conversion of CO_2 in water using ***0.25***Ag/***50***-MgAl/Ga_2O_3 composite photocatalyst. Circle: CO, square: O_2, diamond: H_2. (A) without photocatalyst powder, (B) without irradiation (dark condition), (C) without $NaHCO_3$ additive, (D) without CO_2 gas flow (He gas flow), (E) without Ag cocatalyst, and (F) normal condition. Additive: 0.1 M $NaHCO_3$.

Figure 4 shows the result of control experiments for the photocatalytic conversion of CO_2 in an aqueous $NaHCO_3$ solution using the ***50***-MgAl/Ga_2O_3 composite photocatalyst. The effects of the presence of photocatalyst, photoirradiation, addition of $NaHCO_3$ into the reaction solution, flow of CO_2 gas, and introduction of the Ag cocatalyst on ***50***-MgAl/Ga_2O_3 were investigated. In regions (A) and (B), no photocatalytic reaction was found in the absence of the photocatalyst and in the absence of photoirradiation respectively. When photoirradiation was initiated, stoichiometric amounts of H_2 and O_2 were formed from the photocatalytic splitting of pure water (region (C)). In this experiment, reduction products of CO_2 were not observed despite CO_2 gas being supplied to the system and the pH of the reaction solution was stable at 5.0., which is probably unsuitable for the reduction of CO_2 to CO. Under a He atmosphere (region (D)), water splitting into H_2 and O_2 was also accompanied with a very small amount of CO formation, – presumably owing to the presence of the $NaHCO_3$

additive. No photocatalytic activity for the conversion of CO_2 was achieved in the absence of the Ag cocatalyst (region (E)). These results indicate that all the factors discussed above are important for the catalytic conversion of CO_2 to CO with the ***50***-MgAl/Ga_2O_3 composite photocatalyst.

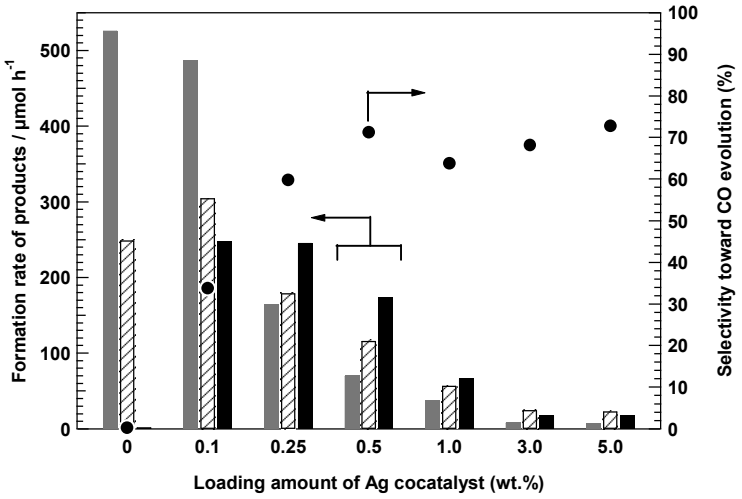

Figure 5 Effect of the amount of Ag cocatalyst on the formation rates of products and the selectivity toward CO evolution in the photocatalytic conversion of CO_2 in water. Left axis: H_2 (gray), O_2 (slash), CO (black). Right axis: selectivity toward CO formation (black circle). Photocatalyst weight: 1.0 g. Additive: 0.1 M $NaHCO_3$. Photoirradiation time: 1 h.

Figure 5 shows the formation rates of products in the photocatalytic conversion of CO_2 in an aqueous $NaHCO_3$ solution using the ***95***-MgAl/Ga_2O_3 composite photocatalyst with various amounts of Ag cocatalyst. The ***95***-MgAl/Ga_2O_3 photocatalyst did not show any activity for the conversion of CO_2 into CO in the absence of the Ag cocatalyst. However, the introduction of 0.1 wt.% Ag caused a dramatic enhancement in CO evolution. The formation rate of CO was 248.0 μmol h^{-1} for 0.1 wt.% of Ag loading, whereas it was only 1.8 μmol h^{-1} for ***95***-MgAl/Ga_2O_3 photocatalyst without any Ag cocatalyst. From this result, it can be concluded that the presence of Ag cocatalyst is necessary for the conversion of CO_2 into CO in this photocatalytic system, as described above. The selectivity toward CO evolution improved on increasing the amount of Ag cocatalyst loaded on the ***95***-MgAl/Ga_2O_3 photocatalyst. However, the actual amount of products evolved was drastically diminished, and the formation rates of H_2, O_2, and CO were 38.0, 56.8, and 67.1 μmol h^{-1}, respectively, when 1.0 wt.% of Ag cocatalyst was loaded. By taking into account both the selectivity and rate of product formation, it can be concluded that the ***0.25***Ag/***95***-MgAl/Ga_2O_3 composite

Table 2 The result of photocatalytic conversion of CO_2 in water for ***0.25***Ag/***95***-MgAl/Ga_2O_3 composite photocatalyst and a series of reference photocatalysts. The content of Ga_2O_3 in photocatalyst powder was fixed at 0.19 g. Additive: 0.1 M $NaHCO_3$. Photoirradiation time: 1 h.

Photocatalyst	Type	Weight / g		Formation rate of products / μmol h^{-1}			Selectivity to CO (%)
		Total	Ga_2O_3	H_2	O_2	CO	
95-MgAl/Ga_2O_3	composite	1.0	0.19	526.7	249.7	1.8	0.3
0.25Ag/***95***-MgAl/Ga_2O_3	composite	1.0	0.19	165.0	179.3	245.6	59.8
95-MgAl/***0.25***Ag/Ga_2O_3	composite	1.6	0.19	183.1	91.6	91.6	40.3
95-MgAl + ***0.25***Ag/Ga_2O_3	mixture	1.0	0.19	373.8	200.6	71.4	16.0
0.25Ag/Ga_2O_3	bare	0.19	0.19	164.3	100.8	55.3	25.1
0.25Ag/Mg−Al LDH	bare	0.50	0.00	trace	trace	trace	–

photocatalyst is the most suitable catalyst for the conversion of CO_2 into CO under UV light irradiation. The formation rate of CO for 0.25 wt.% Ag loading was 245.6 μmol h^{-1}, which is a remarkably high activity as the *real amount* of the reduction products of CO_2 (245.6 μmol h^{-1} per 0.19 g of Ga_2O_3) formed were higher than that reported earlier[6]; the amounts of the products evolved in the photocatalytic reaction were often presented by using the *unreal amounts*, which is normalized with the photocatalyst weight, photoirradiation area, or intensity of the light source (the normalized activity for ***0.25***Ag/***95***-MgAl/Ga_2O_3 was 1292.6 μmol h^{-1} $g_{Ga2O3}{}^{-1}$, g_{Ga2O3}: weight of Ga_2O_3 contained in the composite photocatalyst). In this case, the turnover number (TON) of the consumed electrons per Ag atom for CO evolution was 88.6 for 5 h of photoirradiation. Moreover, the ratio of the consumed electrons to holes, e^-/h^+, was 1.15 during 5 h of photoirradiation, indicating that this photocatalytic system can reduce CO_2 into CO accompanied with the oxidation of H_2O into O_2 in a stoichiometric balance. **Table 2** shows the photocatalytic activities of the ***0.25***Ag/***95***-MgAl/Ga_2O_3 composite photocatalyst and a series of reference samples for the conversion of CO_2 in an aqueous $NaHCO_3$ solution. As shown above, the ***95***-MgAl/Ga_2O_3 composite showed activity for the stoichiometric splitting of water into H_2 and O_2 in the absence of a Ag cocatalyst, and the loading of 0.25 wt.% of Ag cocatalyst helped form a large amount of CO as a reduction product of CO_2 with high selectivity toward CO evolution. Interestingly, ***95***-MgAl/***0.25***Ag/Ga_2O_3, which was prepared via a slightly different procedure from ***0.25***Ag/***95***-MgAl/Ga_2O_3, exhibited a lower formation rate of CO and selectivity toward CO evolution than ***0.25***Ag/***95***-MgAl/Ga_2O_3. For the ***95***-MgAl/***0.25***Ag/Ga_2O_3 composite, all Ag particles are considered to locate on the surface of Ga_2O_3, i.e., Ag/Ga_2O_3 should be

covered with Mg−Al LDH, whereas almost the entire Ag cocatalyst is impregnated on Mg−Al LDH for ***0.25***Ag/***95***-MgAl/Ga_2O_3, which covers Ga_2O_3. Hence, it can be presumed that the photogenerated electron transfer from the conduction band of Ga_2O_3 photocatalyst to Ag particle through Mg−Al LDH permits selective reduction of CO_2 into CO. Moreover, this direct transfer of the photogenerated electron from Ga_2O_3 to Ag cocatalyst may preferentially cause the reduction of H^+ into H_2. Furthermore, the physical mixture of Mg−Al LDH and Ag/Ga_2O_3 did not show any remarkable improvement in the amount of CO evolved than that by Ag/Ga_2O_3 and only showed enhanced water splitting to H_2 and O_2, indicating that the selectivity toward CO evolution diminished. We estimate that the chemical connection between Ga_2O_3 and Mg−Al LDH, as described in the part for XRD patterns, plays an important role in improving the selectivity toward CO evolution.

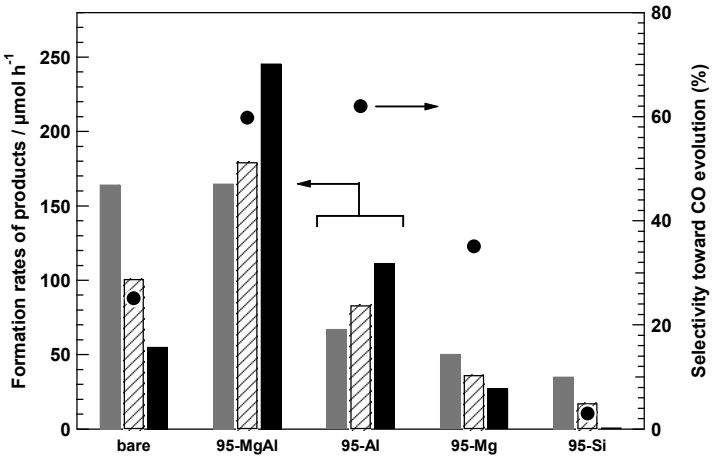

Figure 6 The formation rates of products and the selectivity toward CO evolution in the photocatalytic conversion of CO_2 in water using ***0.25***Ag/***50***-MgAl/Ga_2O_3 composite photocatalyst and a series of reference samples. Bare: Ga_2O_3 (commercial), 95-MgAl: ***0.25***Ag/***95***-MgAl/Ga_2O_3, 95-Al: ***0.25***Ag/***95***-Al/Ga_2O_3, 95-Mg: ***0.25***Ag/***95***-Mg/Ga_2O_3, and 95-Si: ***0.25***Ag/***95***-Si/Ga_2O_3. Left axis: H_2 (gray), O_2 (slash), CO (black). Right axis: selectivity toward CO evolution (black circle). The content of Ga_2O_3 in photocatalyst powder was fixed at 0.19 g. Additive: $NaHCO_3$. Photoirradiation time: 1 h.

Figure 6 shows the formation rates of products and the selectivity toward CO evolution for bare Ga_2O_3, ***95***-MgAl/Ga_2O_3, ***95***-Al/Ga_2O_3, ***95***-Mg/Ga_2O_3, and ***95***-Si/Ga_2O_3 in the presence of 0.25 wt.% of Ag cocatalyst. The photocatalytic activity of ***95***-Si/Ga_2O_3, which has a sufficiently large specific surface area, was much lower than that of bare Ga_2O_3, and CO evolution was also

completely suppressed by SiO_2 modification. Therefore, the increase in the specific surface area was not the sole reason for the improvement in the evolution of CO by the modification of Ga_2O_3 by Mg−Al LDH. The modification by $Al(OH)_3$ increased the specific surface area and improved the selectivity toward CO evolution as compared to that of bare Ga_2O_3. It was reported that Al_2O_3 (or $Al(OH)_3$) can act as an adsorbate for CO_2 capture, i.e., medium strength of basic sites, which result in the desorption of CO_2 at 473−673 K in CO_2-temperature programed desorption (TPD) measurement, are mainly presented.[33] In contrast, the specific surface area of the ***95***-Mg/Ga_2O_3 composite was not altered by modification with $Mg(OH)_2$ because of its low specific surface area, and hence, it did not show any improvement in the selectivity toward CO formation despite the high ability of MgO or $Mg(OH)_2$ as a CO_2-capturing material.[34,35] Hence, the high photocatalytic activity and high selectivity toward CO for the case of ***95***-MgAl/Ga_2O_3 composite photocatalyst were attributed to both the high specific surface area resulted from Mg−Al LDH modification and the excellent ability of Mg−Al LDH as an adsorbent of CO_2,[36,37] which helps preserve CO_2 molecules near the Ag cocatalyst.

Figure 7 shows the result of the isotopic experiment which was conducted in order to confirm the carbon source of CO evolved in the photocatalytic conversion of ^{13}C-labeled CO_2 ($^{13}CO_2$) in an aqueous $NaHCO_3$ solution using the ***0.25***Ag/***95***-MgAl/Ga_2O_3 photocatalyst. The GC-MS profile was obtained by monitoring ion currents of *m/z* = 28 and 29 for the gas-phase products, which were beforehand separated by the gas chromatograph system, accompanied with collecting the TCD-GC chromatogram. Three peaks found in the TCD-GC chromatogram around 100, 150, and 500 s, were respectively assigned to H_2, O_2, and CO. A peak was found in the profile at *m/z* = 29 of the same position to the peak corresponding to CO in the GC chromatogram, indicating that this photocatalytic system produced ^{13}C-labeled CO (^{13}CO, *m/z* = 29) as a reduction product of $^{13}CO_2$. Meanwhile, there was no peak in the profile of *m/z* = 28 (unlabeled CO was not formed in the gas phase). Moreover, the amount of ^{13}CO evolved, as evaluated from the peak area in the *m/z* = 29 profile, matched with the amount of CO quantified by FID-GC. This result clearly indicates that the CO evolved in this reaction originated from CO_2 substrates, and that the decomposition of the $NaHCO_3$ additive or contaminated organic residues did not affect the photocatalytic activity for the conversion of CO_2.

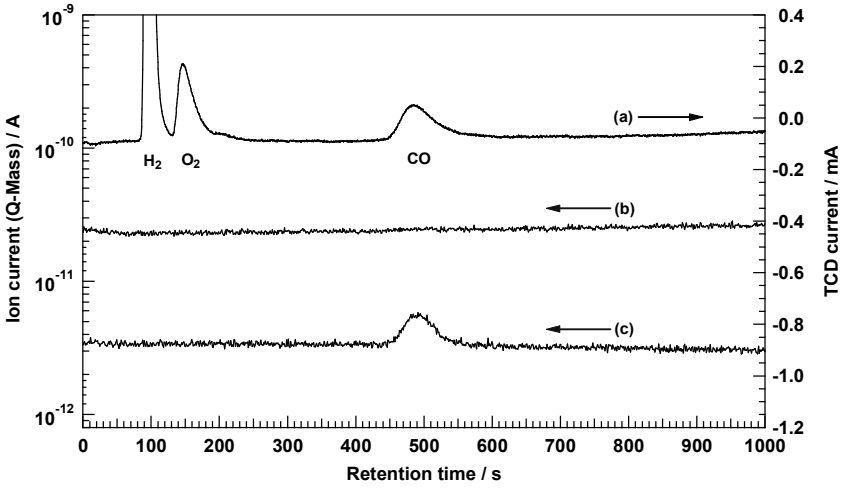

Figure 7 GC-MS profiles in the isotopic experiment for the photocatalytic conversion of CO_2 in water using ***0.25***Ag/***95***-MgAl/Ga_2O_3 composite photocatalyst. (a): TCD-GC chromatogram, (b): Q-Mass profile of *m/z* = 28, (c): Q-Mass profile of *m/z* = 29. Additive: $NaHCO_3$. Substrate: $^{13}CO_2$.

Conclusion

Our work shows that the Mg−Al LDH-Ga_2O_3 composite photocatalyst with a Ag cocatalyst exhibited high photocatalytic activity for the conversion of CO_2 in an aqueous $NaHCO_3$ solution under UV light irradiation. The formation rate of CO for the ***95***-MgAl/Ga_2O_3 photocatalyst was 245.6 μmol h^{-1} in the presence of 0.25 wt.% Ag cocatalyst. The selectivity toward CO evolution among the reduction products was also improved by the modification of the /Ga_2O_3 photocatalyst with Mg−Al LDH, indicating that the photogenerated electron transfer from the Ga_2O_3 photocatalyst to the Ag particle through Mg−Al LDH enabled the selective reduction of CO_2 into CO. The control and isotopic labeling experiments revealed that CO_2 molecules dissolved in the reaction solution were the origin of CO evolved in the photocatalytic conversion of CO_2 using the Ag-loaded ***x***-MgAl/Ga_2O_3 composite photocatalyst. In addition, the stoichiometric formation of O_2 as an oxidation product of H_2O suggested that H_2O acts both as an electron donor and a proton source. Hence, we concluded that both the increase in the specific surface area by Mg−Al LDH modification and the high ability of Mg−Al LDH as an adsorbent for CO_2, which preserves CO_2 molecules near the Ag cocatalyst, improves the selective conversion of CO_2 into CO under UV light irradiation.

References

1. K. Maeda, *Journal of Photochemistry and Photobiology C: Photochemistry Reviews*, 2011, **12**, 237-268.
2. I. Tsuji, H. Kato, H. Kobayashi and A. Kudo, *Journal of the American Chemical Society*, 2004, **126**, 13406-13413.
3. J. Zhang, J. Yu, M. Jaroniec and J. R. Gong, *Nano Letters*, 2012, **12**, 4584-4589.
4. A. Mills and S. Le Hunte, *Journal of Photochemistry and Photobiology A: Chemistry*, 1997, **108**, 1-35.
5. A. Kudo and Y. Miseki, *Chemical Society Reviews*, 2009, **38**, 253-278.
6. J. L. White, M. F. Baruch, J. E. Pander Iii, Y. Hu, I. C. Fortmeyer, J. E. Park, T. Zhang, K. Liao, J. Gu, Y. Yan, T. W. Shaw, E. Abelev and A. B. Bocarsly, *Chemical Reviews*, 2015, DOI: 10.1021/acs.chemrev.5b00370.
7. T. Arai, S. Sato, T. Kajino and T. Morikawa, *Energy & Environmental Science*, 2013, **6**, 1274-1282.
8. K. Teramura, Z. Wang, S. Hosokawa, Y. Sakata and T. Tanaka, *Chemistry - A European Journal*, 2014, **20**, 9906-9909.
9. Z. Wang, K. Teramura, S. Hosokawa and T. Tanaka, *Journal of Materials Chemistry A*, 2015, **3**, 11313-11319.
10. Z. Wang, K. Teramura, Z. Huang, S. Hosokawa, Y. Sakata and T. Tanaka, *Catalysis Science & Technology*, 2015, DOI: 10.1039/C5CY01280E.
11. Q. Li, L. Zong, C. Li and J. Yang, *Applied Surface Science*, 2014, **314**, 458-463.
12. S. Xie, Y. Wang, Q. Zhang, W. Deng and Y. Wang, *ACS Catalysis*, 2014, **4**, 3644-3653.
13. L. Liu, C. Zhao, J. Xu and Y. Li, *Applied Catalysis B: Environmental*, 2015, **179**, 489-499.
14. J. Hong, W. Zhang, Y. Wang, T. Zhou and R. Xu, *ChemCatChem*, 2014, **6**, 2315-2321.
15. K. Teramura, H. Tatsumi, Z. Wang, S. Hosokawa and T. Tanaka, *Bulletin of the Chemical Society of Japan*, 2015, **88**, 431-437.
16. F. Cavani, F. Trifirò and A. Vaccari, *Catalysis Today*, 1991, **11**, 173-301.
17. C. Delhoyo, *Applied Clay Science*, 2007, **36**, 103-121.

18. Z. P. Xu, J. Zhang, M. O. Adebajo, H. Zhang and C. Zhou, *Applied Clay Science*, 2011, **53**, 139-150.

19. R. L. Goswamee, P. Sengupta, K. G. Bhattacharyya and D. K. Dutta, *Applied Clay Science*, 1998, **13**, 21-34.

20. J. Das, B. S. Patra, N. Baliarsingh and K. M. Parida, *Applied Clay Science*, 2006, **32**, 252-260.

21. K. H. Goh, T. T. Lim and Z. Dong, *Water Research*, 2008, **42**, 1343-1368.

22. B. F. Sels, D. E. De Vos and P. A. Jacobs, *Catalysis Reviews*, 2001, **43**, 443-488.

23. S. Abelló, F. Medina, D. Tichit, J. Pérez-Ramírez, J. C. Groen, J. E. Sueiras, P. Salagre and Y. Cesteros, *Chemistry – A European Journal*, 2005, **11**, 728-739.

24. C. Xu, Y. Gao, X. Liu, R. Xin and Z. Wang, *RSC Advances*, 2013, **3**, 793-801.

25. M. K. Ram Reddy, Z. P. Xu, G. Q. Lu and J. C. Diniz da Costa, *Industrial & Engineering Chemistry Research*, 2006, **45**, 7504-7509.

26. K. Ebitani, K. Motokura, K. Mori, T. Mizugaki and K. Kaneda, *The Journal of Organic Chemistry*, 2006, **71**, 5440-5447.

27. K. Teramura, S. Iguchi, Y. Mizuno, T. Shishido and T. Tanaka, *Angewandte Chemie International Edition*, 2012, **51**, 8008-8011.

28. S. Iguchi, K. Teramura, S. Hosokawa and T. Tanaka, *Physical Chemistry Chemical Physics*, 2015, **17**, 17995-18003.

29. S. Iguchi, K. Teramura, S. Hosokawa and T. Tanaka, *Catalysis Today*, 2015, **251**, 140-144.

30. X. Wang, Q. Xu, M. Li, S. Shen, X. Wang, Y. Wang, Z. Feng, J. Shi, H. Han and C. Li, *Angewandte Chemie International Edition*, 2012, **51**, 13089-13092.

31. S. Miyata, *Clays and Clay Minerals*, 1983, **31**, 305-311.

32. R. D. Shannon, *Acta Crystallographica Section A*, 1976, **32**, 751-767.

33. Y. Bang, S. J. Han, S. Kwon, V. Hiremath, I. K. Song and J. G. Seo, *Journal of Nanoscience and Nanotechnology*, 2014, **14**, 8531-8538.

34. R. Philipp and K. Fujimoto, *The Journal of Physical Chemistry*, 1992, **96**, 9035-9038.

35. S. C. Lee, H. J. Chae, S. J. Lee, B. Y. Choi, C. K. Yi, J. B. Lee, C. K. Ryu and J. C. Kim, *Environmental Science & Technology*, 2008, **42**, 2736-2741.

36. Z. Yong, V. Mata and A. r. E. Rodrigues, *Separation and Purification Technology*, 2002, **26**, 195-205.

37. Z. Yong and A. r. E. Rodrigues, *Energy Conversion and Management*, 2002, **43**, 1865-1876.

Summary

In this thesis, the author investigated the photocatalytic conversion of CO_2 in an aqueous media using layered double hydroxides (LDHs) as photocatalysts. It was found that as-synthesized LDHs were active for the photocatalytic conversion of CO_2 under UV light irradiation, and CO was evolved as a reduction product of CO_2. The optimizations of metal components of LDHs, synthesis method, reactor design, and reaction conditions and the development of LDH-semiconductor composite photocatalyst enabled a greatly improvement in the photocatalytic activity for CO evolution. The general conclusion of this thesis is as follows:

In Chapter 1, the author demonstrates the photocatalytic activities of the synthesized LDHs for the conversion of CO_2 in water, and Ni−Al LDH (Ni/Al = 4) prepared from chloride salts as precursors exhibited the highest efficiency for the photocatalytic conversion of CO_2 into CO among kinds of M^{2+}−M^{3+} LDHs (M^{2+} = Mg^{2+}, Zn^{2+}, Ni^{2+}; M^{3+} = Al^{3+}, Ga^{3+}, and In^{3+}). The LDHs which contain In^{3+} as a trivalent cation in the hydroxide sheet (Mg−In LDH and Ni−In LDH) exhibited the high efficiency for the H_2 production, while the amount of CO evolved was totally small. The isotopic experiment using $^{13}CO_2$ as a substrate clearly revealed that the CO evolved in the photocatalytic reaction over these LDHs originated from CO_2 introduced in the gas phase. The influences of residual anions in synthesized LDHs (NO_3^- or Cl^-) derived from precursors of metal components on the photocatalytic activity for the conversion of CO_2 were also clarified.

Chapter 2 describes the effect of chloride ions (Cl^-) on the photocatalytic conversion of CO_2 in an aqueous solution using synthetic Ni−Al LDH as a photocatalyst. The addition of Cl^- to the reaction solution obviously enhanced the photocatalytic activity for the conversion of CO_2 into CO, and simultaneously suppressed the formation of H_2 as a reduction product of H^+. Total amount of CO evolved during 29 h of photoirradiation was 110.9 μmol. *N,N'*-diethyl-*p*-phenylenediamine (DPD) test elucidated that hypochlorous acid (HClO) is stoichiometrically formed as an oxidation product of Cl^-, together with reduction products such as CO and H_2. The author proposed that the Cl^- existing in the reaction solution functions as an effective hole scavenger and that it would be oxidized to Cl_2, which would immediately be converted into HClO in water.

In Chapter 3, the author found that the fluorination of Mg−Al LDH and Ni−Al LDH improved the photocatalytic conversion of CO_2 into CO in an aqueous NaCl solution under UV light irradiation. When the fluorinated Ni−Al LDH was used as a photocatalyst, total amount of CO evolved as a reduction product of CO_2 during 20 h of photoirradiation was 93.3 μmol. With reference to ***F(7.5)imp-***Ni−Al LDH (all F species was impregnated on the surface of Ni−Al LDH), the incorporation of AlF_6^{3-} units in the hydroxide sheets causes significant improvement in the photocatalytic conversion of CO_2 into CO. In addition, a certain amount of hypochlorous acid (HClO) was produced as an oxidation product in the reaction solution. The author concluded that the fluorination of LDH by incorporation of AlF_6^{3-} units in the hydroxide sheets affords surface properties suitable for the photocatalytic conversion of CO_2 in the presence of Cl^-, which acts as a hole scavenger.

Chapter 4 shows the photocatalytic activity of transition metals containing LDHs for the conversion of CO_2 in an aqueous NaCl solution. Particularly, the use of Ni−V LDH (Ni/V = 2) enabled the highest activity for the CO evolution as a reduction product of CO_2, and above 200 μmol of CO was evolved during 8 h of photoirradiation. The amount of H_2 evolved was significantly lower than that of CO, indicating that Ni−V LDH is considered to be suitable for the selective conversion of CO_2 into CO. Through the investigation of photocatalytic activities for different V^{3+} content of Ni−V LDH and Ni−V−Al LDH, the existence of V^{3+} afforded good performance for the conversion of CO_2 into CO in an aqueous solution of NaCl. Although the stability of Ni−V LDH was insufficient due to the leaching into the reaction solution, the co-presence of V^{3+} and Cl^- might make it possible to achieve high photocatalytic activity for the conversion of CO_2 into CO in an aqueous solution.

Chapter 5 reported that a series of LDHs (Ni−Al, Mg−Al, and Zn−Al LDH) were found to produce anodic photocurrent under no external bias, and the order of the initial photocurrent intensities (Zn−Al > Mg−Al > Ni−Al LDH) were in accordance with total amount of electrons consumed in the photocatalytic reaction using these LDH powder samples, while Ni−Al LDH evolved the largest amount of CO. Ni−Al LDH exhibited electrochemical properties corresponding to *n*-type materials; that is, cathodic dark current under cathodic polarization and anodic photocurrent under anodic polarization were found in electrochemical measurements. The potential of the photogenerated electron for the Ni−Al LDH photocatalyst was estimated to be −0.40 V vs. NHE (pH

= 0) based on Mott-Schottky plot, which is enough to induce the two-electron reduction of CO_2 into CO. Moreover, the change of M^{3+} metal in Ni−M^{3+} LDH clearly influenced the potential of the photogenerated electrons and holes.

In Chapter 6, the author showed the excellent improvement in the photocatalytic conversion of CO_2 into CO by the modification of Ga_2O_3 with Mg−Al LDH. The formation rate of CO for the ***95***-MgAl/Ga_2O_3 with 0.25 wt.% Ag cocatalyst was 245.6 μmol h^{-1}, the largest value in this thesis. The control and isotopic labeling experiments revealed that CO_2 molecules dissolved in the reaction solution were the origin of CO evolved in the photocatalytic conversion of CO_2 using the composite photocatalysts. In addition, the stoichiometric formation of O_2 as an oxidation product of H_2O suggested that H_2O acts both as an electron donor and a proton source. The author concluded that both the increase in the specific surface area by Mg−Al LDH modification and the high ability of Mg−Al LDH as an adsorbent for CO_2, which preserves CO_2 molecules near the Ag cocatalyst, improves the selective conversion of CO_2 into CO under UV light irradiation.

In short, the author developed the photocatalytic systems using various synthetic LDHs as photocatalysts which can induce the selective conversion of CO_2 into CO in an aqueous media. The H_2 evolution via reduction of H^+, which competitively takes place in the photocatalytic reaction in water, was significantly suppressed owing to the superior surface properties of LDHs. Although LDHs photocatalysts are not capable of oxidizing H_2O into O_2, the new photocatalytic system using Cl^- as a hole scavenger which might be oxidized into Cl_2 was demonstrated in this thesis. Here, the author proposes LDHs as a promising material for constructing high water tolerant system intended to convert CO_2. Generally, the author believes these results to contribute to the development in the field of photocatalysis aiming to overcome the global climate changes.

Appendix

$ZnTa_2O_6$ Photocatalyst Synthesized via Solid State Reaction for Conversion of CO_2 into CO in Water

Abstract

Because of the environmental problems and the resulting exigent demand for CO_2 recycling processes, great attention is being paid to the photocatalytic conversion of CO_2 into useful chemicals such as CO, HCOOH, HCHO, CH_3OH, and CH_4. We have previously reported that the Ag-loaded, Zn-modified Ga_2O_3 photocatalyst exhibits excellent photocatalytic activity required for the conversion of CO_2 into CO by using H_2O as a reductant, and that the Ag particles that exist together with the Zn species act as good cocatalysts for the selective formation of CO. In this study, we demonstrated the photocatalytic activity of $ZnTa_2O_6$ under UV light irradiation, which was prepared via a solid-state reaction, for the conversion of CO_2 in an aqueous $NaHCO_3$ solution. Ag cocatalyst-loaded $ZnTa_2O_6$ photocatalyst evolved CO as a reduction product of CO_2 with 46% of the selectivity toward CO evolution among the reduction products. In contrast, when Pt and Au were introduced as cocatalysts, more than 99% of photoexcited electrons were consumed to reduce the protons to H_2.

Introduction

Artificial carbon cycling systems based on the catalytic conversion of CO_2 into useful carbon sources such as CO, HCOOH, HCHO, CH_3OH, and CH_4 are receiving a great deal of attention because of environmental issues such as global warming and natural resource depletion [1-3]. In heterogeneous catalysis, it is generally necessary to introduce a reducing reagent such as H_2 or a hydrocarbon at a high temperature in order to reduce CO_2 [3, 4]. However, H_2O is a more favorable reductant, because it is harmless and is an abundant source of protons. The photocatalytic conversion of CO_2 by means of H_2O, also known as artificial photosynthesis, is considered an uphill reaction involving photoexcited electrons and positive charge holes [5, 6]. H_2 evolution via reduction of protons (H^+) takes place competitively during the photocatalytic conversion of CO_2 in water, because the standard reduction potential of CO_2 ($E°(CO_2/CO) = -0.11$ V vs. SHE) [7] is more negative than that of H^+ ($E°(H^+/H_2) = 0.0$ V vs. SHE) [7]. In order to convert CO_2 to CO, rather than H_2 evolution from H^+, the photocatalyst surface should be design in such a way that it helps improve the selectivity of photogenerated electrons toward CO_2 reduction. The primary strategy for designing such a photocatalyst is to provide suitable surface properties to enable the absorption of CO_2. We previously reported that ZrO_2 [8-11], MgO [12, 13], and Ga_2O_3 [14], which can act as solid base materials, were active for the photocatalytic conversion of CO_2 in the presence of H_2 as a reductant. Detailed analyses of the adsorbed species formed on the surface of these photocatalysts showed that the adsorption of a CO_2 molecule on the photocatalyst material is an essential step for the photocatalytic conversion of CO_2 [13, 14]. Moreover, the photocatalytic activities of layered double hydroxides (LDHs), which have high water-tolerant base sites, for the conversion of CO_2 in water were found [15, 16]. In particular, the use of a Ni−Al LDH enables the selective evolution of CO as a reduction product of CO_2 [17]. Another method for the selective conversion of CO_2 is the introduction of a metal cocatalyst onto the photocatalyst. Our research group also found that the Zn-modified Ga_2O_3 photocatalyst exhibited excellent activity for the conversion of CO_2 into CO and O_2 in the presence of Ag as a cocatalyst, with stoichiometric amounts of O_2 being formed as an oxidation product of H_2O [18, 19]. We presume that Ag particles, in combination with the zinc species, can act as an effective cocatalyst for the conversion of CO_2 to CO, because the consumption of the photogenerated electrons by H^+ derived

from H_2O was completely suppressed. These results indicate that a Ag cocatalyst in combination with a Zn-based mixed oxide semiconductor photocatalyst should enable the conversion of CO_2 with high selectivity under photoirradiation.

In this study we focused on the zinc tantalum mixed oxide as a photocatalyst for the conversion of CO_2 in water. A series of isostructural zinc tantalum mixed oxides: $ZnTa_2O_6$ [20-22], $Zn_3Ta_2O_8$ [23], and $Zn_4Ta_2O_9$ [24], have been successfully synthesized. Moreover, Kato and Kudo (1998) showed the photocatalytic activity of $ZnTa_2O_6$ for water splitting in their summary of various tantalate photocatalysts; NiO-loaded $ZnTa_2O_6$ evolved H_2 at a rate of 15 μmol h^{-1} and O_2 at a rate of 6 μmol h^{-1} from distilled water under UV light irradiation [25]. Recently, Wu et al. demonstrated the photocatalytic degradation of methyl orange using $ZnTa_2O_6$ [20] and Hong et al. demonstrated the photocatalytic evolution of H_2 from an aqueous methanol solution using $Zn_3Ta_2O_8$ [23]. As reviewed by Kudo et al., tantalum-based mixed oxides ($M_xTa_yO_z$) have excellent photocatalytic abilities, where M = Li, Na. K, Mg, Ca, Sr, Ba, Ni, Rb, or La, and showed stoichiometric decomposition of H_2O into H_2 and O_2 (H_2:O_2 = 2:1) [25]. Takayama et al. reported that $KCaSrTa_5O_{15}$ photocatalyst, which shows good activity for the overall splitting of water using NiO as a cocatalyst, exhibited good activity for the reduction of CO_2 in water when Ag was loaded as a cocatalyst. Turnover number (TON) of electrons utilized for CO formation per the number of Ag atoms was 8.6 after 20 h of photoirradiation [26]. In contrast to the successful investigation of complete photocatalytic water splitting, the investigation on the photocatalytic conversion of CO_2 remains incomplete. In the present study, we demonstrate the photocatalytic activity of $ZnTa_2O_6$, synthesized via a solid-state reaction method, for the conversion of CO_2 to CO in an aqueous solution under UV irradiation.

Experimental

$ZnTa_2O_6$ photocatalyst was prepared via a solid state reaction with referring the previous report [22]. The calculated amount of high purity Ta_2O_5 powder (Kojundo Chemical Laboratory) was added into an aqueous solution of $Zn(NO_3)_2{\cdot}6H_2O$ (Wako Pure Chemical) with molar ratio of Zn/Ta = 0.5. An aqueous NaOH solution was dropped to the suspension with vigorous stirring in order to adjust the pH at around 10.0−10.3, and then the resulting suspension was kept stable for 30 min at

room temperature. The white suspension was aged at 363 K for 6 h with stirring by a magnetic stirrer. The resulting cake was collected by a vacuum filtration, and dried at room temperature under air condition. $ZnTa_2O_6$ was obtained through the calcination of this precursor using an electric furnace at a specified temperature. $ZnTa_2O_6$ samples which were calcined at 1073, 1173, 1273, and 1373 K were hereinafter called ZTO_1073, ZTO_1173, ZTO_1273, and ZTO_1373, respectively. In addition, the polymerized complex method was used to synthesize $ZnTa_2O_6$. The required amount of $TaCl_5$ (Wako Pure Chemical) methanol solution and $Zn(NO_3)_2 \cdot 6H_2O$ (Wako Pure Chemical) were added into an aqueous citric acid solution, and stirred at room temperature. Ethylene glycol (Wako Pure Chemical) was added into this solution, and then stirred at 353 K to form a gelatinous solution. After the gel was heated at 723 K for 3 h with vigorous mixing, the resulting powder was calcined at 1273 K. $ZnTa_2O_6$ synthesized via the polymerized complex method would be presented as ZTO_PC. As a reference material, physical mixture of Ta_2O_5 and ZnO was prepared via a grinding of Ta_2O_5 and ZnO powder using an agate mortar, in advance, each of two powders was respectively calcined at 1273 K under an air atmosphere. One of the metal species (Ag, Au, Pt, Ni, and Cu) was loaded to the synthesized $ZnTa_2O_6$ as a cocatalyst for the photocatalytic reaction by impregnation, photodeposition, and chemical reduction methods. The cocatalyst loading procedures of these methods are described below based on the case of Ag. For the impregnation methods, an aqueous $AgNO_3$ solution including $ZnTa_2O_6$ powder was thoroughly evaporated at 353 K, and calcined at 723 K for 2 h in air. For the photodeposition method, $ZnTa_2O_6$ powder was dispersed in 1.0 L of ultra-pure water containing a required amount of $AgNO_3$, and the dissolved air in the solution was completely degassed by a flow of He gas. The suspension was irradiated under a 400 W high-pressure Hg lamp with a quartz filter using an inner-irradiation-type reaction vessel with He gas flowing. For the chemical reduction method, an aqueous solution of $NaPH_2O_2$ was added to a suspension of the $ZnTa_2O_6$ containing a given amount of $AgNO_3$. After stirring at 353 K for 2 h, the modified photocatalyst was filtered and washed with 1.0 L of ultra-pure water, and then dried at room temperature.

For photoelectrochemical measurements, film form $ZnTa_2O_6$ samples were prepared by an electrophoresis method. The photocatalyst powder was dispersed to an acetone solution containing iodine (I_2) as an electrolyte, and 10 V of a direct current (DC) was applied to the suspension using a two-electrode electrochemical cell to deposit the photocatalyst on a glass substrate covered with

fluorine-doped tin oxide (FTO) as a conductive layer. The prepared film sample, hereinafter called $ZnTa_2O_6$/FTO, was heated at 773 K for 2 h before use.

X-ray diffraction (XRD) patterns of prepared samples were collected by using an X-ray diffractometer (Multi Flex, Rigaku), using Cu K_α radiation (λ = 0.154 nm) at a scan rate of 4 ° min^{-1}. Specific surface areas of the photocatalysts were estimated from their N_2 adsorption isotherms at 77 K using an adsorption analyzer (BELSORP-miniII, BEL Japan, Inc.). Prior to the measurements, each sample was evacuated at 673 K for 1 h using a pretreatment system (BELPREP-vacII, BEL Japan, Inc.). UV/Vis diffuse reflection spectra of synthesized materials were measured using a UV-Visible Spectrometer (V-650, JASCO) equipped with an integrated sphere accessory. Zn K-edge and Ta L_{III}-edge XAFS spectra of $ZnTa_2O_6$ were collected at the BL01B1 of SPring-8 with the approval of the Japan Synchrotron Radiation Research Institute (JASRI). The spectra were recorded in a transmittance mode at room temperature, using Si(111) double crystal monochromator. The photon energy was calibrated by using Zn foil. SEM images were captured using a Field Emission Scanning Electron Microscope (FE-SEM, SU-8220, Hitachi High-Technologies) at an acceleration voltage of 3.0 kV. In order to evaluate the photocurrent under UV light irradiation, photoelectrochemical measurement was performed in a three-electrode type cell; $ZnTa_2O_6$/FTO, Ag/AgCl electrode, Pt wire, and 0.1 M Na_2SO_4 aq. were used as working electrode, reference electrode, counter electrode, and electrolyte solution, respectively. The $ZnTa_2O_6$/FTO electrode was irradiated with a 200 W Hg-Xe lamp (San-ei electric) through a quartz window under N_2 atmosphere without external bias, and the value of phorocurrent was recorded by using an electrochemical measurement system (HZ-5000, Hokuto Denko Corp.). The irradiated area (effective area) of $ZnTa_2O_6$/FTO was fixed at 1 cm × 3 cm (3 cm^2) in the photoelectrochemical measurements in this study. FT-IR spectra of adsorbed species on a $ZnTa_2O_6$ were recorded with a FT-IR spectrometer (FT/IR-4000, JASCO) in a transmission mode at room temperature. A $ZnTa_2O_6$ sample (ca. 100 mg) was pressed into a wafer (diameter = 10 mm) and placed in an *in-situ* IR cell equipped with CaF_2 windows. The cell enabled to perform evacuation, heating, O_2 treatment, introduction of CO_2, and measurement of spectra in situ. Prior to measurement, the sample was evacuated at 673 K. followed by treatment with 5 kPa of O_2 for 1 h and evacuation for 15 min at 673 K. The background spectrum was obtained after the pretreatment at room temperature under evacuation. The data from 128 scans

were accumulated at a resolution of 4 cm^{-1}.

Photocatalytic reactions were performed by using an inner-irradiation type reactor vessel under a flow of CO_2 gas. 0.5 g of the photocatalyst powder was dispersed to 1.0 L of an ultra-pure water (if necessary, 0.1 M of $NaHCO_3$ was added to the reaction solution as an additive), and the suspension was thoroughly degassed by a flow of CO_2 or He gas with a vigorous stirring. The reaction solution including a photocatalyst powder was illuminated by a 400 W high-pressure Hg lamp through a quartz glass jacket equipped with a water cooling system. Gas phase products were detected and quantified by using an online gas chromatograph (Tracera GC-2010plus, Shimadzu) equipped with a barrier discharge ionization detector (BID) using He gas as a carrier. The selectivity toward CO evolution among the reduction products was given by formula (1) as below,

Formula (1) Selectivity toward CO evolution (%) = $100 \times \boldsymbol{R}_{CO} / (\boldsymbol{R}_{CO} + \boldsymbol{R}_{H2})$

where $\boldsymbol{R}_{CO}$ and $\boldsymbol{R}_{H2}$ was formation rates of CO and H_2, respectively.

For an isotopic experiment using ^{13}C-labeled CO_2 as a substrate, the photocatalytic reaction was conducted by using a closed circulation system connected to a rotary vacuum pump. 0.5 g of the photocatalyst powder was dispersed to 380 mL of an aqueous $NaHCO_3$ solution in the inner-irradiation type reaction vessel, and dissolved air in the reaction solution was degassed under a vacuum condition. 7.6 mmol of $^{13}CO_2$ (isotopic purity: 99 %, purchased from SI Science Co., Ltd.), which was purified by a freeze distillation, was introduced to the dead space. After the circulation for 30 min, the suspension was illuminated from an inner of the reaction vessel through the quartz filter by a 400 W high-pressure Hg lamp. A thermal conductivity detector gas chromatograph (GC-8A, Shimadzu) and a quadrupole mass spectrometer (BELMASS, MicrotracBEL) were used to detect the CO evolved in the gas phase.

Results and discussion

Figure 1 shows X-ray diffraction (XRD) patterns of $ZnTa_2O_6$ prepared via a solid-state reaction method; $ZnTa_2O_6$ was calcined at various temperatures. When compared to a reference pattern of $ZnTa_2O_6$ (**Figure 1(d)**, ICSD #36289), our observations showed that $ZnTa_2O_6$ was successfully synthesized with no impurity phases, and that the diffraction peaks corresponding to

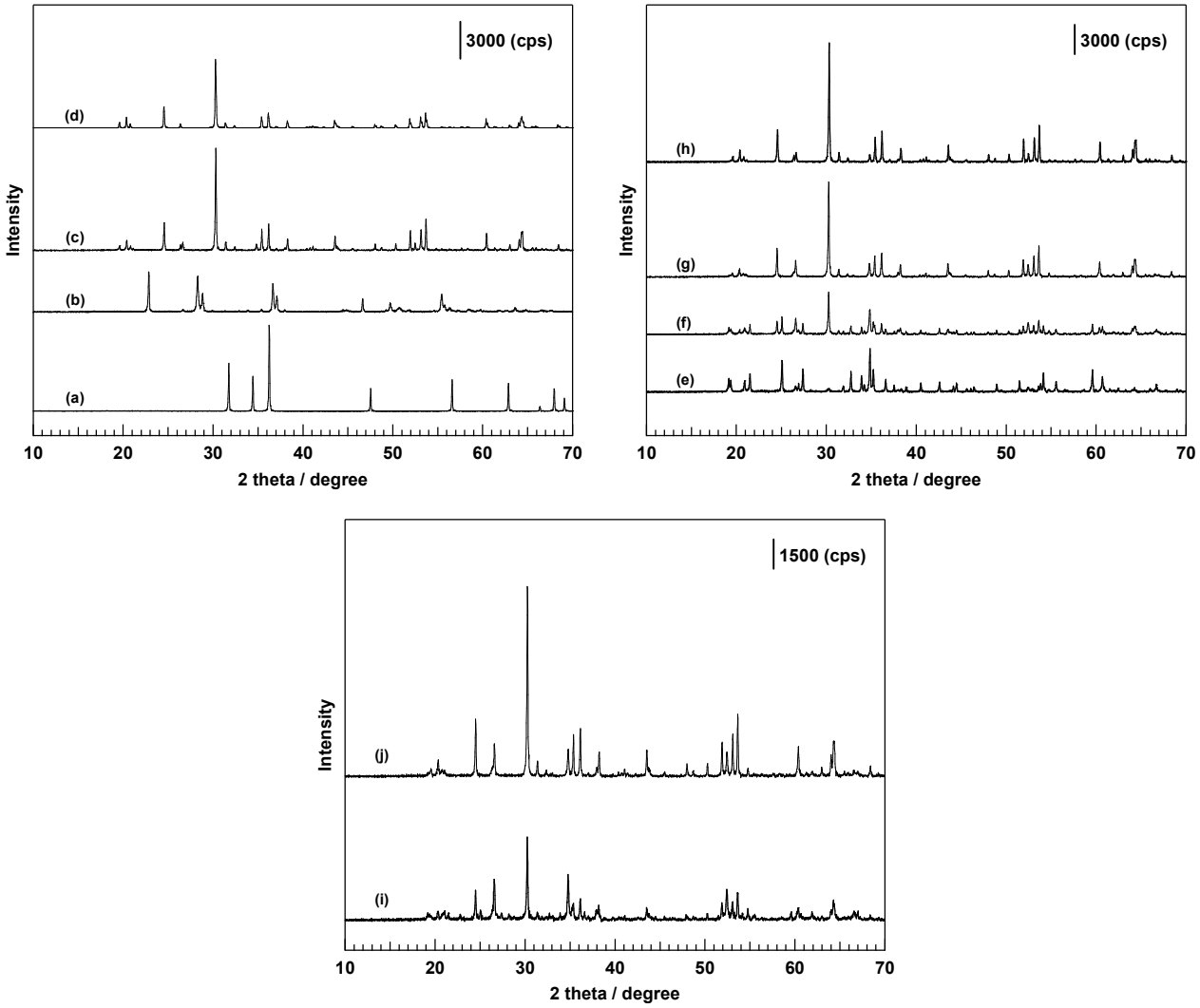

Figure 1 XRD patterns of (a) ZnO, (b) Ta_2O_5, (c), (g), and (j) ZTO_1273, (d) reference pattern of $ZnTa_2O_6$ (ICSD #36289), (e) ZTO_1073, (f) ZTO_1173, (h) ZTO_1373, and (i) ZTO_PC.

ZnO (**Figure 1(a)**) and Ta_2O_5 (**Figure 1(b)**) were not found at all. No diffraction peaks corresponding to isostructural zinc tantalum mixed oxides such as $Zn_3Ta_2O_8$ and $Zn_4Ta_2O_9$ were observed in the XRD patterns of $ZnTa_2O_6$ (ZTO_1273, **Figure 1(c)**). In contrast to this, several impurity phases were observed in the XRD patterns of ZTO_1073 (**Figure 1(e)**) and ZTO_1173 (**Figure 1(f)**). In the case of ZTO_1173, a noticeably sharp diffraction peak was observed around 30°, confirming the formation of $ZnTa_2O_6$; in contrast, the XRD pattern of ZTO_1073 showed no clear peak in this region. These results indicate that the formation of the $ZnTa_2O_6$ starts at 1173 K and ends at 1273 K. As shown in **Figure 1(i and j)**, the characteristic diffraction peaks assigned to the $ZnTa_2O_6$ structure appeared in the XRD patterns of ZTO_PC. Hence, the polymerized complex

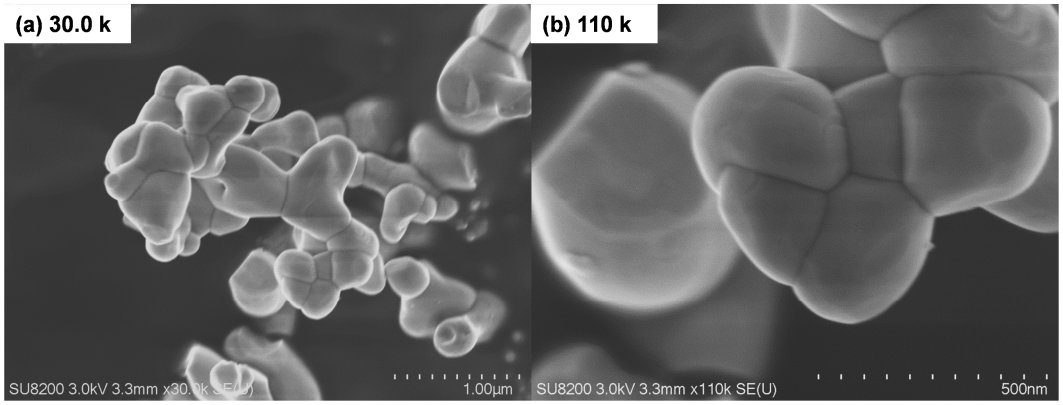

Figure 2 SEM images of ZTO_1373 at magnification of (a) 30k and (b) 110k.

method resulted in poor crystallinity of ZTO_PC compared to ZTO_1273, which was prepared via a solid-state reaction. **Figure 2** displays scanning electron microscopy images of ZTO_1373. The micrometer-sized particles were observed to have a very smooth surface, and were created by combining several submicron-sized particles with each other. **Figure 3** shows UV/Vis diffuse reflectance spectra of $ZnTa_2O_6$ prepared at various temperatures and with different compositions of Ta_2O_5 and ZnO, as described in the experimental section. The results showed that an absorption edge of $ZnTa_2O_6$ was locates around 270 nm, whereas the absorption edge corresponding to Ta_2O_5 was found at 330 nm in the spectrum of the mixed sample. Based on the Davis-Mott equation [27] using the Kubelka-Munk function $\boldsymbol{F(R_\infty)}$ obtained from diffuse reflectance spectrum, the energy band gap of the $ZnTa_2O_6$ photocatalyst was estimated to be 4.5 eV.

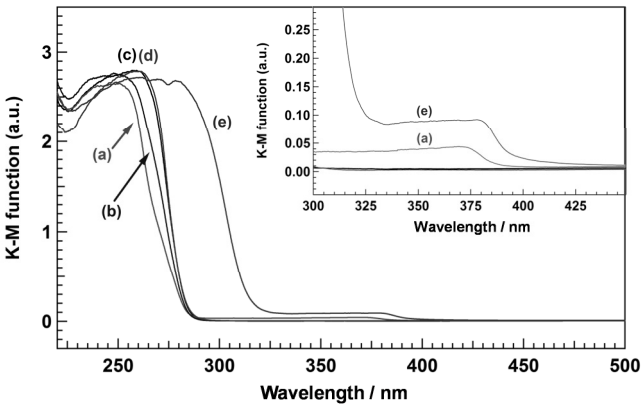

Figure 3 UV/Vis diffuse reflectance spectra of (a) ZTO_1073, (b) ZTO_1173, (c) ZTO_1273, (d) ZTO_1373, and (e) mixture of ZnO + Ta_2O_5 (molar ratio Zn : Ta = 1 : 2). The inserting figure is enlarged view of small y-axis range.

Formula (2) $[F(R_\infty)hv]^{-n} = A(hv - E_g)$

where h, v, and A are Planck's constant, frequency of vibration, and proportional constant, respectively. The ZTO_1073 spectrum showed weaker absorption of ZnO than that of the mixture sample. The absorption peak of ZnO completely disappeared when the sample was calcined above 1173 K, indicating that the zinc species was completely conjugated with tantalum to form the $ZnTa_2O_6$ structure. Moreover, a broad absorption peak was observed in the spectra of the Ag-modified $ZnTa_2O_6$ samples, which can be ascribed to plasmonic absorption of Ag particles. **Figure 4** shows the photocurrent value of the $ZnTa_2O_6$ photocatalyst measured by using a three-electrode–type photoelectrochemical cell without any external bias, during the repetition of turning on and off the illumination. The setup details of the photoelectrochemical cell are presented in the experimental section. When the photoirradiation through a quartz window started, a clear anodic photocurrent was found, indicating that $ZnTa_2O_6$ is an *n*-type semiconductor photocatalyst. Furthermore, the anodic photocurrent was effectively diminished when a UV-29 long-pass filter is used. This result suggested that UV irradiation at wavelengths below 290 nm is necessary to induce the photocatalytic reaction over $ZnTa_2O_6$, which is consistent with the results obtained from UV/Vis absorption spectra.

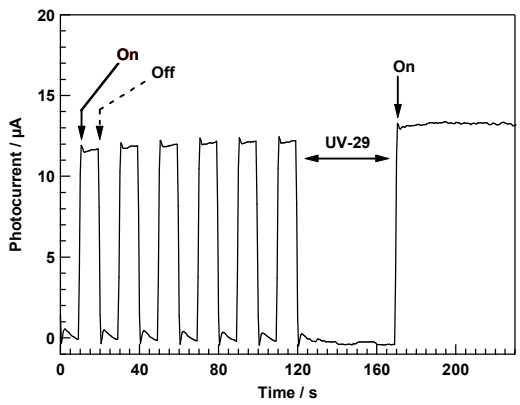

Figure 4 Photocurrent value of ZTO_1373 photoelectrode measured by using a three electrode type photoelectrochemical cell without external bias. Electrolyte: 0.1 M Na_2SO_4 aqueous solution. Turning on and off of photoirradiation was repeated every 10 s from 0 to 120 s. UV-29 long-pass filter was used from 120 to 170 s. Photoirradiation was kept on after 170 s.

Table 1 Formation rates of products evolved (H_2, O_2, and CO) and selectivity toward CO evolution in the photoacatalytic conversion of CO_2 in an aqueous $NaHCO_3$ solution. Photocatalyst powder: 0.5 g. Additive: 0.1 M $NaHCO_3$. Amount of cocatalyst loaded: 1 wt. %.

Photocatalyst	[a] Formation rates of products / μmol h^{-1}			[b] Selectivity toward CO evolution (%)
	H_2	O_2	CO	
Bare ZTO_1273	19.7	9.3	6.6	25.1
[c] Pt/ZTO_1273	703.5	397.6	0.3	0.04
[c] Au/ZTO_1273	253.6	80.8	0.4	0.2
[c] Ni/ZTO_1273	135.0	67.6	0.2	0.1
[c] Cu/ZTO_1273	72.6	45.2	1.5	2.0
[d] Ag/ZTO_1273	25.1	18.6	19.3	43.4
[d] Ag/Ta_2O_5	6.5	3.3	2.1	24.4
[d, e] Ag/(ZnO + Ta_2O_5)	8.8	3.7	0.8	8.3
[d, f] Ag/ZTO_PC	14.7	4.2	2.4	13.8

[a] After 1 h of photoirradiation. [b] Calculated in accordance with equation (1).
[c] Cocatalyst was loaded via photodeposition method. [d] Cocatalyst was loaded via impregnation method.
[e] ZnO + Ta_2O_5: physical mixture. [f] ZTO_PC: synthesized via polymerized complex method.

Table 1 displays the formation rates of the products evolved (H_2, O_2, and CO) and the selectivity toward CO evolution during the photoacatalytic conversion of CO_2 in an aqueous $NaHCO_3$ solution using various metal-loaded ZTO_1273 and reference samples. Unmodified ZTO_1273 also exhibited photocatalytic activity under UV irradiation and generated reduction (H_2 and CO) and oxidation products (O_2). However, no photocatalytic activity was observed when the quartz jacket was replaced with a pyrex jacket. The photocatalytic activity was evidently influenced by modifying the $ZnTa_2O_6$ photocatalyst with a metal species as a cocatalyst. Loading of Pt, Au, Ni, and Cu cocatalysts enabled the splitting of water into H_2 and O_2 while simultaneously generating small amounts of CO as a reduction product of CO_2, indicating that almost all photoexcited electrons stimulated by UV irradiation were consumed in the reduction of H^+ to H_2. In particular, Pt/ZTO_1273, which was prepared via photodeposition method, showed fairly high overall water splitting activity and produced over 700 μmol of H_2 during 1 h of photoirradiation, whereas the formation rate of CO was only 0.3 μmol h^{-1}. In comparison, Ag-modified ZTO_1273 exhibited good activity for the conversion of CO_2 into CO. Although the total number of electrons consumed in the

photocatalytic reaction was less than a tenth of Pt/ ZTO_1273, the formation rate of CO (19.3 μmol h^{-1}) was significantly higher than that of other cocatalyst. The selectivity toward CO evolution among the reduction product was 43.4% for the Ag/ZTO_1273 photocatalyst, whereas the percentage for ZTO_1273 modified with other cocatalysts was smaller by several percent points. The turnover number of electrons consumed for reduction of CO_2 into CO was 3.4 per Ag atom for 5 h of photoirradiation. Ag particle is considered to be an excellent cocatalyst for selective CO evolution in the photocatalytic conversion of CO_2, as it is recently known in the field of photocatalysis. Moreover, the formation rate of CO for ZTO_1273 was significantly higher than those for Ta_2O_5, ZTO_PC, and the physical mixture of ZnO and Ta_2O_5, indicating that the $ZnTa_2O_6$ photocatalyst, synthesized by the solid-state reaction, is more suitable for the conversion of CO_2 into CO in an aqueous $NaHCO_3$ solution under UV irradiation.

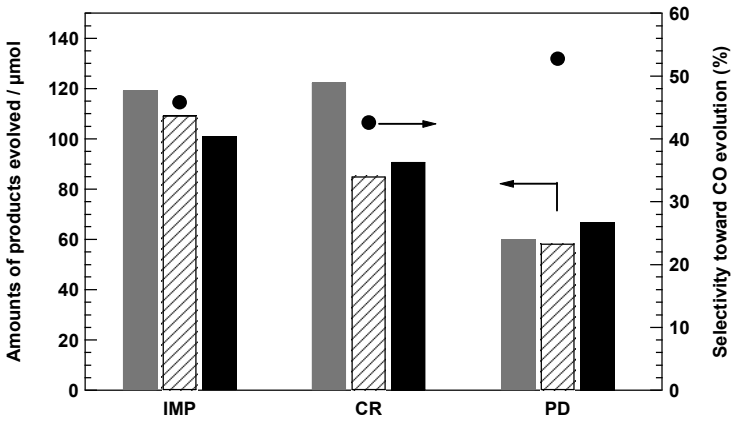

Figure 5 Amounts of products evolved in the photocatalytic conversion of CO_2 in an aqueous $NaHCO_3$ solution using ZTO_1273 photocatalyst modified with Ag via impregnation (IMP), chemical reduction (CR), and photodeposition (PD) methods. Photocatalyst powder: 0.5 g. Additive: 0.1 M $NaHCO_3$. Amount of Ag loaded: 3 wt. %. Black: CO, gray: H_2, slash: O_2, and circle: selectivity toward CO formation.

Figure 5 shows the amount of product evolved in the photocatalytic conversion of CO_2 in an aqueous $NaHCO_3$ solution using ZTO_1273 modified with Ag via impregnation (IMP), chemical reduction (CR), and photodeposition (PD) methods. The Ag-loading method affected both the photocatalytic activity and selectivity toward the evolution of CO. Ag/ZTO_1273, prepared via impregnation methods, exhibited the largest amount of CO evolved as a reduction product of CO_2. In

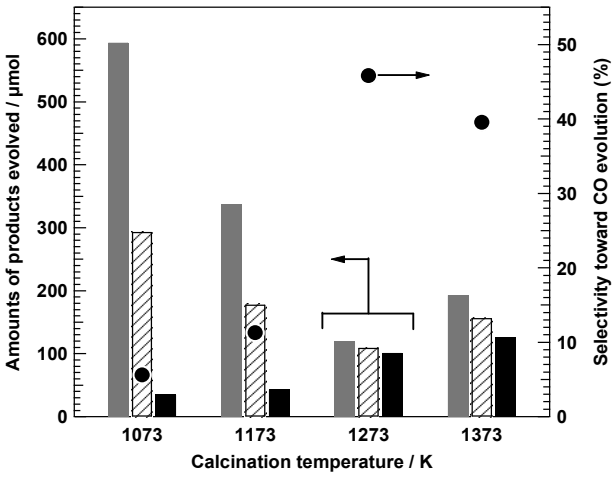

Figure 6 Amounts of products evolved and the selectivity toward CO evolution in the photocatalytic conversion of CO_2 in an aqueous $NaHCO_3$ solution using ZTO_1073, ZTO_1173, ZTO_1273, and ZTO_1373 as photocatalysts. Photocatalyst powder: 0.5 g. Additive: 0.1 M $NaHCO_3$. Amount of Ag loaded: 3 wt. % (IMP). Black: CO, gray: H_2, slash: O_2, and circle: selectivity toward CO formation.

comparison to previously developed compounds for the conversion of CO_2, the influence of the Ag-loading method on the photocatalytic activity and selectivity toward CO evolution was not as obvious; these compounds include Zn-modified Ga_2O_3 [18, 19], $ZnGa_2O_4$ [28], and SrO-modified Ta_2O_5 [29] reported by our group, and $BaLa_4Ti_4O_{15}$ [30], and $KCaSrTa_5O_{15}$ [26, 31] reported by Kudo et al. After 5 h of photoirradiation, Ag/ZTO_1273, which was prepared by IMP, CR and PD methods, showed similar absorption peaks that corresponded to the plasmonic absorption of Ag in UV/Vis DR spectra. Thus, Ag/ZTO_1273 prepared via impregnation was used in the subsequent studies. As shown in **Figure 6**, the calcination temperature of the $ZnTa_2O_6$ photocatalyst drastically changed the photocatalytic activity for the conversion of CO_2 under UV irradiation. When $ZnTa_2O_6$ was synthesized through the calcination process at less than 1173 K (for ZTO_1073 and ZTO_1173), the main process was water splitting into H_2 and O_2. In contrast, only small amounts of CO were evolved as the reduction product of CO_2. Here, the selectivity toward CO evolution among the various reduction products was equal to or less than 10%. However, the photocatalytic activity changed at 1273 K, at which the selectivity toward CO evolution greatly increased to ca. 40% because H_2 generation via reduction of H^+ was effectively suppressed at 1273 K. The specific surface area (S_{BET}) of as synthesized $ZnTa_2O_6$ gradually decreased with the increase in the calcination temperature;

specifically, when $ZnTa_2O_6$ was calcined at 1073, 1173, 1273, and 1373 K, the S_{BET} values became 2.5, 2.1, 1.8, and 1.4 $m^2\ g^{-1}$, respectively. It is estimated that the decrease in the surface area of $ZnTa_2O_6$ is one of the reasons why the total number of consumed electrons in the photocatalytic reaction noticeably decreased at high calcination temperatures. Furthermore, the Zn-K edge XANES spectra of $ZnTa_2O_6$ materials showed that the structure was altered by the calcination temperature, as shown in **Figure 7(a−e)**. Compared to the spectrum of the mixture sample (ZnO + Ta_2O_5), which shows the characteristic Zn^{2+} peak in ZnO, the Zn species in ZTO_1073 was different from ZnO; if anything, it should be similar to a four-fold coordination of Zn^{2+}, just like ZnS [32]. The XANES spectra of ZTO_1273 and ZTO_1373 were different from that of ZTO_1073, because the crystal structure of $ZnTa_2O_6$ is classified as a α-PbO_2 structure, in which Zn^{2+} species are in a six-fold coordination [33]. This result indicates that Zn species in the precursor should be transformed to six-fold coordination in order to construct the $ZnTa_2O_6$ structure during the calcination above 1273 K.

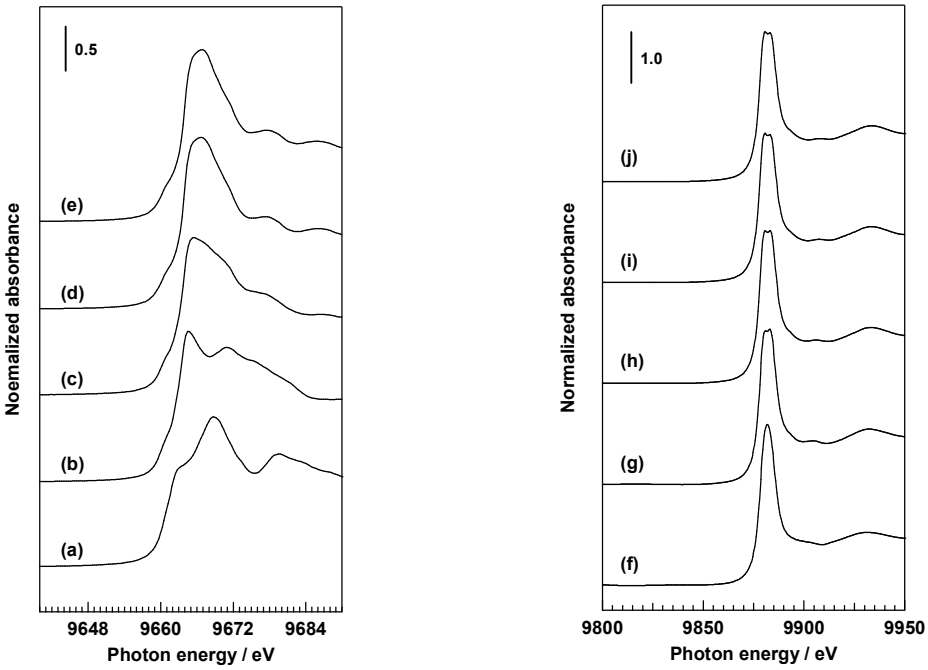

Figure 7 Normalized (a−e) Zn-K edge and (f−j) Ta-L_{III} edge XANES spectra of (a, f) mixture of ZnO and Ta_2O_5, (b, g) ZTO_1073, (c, h) ZTO_1173, (d, i) ZTO_1273, and (e, j) ZTO_1373.

Therefore, the Zn-K edge XANES spectrum of ZTO_1173 was found to be between those of ZTO_1073 and ZTO_1273. As shown in **Figure 7(f–j)**, in contrast, the XANES spectra of the Ta-L_{III} edge did not change on increasing the calcination temperature. Hence, we can conclude that based on the results of XRD and XAFS, the improvement in the selectivity toward CO evolution was due to the structural change of Zn species, which in the ZnO phase were incorporated into Ta_2O_5 to form a $ZnTa_2O_6$ structure when calcined above 1273 K, and because the potential of the photogenerated electrons in the conduction band of ZnO was not enough to reduce CO_2 [34]. The *in situ* FT-IR spectra of CO_2 adsorbed species on ZTO_1173 and ZTO_1273 are presented in **Figure 8**. Both of them showed absorption peaks corresponding to the C-O stretching of the CO_2 species adsorbed on the metal oxide materials, with reference to the review about the CO_2 species adsorbed on other simple metal oxides [35]; in contrast, it is difficult to determine the adsorbed CO_2 on the surface of Ta_2O_5. The absorption peaks observed at 1320, 1375, and 1632 cm^{-1} for both ZTO_1173 and ZTO_1273 can be assigned to the carbonate species [35]. The peaks at 1450 and 1730 cm^{-1} corresponding to bicarbonate species [35] were found in ZTO_1273, indicating that the surface properties of $ZnTa_2O_6$ were altered on changing the calcination temperature. Hence, it can be considered that changes in the chemical properties, which alter the adsorbed CO_2 species, improve the selectivity toward CO evolution.

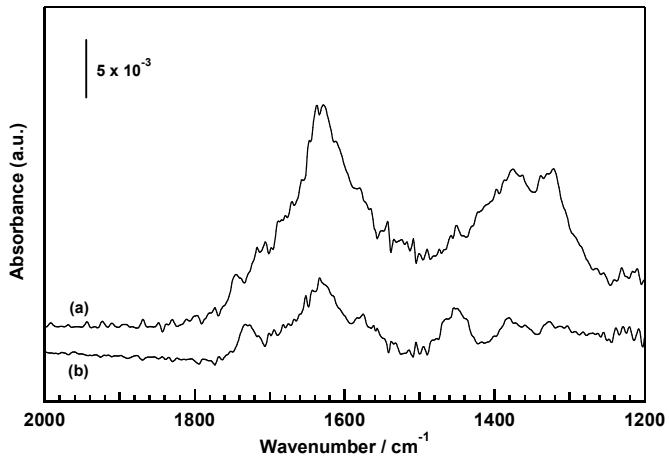

Figure 8 *In-situ* FT-IR spectra of (a) ZTO_1173 and (b) ZTO_1273. Pellet: 100 mg. Detector: MCT. Resolution: 4 cm^{-1}. Accumulation: 128 scans. Temperature: R.T. CO_2 introduction: 1.1 kPa.

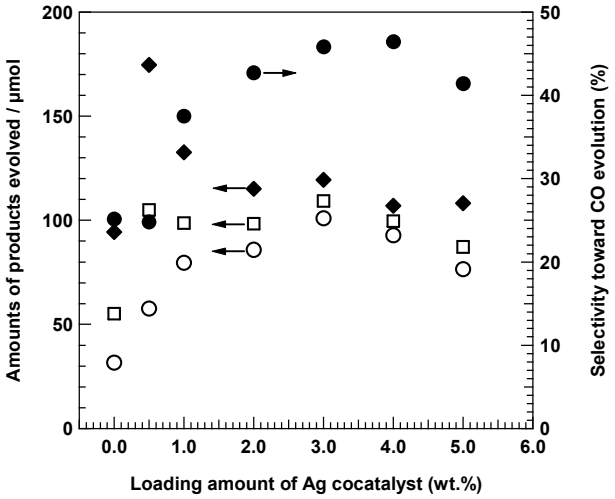

Figure 9 Effect of Ag loading amount on the photocatalytic conversion of CO_2 in an aqueous $NaHCO_3$ solution using ZTO_1273 as a photocatalyst. Photocatalyst powder: 0.5 g. Additive: 0.1 M $NaHCO_3$, Ag loading method: impregnation (IMP). White circle: CO, diamond: H_2, square: O_2, and black circle: selectivity toward CO formation.

Figure 9 displays the effect of the loading amount of Ag on the photocatalytic activity for the conversion of CO_2 in an aqueous $NaHCO_3$ solution using ZTO_1273 as a photocatalyst. As the loading amount of Ag was increased to 3.0 wt.%, the amount of CO evolved also increased, which was accompanied with a decrease in H_2 evolution. This is an indication that the selectivity toward CO evolution clearly improved on increasing the loading amount of Ag. As mentioned above, Ag particles loaded on a $ZnTa_2O_6$ photocatalyst are considered to be effective cocatalysts for the conversion of CO_2 into CO. The results of the control experiments using Ag-loaded ZTO_1273 are presented in **Figure 10**. At region (A), no photocatalytic reaction was observed under dark condition under He gas flow. Small amounts of H_2 and O_2 were produced in the He atmosphere under UV irradiation, as shown in region (B). At region (C), small amounts of H_2 and O_2 were evolved from pure water under photoirradiation and CO_2 gas flow,. Prior to starting the region (D), $NaHCO_3$ (0.1 M) was added into the reaction solution and the dissolved air was completely degassed by the He gas flow. During illumination, small stoichiometric amounts of H_2, O_2, and CO were formed in the gas phase. The selectivity toward CO evolution was ca. 10% in region (D), indicating that the main photocatalytic process was water splitting, which was accompanied by the conversion of $NaHCO_3$-derived CO_2. With the start of CO_2 gas flow in region (E), the evolution of CO noticeably improved. Moreover, the selectivity toward CO evolution was over 40% after 2 h of photoirradiation.

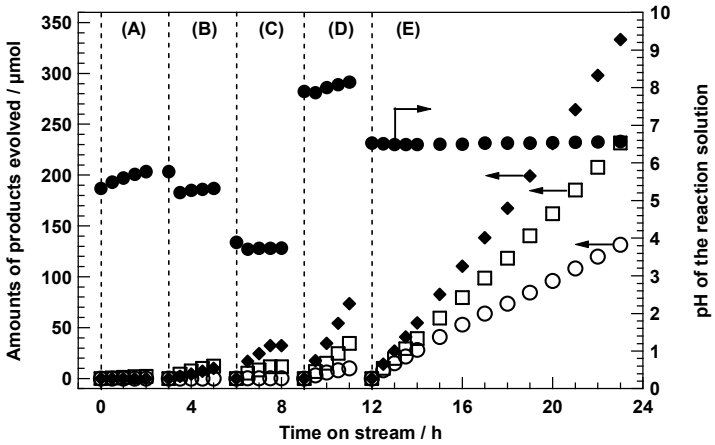

Figure 10 Result of control experiments for the photocatalytic conversion of CO_2 using in water Ag/ZTO_1273 as a photocatalyst. (A) no additive; He gas flow; dark, (B) no additive; He gas flow; photoirradiation, (C) no additive; CO_2 gas flow; photoirradiation, (D) 0.1 M $NaHCO_3$ additive; He gas flow; photoirradiation, (E) 0.1 M $NaHCO_3$ additive; CO_2 gas flow; photoirradiation. Photocatalyst powder: 0.5 g. Ag loading: 3 wt. % (IMP). White circle: CO, diamond: H_2, square: O_2, and black circle: selectivity toward CO formation.

The formation rate of CO gradually decreased with the irradiation duration, whereas that of H_2 remained stable during the 12 h of photoirradiation. Furthermore, the isotopic experiment was performed using ^{13}C-labeled CO_2 in order to confirm that carbon source of CO evolved in the photocatalytic conversion of CO_2 over Ag-modified ZTO_1273. **Figure 11** shows the result of GC-MS analysis for the isotopic experiment. In the TCD-GC chromatogram, the clear peak at 10.5 min was assigned to CO, and the others peaks corresponded to H_2, O_2, and contaminated N_2. With a Q-Mass profile of m/z = 29, one peak was found at the same retention time to CO in the GC chromatogram, indicating that this peak can be considered to originate from the ^{13}C-labeled CO. In contrast, no peak was observed in the profile of m/z = 28. Hence, it can be concluded that the CO evolved in this study originated from CO_2. Therefore, other carbon sources such as the contamination of organic residues did not influence this photocatalytic reaction. Further investigation on the synthesis procedure of photocatalyst and cocatalyst modification is necessary, because the photocatalytic activity and selectivity toward CO evolution have not been insufficiently investigated. We found that the $ZnTa_2O_6$ photocatalyst is active for the conversion of CO_2 into CO under UV irradiation. The formation of stoichiometric amounts of O_2 indicates that H_2O can act both as an electron donor and a proton source for this reaction.

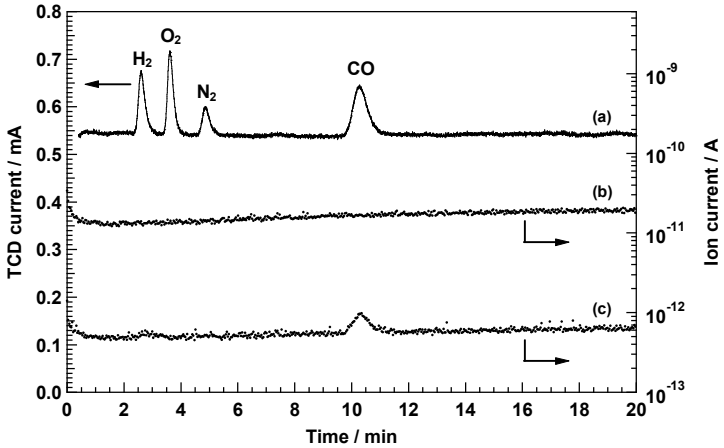

Figure 11 GC-MS profile in the isotopic experiment for the photocatalytic conversion of ^{13}C-labeled CO_2 using ZTO_1273 as a photocatalyst. (a) TCD-GC chromatogram, Q-Mass profile of (b) *m/z* = 28, and (c) *m/z* = 29.

Conclusion

We found that the Ag cocatalyst-loaded $ZnTa_2O_6$ photocatalyst showed activity for the conversion of CO_2 into CO in an aqueous $NaHCO_3$ solution under UV irradiation. After 5 h of photoirradiation of Ag-loaded ZTO_1273 (3 wt.%), the amount of CO evolved was 109.3 μmol and the selectivity toward CO evolution among the reduction products was 45.8%. The formation of stoichiometric amounts of O_2 indicates that H_2O can act both as an electron donor and a proton source for this reaction. In contrast, Pt/ZTO_1273, which was prepared by the photodeposition method, showed good overall water splitting capabilities and over 700 μmol of H_2 was produced over 1 h of photoirradiation. Through control and isotopic experiments, we concluded that CO evolved during the photocatalytic conversion of CO_2 in an aqueous $NaHCO_3$ solution using the Ag cocatalyst-loaded $ZnTa_2O_6$ photocatalyst originated from the CO_2 introduced as a substrate. Calcination at high temperatures altered both the chemical and structural properties of $ZnTa_2O_6$ and improved the selectivity toward CO evolution.

References

1. W. Wang, S. Wang, X. Ma and J. Gong, *Chemical Society Reviews*, 2011, **40**, 3703-3727.
2. G. Centi, E. A. Quadrelli and S. Perathoner, *Energy & Environmental Science*, 2013, **6**, 1711-1731.
3. E. V. Kondratenko, G. Mul, J. Baltrusaitis, G. O. Larrazabal and J. Perez-Ramirez, *Energy & Environmental Science*, 2013, **6**, 3112-3135.
4. M.-S. Fan, A. Z. Abdullah and S. Bhatia, *ChemCatChem*, 2009, **1**, 192-208.
5. A. Kubacka, M. Fernández-García and G. Colón, *Chemical Reviews*, 2012, **112**, 1555-1614.
6. W. Fan, Q. Zhang and Y. Wang, *Physical Chemistry Chemical Physics*, 2013, **15**, 2632-2649.
7. *Standard Potentials in Aqueous Solution*, Marcel Dekker, 1985.
8. Y. Kohno, T. Tanaka, T. Funabiki and S. Yoshida, *Chemical Communications*, 1997, 841-842.
9. Y. Kohno, T. tanaka, T. Funabiki and S. Yoshida, *Chemistry Letters*, 1997, **26**, 993-994.
10. Y. Kohno, T. Tanaka, T. Funabiki and S. Yoshida, *Journal of the Chemical Society, Faraday Transactions*, 1998, **94**, 1875-1880.
11. Y. Kohno, T. Tanaka, T. Funabiki and S. Yoshida, *Physical Chemistry Chemical Physics*, 2000, **2**, 2635-2639.
12. Y. Kohno, H. Ishikawa, T. Tanaka, T. Funabiki and S. Yoshida, *Physical Chemistry Chemical Physics*, 2001, **3**, 1108-1113.
13. K. Teramura, T. Tanaka, H. Ishikawa, Y. Kohno and T. Funabiki, *The Journal of Physical Chemistry B*, 2004, **108**, 346-354.
14. H. Tsuneoka, K. Teramura, T. Shishido and T. Tanaka, *The Journal of Physical Chemistry C*, 2010, **114**, 8892-8898.
15. K. Teramura, S. Iguchi, Y. Mizuno, T. Shishido and T. Tanaka, *Angewandte Chemie International Edition*, 2012, **51**, 8008-8011.
16. S. Iguchi, K. Teramura, S. Hosokawa and T. Tanaka, *Catalysis Today*, 2015, **251**, 140-144.
17. S. Iguchi, K. Teramura, S. Hosokawa and T. Tanaka, *Physical Chemistry Chemical Physics*,

2015, **17**, 17995-18003.

18. K. Teramura, Z. Wang, S. Hosokawa, Y. Sakata and T. Tanaka, *Chemistry - A European Journal*, 2014, **20**, 9906-9909.
19. Z. Wang, K. Teramura, Z. Huang, S. Hosokawa, Y. Sakata and T. Tanaka, *Catalysis Science & Technology*, 2015, DOI: 10.1039/C5CY01280E.
20. Z. Ding, W. Wu, S. Liang, H. Zheng and L. Wu, *Materials Letters*, 2011, **65**, 1598-1600.
21. G. B. Kunshina, I. V. Bocharova, O. G. Gromov, E. P. Lokshin and V. T. Kalinnikov, *Inorganic Materials*, 2012, **48**, 62-66.
22. A. V. B. M. Birdeanu, E. Fagadar-Cosma, C. Enache, I. Miron, I. Grozescu, *Digest Journal of Nanomaterials and Biostructures*, 2013, **8**, 263-272.
23. T. H. Noh, I.-S. Cho, S. Lee, D. W. Kim, S. Park, S. W. Seo, C. W. Lee and K. S. Hong, *Journal of the American Ceramic Society*, 2012, **95**, 227-231.
24. M. Waburg and H. Müller-Buschbaum, *Zeitschrift für anorganische und allgemeine Chemie*, 1985, **522**, 137-144.
25. H. Kato and A. Kudo, *Chemical Physics Letters*, 1998, **295**, 487-492.
26. T. Takayama, K. Tanabe, K. Saito, A. Iwase and A. Kudo, *Physical Chemistry Chemical Physics*, 2014, **16**, 24417-24422.
27. E. A. Davis and N. F. Mott, *Philosophical Magazine*, 1970, **22**, 0903-0922.
28. Z. Wang, K. Teramura, S. Hosokawa and T. Tanaka, *Journal of Materials Chemistry A*, 2015, **3**, 11313-11319.
29. K. Teramura, H. Tatsumi, Z. Wang, S. Hosokawa and T. Tanaka, *Bulletin of the Chemical Society of Japan*, 2015, **88**, 431-437.
30. K. Iizuka, T. Wato, Y. Miseki, K. Saito and A. Kudo, *Journal of the American Chemical Society*, 2011, **133**, 20863-20868.
31. T. Takayama, A. Iwase and A. Kudo, *Bulletin of the Chemical Society of Japan*, 2015, **88**, 538-543.
32. R. Kretzschmar, T. Mansfeldt, P. N. Mandaliev, K. Barmettler, M. A. Marcus and A. Voegelin, *Environmental Science & Technology*, 2012, **46**, 12381-12390.
33. M. Waburg and H. Müller-Buschbaum, *Zeitschrift für anorganische und allgemeine Chemie*,

1984, **508**, 55-60.

34. Y. Xu, and M.A.A. Schoonen, *American Mineralogist*, 2000, **85**, 543-556.

35. G. Busca and V. Lorenzelli, *Materials Chemistry*, 1982, **7**, 89-126.

List of Publications

Chapter 1

1. Kentaro Teramura, Shoji Iguchi, Yuto Mizuno, Tetsuya Shishido, and Tsunehiro Tanaka
   Photocatalytic Conversion of CO_2 in Water over Layered Double Hydroxides.
   Angewandte Chemie International Edition, 2012, **51**, 8008-8011.

2. Shoji Iguchi, Kentaro Teramura, Saburo Hosokawa, and Tsunehiro Tanaka
   Photocatalytic conversion of CO_2 in an aqueous solution using various kinds of layered double hydroxides.
   Catalysis Today, 2015, **251**, 140-144.

Chapter 2

3. Shoji Iguchi, Kentaro Teramura, Saburo Hosokawa, and Tsunehiro Tanaka
   Effect of the chloride ion as a hole scavenger on the photocatalytic conversion of CO_2 in an aqueous solution over Ni−Al layered double hydroxides.
   Physical Chemistry Chemical Physics, 2015, **17**, 17995-18003.

Chapter 3

4. Shoji Iguchi, Kentaro Teramura, Saburo Hosokawa, and Tsunehiro Tanaka
   Photocatalytic conversion of CO_2 in water using fluorinated layered double hydroxides as photocatalysts.
   Applied Catalysis A: General, in press (DOI: 10.1016/j.apcata.2015.11.023).

Chapter 4

5. Shoji Iguchi, Yudai Hasegawa, Kentaro Teramura, Saburo Hosokawa, and Tsunehiro Tanaka
   Preparation of transition metal-containing layered double hydroxides and application to the photocatalytic conversion of CO_2 in water.
   Journal of CO_2 Utilization, submitted.

Chapter 5

6. Shoji Iguchi, Soichi Kikkawa, Kentaro Teramura, Saburo Hosokawa, and Tsunehiro Tanaka
   Investigation on electrochemical and photoelectrochemical properties of Ni−Al LDH photocatalyst.
   Physical Chemistry Chemical Physics, to be submitted.

Chapter 6

7. Shoji Iguchi, Yudai Hasegawa, Kentaro Teramura, Saburo Hosokawa, and Tsunehiro Tanaka
   Improvement in the photocatalytic activity for the conversion of CO_2 in water by modification of Ga_2O_3 with Mg−Al layered double hydroxide.
   Journal of the American Chemical Society, to be submitted.

Appendix

8. Shoji Iguchi, Kentaro Teramura, Saburo Hosokawa, and Tsunehiro Tanaka
   $ZnTa_2O_6$ photocatalyst synthesized via solid state reaction for conversion of CO_2 into CO in water.
   Catalysis Science & Technology, submitted.